Velocity and mixing characteristics of stirred vessels with two impellers.

Seyed Mahmoudi, Seyed Mohammad

VELOCITY AND MIXING CHARACTERISTICS OF STIRRED VESSELS WITH TWO IMPELLERS

A thesis submitted for the degree

of

DOCTOR OF PHILOSOPHY

in the

Faculty of Engineering

of the

University of London

by

Seyed Mohammad SEYED MAHMOUDI

Mechanical Engineering Department

King's College London

December 1993

To my parents

ABSTRACT

This thesis describes an experimental investigation of the mixing characteristics of stirred vessels agitated by single and double Rushton or pitched blade impellers. Flow visualization experiments were performed to observe the flow patterns induced by different impeller configurations with different clearances prior to velocity measurements by laser-Doppler anemometry (LDA). Strain gauges were employed together with a telemetric system for power consumption measurements and a conductivity probe was used for mixing time studies.

Variation of the spacing between two Rushton impellers was found to affect significantly the induced flow pattern, power consumption and mixing time in the vessel. Three stable and four unstable flow patterns were identified with different impeller clearances. The unstable flows resulted in longer mixing times and a variation of the power consumption with time. The three stable flow patterns were quantified with detailed measurements obtained by LDA. The distributions of the turbulence kinetic energy for these three flow patterns were considerably different.

A similar investigation was performed with two pitched blade impellers and with combinations of pitched blade and Rushton impellers. The flows were found to be always unstable except in the case when two pitched blade impellers pumping towards each other were employed. The flow pattern in the latter case was quantified by LDA measurements and the results were compared with those for a similar pattern obtained with two Rushton impellers.

The power measurements showed a time-varying power consumption

with all impeller combinations. In the case of unstable flow patterns, the fluctuation level was comparatively higher than that for stable flow patterns. The power numbers for each of the impellers in the double Rushton configuration were different and in general smaller than that for a single impeller.

The effect of the Rushton impeller geometry and speed for both single and double-impeller systems on the velocity and mixing characteristics was also investigated. The impeller blade and disk thickness was found to affect both the flow number and power consumption.

The results are analysed and their implications for the calculation of the flows and process design are discussed in detail.

ACKNOWLEDGEMENTS

I am indebted to Dr. M. Yianneskis for his supervision and guidance, his continuous encouragement and support and constructive criticism throughout my research.

I am also grateful to:

Dr. H. Fu and Dr. K.O. Suen for their advice and assistance during early stages of my study.

Dr. J. Fendley and Mr. M. Jessop for their help with the graphics programs.

My colleagues in the Centre for Heat Transfer and Fluid Flow Measurement for their useful suggestions and assistance.

Messrs. M. Harrington, D. Elgar, B. Hoskins, J. Greenberg D. Green and S. Wooton for constructing the rig and measuring tools.

Finally I must mention all my close friends in London for their encouragement and warmth and for providing a light-hearted side of life.

CONTENTS

NOMENCLATURE and ABBREVIATIONS

C	Clearance of the impeller in single-impeller system
C_1	Lower impeller clearance in the two-impeller system
C_2	Spacing between impellers in two-impeller system
C_3	$C_3 = H - (C_1 + C_2)$
C_c	Concentration in probe calibration experiments
C_{m1}	Local mean concentration
C_{m2}	Mean concentration in the whole vessel
C_f	Concentration in the vessel when mixing is completed
C_i	Instantaneous concentration
d	Impeller diameter
d_{ph}	Diameter of the pinhole in the photomultiplier
dR	Change in the electrical resistance of a strain gauge
d_s	Shaft diameter
E	Wheatstone bridge excitation voltage
F	Weight in the calibration of the torque measuring system
f_1, f_2, f_3	Focal lengths of the LDA lenses
F_l	Impeller flow number
F_D	Doppler frequency
F_s	Frequency shift
h	Impeller blade width
H	Height of liquid in the stirred vessel
K	Gauge factor
k	Turbulence kinetic energy
k_{avr}	Area-weighted average turbulence kinetic energy
L	Impeller blade length
m	Order of the beams diffracted from grating

n	Number of the lines in the diffraction grating
N	Impeller speed
N_g	Diffraction grating rotational speed
N_p	Power number
$\overline{Np}$	Average peak power number
P	Power consumption
Q	Radial volumetric flow rate
Q_g	Gas flow rate
R	Radial distance from the tip of the impeller in LDA measurements; resistance of strain gauges in torque measurement system
r	Radius of measurement location
r*	Non-dimensional coordinate, r* = 1 + 2R/d = r/(d/2)
S	Torsion
t	Impeller thickness; time
t_c	Circulation time
t_{in}	tracer insertion time
t_b	Impeller blade thickness
t_d	Impeller disc thickness
t_f	Mean mixing time (equal to ζ_{av})
T	Vessel diameter
T_c	Temperature
T_q	Torque exerted on the shaft
U,V,W	Axial, radial and tangential mean velocities
u, v, w	Axial, radial and tangential rms velocities
U_{is}, V_{is}, W_{is}	Instantaneous axial, radial and tangential velocities
V_1 and V_2	Mean voltages in the conductivity measurements

V_{45}	Velocity in a direction 45° to the radial direction
V_c	Voltage in conductivity probe calibration
Vi	Instantaneous voltage in conductivity measurements
V_o	Measured 'no load' voltage in torque measurements
V_q	Voltage in torque measurements
V_{tip}	Impeller tip speed
V_{out}	Wheatstone bridge output voltage
W_b	Width of baffles
X,Y,Z	Orthogonal directions for movement of the traversing tables
z	Axial distance from the bottom of the vessel
z'	Axial distance from the elevation of the impeller
z*	Non-dimensional axial coordinate, z* = z' / (h/2)

Greek symbols:

$(\delta Np)_{max}$	Maximum fluctuation in power number
$(\delta Tq)_{max}$	Maximum fluctuation in exerted torque
$(\delta N)_{max}$	Maximum fluctuation in impeller speed
$(\delta P)_{max}$	Maximum fluctuation in power consumption
δR	Change in the electrical resistance of a strain gauge
ε	Strain
ζ_i	Mixing time for a specific degree of mixing
ζ_{av}	Mean mixing time
θ	Intersection angle between the laser beams; r - z measurement plane angle
λ	Wavelength of the laser light
λ^*	Fringe spacing

μ	Fluid viscosity
ρ	Fluid density
τ	Circulation time group; $\tau = N\, t_c\, (d/T)^2$

Abbreviations

DT	Disk turbine (Rushton impeller)
FC	Flow configuration
LDA	Laser-Doppler anemometry
M. D.	Merging / diverging flow in Figures 3.3 to 3.8
PBD	Downward pumping pitched blade impeller
PBT	Pitched blade turbine
PBU	Upward pumping pitched blade impeller
P. D.	Parallel / diverging flow in Figures 3.3 to 3.8
P. M.	Parallel / merging flow in Figures 3.3 to 3.8
P. M. D.	Parallel / merging / diverging flow in Figures 3.3 to 3.8
rpm	Revolutions per minute
rms	Root mean square
$[rms]_{Np}$	Rms level in the fluctuating power number
Re	Reynolds number; $Re = (\rho N d^2/\mu)$
S.G. (L)	Lower strain gauge Wheatstone bridge
S.G. (U)	Upper strain gauge Wheatstone bridge
SRI	Standard Rushton impeller with a geometry ratio of d : L : h = 20 : 5 : 4
Tech	Experimental technique
TR	Tracer in conductivity experiments
WF	Working fluid

CHAPTER 1

INTRODUCTION

1.1 Background

The performance of stirred vessels has been the subject of research by a great number of investigators as these have been extensively used for mixing in the chemical, food, petroleum and pharmaceutical industries. These vessels are generally involved in mixing of miscible or immiscible liquids, dispersion of gas in liquids, suspension of solid particles in liquids and quite often in three-phase mixing processes.

Over the years a great deal of effort has been devoted to the optimisation of mixing processes in stirred tanks with respect to power consumption, quality of mixture product, duration of the process and capital and operating costs, (see, for example, Benkreira, 1990). For a particular mixing system, vessels with different geometries employing a variety of impeller types have been used. However, there is no universal design of impeller or mixing tank which can be employed for all mixing applications.

The modification of existing stirred reactors for better efficiency, as well as the design of new mixing systems or new type of impellers, require an accurate knowledge of the flows induced by the impellers in the vessel. This necessity has urged investigators to undertake many experimental investigations employing various techniques, for example, mixing time measurements by Holmes et al (1964), flow visualisation by van't Riet and Smith (1975), power measurements by Bujalski et al (1986) and laser-Doppler anemometry (LDA) measurements of the mean and rms

velocities by Yianneskis et al (1987). For the purposes of economy and ease of experimentation the majority of the mixing process investigations have been carried out in small scale vessels. The results may be scaled up to process-size systems employing geometric, kinematic and dynamic similarity. However, in many applications such scaling-up is not appropriate and experiments in larger vessels are necessary.

Rushton and pitched blade impellers are two of the most-commonly used impellers in industrial turbulent mixing processes. The former produces a high-shear radial flow which results in better dispersion whilst the latter generates a 'mixed', axial and radial, flow with a larger pumping capacity resulting in better circulation in the tank.

A number of mixing processes make use of two impellers on the same shaft. In these systems in addition to the geometries of the tank and the impellers, impeller spacing and impeller combination are the main features of system design for mixing processes. The importance of impeller spacing stems from the fact that if the impellers are positioned comparatively close to each other the impeller streams may interact and influence each other and flow entrainment may occur from the field of action of one impeller to that of another. This influence will result in a more complex flow in a two-impeller system in comparison with that in a single-impeller system. On the other hand if the impellers are located far apart, stagnant regions will appear in the vessel in the region between the impellers which should be avoided in an efficient mixing system. Depending on the nature of the mixing process, combinations of two Rushton impellers, two pitched blade impellers and pitched and Rushton impellers are often used in industry.

The published literature for two-impeller mixing systems is not as extensive as that for single-impeller systems albeit the former are widely used in the mixing industry. Most of the research carried out on two-impeller systems has been involved with gas dispersion in liquids and most attention has been paid to the power consumption, e.g. Kuboi and Nienow (1982), Cronin (1988) and Hudcova et al (1989); these investigations have been only partly concerned with non-gassed systems. A small number of flow visualisation investigations has also been reported for different combinations of Rushton and pitched blade impellers. Quantitative data on the flows in two-impeller systems is very sparse. This lack of data may pose serious design shortcomings. For example, Crozier (1989) reported that in stirred tanks with a liquid height equal to twice the vessel diameter some stagnant regions appear in the mid-height of the vessel when two Rushton impellers are located with a separation equal to the vessel diameter.

Notwithstanding the numerous applications of dual-impeller systems in mixing processes and the differences in flow patterns between single and two-impeller combinations, little is known about the latter. This thesis aims to redress this lack of knowledge by a methodical investigation of fundamental and practical aspects of dual-impeller mixing.

In order to identify the methods and the parameters of importance in such mixing systems, the experimental techniques and the findings of previous stirred tank investigations are reviewed in the following two sections. Some single-impeller systems have also been reviewed in order to distinguish between single- and dual-impeller effects and to identify parameters requiring further study. The survey was used to formulate the

specific objectives of the present investigation which are listed in section 1.4. The chapter closes with an outline of the thesis given in section 1.5.

1.2 Review of experimental techniques employed in stirred tanks

A large number of papers have been reviewed and they are tabulated in table 1 in chronological order. The most relevant ones are reviewed in more detail in this section and in section 1.3.

Many types of experimental techniques have been developed for or introduced to stirred tanks in order to obtain more information about the mixing process. These techniques may be grouped as follows:

a) Flow visualisation methods;
b) Measurement of power consumption;
c) Measurement of velocity characteristics; and
d) Measurement of mixing time.

The main applications of each of the above groupings are reviewed below.

1.2.1 Flow visualisation techniques

Flow visualisation is a simple, relative rapid and powerful means of obtaining a qualitative picture of the fluid movement during agitation. This technique is generally applied by illumination of a plane of interest in the flow so that the path of added particles can be visualised, photographed and/or filmed. However, the application of the techniques in stirred vessels is not always simple and informative: the flow in some

cases is strongly three dimensional, and illumination of one (two-dimensional) plane at a time does not offer much insight into the processes involved.

In other cases the flow must be visualised with respect to the rotation of the impeller, for example when studying the trailing vortices in the impeller stream which are three-dimensional structures rotating with the impeller. In order to visualise the trailing vortices behind the impeller blades, investigators have used different techniques. Van't Riet and Smith (1973) used a rotating camera which was coupled to the impeller shaft. Kuboi et al (1983) used a rotating device consisting of a prism which when rotated caused the trailing vortices to appear stationary.

Sachs and Rushton (1954) and van't Riet and Smith (1975) used a photographic technique to measure the mean velocities in the impeller stream and the trailing vortices respectively. With this technique the exposure time and the length of the streaks produced by illuminated particles or the dimensions of the route of a particle were used to determine the mean velocity field. However, as the flow in stirred tanks is often highly three dimensional, Sachs and Rushton suggested that a comparatively large error may occur in the velocity assessment with flow visualisation methods .

1.2.2 Power measurement techniques

The power consumed for a mixing process can be measured by recording the speed of agitation and the torque exerted on the shaft during mixing. The power consumed is given by;

$$P = 2\pi N T_q \qquad (1.1)$$

where N is the impeller speed and T_q is the torque exerted on the shaft. A non-dimensional number called the power number is used to characterise power consumption:

$$N_p = \frac{P}{\rho N^3 d^5} \qquad (1.2)$$

where d is the impeller diameter and ρ is the density of the fluid in the vessel.

Researchers have applied various techniques using dynamometers for the measurement of power consumption in stirred tanks. Nagata (1975) reviewed the principles of these techniques and clarified the reasons for disagreement in the power data reported by different investigators employing different types of dynamometers. He emphasised the significance of the effect of the friction in the moving parts of the measurement system and of the friction resulting from mechanical contact between the shaft and any fixed part prior to the shaft entering the agitated liquid on the torque measured. Bader (1986) measured the power consumption with and without water in the vessel and subtracted the latter from the former in order to eliminate frictional effects. This method may suffer, however, from the inaccuracies caused by air resistance to the impeller rotation.

Air bearings have also been used for power measurements, e.g. by Yianneskis et al (1987). This is a friction free method as the tank and measuring load cell are separated by a film of air. However, air bearings can only measure the total power consumption in two-impeller systems,

not the individual power consumed by each impeller and therefore are not very useful for double-impeller studies.

Strain gauge telemetric systems, which have been used in mixing tanks by, among others, Kuboi and Nienow (1982), Cronin (1988) and Hudcova et al (1989) provide a power measurement technique which allows the determination of the power consumption of each impeller in two-impeller systems. The principles of this technique will be discussed in Chapter 2.

1.2.3 Velocity and turbulence measurement techniques

Before the application of laser-Doppler anemometry to stirred vessels several measurement techniques had been used to measure velocity and turbulence characteristics in stirred vessels.

Measurements have been made by hot wire anemometry or pitot tubes by many investigators. Such techniques suffer from inaccuracies as the probes disturb the flow. Although these techniques may seem to be convenient for velocity measurements in-between the impeller blades as they can be fixed to the impeller, the disturbance of the flow by the probe and the probe support may result in a wrong interpretation of the structure of the flow. The existence of four trailing vortices between two adjacent Rushton impeller blades which was claimed by Gunkel and Weber (1975) is an example of this type of error.

Laser-Doppler anemometry is a non-obtrusive technique and at present the most convenient technique for the measurement of velocity characteristics in stirred tanks. This technique has been used by many workers since its first application in a stirred tank by Reed et al (1977).

The principles of this technique and its application to stirred tank flows is discussed in detail in Chapter 2.

1.2.4 Techniques for mixing time measurements

Schofield (1974) reviewed the experimental techniques employed for the measurement of mixing time in stirred vessels. For liquid-liquid mixing, these techniques can be generally classified into two groups:

a) Observation methods; and
b) Transducer methods.

In observation methods, the change in the colour of the liquid contained in the tank caused by the insertion of either a dye or a reacting liquid is observed as the mixing process proceeds. In the latter case the addition of the liquid initiates a chemical reaction which results in a colour change. Large inaccuracies can be encountered using this technique which may lead to significant underestimation of the mixing time. One advantage of the method is that in some situations 'dead' or stagnation zones may be identified quickly.

The most commonly employed methods of the second group make use of a conductivity probe or a thermocouple to detect the variation of the conductivity or temperature of the fluid in the vessel, respectively. This variation is produced by introducing a small amount of another liquid with a different property appropriate to the technique. Although only local concentration can be measured by this technique, repeating the measurement in different locations can give a more accurate overall mixing time. In addition, the degree of mixing at different stages of

process can be measured. Most of the researchers have used a pulse injection of a tracer of higher conductivity than the fluid in the vessel to obtain the conductivity-time history, as this technique can yield more information than observation methods.

Khang and Fitzgerald (1975) considered the effect of stray currents in mixing time measurements obtained by conductivity probes of different designs. The stray currents were considered to be due to several effects such as 'internal batteries'. Internal batteries are formed as a result of the resistance from each electrode of the probe to the bulk fluid and the presence of metal parts other than platinum in the rig. This battery effect creates a potential between the probe electrodes and other metal parts used in the rig and can result in a biased output voltage. As stray currents result in false information in the concentration time-history, Khang and Fitzgerald designed a new type of probe which was free of such currents and had a linear response. The probe consisted of a coiled electrode in the form of a cage which surrounded the point electrode. Both electrodes were made of platinum and their exposed parts were platinised in order to avoid polarisation.

The effect of probe volume size in the mixing time was investigated by Thyn et al (1976) employing 14 probes with different sizes. They classified their mixing time experiments into two groups on the basis of probe-to-tracer volume ratio. Depending on whether the value of this ratio was smaller or bigger than unity, they obtained two different correlations between mixing time and probe-to-vessel volume ratio. However, it is interesting to note that the probes employed consisted of two parallel plates positioned in front of each other. The effective probe volume, which is greater than the actual volume between the two plates,

was determined experimentally using a constant for each probe and the distance between two electrodes.

1.3 Review of the findings of previous studies

In this section the main findings reported in the literature are reviewed in order to assess the present state of knowledge on the fluid mechanics of mixing processes. Rushton impeller systems are initially considered for single- and then dual-impeller configurations. Subsequently pitched-blade turbine systems are considered.

1.3.1 Single Rushton impeller

As mentioned earlier the Rushton impeller is the most commonly used design in stirred tanks. Many investigations have been carried out in order to understand the flow induced by these impellers particularly in the impeller region and impeller stream. In the following text, the pioneering early investigations are considered first, followed by the studies concerned with the flow structure around the impeller stream. Subsequently parametric studies of the flow in the bulk of the vessel and of average quantities such as the power number are reviewed.

Rushton et al (1950) found the power number to be constant for Re greater than 20000* . Sachs and Rushton (1954) studied the flow in the impeller stream of a four flat-blade turbine using a photographic technique. The results showed that the radial velocity profiles in the impeller stream flattened out with increasing radius while the radial flow increased. The latter increase persisted up to a radius r = T/3 after which

* The Reynolds number is defined by $Re = (\rho N d^2) / \mu$ where d is the impeller diameter, N is the impeller speed, ρ is the fluid density and μ is the fluid viscosity

the radial volumetric flow dropped off. The authors also noted the periodicity of the flow in the vicinity of the impeller by measuring a peak value of radial velocity at an angle of 50° ahead of the trailing blade.

Employing three vessels of different sizes with a variety of Rushton impeller to vessel diameter ratios, Holmes et al (1964) used the conductivity technique to investigate the rate of mixing in stirred tanks. In the concentration-time histories obtained several peaks with decreasing amplitude were observed. It was shown that the intervals between the successive peaks were equal to the circulation time (t_C) in the vessel. The circulation time was defined as the time required for a fluid element to move once around the average circulation loop in the tank. Using dimensional analysis they introduced a dimensionless group $\tau = N\, t_C\, (d/T)^2$ which was a function of Reynolds number and τ was constant (equal to 0.85 ± 0.05) at Reynolds numbers above 20000. The reduction in the amplitude of the peaks in the concentration-time history characterises the dispersion of the tracer during each circulation loop (Voncken et al, 1964).

Employing a photographic technique Cutter (1966) measured mean and rms velocities in the impeller stream and concluded that both mean and rms velocities are independent of Reynolds number when they are normalised by the impeller tip speed:

$$V_{tip} = \pi N d \qquad (1.3)$$

However, much scatter can be seen in Cutter's data. He estimated that the input energy to the impeller dissipated mostly in the impeller stream.

Using a pitot tube and a hot-wire anemometer Cooper and Wolf (1968) examined the magnitude and direction of the velocities in the impeller stream and showed that the flow at the outer extremes of the blades of height (h) less than 0.3d is mostly tangential and becomes increasingly radial towards the centre of the blades. However, an increase in the height of the blade h > 0.3d resulted in a more radial flow at the outer edge of the blades and a more tangential flow at the centre of the blades. A linear relationship was found between the impeller speed and the pumping capacity while the pumping capacity was found to be proportional to the cube of the turbine diameter. The authors identified an optimum value for the blade height (h = d/5) above which the pumping capacity did not vary significantly.

Van't Riet and Smith (1973) visualised the trailing vortices behind the impeller blades using 2 mm polystyrene particles as tracers and a camera rotating at the stirrer speed. The axes of the vortices were found to be horizontal and the vortices maintained their identity for at least two or three blade lengths with a fluid of low kinematic viscosity like water. The importance of these vortices on the dispersion and coalescence in liquid-gas mixing was pointed out. In a later study (van't Riet and Smith, 1975) the authors attempted to measure the velocity and pressure distribution within the trailing vortices. They employed a photographic technique for the velocity measurements and an impact tube (fixed to the blade) for the pressure measurements. The trajectory of a particle trapped in the vortex was photographed and it appeared as a sine wave. From the length of this trajectory and the exposure time the particle velocity was determined. Their results showed that the angular velocities in the vortex were independent of the distance along the vortex axis and dependent only on the Reynolds number when they are normalised with the impeller angular

speed ($2\pi N$). However, at higher Reynolds numbers, $15000 < Re < 90000$, the angular velocities in the trailing vortices did not show many differences. The axial velocities exhibited a linear relation with distance along the vortex axis but were almost independent of the distance from the axis. The radial velocities could not be measured, however, due to their small magnitude.

Gunkel and Weber (1975) measured the mean and rms velocities between two successive blades of a Rushton impeller by mounting a hot wire probe in-between the impeller blades. A shielded hot-wire anemometer and a yaw tube were also used to measure the velocities in the impeller stream. The shielded wire was claimed to allow reverse flow regions to be detected. The working fluid used was air, following the justification given by Mujumdar et al (1970). The measurements between two blades indicated the existence of two smaller vortices with larger radial velocities behind the leading blade and two larger vortices with smaller radial velocities ahead of the trailing blade. The former pair had also been identified by van't Riet and Smith (1973). The rms velocities measured between the blades were independent of the angular position. In the centre line and the vicinity of the impeller they measured a maximum radial mean velocity of 0.8 V_{tip} that was in agreement with the data obtained by Cutter (1966) and Mujumdar et al (1970). Using an energy conservation equation and assuming that no energy is dissipated within the control volume surrounding the impeller, Gunkel and Weber concluded that most of the input energy is dissipated in the bulk flow. It must be noted that the reliability of the data obtained by Gunkel and Weber must be questioned as they obtained differences of 20% between the velocities measured with three methods in the same location.

More reliable velocity data have been provided by the application of laser-Doppler anemometry (LDA) methods for measurements in stirred tanks. The advantages of this technique over hot-wire and hot-film anemometry are well known. A comparison of the hot wire anemometry and laser-Doppler velocimetry has been given by Nadaradjah (1992). The primary advantage is that it is a non-obtrusive technique and therefore very suitable for complex three-dimensional recirculating flows.

Using LDA Reed et al (1977) studied the flow in a stirred tank agitated by a Rushton impeller located at a clearance C = T/3. The results of this investigation revealed that the flow was highly three-dimensional. The ring vortex below the impeller was found to be stronger than that above the impeller. The difference in the strength of the two vortices resulted in an inclination of the impeller stream slightly upwards. Reed et al also noticed that the baffles had an extensive influence on the mean flow and emphasised the existence of strong helical vortices in front of the baffles.

In an investigation carried out by van der Molen and van Maanen (1978), the periodic component of the velocities in the vicinity of the impeller was measured and the existence of the trailing vortices behind the blades was confirmed. Their results showed that the peak-to-peak value of the periodic axial velocities in the vicinity of an impeller increased by a factor of three as the blade and disk thickness of the impeller decreased from 1.5 mm to 0.5 mm. From their results a slight increase of the above mentioned velocity with Reynolds number can be observed. They employed different impellers with two different blade/disk thickness to diameter ratio and the same impeller to vessel diameter ratio. However, the effect of vessel size on the periodic axial velocity profiles can not be

determined from their results as the measurements were performed at different Reynolds numbers.

The structure of the flow around the impeller blades and in the rest of the vessel was quantified in detail by Yianneskis et al (1987). Employing laser-Doppler anemometry, ensemble-averaged velocity measurements were performed over 1° and over 360° of impeller rotation. The influence of the ring vortices on the trailing vortices was found to be significant at about 25° behind the leading blade, while at an angle of 30° the trailing vortices were almost dissipated. The measurements showed that the rms velocities measured over 1° were similar to those obtained over 360° behind the leading blade (due to the presence of the trailing vortex) and decreased to 25% of the 360° averages where no trailing vortices are present, i.e. in front of the trailing blade. The maximum value of turbulence kinetic energy was measured at 20° behind the blade and valued at $k = 0.17\ V_{tip}^2$. The turbulence in the impeller stream was found to be anisotropic. The existence of second vortex behind the blade as claimed by Gunkel and Weber (1975) was rejected. The inclination of the impeller stream to the horizontal was found to decrease with increasing impeller spacing and impeller rotational speed. The instantaneous axial velocity measurements at the bottom and top edge of the impeller showed that the flow immediately above and below the disk was nearly symmetric. The periodicity and vortical structure of the flow in the impeller region persisted up to a radius of 0.7 d and at a radius r = d the vortices were broken up. The power number was found to be 4.8 for the d = T/3, t = 3 mm impeller located at C = T/3.

Wu and Patterson (1989) carried out a LDA study concerned with the influence of the trailing vortices on the velocity measurements in the

impeller stream. The results showed that the periodicity of the flow, as a result of the trailing vortices, strongly influences the rms velocities in the impeller stream close to the impeller. The largest contribution of the flow periodicity to the total radial and tangential rms velocities occurred in the impeller elevation and in the vicinity of the impeller. For the axial rms velocities the maximum contribution occurred on both sides of the impeller disk at a distance $\pm$ h/4 from the impeller elevation. The results also showed that the periodicity of the flow decayed rapidly with increasing distance from the tip of the impeller. At a location r* = 1.08 (where $r^* = \frac{2r}{d}$) the periodicity of the flow accounted for as much as 85% of the total turbulence in terms of mean-square fluctuation velocity. This contribution decreased to 20% at r* = 1.5 and the periodicity disappeared completely at r* = 1.9. Wu and Patterson also reported that the random rms velocities developed from the impeller tip, reaching to a maximum value at around r* = 1.5 and then decreasing with increasing radius.

In order to avoid the difficulties of the trailing vortex quantification relative to the impeller blade, Calabrese and Stoots (1989) simulated the environment of an impeller blade in a channel with a well conditioned flow with low turbulence intensity. The blade was positioned at an angle of 45° to the flow direction and velocity measurements were carried out employing laser-Doppler anemometry. The results showed that the inner edges of the trailing vortices merged at a very short distance from the blade tip. At the blade tip the turbulence kinetic energy was found to be relatively small increasing with distance from the tip along the vortex. The trailing vortices started to break down at a distance of about one blade width from the blade tip where the maximum kinetic energy was

measured. Similar results were obtained inside a stirred tank of 300 mm diameter.

A similar approach for the study of the flow behind the impeller blade is described in an earlier but less detailed investigation by Nienow and Wisdom (1974). They visualised the trailing vortices behind a single blade attached to a semi-circular disk placed in water channel with an angle of 45° to the flow direction. Observations were made by injecting dye or air upstream of the blade. They found separation regions both behind and in front of the blade. However, they observed that the separation region in front of the blade diminishes at higher flow velocities. As has already been remarked, the presence of any vortex in front of the blade has been discounted by the findings of Yianneskis et al (1987). Nienow and wisdom also visualised the trailing vortices around an impeller in a gassed system with a stroboscope and found a close resemblance between the flow characteristics of the vortices in the channel and in the stirred vessel.

The effect of impeller geometry on the flow field in the vicinity of the impeller was also investigated by Armstrong and Ruszkowski (1986) who employed two Rushton impellers identical in all aspects except for the blade thickness which was altered from 1.5 mm to 3 mm. They also used another impeller identical to the former in all except the disk diameter which was increased from 2d/3 to 3d/4. The LDA measurements performed at the $\theta = 45^{\circ}$ r-z plane (the vertical plane containing two baffles) showed an identical flow number for all three impellers. It was argued that the effect of thickness is only focused on the circulation velocities in the trailing vortices and the peak-to-peak value of the periodic component in the axial velocities, as stated by van der Molen and van Maanen (1978). However, Armstrong and Ruszkowski did not

mention the disk thickness of the impellers (t_d) they used and if there was any variation in t_d among the three impellers. They obtained a slightly higher flow number (F_l = 0.8) from the measurements performed at $\theta = 0^\circ$ in comparison with that obtained at $\theta = 45^\circ$ (F_l = 0.75). Armstrong and Ruszkowski also used a marine propeller and a four-bladed 45° pitched blade impeller and obtained flow numbers of 0.41 and 0.9 respectively.

Nouri et al (1987) investigated the effect of impeller rotational speed and size on the velocity field in the impeller stream and bulk flow. They employed three impellers with diameters d = T/4, T/3 and T/2 which were scaled up geometrically in every respect except for the blade/disk thickness which remained the same (3 mm). In that study the effect of impeller speed on the mean and rms velocities was found to be negligible when these velocities are normalised with the impeller tip speed. However, at a lower impeller speed, N = 50 rpm, the normalised velocities were found to be lower. The mean and rms velocity profiles (normalised with the impeller tip velocity) in the impeller streams of the three impellers with different diameters showed no differences when they were plotted in non-dimensional co-ordinates, defined as $r^* = r / (d/2)$ and $z^* = z' / (h/2)$. However, the impeller with diameter d = T/2 produced higher normalised velocities in the region away from the impeller.

Weetman and Oldshue (1988) studied the power, flow and shear characteristics of several impeller designs varying from a highly efficient axial flow impeller to the Rushton impeller which produces a high shear rate. They calculated the velocity gradients in the discharge of impellers of different sizes. The results showed that the average velocity gradient in the vicinity of a Rushton impeller was dependent only on the Reynolds

number and not on the impeller size. The maximum shear gradient was found to be dependent on the impeller tip speed (or N.d). A similar calculation for the four-bladed pitched-blade and fluidfoil impellers showed that both the mean and the maximum shear gradient are dependent on the impeller speed and size. They also measured higher fluctuation levels in the instantaneous velocities obtained with a Rushton impeller in comparison to those obtained with pitched-blade and/or fluidfoil impellers.

Greaves and Kobbacy (1981) investigated the effect of surface aeration on the power number. Some of their results were concerned with non-aerated flows and are relevant to the present investigation: the variation of power number with Reynolds number was found to depend on the impeller clearance, impeller diameter and impeller blade thickness to diameter ratio, particularly at lower impeller speeds. They suggested that further investigation of the effect of variation in impeller blade thickness on the variation of power number with Reynolds number was needed.

Bujalski et al (1986) looked at the influence of impeller geometry on the power consumption and used their experimental data to correlate the power consumption with the impeller and vessel geometries. The average power number $\overline{Np}$ was obtained from the average of measurements made over a range of Reynolds numbers $20000 < Re < 2\ Re_{SA}$, where Re_{SA} is the value of Re for which aeration from the free surface commences. Bujalski et al reported the following equation for the determination of $\overline{Np}$:

$$\overline{N_p} = 2.5 \left(\frac{t_d}{d}\right)^{-0.2} T^{0.065} \qquad (1.4)$$

where t_d is the impeller disk thickness, d is the impeller diameter and T is the vessel diameter in meters.

The effect of vessel size on the velocities in the impeller stream and bulk flow was investigated by Nouri and Whitelaw (1990). They employed two vessels with diameters T = 144 and 294 mm agitated by Rushton impellers scaled with respect to the vessel diameters. LDA measurements showed that the axial and radial velocities in the impeller stream and bulk flow exhibit no dependency on the vessel size when the velocities are normalised with the impeller tip velocity and plotted in non-dimensional co-ordinates $r^* = r / (d/2)$ and $z^* = z' / (h/2)$. They also found a negligible difference in the velocities due to the confinement of the vessel.

Numerous papers in the literature have been concerned with comparisons of the performance of Rushton impellers with that of other commonly-used single impellers. Comparisons with PBTs are discussed in section 1.3.3 below. The third most common design used is the axial flow impeller, normally a propeller.

An investigation of mixing time in the stirred reactors was carried out by Kramers et al (1953) employing the conductivity technique. In this investigation a propeller was found to be superior to a Rushton impeller as although both designs yielded the same mixing time, the power number for a Rushton impeller was found ten times higher than that for propeller. They observed that mixing was first completed in the immediate surrounding of the impeller and as mixing proceeded the homogeneous region is expanded until finally it contained the whole of the vessel. It was also found that the mixing time is inversely proportional to the impeller speed.

However, in view of the large variety of impeller designs, only the Rushton and PBT are considered in this thesis as the number of combinations and spacings possible with just these two types is enormous, as will become evident from the following text.

1.3.2 Two Rushton impeller system

A schematic representation of a stirred tank with two Rushton impellers is shown in Figure 1.1, in order to define the various geometrical characteristics of a double-impeller configuration.

An early investigation of the performance of multi-impeller systems was carried out by Richards (1963) who studied the flow patterns and power consumption in a stirred tank agitated by three Rushton impellers. He noted the influence of impeller spacing on the mixing process observing a critical impeller spacing which could result in an unstable flow pattern and fluctuations in power consumption. He suggested that an impeller spacing of between one and two impeller diameters should be used in multiple-impeller systems.

Employing a wide range of impeller diameters Taguchi and Kimura (1970) investigated the influence of impeller spacing on the power consumption of Rushton impellers in a multi-stage mixing tank (with H = 1.9 T and 2.4 T). They correlated the optimum impeller spacing between the impellers with the liquid height and the impeller diameter for maximum power consumption. The correlation for a two-impeller system was $C2 = (H - 1.9\ d) / 2$. The range of spacing between the impellers used in their investigation was $0.5d < C2 < 3d$. However, the experiments were

carried out in a vessel with liquid height H = 1.9 or 2.4T as mentioned above and the correlation is not necessarily applicable for H = T.

The power consumption of a two Rushton impeller combination with d_1 = d_2 = T/4 located at spacings C_1 = T/4 and C_2 = T/4 or 3T/8 in a standard vessel (T = H) was measured by Nienow and Lilly (1979). The results for both spacings showed identical power numbers which were twice those obtained in a single-impeller system with C = d = T/4.

A combination of two Rushton impellers (d_1 = d_2 = T/3) located at C_1 = C_2 = T/3 for gas dispersion was investigated by Kuboi and Nienow (1982) who observed that at higher impeller speeds the impeller streams merge and form only two ring vortices and the total power consumption is significantly less than the addition of the power consumed by each impeller if they had acted in single impeller systems. However, they suggested that this may happen only in gassed systems and not in un-gassed systems. They also stated that at Reynolds numbers above 40000 the power number remains constant within ± 5%.

Employing two or three impellers in a tall tank (H = 2T) Roustan (1985) measured a total power number Np = 14.2 for three impellers and Np = 10.4 for two impellers in un-gassed systems. In gassed systems introducing the third impeller increased the power consumption in the same manner as in an un-gassed system but the gas hold-up remained the same, presumably due to the variation in flow pattern (Richards 1963).

Employing eight-bladed Rushton impellers with a larger impeller to vessel diameter ratio (d = 0.4T), Bader (1986) investigated the influence of the impeller spacing on the power consumption. With a single-impeller

system the results showed a linear increase of power number with liquid level above or below the impeller in the range of 0.2T to 0.85T. In multiple-impeller systems, comprising up to five impellers located on the same shaft with equal spacings, the variation of the power number for each impeller with liquid level above or below that impeller was found to be the same as that for the single-impeller system (defining the spacing between the impellers as the liquid level above or below the impeller). The power number did not vary with impeller spacing for spacings above 0.85T.

The power consumption and flow patterns in a dual impeller system (with d = T/3 and H = 2T) were investigated by Hudcova et al (1989) employing a strain gauge telemetric device. This system can measure the power consumed by each impeller separately. Altering the spacing between two impellers in the range of $0.066T < C2 < T$ and locating the lower impeller at C1 = T/3 the power consumption of each impeller was measured. With the spacing C2 = 0.066T (when the blades touched) the power number increased, but only by around 30% in comparison to that of a single impeller. With impeller spacings in the region of $0.16T < C2 < 0.5T$ they observed a flow pattern in which the impeller streams were merged and only two ring vortices were observed in the vessel. With this pattern they measured a total power number Np = 8.4 which was less than twice that obtained in a single impeller system. This result is in good agreement with that obtained by Kuboi and Nienow (1982) although the vessel height in the latter study was H = T. Hudcova et al reported an independent behaviour of the impellers for impeller spacings of C2 above 0.66 T. Their results showed that the lower impeller drew slightly more power than the upper one. In this investigation the transition of flow from one pattern to another as a result of change in impeller spacing went unnoticed

and the border line of the impeller spacing for a specific flow pattern was not determined. They recommended an impeller spacing of C2 = T in order to draw the maximum power.

A similar investigation of the influence of impeller spacing on the power consumption was performed by Cronin (1988) who employed two impellers with diameters d = 0.5T on the same shaft. He located the lower impeller at a clearance of C = T/4 and measured the power consumption as the spacing between two impellers was varied. The results showed a trend similar to those obtained by Hudcova et al (1989). Cronin also looked at the effect of impeller spacing on the mixing time and obtained the shortest mixing time with an impeller spacing of C2 = T in a vessel with H = 2T.

Crozier (1989) employed laser-Doppler anemometry to study the behaviour of a two-impeller agitation system with the impellers located at C1 = T/3 and C2 = T. The results showed an independent behaviour of the impellers as if the mixing vessel was divided into two equal parts, each part being agitated by one impeller. The results also indicated some stagnant regions in the area where the mixing tank is divided by the field of action of the two impellers. The appearance of the stagnant region brings the suggestion made by Hudcova et al (1989) and Cronin (1988), who recommended an impeller spacing of C2 = T to be used as this spacing results in a maximum drawn power by the impellers, into question as the power consumption may be maximised under this condition but mixing may be poor in some regions in the vessel.

1.3.3 Single down-pumping pitched-blade impeller (PBD)

The flow pattern generated by a 60° PBD (d = T/3 and C = T/3) was studied by Hockey (1988a), employing flow visualisation and laser-Doppler anemometry. The flow visualisation for the flow pattern generated by this impeller was not found as successful as that by Rushton impeller due to the strong three-dimensionality of the flow. However, it was found that the PBD impeller stream produced an axial jet with a strong swirl and that only one ring vortex was formed in the bulk of the tank. The LDA measurements in the impeller stream showed a maximum axial velocity at a radius of r = 0.71 d/2 near the lower edge of the impeller. At a location r = 0.15 d in the impeller stream, reverse flow was found in both the axial and tangential directions. Hockey obtained a flow number of 0.9 which is considerably higher than that for a Rushton impeller. This flow number was in agreement with that obtained for a 45° PBD by Armstrong and Ruszkowski (1986).

In another paper (Hockey, 1988b), the periodicity of the flow at the impeller discharge region was quantified by performing angle-resolved LDA measurements. It was shown that this periodicity, which lasted for a distance equal to two impeller blade heights, strongly influences the rms ensemble-averaged velocities measured over 360° of impeller rotation. The angle-resolved measurements showed the existence of a small vortex originating at the impeller tip. However, this vortex was destroyed quickly as the flow moved downwards away from the impeller. It was also found, from a comparison made with the data of Yianneskis et al (1987), that the turbulence kinetic energy level in the impeller suction region was the same as that of the Rushton impeller but in the discharge region it was slightly lower with the PBD.

Jaworski et al (1991) looked at the flow induced by a 45° PBD with two clearances, C = T/4 and C= T/2. LDA measurements indicated that a higher impeller clearance from the bottom of the vessel results in a small decrease of the intensity of the main circulation in the vessel. The results also showed that the reverse flow region, occurring beneath the impeller, extended to the bottom of the tank as the impeller spacing increased from C = T/4 to C = T/2.

A comparison of several mixing systems for homogenisation of immiscible liquids was made by Hemrajani (1985) on the basis of the power required for good mixing. In that investigation a pitched-blade impeller was found to be superior to the other types of impeller and particularly to the flat-blade turbine. For a given impeller the width of the baffle was found to be quite important for the efficiency of the system. In a mixing tank the most efficient system comprised of a pitched-blade impeller and a baffle width of w_b = 0.02T. The power consumption increased by 1000% when a flat blade turbine and baffles with a width of w_b = 0.08T were employed in the tank. The importance of the influence of the baffles on the mean flow is also reported by Reed et al (1977). In the so-called most efficient system used by Hemrajani the power consumption per unit volume was found to be independent of the liquid height as well as of the impeller to vessel diameter ratio. The latter finding is in agreement with the finding of Bujalski et al (1986) if the blade/disk thickness to diameter ratio of the impellers remains constant. However, in the comparative study of Hemrajani the mixing times are not given, so the energy required for the blending process with different systems can not be quantified.

1.4 Objectives of the present research

The preceding review of the published literature and the findings of the previous investigations listed in table 1, indicate clearly that the knowledge of the flows in stirred tanks agitated by one or more Rushton and/or pitched blade impellers is far from complete. A number of differences between one- and two-impeller flows have been indicated but not studied in any detail and there is some evidence that the effects of various geometrical parameters may be important for mixing and power consumption. However, there is a number of inconsistencies in the findings reported by different researchers and its evident that there is a lack of systematic documentation of dual-impeller systems.

A number of studies have reported the flows produced by Rushton impellers, e.g. Mujumdar et al (1970) and Reed et al (1977), and by pitched-blade impellers, e.g. Hockey (1988a, b) and Jaworski et al (1991). Although some of these studies have been concerned with the detailed characteristics of the flows (Yianneskis et al, 1987), there is still uncertainty as to the effect of impeller blade and disk thickness and diameter (van der Molen and van Maanen, 1978, Greaves and Kobbacy, 1981 and Armstrong and Ruszkowski, 1986).

It would therefore be useful to quantify precisely the effect of thickness and/or thickness to diameter ratio (Bujalski et al, 1986) as this could lead to small but non-negligible power savings. It is also helpful to compare the behaviour of impellers with different types of hubs used by various investigators, e.g. Calabrese and Stoots (1989) and Yianneskis et al (1987).

Although the effect of Reynolds number or impeller speed has been looked at by some investigators (Cutter, 1966, Nouri et al, 1987), there is still uncertainty as to the scaling of the flows with speed (or equivalently, Reynolds number). More experimentation is necessary in order to determine impeller speed effects more definitely as in many mixing processes different impeller speed ranges may be employed for different fluids.

There is some indication that in systems with two Rushton impellers, the impeller spacing may affect significantly the power consumption, (Smith et al, 1986, Hudcova et al, 1989), and may even influence the flow pattern (Richards, 1963, Kuboi and Nienow, 1982). However, systematic studies of the effect of the lower and the upper impeller spacing have not been carried out. Therefore it would be very interesting and useful to investigate quantitatively such effects on the mixing time, power consumption, mean flow and turbulence.

The flow patterns produced by combinations of different impellers have only been scantily investigated. It is not known under what conditions the flows are stable (Kuboi and Nienow, 1982), therefore further qualitative and quantitative data is required to establish when the flows with combinations of commonly-used impeller designs, e.g. Rushton and pitched-blade, will result in stable flows and therefore stable mixing processes. The impeller combinations to be studied are outlined below and were determined from both the above review of the published literature as well as from consultations with chemical engineering industry and in particular Imperial Chemical Industries, Unilever and Dow Chemicals.

In addition, in situations where a similar flow pattern can be produced by more than one impeller combination, it is necessary to know which combination will be the most efficient in terms of power consumption and mixing characteristics.

Therefore the above survey of the literature and recommendations from chemical industry has indicated that new and/or more detailed and better clarified knowledge is required in the following areas:

1. The effect of impeller blade and disk thickness on the power consumption, mixing time, mean flow and turbulence in single- and dual-impeller systems;

2. More detailed quantification of the effect of impeller rotating speed;

3. The effect of impeller spacing on the flow patterns in dual-impeller systems and the resulting effects of flow pattern on the mean velocities, turbulence, mixing time and power consumption; in particular, the effect of combinations of two Rushton impellers;

4. Similarly for combinations of two pitched-blade turbines, both with one pumping upwards and one downwards, as well as with both turbines pumping downwards;

5. Similarly for combinations of downward-pumping PBD and/or upward-pumping PBU located above a Rushton impeller; and

6. Comparison of impeller combinations producing similar flows, to determine their relative merits for mean flow and turbulence generation.

1.5 Outline of thesis

The rest of this thesis is divided into five Chapters. In the following Chapter the design and construction of the test rig, the impellers employed and also the experimental techniques used for the investigation of flow pattern, power consumption, velocity, turbulence and mixing time in the vessel are described. In Chapters 3, 4 and 5 the results of the investigation and the implication of the results for calculation of the flows and process design are presented and discussed.

Chapter 3 is concerned with the mixing characteristics of the vessel stirred by two Rushton impellers. More attention has been paid to the variation of impeller spacing which is a very effective parameter in determining the behaviour of impellers and consequently the performance of the mixer.

Chapter 4 presents the results of a parametric study to determine the effect of impeller rotational speed and impeller geometry on the power consumption, mean and rms velocities and mixing time in single- and dual-Rushton impeller systems.

In Chapter 5 different combinations of Rushton and PBT impellers are considered and the mixing characteristics of these impeller combinations are studied. The stable flow generated by two PBT impellers, pumping towards each other is quantified and similarities between this flow pattern and that obtained by two Rushton impellers are discussed.

Finally, in Chapter 6 a brief overview of the research carried out is given, the findings of the investigation are summarised and recommendations for future work are made.

Table 1. Experimental investigations of the flows in stirred tanks

The following assumptions have been made in the completion of this table, unless otherwise stated.

1. A single impeller is considered on the shaft.

2. The vessel is a cylindrical flat bottomed tank. Four vertical baffles with a width of $W_b = 0.1T$ are located symmetrically in the vessel as shown in Figure 1.1

Author	Experimental technique (Tech), working fluid (WF), flow configuration (FC), Tracer (TR)	Quantity measured, impeller speed / Re	Main findings
Kramers et al (1953)	Tech: Conductivity probe and dynamometer WF: water TR: KCl solution FC: T = H = 320 and 640 mm, unbaffled and baffled vessels (three different baffle arrangements), Three bladed marine propeller and Rushton impeller, d = T/4, C = T/4 - T/2	Mixing time and power consumption 45000 < Re < 200000	1) For blending process propellers are more efficient than Rushton impellers. 2) Vertical baffles attached to the vessel wall were found more favourable than the baffles located at some distance from the vessel wall. 3) A sufficient excentricity of the propeller improves the mixing performance considerably provided the propeller is not located too near to the bottom of the vessel. 4) Mixing time is inversely proportional to the impeller rotational speed

Sachs & Rushton (1954)	Tech Photographic technique WF Water FC: T = 292 mm, H = 406.4 mm, four bladed disk turbine, d = C = T/3, four baffles, W_b = T/11 5	U, V and W in the impeller stream N = 100 - 200 rpm	1) V profiles flatten out with increasing radius. 2) Volumetric flow rate increases with radius up to a radius r = T/3 and then falls down 3) The periodicity of the flow in the impeller stream persists up to a radius r = T/3
Richards (1963)	Tech Flow visualization, Power measurements by three methods, Dynamometer, temperature rise, electrical input. WF: Water or fermentor mash FC: Three Rushton impellers on the same shaft	Power consumption, flow visualisation	1) Impellers should not be fitted with spacing less than impeller diameter. 2) Unstable flow patterns were observed with a critical spacing between the adjacent impellers.
Holmes et al (1964)	Tech. Conductivity probe, Miniature propeller flow meter WF: Water or aqueous glycerine TR: H2SO4 solutions FC H = T = 220, 600 and 1000 mm, SRI, d = 0 174 - 0.5T, C = T/2	V and circulation time in the ring vortices (t_c) N = 30 - 1500 rpm	1) In the response of a conductivity probe to a tracer insertion the intervals between the peaks are equal to the circulation time around the tank . 2) Dimensionless group $\tau = N\, t_c\, (d/T)^2$ is a function of Reynolds number and at Re > 2 x 10^4 is constant valued at $\tau = 0\ 85 \pm 0\ 05$.
Cutter (1966)	Tech. Photographic and impact tube (kiel tube) WF· Water FC Covered vessel, T = 292.1 mm, H = 304 8 mm, single Rushton impeller, d = 101.6 mm	U, V and W in the impeller stream Power consumption N = 200 - 700 rpm	1) Normalised radial mean and rms velocities in the impeller stream are independent of Reynolds number. 2) V and W are about equal near the impeller but W decreases more rapidly than V with increasing radial distance. 3) It was estimated that from the input energy 20% was dissipated in the impeller, about 50% in the impeller stream and about 30% in the bulk flow.

Cooper and Wolf (1968)	Tech. Hot wire anemometry for air, Pitot tube for either air or water WF: Water or Air FC: T = 381 mm, H = 508 mm SRI or marine propeller	U, V and W in the impeller stream N = 50 - 600 rpm	1) Flow number of a propeller (d = 0.203 m) at N = 200 - 300 rpm was found to be 0.53 ± 0 03 and 0.52 ± 0 01 using water and air respectively. 2) The angle of the flow to the plane of impeller blade in the stream of a Rushton impeller varies between 48° and 70°, being maximum at outer extremes of the blades (Pure radial flow has an angle of 0°). 3) Pumping capacity of turbine is proportional to N and D^3. 4) Np does not vary with impeller speed but depends on the impeller diameter 5) An Increase in the blade height from h = 0 3d results in more radial flow at the outer edge of the blade and more tangential flow towards the centre of the blade.
Mujumdar et al (1970)	Tech Constant temperature hot wire anemometry WF: Air FC. T = 381 mm, H = 508 mm, Rushton impeller (d = 127 or 152 4 mm), C1 = 0 47T	V and v in the impeller stream N = 600, 725 and 1100 rpm	1) V / V_{tip} versus r* does not change with N while v / V_{tip} does change with N. 2) Large correction must be made to the turbulence intensity at the vicinity of the impeller due to the periodicity of the flow with a frequency equal to the passage of each impeller blade
Taguchi and Kimura (1970)	Tech. Strain gauge dynamometer WF: Sulphite solution and mycelial suspension of Aspergilus niger FC: T = 345 mm, H = 1.9T and 2 4T, Multi-Rushton impeller system, d = T/4, T/3, 2T/5 and T/2	Power consumption and volumetric oxygen transfer coefficient 950 < Re < 3300	1) A correlation was suggested by which the impeller spacing was calculated to draw the maximum power in a m-stage stirred reactor. For two-impeller system the correlation was: $C_2 = (H - 1\,9\,d) / 2$

Nienow and Miles (1971)	Tech. Air bearing dynamometer WF: Water FC: Closed and open vessel, T = 150 and 300 mm, H = T Single impeller: 2-blade flat paddles and 4-blade 45° PBD	Power consumption (non-gassed) N = 20 - 2400 rpm	1) Power number for a Rushton impeller varies significantly with the impeller disk to blade width ratio 2) They suggested that the power consumed by Rushton impeller may increase with increasing impeller to vessel diameter ratio. 3) The power number of a Rushton impeller decreases as the impeller is located closer to vessel base or free surface
Van't Riet and Smith (1973)	Tech Flow visualization and Photographic technique for velocity measurements FC. T = H = 450 mm, Rushton impeller, d = 176 mm, C = T/2	Circumferential velocity in the trailing vortex N = 83 - 130 rpm	1) The trailing vortices behind the blades maintain their identity for at least two or three blade length 3) The trailing vortices were found to have an important roll on gas dispersion or coalescence
Bruijn et al (1974)	Tech Air bearing Torque meter WF. Aerated and unaerated distilled water FC. Two cylindrical vessels, T = 440 mm, 1200 mm. One square tank with a diameter of 500 m, H = T 6, 9, 12 and 18 blade turbines, d h.L = 20 4 5, d = 76, 176 and 480 mm	Aerated and unaerated power consumption N =120 - 1000 rpm	1) The rate of reduction in the power consumption as a result of aeration is related to the size and shape of the cavities formed behind the blades. 2) Power consumption for both gassed and ungassed systems increase with number of blades 3) Impellers with higher number of blades have a higher gas handling capacity.
Gunkel and Weber (1975)	Tech Shielded and standard hot wire anemometer and Yaw tube WF. Air FC. T = H = 457 and 914 mm, SRI, d = 228 - 475 mm, C = T/2	U, V, W and u, v and w in the impeller stream, in the bulk flow and in between the blades N = 200 - 950 rpm	1) The input energy dissipates mostly in the bulk of the tank which is opposite to the finding of Cutter (1966). 2) The turbulence in the bulk of the tank is essentially homogeneous and isotropic. 3) Two pairs of roll vortices were found in the region confined between two successive blades, one behind the leading blade and one in front of the trailing blade

Ito et al (1975)	Tech Multi-electrode spherical probe WF: A solution of $K_4Fe(CN)_6$, $K_3Fe(CN)_6$ and KCl ($\mu = \mu_{water}$) FC: T = H = 312 mm, SRI, d = T/3, C = T/2	U, V, W, u, v, w $\overline{vw}$, $\overline{uv}$ and $\overline{wu}$ in the impeller stream N = 60, 90 and 120 rpm	1) The flow in the impeller stream is not homogeneous isotropic. 2) $\overline{vw}$ is much larger than $\overline{uv}$ and $\overline{wu}$ so the flow in the impeller stream is intense shear flow.
van't Riet and Smith (1975)	Tech. Photographic velocity measurements and Pressure measurements by impact Pitot tube WF: Water and aqueous glycerol FC: T = 440 m, 1200 mm, SRI, d = 0 4T, C = 0 4T	Axial and tangential velocities and pressure distribution in the trailing vortices N_{max} = 300 rpm	1) The trailing vortices form at Re > 150 and at Re > $5x10^3$ the axes of the vortices do not change position 2) In the trailing vortex the angular velocity is independent of the distance along the vortex axis and at $1.5 \times 10^4 < Re < 9 \times 10^4$ the angular velocities normalised with that of the impeller is independent of Reynolds number. The axial velocities in the vortex is dependant on the distance along the vortex axis 3) Cavitation starts at low pressure and disperses with turbulence
Khang and Levenspiel (1976)	Tech Conductivity WF: Tap water or 70% glycerol TR: saturated solution of NaCl (5 cm^3 for small tank and 15 cm^3 for large tank) WF: Tap water and/or 70% glycerol FC: T = H = 559 and 1219 mm, SRI, d = 127 - 488 mm Three blade marine type impeller, d = 114 and 254 mm, C = T/2	Mixing time 800 < Re < 200000	1) Rushton impellers give a smoother response to a tracer injection in comparison to that by propellers. 2) The response of the probe in larger tanks is smoother than that obtained in smaller tanks.

Thyn et al (1976)	Tech. Conductivity WF. Distilled water TR· NaCl solution FC. T = 200 and 600 mm, SRI, d = C = T/3, 16 conductivity probes with different sizes	Mixing time and effective conductivity probe volume N = 300 rpm	1) Probe volume size affects measured mixing time in conductivity technique 2) Two different correlation between mixing time and probe to vessel volume ratio were obtained depending on the probe to tracer volume ratio value, smaller or bigger than one.
Reed et al (1977)	Tech: Flow visualization and laser Doppler anemometry WF: Water FC· T = 192 mm, SRI, d = T/3, C = T/3	U, V, W and u, v, w in the impeller stream and in the bulk flow N = 1000 rpm	1) The ring vortex below the impeller is stronger than the one above the impeller 2) The impeller stream is slightly inclined upwards and is angular dependant due to the influence of the baffles. 3) Turbulence intensity of 100% is typical in the impeller stream
van der Molen and van Maanen (1978)	Tech Laser-Doppler anemometry WF Water FC: One closed vessel , T = H = 120 mm, Two open vessel T = H = 290 and 900 mm SRI, d = T/3, t = 0 5 - 3 mm , C = T/2	U, V, W and u, v and w in the impeller stream and in the bulk flow and also circulation velocities in the trailing vortices N = 300, 170 and 80 rpm	1) Normalised central line radial velocities in the impeller stream are independent of the vessel size but a function of measurement radius. $V/V_{tip} = 0\ 85\ (2r/d)^{-7/6}$ 2) Circulation velocity in the trailing vortices and peak to peak value of periodic axial velocity component in the vicinity of the impeller is strongly dependent on the impeller blade thickness.
Nienow and Lilly (1979)	Tech· Air bearing dynamometer WF: 0 2% Nacl solution FC: T = 560 m, H = T, two-Rushton impeller system, d = T/4, C1 = T/4, C2 = T/4 or 3T/8	Power consumption (gassed and ungassed systems)	1) For single Rushton impeller Np = 4 9 2) For two-impeller system Np = 10 2, i e. two times higher than that of single impeller 3) The plots of gassed to ungassed power number ratio versus Qg for single and double impeller systems are markedly different

Tatterson et al (1980)	Tech: Stereoscopic flow visualization WF. Water FC(1). H = T = 295 mm, 6 bladed 45° PBD, d = 102 mm FC(2)· H = T = 914 mm, 4 bladed 45° PBD, d = 305 mm	Flow visualisation N_1 = 300 rpm N_2 = 100 and 250 rpm	1) Weak trailing vortices exist at the bottom outside tip of the blades of 6 bladed 45° PBD impeller 2) The trailing vortices are stronger with the 4 bladed 45° PBD impeller. 3) In the impeller stream of 45°PBD usually 3 jets with no vortical character were observed.
Greaves and Kobbacy (1981)	Tech: Strain gauge transducer WF: Tap water, distilled water and 0 11 mol K_2 SO_4 solution FC: T= H = 203, 152 mm d = 76 2, 106 and 135 mm	Power consumption and impeller speeds at which the first surface aeration and the first drop on the power number occurs N = 60 - 1200 rpm	1) The impeller speed at which the first aeration occurs is 0 54 times less than the impeller speed at which the first drop in the power number appears when the working fluid is water. 2) These two impeller speeds were correlated with the impeller and tank geometry, impeller spacing, vessel working pressure and the working fluid 3) The influence of the impeller spacing, diameter and blade thickness to diameter ratio on the power number is more pronounced when the impeller speed is well below that at which the surface aeration starts
Kuboi and Nienow (1982)	Tech: Strain gauge telemetric system WF: Aerated water FC: T = 450 m, H = T combinations of Rushton and 45° pitched blade impellers, d = T/3 or 4/9T, C1 = C2 = T/3	Power consumption N_{max} = 390 rpm.	1) In aerated systems with two Rushton impellers (C1 = C2 = T/3) the impeller streams merge at higher impeller speeds and the normal figure-of-eight flow pattern associated with Rushton impeller does not appear. 2) Flow patterns produced by different combination of Rushton and pitched blade impellers were observed and their convenience for gas dispersion was discussed. 3) Complete dispersion of gas in liquid with the combination of two PBT impellers pumping towards each other occurs at a speed and power level smaller than that with the combinations of two Rushton impellers and/or of PBU above a Rushton impeller.

Revill (1982)	Review of pumping capacity of a Rushton impeller	1) Differences among flow numbers obtained for Rushton impeller in the mixing literature are mostly due to the different definition of flow number used by researches 2) The variation in the flow number found by different researchers can be reduced to $F_l = 0.75 \pm 0.15$ for; $0.2 < d/T < 0.5$ and $0.3 < C/T < 0.5$ if the flow number is defined as $Fl = Q/N\,d^3$ and $Q = \pi d \int_{-h/2}^{h/2} V dz$	
Nienow and Kuboi (1984)	Tech. Flow visualization WF: Corn syrup solutions FC: T = 290 mm, H = T Combination of upward or downward pumping 45° pitched blade and Rushton impeller, d = T/2, C1 = T/4 and C2 = 0.375T. Rushton impeller, d h L = 24 4·6 Pitched blade impeller, d h = 20 4	Impeller pumping rates, circulation time within each vortex, exchange flow rate between vortices	1) Stable flow patterns were observed in the vessel with both combinations DT / PBD and DT / PBU. 2) Four and three gross circulation vortices were observed with the DT / PBU and DT / PBD impeller combinations respectively. 3) Flow interchange between the adjacent vortices increases with increasing impeller speed The rate of inrease in flow interchange between the impellers is higher than that between the vortices of each impeller.
Hemrajani (1985)	Tech· Photographing of the position of two immiscible liquid interface as the mixing prosses preceded power measurements technique is not given. WF· Coloured water and Isobar-M FC: T = 300 mm, H = 700 mm, W_b = 0.02-0.08T. Single and dual impeller system; d = 0.33 - 0 58T. The Impellers used was. Pitched blade turbine, 3 bladed Burmagin impeller, flat blade turbine and retreat curve impeller	Power consumption N is not given, however it increased as the mixing process preceded until complete homogeneity was achieved	1) Pitched blade impellers are superior to all the type of impellers studied in this work particularly to the flat blade impellers. 2) The power consumption per vessel volume decreases with decreasing baffle width. 3) The power number is independent of impeller to vessel diameter ratio and/or the liquid height in the vessel.

Machon et al (1985)	Tech Dynamometer WF: Water and/or aerated water FC: H = T = 290 mm, SRI, d = T/3 H = 2T, combinations of two SRI, and of a PBD and/or PBU above a SRI, C1 = T/3, C2 = T	Power consumption in aerated and unaerated systems N= 250 -500 rpm Qg = 2 - 60 l/min	1) No interaction was found between the streams of two impellers located with a spacing equal to the tank diameter 2) With C2 = T, the total N_p is equal to the some of the N_ps of the corresponding single impellers in all combinations studied. 3) Combination of downward pumping pitched blade impeller above Rushton impeller is not a desirable set up in gassed systems.
Armstrong and Ruszkowski (1986)	Tech. Laser-Doppler anemometry WF: Water FC: T = H = 305 mm, Single impeller 45°PBD, Marine propeller, Rushton impeller d = C = T/3, t = 1.5 and 3 mm	U, V and W in the impeller stream N = 150 - 720 rpm	1) Change in the disk diameter or in the blade thickness of a Rushton impeller does not affect the radial velocities in the vicinity of the impeller. 2) Flow numbers obtained at different measurement planes are different 3) Flow numbers were found as, 0 73 - 0 8 for Rushton impeller 0 41 for marine propeller and 0 90 for 45° PBD
Bader (1986)	Tech. Power measurements by electrical input power to the driving motor WF. Water FC· T = 596 9 mm, H = 1650 mm, 1 - 5 eight-blade Rushton impeller on the same shaft, d = 241.3 mm	Power consumption N_{max} = 371 rpm	1) Np in a single ungassed agitation system increases linearly with the height of liquid above and/or below the Rushton impeller through the range of 0 2T < C < 0.85T and 0.2< H-C < 0.85T. With the liquid levels above these the power demand remains constant. 2) The variation of the power number with the liquid level above or below the impeller in multiple-impeller systems is the same as that in single impeller systems if the liquid level below or above the impeller is considered as the impeller spacing for the middle impellers 3) When the spacings between identical impellers are equal, the power consumption by each impeller is equal to total power divided by the number of impellers

Bujalski et al (1986)	Tech. Strain gauge telemetry system WF: Water FC. T = 220, 290, 300, 450, 610, 1830 mm H = T, 0 92T, Rushton or pitched blade impeller, d = 73 5 - 902 mm, t = 1.7 - 11 mm, C = T/4	Power consumption $20000 < Re < 2\ Re_{sa}$, Re_{sa} = Reynolds number by which surface aeration occurs	1) Power number depends on t_d/d for Rushton impellers and on t_b/d for pitched blade impellers with 45° blade inclination 2) With $t_d/d \leq 0\ 05$ for Rushton impellers $\overline{N_p} = 2.5\ (t_d/d)^{-0\ 2}\ T^{0\ 065}$ With d/T ≤ 0.5 for 45° pitched blade impellers $\overline{N_p} = 0.78\ (t_b/d)^{-0\ 14}\ (d/T)^{-0\ 17}$ 3) For Rushton impellers provided (t_d/d) = constant, $\overline{N_p}$ is independent of d/T
Nouri et al (1987)	Tech. Laser-Doppler anemometry WF: Water T = H = 294 mm SRI, d = T/4, T/3 and T/2, t = 3 mm, C = T/3	U, V, W and u, v, and w in the impeller stream and in the bulk flow N = 50 - 300 rpm	1) Mean and rms velocities (normalized with the impeller tip speed) in the impeller stream and bulk flow scale with impeller rotational speed at N = 150 - 300 rpm and lower normalised velocities are obtained at N = 50 rpm. 2) The effect of impeller size on the normalized velocity profiles in the impeller stream is negligible when the profiles are plotted in non-dimensional coordinates (r* and z*) while in the region away from the impeller stream the impeller with d = T/2 generates higher velocities 3) The impeller tip velocity is an appropriate scaling factor to account for the effect of change in rotational impeller speed (Reynolds number)
Yianneskis et al (1987)	Tech. Flow visualization, laser-Doppler anemometry and air bearing WF: Water FC: T = H = 294 mm, SRI, d = T/3 and t = 3 mm, C = T/4, T/3 and T/2	U, V, W and u, v and w in the impeller stream and in the bulk flow and also velocities in the trailing vortices N = 100 - 300 rpm	1) The trailing vortex behind the blade is influenced by the ring vortex at 25° behind the leading blade and gets destroyed at 30°. 2) The inclination of the impeller stream to the horizontal decreases with increasing impeller spacing or impeller speed. 3) The flow in the impeller stream is anisotropic 4) The power number was found to be 4 2, 4.8 and 5 for the impeller spacings C = T/4, T/3 and T/2 respectively

Armstrong and Ruszkowski (1988)	Tech. Two component LDA WF: water FC: T = H = 305 mm, four baffles; 5 mm spaced from the tank wall, W_b = 25 5 mm Two non-standard Rushton impellers with the same d, d = T/3, C = T/3	U, V, u and v in the impeller stream N = 200 and 300 rpm	1) Impellers with smaller hub produce higher mean velocities in the vicinity of the impeller 2) Impellers with smaller hub and thinner blade and disk produce higher periodicity and similar fluctuation component.
Hockey (1988a)	Tech. Flow visualization and laser - Doppler anemometry WF· Water FC. T = H = 294 mm 60° pitched blade impeller d = T/3, C = T/3 and t = 3 mm	U, V and W, u, v and w in the impeller stream and bulk flow N = 300 rpm	1) Pitched blade impeller generates an axial jet with strong swirl (F_l = 0 9) forming one ring vortex in the vessel. 2) At the discharge side of the impeller the flow changes direction axially and tangentially at a radius r = 0 15T. 3) In the location r = d/2 and 1 mm below the lower edge of the impeller maximum rms velocity and highest mean velocity gradient (0.62 s^{-1}) was measured. 4) The flow generated by pitched-blade and Rushton impeller is of similar strength in the region below the impeller but weaker for the pitched blade impeller in the region above the impeller. 5) The turbulence is not isotropic and usually stronger in the direction of the flow

Hockey (1988b)	Tech Laser-Doppler anemometry WF. Water FC: T = H = 294 mm 60° pitched blade impeller d = T/3, C = T/3 and t = 3 mm	Time resolved and gated velocity measurements in the impeller region N = 300 rpm	1) In the vicinity of the impeller the periodicity of the mean flow strongly influences the rms velocities measured over 360° of impeller rotation. 2) Maximum mean velocity gradient calculated from the measurements over 1.08° of impeller rotation is four times higher than that obtained from the measurements over 360° of impeller rotation. 3) The periodicity of the flow lasts for about two blade height away from the impeller. 4) At the discharge side of the impeller in the cylindrical planes of r = 45 and 50 mm a small vortex was found which was coming off of the impeller tip and diffused quickly as the flow moved downward. 5) The turbulence kinetic energy in the flow entering the pitched blade impeller is similar to that for Rushton impeller. In the flow leaving the pitched blade impeller the turbulence kinetic energy is slightly lower than that obtained for Rushton impeller
Weetman and Oldshue (1988)	Tech. Hot wire anemometer, OTT flow meters and two dimensional laser-Doppler anemometry WF Water FC: Three types of impellers, Rushton, four-bladed 45° PBD and fluid foil impellers d = 100 - 1590 mm	U, V, u, v, U_{IS} and V_{IS} in the vicinity of the impeller N = 40 - 350 rpm	1) For a Rushton impeller the average shear gradient of the velocities in the vicinity of the impeller is independent of the impeller size but dependent on the impeller speed. The maximum shear gradient is a function of impeller tip speed. 2) For a four-bladed 45° PBD both the mean and maximum shear gradients of the velocities in the impeller stream are a function of impeller speed and size. 3) For the same volumetric discharge flow Rushton impeller produces a shear gradient of about 1 5 times more than a four bladed 45° PBD. 4) Larger four bladed 45° PBD impellers produce lower shear gradient

Wu and Patterson (1989)	Tech· Laser-Doppler anemometry WF: Water FC: T = H = 270 mm, SRI, d = T/3 and C= T/3	U, V, W and u, v, and w in the impeller stream N = 100, 200 and 300 rpm	1) F_l is independent of N and increases with R due to the fluid entrainment 2) Both the random and the periodic rms velocities near the impeller tip are proportional to N 3) The diameters of each of the trailing vortices are about h/2. 4) The random rms velocities in the impeller stream starts dominating the total rms velocities at r* = 1.5. 5) The periodicity of the flow in the impeller stream disappears completely at r* = 1 9
Crozier (1989)	Tech Laser-Doppler anemometry WF(1). Water FC(1) T = 250 mm, H = 2 T, two-Rushton impeller system, d = T/3, C1 = T/3, C2 = T WF(2) Water, 80% Glycerol and 3% CMC concentration in water FC(2): T = 300 mm, H = T, d = T/3, C = T/3	U and V in the impeller stream and in the bulk flow N = Not given	1) With non-Newtonian fluids the radial velocity profiles in the impeller stream are much broader with a drop in the impeller elevation in comparison with those obtained with newtonian fluids. 2) In dual impeller system (H = 2T) the flow generated by Rushton impellers appears to behave as two independent systems 3) Flow number (F_l = 0.73) was obtained for the lower impeller and F_l = 0 68 for the upper impeller
Hudcova et al (1989)	Tech. Strain gauge telemetry WF. Water and/or aerated water FC: T = 560 mm, H = 2T, Single and Double impeller, d = T/3, C1 = T/3, C2 = 0.2 - 3d	Power consumption N = 120 - 300 rpm	1) In ungassed system an impeller spacing of C2 = 2d - 3d is required for the impellers to draw a power as much as two times higher than that of single impeller system. 2) Np for single impeller located at C = T/4 or T/3 was 5.5. 3) In two-impeller system with C2 larger than 2d the lower impeller draws a power slightly higher than the upper impeller

Nouri and Whitelaw (1990)	Tech. Laser-Doppler anemometry WF: Water FC Two geometrically similar vessels T = 144 and 294 mm, the former was used as both open and closed vessel The thickness of the baffle was 3 and 1 5 mm for larger and smaller vessel respectively SRI, d = T/3 and t = 3 and 1.5 mm for the impellers used in larger and smaller vessels respectively, C = T/3	U, V, u, v in the impeller stream and bulk flow N = 150 and 600 rpm for larger and smaller vessels respectively resulting equal Reynolds number in both systems	1) The normalized mean and rms radial and axial velocities scale with the vessel size when the velocities are plotted in non-dimentional coordinates of r* and z*. 2) The confinement of the vessel makes little difference to the flow in the impeller stream and above the impeller except in the immediate vicinity of the impeller 3) The Power numbers in both open vessels were 4 2 at a Reynolds number Re = 24000.
Jaworski et al (1991)	Tech. Laser-Doppler anemometry WF Distilled water FC: T = H = 146 mm, Single 45° PBD impeller, d = T/3, C = T/4 and T/2, h (projected) = d/5 and t = 1 mm	U, V, u and v in the impeller stream and in the bulk flow N = 600 rpm	1) Lower impeller spacing results in higher radial and axial velocities in the impeller stream. 2) Impeller spacing affects the reverse flow beneath the impeller, this flow is spread to the bottom of the tank at C = T/2. 3) Turbulence level produced by pitched blade impellers are similar to those obtained by Rushton turbines. 4) The flow number was found 0 71 which is similar to the value obtained with Rushton impeller reported by Weetman and Oldshue (1988)
Dyster et al (1993)	Tech. LDA, Patent Gear mechanism (Torque measurements) WF· Water and solutions of glycerol glucose and polyethylene glycol (PEG) FC. H = T = 150 mm, single Ruhton impeller, d = T/3 or T/2, C = T/2	U, V, u and v in the impeller stream N = 50 - 800 rpm	1) With water as working liquid the normalized radial mean and rms velocities are independent of impeller speed. 2) Normalized radial mean velocities in the elevation of impeller are corrolated to the measurement locations and Reynolds number as $V/V_{up} = 0.85\ \sigma\ (2r/d)^{-7/6}$ where σ is a function of viscosity of the fluid (or of Re). 3) Fl starts falling down at Re = 500 as Reynolds number decreases

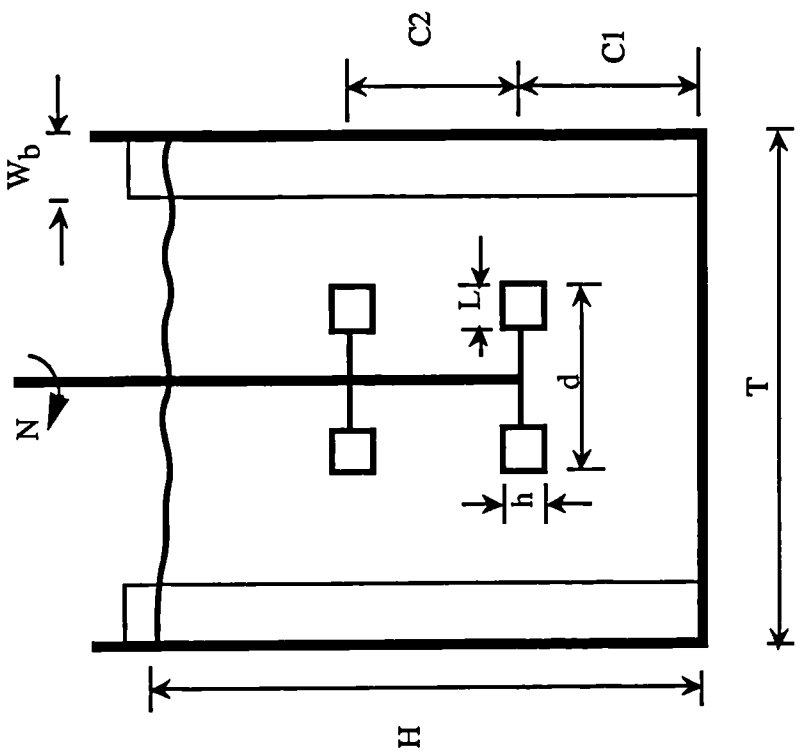

Figure 1.1 Schematic diagram of the two-Rushton impeller system

CHAPTER 2

MIXING VESSEL CONFIGURATION AND EXPERIMENTAL TECHNIQUES

2.1 Introduction

This Chapter describes the stirred tank configuration and the experimental techniques for flow visualisation, mixing time studies and measurements of torque and mean and rms velocities used in this investigation. Tap water was used as the working fluid and all the measurements and the flow visualisation experiments were performed at a constant temperature. Mixing time measurements were carried out by detecting the change in the conductivity of the liquid in the tank resulting from the insertion of a solution of potassium chloride (KCl). This change was detected by a small conductivity probe. For the measurements of power consumption strain gauges were employed and the change in their electrical resistance due to the applied torque was recorded with a telemetric transmission system. Laser-Doppler anemometry in forward scattered mode was employed for the mean and rms velocity measurements. All of these techniques will be dealt with in detail separately in the following sections.

2.2 Flow configuration

A mixing vessel was designed, manufactured and commissioned for the experiments. The same vessel was employed for all the investigations in this project. It was a baffled cylindrical vessel with a flat bottom and a diameter T = 294 mm, height H = 490 mm and wall thickness 3 mm as

shown in Figure 2.1. Four vertical baffles with a width of W_b = T/10 and a thickness of 3 mm were fitted symmetrically along the vessel periphery. The vessel geometry was identical to the 'standard' configuration used in mixing research (Uhl and Gray, 1966). The baffles prevented the formation of a vortex at the free surface of the water. The baffles also produced strong vertical flow in the vessel which promotes good circulation in the tank (Bissel et al, 1947). The vessel was made of clear cast acrylic plastic (Perspex) and for optimisation of optical access it was placed inside a Perspex trough (with 10 mm walls thick and 388 mm x 388 mm in cross section) which was filled with water.

A heat exchanger was designed and located at the bottom of the vessel to remove the heat generated by the impellers in order to maintain a constant temperature in the vessel during the experiments. The temperature of the water in the tank was checked continuously and the water flow through the heat exchanger was adjusted so that the temperature variation in the vessel did not exceed $\pm 1^{\circ}$ C. The heat exchanger was mostly needed for the flow visualisation and velocity measurements by laser-Doppler anemometry as these experiments took relatively long time to complete in comparison with the torque and mixing time measurements.

The vessel could be rotated around its vertical axis relative to the trough and the periphery of the vessel at the top edge was marked and divided into 360 one-degree intervals. A marker was fixed to the top cover of the vessel in front of the divisions on the vessel for the purpose of determining accurately and reproducibly the angle by which the vessel was rotated when measurements were made at different planes. The

vertical and horizontal cross sections of the mixing system are shown in Figure 2.2.

The trough was placed in a frame with a fixed base and a detachable top cover (Figure 2.3). The vessel and the trough were filled with water up to a height of 1.0 - 1.5T. A line marking the height H = T was drawn on the vessel periphery. A 0.25 hp electrical motor (Parvalux) was mounted on the test section frame to supply the required torque for the impellers. The speed of the motor was monitored continuously through a shaft encoder (Hewlett Packard model HEDS 6310 036) mounted on the motor shaft.

Two traversing tables were used to enable the test section to be moved in three orthogonal directions. As the vessel could also be rotated, LDA measurements could be made everywhere within the vessel except at those locations where either one of the incident beams to the control volume or the collection of the scattered light by detector was blocked by the impeller or the shaft. The accuracy of the test section traverse in X and Y directions was 0.05 mm and in the Z direction 0.25 mm (Figure 2.3). The impeller speed fluctuation was less than $\pm$ 1 rpm which is around $\pm$0.4% of the impeller rotational speed used in most of the experiments (250 rpm). The general arrangement of the mixing rig is shown schematically in Figure 2.3.

A number of Rushton and pitched blade impellers were employed in this work. The geometries of the Rushton impellers which had either a symmetrical or an asymmetrical hub, a diameter d = T/3 and different thicknesses are shown in Figure 2.4. An impeller of identical proportions but with a larger diameter (d = 0.4T) was also used. In each impeller,

the blade thickness (t_b) and the disk thickness (t_d) were the same and hereafter they will both be referred to as the impeller thickness, $t = t_b = t_d$. The thickness to diameter ratio in the larger impeller (d = 0.4T) was the same as that of the d = T/3 impeller with t = 1.65 mm.

Pitched blade impellers with 60° or - 60° blade inclination were also employed in this project and their geometries are shown in Figure 2.5. Depending on the direction of the impeller rotation these impellers can pump either downward or upward. In order to minimise the scattered or reflected light from the impellers in the flow visualisation and the LDA measurements the impellers were sand-blasted and painted matt black. In all the investigations the impeller shaft coincided with the vertical axis of the vessel and had a diameter d_s = 20 mm except in the torque measurements for which a shaft with smaller diameter (d_s = 10 mm) was employed. The purpose of the reduction of the shaft diameter was to obtain a greater deflection and therefore response and output of the strain gauges to torque variations. The shaft was covered with black plastic tape to minimise light reflection and scattering in all the experiments.

2.3 Flow visualisation technique

Flow visualisation was carried out in order to determine qualitatively the general structure of the flow before detailed velocity measurements were made by laser-Doppler anemometry as well as to determine the locations where LDA results should be obtained.

Three sides of the test section were covered with thick black paper to prevent any extraneous light penetrating into the vessel. A 2 W Argon-Ion laser or a 1 kW white light source were employed together with a

cylindrical lens to illuminate the plane of interest in the mixing vessel. The illumination was achieved through a 2 mm slot in the side cover facing the white light source or laser. The slot could be moved so that any horizontal or vertical plane of interest in the vessel could be illuminated.

Approximately 5 g of Diakon particles with a diameter range of 590 to 730 μm and a density of 1.18 x 10^3 kg/m^3 were suspended in the liquid to act as flow followers and to scatter the incident light. The particles could follow the flow faithfully as their sink velocity was only 0.02 m/s. The flow in the illuminated plane was photographed and recorded by still and video cameras. The focus of attention of the experiments was the direction(s) of the impeller stream(s) which were greatly dependent on the impeller spacings. The results of flow visualisation will be discussed below in section 3.2 and Chapter 5.

2.4 Conductivity measurement technique

As mentioned in Section 1.2.4, this technique makes use of a conductivity probe to detect the variation of the conductivity of the fluid in the vessel as the mixing process proceeds. The difference between the conductivities of the two liquids must be comparatively high in order to have a better sensitivity in the response of the probe used.

In this work a solution of potassium chloride (KCl) in water was used as the tracer and the instantaneous local concentration was measured by a small conductivity probe of the design recommended by Khang and Fitzgerald (1975). The probe was minimised in size in order to increase the sensitivity of the probe for detection of small scale concentration

fluctuation (Thyn et al, 1976) as well as to decrease the intrusion of the probe to the flow. The position of the probe was determined by placing it at various locations where two laser beams crossed each other, i.e. the positions of the control volume in laser-Doppler anemometry measurements which could be accurately determined. The procedure of locating the control volume inside the vessel will be described later in Section 2.6.3.

The vessel bottom and the shaft, which were both made of metal, were insulated to minimise any possible stray currents passing through the probe albeit that the conductivity probe design was purported to be free of stray currents (Khang and Fitzgerald, 1975). Current was supplied to the probe by a 9 Volt battery incorporated in a conductivity meter (WPA CM35). The mains adapter (PS100) supplied with the meter was not used as it resulted in a higher noise level in the output signal of the conductivity probe.

A tracer volume of either 50 or 70 ml with a concentration of 3.35 or 2.24 mol/l respectively was inserted from the free surface of the water into the tank at the $\theta = -135^{\circ}$ r-z plane. The conductivity meter output was low-pass filtered (at 2 kHz) by a variable active filter (Krohn-Hite model 3200) to remove any noise present. The signal was then fed in to a computer via an analogue to digital converter. The system is shown schematically in Figure 2.6.

The tracer insertion was performed manually and the syringe was located at the same height as the insertion location in the vessel to avoid any tracer flowing into the vessel before the start of the insertion. Before every experiment it was ensured that there were no air bubbles trapped in

the tube connecting the syringe to the insertion location as the air bubbles would result in a discontinuous tracer insertion.

Each experiment was started by first simultaneously triggering the computer and starting a stop watch. A few seconds later the first lap in the stop watch was stopped and the second lap was started simultaneously with the start of the insertion. The second lap was stopped when the tracer insertion was completed. This method was used for the experiments as it was not possible for an operator to insert the tracer simultaneously with triggering the computer and starting the stop watch. The recorded time in the first lap corresponded to the time in the obtained signal when the insertion started and that in the second lap was the insertion duration.

The rate of data recording was set at 200 Hz and every measurement lasted 80 seconds, i.e. 16000 data points were captured during each measurement. The captured data were first displayed on the computer screen and then stored on the pc's hard disk and subsequently transferred to the Vax main frame computer for further processing.

After the end of each test the mixture was drained by a pump and the vessel was washed thoroughly and refilled with tap water. The water temperature in the vessel was measured and adjusted if necessary. This was done to avoid a rise in concentration in the vessel when carrying out many measurements. The concentration rise would result in a smaller sensitivity of the probe to the concentration variation, and therefore lower signal to noise ratio.

2.4 1 Conductivity probe and its calibration

The mechanism of electrical conduction in liquids is characterised by a charge being transported through the medium by means of ions. As a result of electro-chemical reaction, gases are generated at the electrodes of the probe. These gases cause a reduction when a (constant) conductivity value is measured over a period of time. In conductivity measurements by probes this effect is called polarisation and must be avoided by removal of the gases from the surface of the probe electrodes.

The connecting wires of the conductivity probe employed in this project were located inside a glass tube and only the electrodes were exposed to the liquid in the vessel. The tip of the probe is shown in Figure 2.7. The electrodes at the tip of the probe were made of platinum. They were platinised in order to avoid polarisation as the platinised platinum (platinum black) adsorbs the generated gases in the surface of the probe electrodes. The probe was designed to be free of errors caused by stray currents and also to have linear response to the variation of concentration according to the recommendations of Khang and Fitzgerald (1975). The connecting wires between the probe and conductivity meter were made from a twin cable and individually screened. The cable was minimised in length and insulated with a 20 mm diameter pipe legging. These considerations minimised the capacitive pickup between the wires as well as interferences from the surroundings. The signal to noise ratio during the measurements was determined to be around 25.

The probe was calibrated extensively under steady-state conditions for four different temperatures: 10 °C, 15 °C, 20 °C and 30.5 °C and for the concentration range 0.0 - 0.015 mol / l. The calibration was carried out

in a constant temperature water bath (Grant instrument type LTD6) as shown schematically in Figure 2.8.

The results of the calibration are presented in Figure 2.9. As can be seen the variation of the conductivity with a change in concentration is linear for all temperatures in the range of concentrations used. All the data in each calibration temperature could be fitted to a linear equation of the form:

$$V_c = A\ C_c + B \qquad (2.1)$$

where V_c is the voltage in Volts, C_c the concentration in mol / l and A and B are constants which depend on the calibration temperature (T_c). In order to obtain an equation to determine these constants under any condition, the values of A and B obtained were plotted against the corresponding temperatures. The variations of A and B with temperature were linear as shown in Figure 2.10. The calibration equation is given by:

$$V_c = 0.05 + 0.002\ T_c + (0.315 + 0.013\ T_c)\ C_c \qquad (2.2)$$

2.4.2 Mean and fluctuating concentration

The instantaneous concentration at any time may assumed to be the sum of a mean value and a fluctuating component, as is usually the case in all turbulent flows. In order to estimate the levels of the fluctuating component, two types of transient mean concentration value were used in the processing of the data:

a) The variation of local mean concentration with time $C_{m1}(t)$ obtained from the data.

b) The variation of the mean concentration value with time $C_{m2}(t)$ calculated from the total volume of tracer inserted in the vessel during the measurement.

2.4.3 Signal processing

Each measurement was obtained in the form of a digitised voltage variation with time which was first stored and subsequently displayed on the computer screen (see, for example, Figure 2.11(a)). The stored file was then converted to a form transferable to the Vax mainframe computer where specifically-written software were used to obtain the time history of the instantaneous concentration, mean concentration and the fluctuating component of the concentration. Mixing time was determined for different degrees of homogeneity as described below.

In order to confirm that the calibration of the conductivity probe did not vary with time, the probe was re-calibrated for each test by recording the mean values of the voltage and concentration at the start and at the end of the experiment.

The mean voltage value obtained in the first five seconds of the experiment, before the insertion of the tracer, was calculated and considered to correspond to zero tracer concentration in the vessel. A concentration of 6.72×10^{-3} mol/l (i.e. a total of 10 grams of KCl in the vessel) was considered for the calculated mean value of the voltages obtained in the last five seconds of the experiment. As the maximum

voltage recorded in the linear calibration was around 1.5 times higher than the greatest voltage recorded in the conductivity measurements, the variation of the voltage with concentration and temperature in the voltage time history was always linear. The instantaneous concentration for each data point can be obtained by the following equation:

$$C_i = (V_i - V_1) \times \frac{0.00672}{V_2 - V_1} \qquad (2.3)$$

where V_i is the voltage for each data point and V_1 and V_2 are the mean voltages at the start and at the end of the experiment. A typical variation of instantaneous concentration (C_i) with time is shown in Figure 2.11(b).

The concentration trace was scanned from the end to the beginning of the recording and a mean value C_{m1} was found for every 49 points by moving 1 data point backward each time. Every mean value was located at the corresponding 25th point. In this way a local mean concentration-time history was obtained (Figure 2.11(c)). The difference between the mean and the corresponding instantaneous concentration values was used to determine the concentration fluctuation time history ($C_i - C_{m1}$, Figure 2.11(d)). The mixing time for a prescribed degree of homogeneity was determined as described below.

In the scanning of the instantaneous concentration time history (from the end to the start of the trace) every mean value obtained was compared to the final concentration value (6.72×10^{-3} mol/l). When the difference between the two values exceeded a certain percentage for the first time in the scan, the corresponding time was recorded. The difference between the time obtained and the time when the insertion had started gave the mixing time for the degree of homogeneity specified.

Non-dimensional concentration traces were also obtained by normalising the instantaneous concentration trace at every instant by the concentration corresponding to the mean mixing time (C_f) and normalising the time with the mixing time (t_f, see Figure 2.11(e)). The start of these traces was the instant when the tracer insertion was commenced.

The fluctuating concentration trace was also plotted with respect to the second type of mean concentration [$C_{m2}(t)$], as shown in Chapter 3 below.

2.4.4 Mixing time and degree of mixing

In any mixing process, the mixing time is defined to be the time in which a certain degree of homogeneity is achieved throughout the vessel (Harnby et al - 1985). Although with the conductivity method only the local mixing time can be measured, the results are however more accurate than those obtained by visual observation techniques (Schofield - 1974). Repeating the experiments with the probe placed in several locations can partly remove the shortcomings of the conductivity technique.

Due to the complex and turbulent nature of the flow the traces obtained from repeated experiments at the same probe location and with the same experimental parameters are not unique and they may result in different local mixing times for a specific degree of homogeneity. In the present work a mean mixing time has been defined and used to minimise the number of required experiment repetitions.

Figure 2.12 shows the variation of mixing time obtained from recordings at various locations for different degrees of mixing. These experiments have been carried out with different probe locations keeping all the other experimental parameters the same. As it can be seen the curves are not smooth and they often cross each other. For example the local mixing time at z = 0.125 T and r = 80 mm is higher than that obtained for z = 0.125 T and r = 30 mm if a higher degree of mixing is used. Also in some curves there are step changes, for example the mixing time for the location z = T/2 and r = 30 mm is about 8 seconds for a degree of mixing of 92% to 95.5% while this value changes to 10 seconds for a degree of mixing of 96% to 97.5%.

In order to minimise such variations in this work the mixing time was defined as the average value of the mixing times obtained for 13 homogeneity degrees from 92% to 98% at intervals of 0.5%. The mathematical expression for this average mixing time is given by equation 2.4 below:

$$\xi_{av} = \sum_{i=1}^{13} \frac{\xi_i}{13} \qquad (2.4)$$

where ξ_i is the mixing time for a specific degree of mixing. The mixing time obtained for each interval of the degree of mixing has been calculated from the local mean concentration time histories, such as that shown in Figure 2.11(c).

2.5 Torque measurement technique

The use of the strain gauges together with telemetric devices has been introduced to the torque measurement in agitated tanks relatively

recently. As mentioned in Chapter 1, this technique is very well suited for the measurement of power consumption in two-impeller systems as with this technique the power consumed by each impeller can be individually measured.

This technique is based on the change of electrical resistance in a strain gauge due to the imposed strain. The technique, although it does not suffer from common error sources, e.g. due to mechanical friction between the shaft and bearing, some errors may arise in measurements with strain gauges and they will be dealt with later. The sensitivity of a strain gauge to an applied strain can be determined from its gauge factor K given by:

$$K = \frac{\delta R}{R\varepsilon} \qquad (2.5)$$

where R is the gauge electrical resistance, ε is the strain due to an applied torque and δR is the variation of R due to ε.

Wire and foil strain gauges are normally used for torque measurements. These two types of strain gauges are shown in Figure 2.13. Foil gauges have almost replaced the wire ones firstly due to their linear response and secondly because of their insensitivity to the strains across the grids. These advantages are mainly due to the lower resistance of the tabs at each conductor path in foil strain gauges. In addition they have a greater ratio of surface to cross sectional area than wire gauges which results in higher heat dissipation rate at higher excitation voltages. Therefore the temperature rise in foil gauges is comparatively small and will result in smaller errors, as will be discussed later.

The change of the electrical conductivity due to the imposed strain (gauge factor) is rather small and can be of the order of one thousandth of an ohm. In order to improve the gauge factor and eliminate the measurement errors due to the temperature variation, it is more convenient to use the strain gauges in a full Wheatstone bridge. The locations where the strain gauges are attached to the shaft are quite important and for a better sensitivity they must be placed where the normal stresses are maximum and shearing stresses are zero.

Figure 2.14 shows a solid circular shaft under a torsion S. A small element ABCD on the surface of the shaft is in pure shear and the principal planes (no shearing stresses) occur in the directions making an angle of 45° with the shaft axis. Having the same magnitude, the direct stresses on AC and BD are tensile and compressive respectively. These directions were chosen for the strain gauges attachment in the Wheatstone bridge circuit as shown in Figure 2.15.

Considering an identical resistance for the strain gauges in the four arms of the Wheatstone bridge, the variation of the strain gauge resistance due to an applied torsion will be $+\delta R$ in the stretched gauges and $-\delta R$ in the compressed ones as shown in Figure 2.16. The bridge output voltage will be:

$$V_{out} = \pm E \frac{\delta R}{R} \tag{2.6}$$

where E is the bridge excitation voltage. V_{out} is four times higher than the voltage that can be obtained in a quarter bridge (i.e. one arm being a strain gauge and three arms being resistances).

Employing eight identical strain gauges (type FLA-6, 1000 Ω) supplied by Techni Measure Ltd, two identical Wheatstone bridges were fitted on the shaft, one above the lower impeller and one above the upper impeller. The former was used for the measurement of the power consumption by the lower impeller and the latter for the power consumed by both impellers. Both bridges were balanced by shunt resistors valued at R_{S1} = 3.5 MΩ for the lower bridge and R_{S2} = 5.2 MΩ for the upper bridge. The effective gauge factor of the bridges is given by Baker (1974) as

$$\text{Modified K} = \text{Original K} \times \frac{4R_S + R}{4R_S + 2R} \qquad (2.7)$$

The difference between the original and the effective gauge factor was extremely small due to the higher resistance of the balancing resistors in comparison to the resistances of the strain gauges.

A single channel telemetric torque measurement system supplied by Astech Electronics Ltd was employed in this project. The components of this system associated with the Wheatstone bridge circuits are shown in Figure 2.17. A five Volt battery supplied the excitation voltage for the bridge and the bridge output voltage controlled the frequency of a square wave oscillator (Os. in the Figure) in the transmitter. The oscillator output is transmitted telemetrically by the transmitting (T. A.) and receiving (R. A.) aerials. The signal is transmitted in the form of a frequency and the indicator converted this frequency back into a voltage.

The analogue output signal from the indicator was converted to digital form in an A-D converter before being measured in a micro-computer. The transmitter could operate in two ranges of torque, 0 - 1 and 0 - 5 N m. Since the total torque developed by the two impellers did not exceed 1

N m in all tests, the lower range of the transmitter was used in all the measurements for better sensitivity.

Simultaneous measurement of the power consumption by each impeller was not possible as the employed system had only one channel. For the measurements of power consumption by both impellers and that by lower impeller separately, two change-over switches were mounted on top of the transmitter housing to switch from one bridge circuitry to another. The wiring around the change over switches was made and insulated properly in order to avoid noise interference, as without taking this precaution there were large fluctuations in the output signal.

Although the variation of the distance between the two aerials (which was varied up to 75 mm), did not affect the signal, the receiving aerial was located as close to the transmitting aerial as possible and the pick up sensitivity of the indicator was reduced to 50%. This was done in order to minimise the noise interference from the surroundings according to the recommendations given by the manufacturer (Baker, 1992).

2.5.1 Calibration of the system

The calibration was performed experimentally in order to avoid errors due to several parameters like the gauge factor tolerance, error in the direction of strain gauge installing, imperfections in the application of the adhesive, etc.

For the calibration, two Rushton impellers (d = T/3) were fitted to the shaft, one below the lower bridge and the other between the two bridges as shown in Figure 2.18. The shaft assembly was placed horizontally and

the lower bridge was connected to the circuit of the system by the change-over switches and the 1 N m range of the transmitter was selected. One of the blades of the lower impeller was positioned horizontally (at an angle to the horizontal $\alpha = 0^{\circ}$) and the shaft was held by a clamp placed between the lower bridge and the upper impeller. Measurements were carried out by suspending a number of weights ranging from 0.1 to 1.2 kg from the tip of this blade. This procedure was repeated for all six blades by rotating the shaft in increments of 60° and suspending the weights from the blade at $\alpha = 0^{\circ}$.

Due to the effect of the bending moment, there were some differences in the measurements obtained with the six blades. However, the average of the readings from every two blades with an 180° phase difference was the same with a negligible discrepancy. This was expected due to the reverse bending moment effect of forces acting from two blades opposite to each other. The average of the readings from six blades was used for the bridge calibration. The whole procedure was repeated for the upper bridge by loading the upper impeller, selecting the change-over switches for the upper bridge circuit and holding the shaft just above the upper bridge. The results of these calibrations are shown in Figure 2.19.

In the power measurements the 'no load' voltage was measured immediately before and after the experiment in order to check the zero drift. Although the no load voltage was changing slightly from one day to another, the gradient of the calibration curve was found to be the same when re-calibrating the system. Therefore the calibration equations for the lower bridge (a) and the upper bridge (b) were as:

$$\text{(a)} \quad V_q = V_o + 14.742\, T_q \qquad (2.8)$$

$$(b) \quad V_q = V_o + 14.837\ T_q \qquad (2.9)$$

where V_q is the measured voltage for an applied torque T_q and V_o is the measured 'no load' voltage.

2 5.2 Power number fluctuation

Although the power number in a single impeller system was constant and easy to measure due to the stability of the impeller speed, however this was not the case for the two-impeller system. The interaction of the impeller streams even when the flow was stable (i.e. when the impeller streams did not change direction) resulted in fluctuations of the impeller speed and of the torque. For the measurements of the power number in a two-impeller system two methods were followed.

(1) Simultaneous measurements of impeller speed and required torque were carried out by recording the signals from the shaft encoder and the torque indicator respectively. The signal from the shaft encoder was in the form of a train of pulses whose intervals were used for the measurement of impeller speed variation. For better accuracy in the impeller speed measurement a recording with a higher sampling rate was required and as the maximum number of data that could be captured per sweep was 16000, the duration of the signals recording in each experiment was limited to a few seconds, i.e. around 10 cycles of the shaft rotation.

The results of a typical experiment in a two-impeller system are shown in Figures 2.20 (a) and (b). Figure 2.20 (a) shows that the torque varies in inverse proportion to the impeller speed. This variation is not as large in

single-impeller systems as the induced flow pattern is comparatively more stable. With this method, due to the short duration of the measurements the detection of the torque fluctuation over a long period of time was not possible.

A typical variation of the power and the power number over a number of impeller revolutions is shown in Figure 2.20(b). The power number can be seen to vary from 7.3 to 8.6, i.e. by as much as 17% over ten impeller revolutions. This may have significant implications for both process uniformity and mixing gear wear and clearly needs further investigation in a purpose designed rig.

(2) In order to minimise the impeller speed fluctuation a heavy flywheel was fixed on top of the shaft. This resulted in stabilising the shaft speed and in a higher fluctuation of the required torque and consequently of the power number. The duration of the experiments was long enough (40 seconds) to record any possible fluctuation of the required torque in any stable flow pattern.

2.5.3 Experimental errors

The use of a full Wheatstone bridge cancels out all the errors due to the temperature sensitivity of the strain gauges and the unwanted stresses generated. The latter stresses are a result of differences between the thermal expansion factor of the gauge and of the material on which the gauge is mounted. However, the employment of a full bridge does not resolve the errors due to the variation of the resistance of the supply leads and the balancing resistors as a result of ambient temperature variations. These errors may result in a zero load voltage variation

measured by the indicator. As mentioned before the identical calibration curve gradients obtained at the start and at the end of investigation and the determination of zero load voltage in every experiment indicate that the error due to this zero load voltage variation was accounted for. This method also eliminates the effect of zero load voltage variation with time which was possibly due to the imperfection in the used adhesive (CN type supplied by Techni Measure) or the water proof coating material (W-1 type supplied by Techni Measure) used for the bridge installation.

The static and dynamic behaviour of the measuring system was studied by performing torque measurements without any impeller at zero speed and at 300 rpm with the vessel empty of water. The results of these two experiments showed almost no difference. This was also confirmed by the manufacturers (Ramage 1992). As these torque measurements showed no differences, it can be concluded that the friction between the shaft surface and the water in the vessel is negligible.

The variation of the impeller diameter due to manufacturing tolerances (maximum $\pm$ 0.2 mm, measured on three opposite blades) was also considered and the average value between them was used for power number calculations in the measurements. Although the variation of the impeller speed with the flywheel attached to the shaft was $\pm$ 1 rpm, any measurement in which the variation of the impeller speed was more the $\pm$ 0.5 rpm was rejected and repeated. This variation resulted in a maximum experimental error of 2% at 100 rpm and 0.7% at 300 rpm in the power number.

Employing a similar technique but in larger scale measurements Kuboi and Nienow (1982) reported an accuracy of 3% in the linearity of the response of the strain gauges.

It was ensured that the excitation voltage (5 Volts) did not change from the calibration experiments to the actual measurements. The high resistance of the employed strain gauges (1000 Ω) aided this matter and the battery was charged every 5 hours.

2.6 Laser-Doppler anemometry

Laser-Doppler anemometry (LDA) is probably the most suitable technique for the measurement of the flow characteristics of stirred vessels. The LDA technique makes use of the variation in the intensity of the laser light scattered by a small particle moving through a fringe pattern. This fringe pattern, shown in Figure 2.21, is formed as a result of the intersection of two laser beams. The spacing between the light and dark bands (λ^*), the fringe spacing, depends on the angle of the intersecting beams θ and the wavelength of the laser light λ.

$$\lambda^* = \frac{\lambda}{2 \sin(\theta/2)} \qquad (2.10)$$

A particle crossing the control volume (fringe pattern) with a velocity V in a direction perpendicular to the fringes will scatter laser light. The frequency of the variation of the intensity of this scattered light, F_D, is proportional to the velocity V and the fringe spacing λ^* and given by:

$$F_D = \frac{2\ V.\ \sin(\theta/2)}{\lambda} \qquad (2.11)$$

The intensity of the scattered light depends on the size, shape and refractive index of the particle and on the direction of observation. However, in addition to the frequency of the Doppler burst the scattered light will always have a low frequency component of intensity variation (pedestal).

The frequency of the Doppler burst does not specify the direction of the particle velocity and in order to resolve this ambiguity the fringe pattern can be moved within the control volume by imposing a different optical frequency on the two laser beams. Considering an applied frequency shift F_S, the equation (2.11) can be rewritten as:

$$V = \frac{\lambda\,(F_D \pm F_S)}{2\,\sin(\theta/2)} \qquad (2.12)$$

A diffraction grating is a convenient way of providing a frequency shift. This frequency shift is given by:

$$F_S = \frac{2\,m\,n\,N_g}{60} \qquad (2.13)$$

where m is the order of the diffracted beams, n is the number of lines on the grating and N_g is the grating rotational speed in rpm.

Equation 2.12 gives the instantaneous velocity of the particle. If the particle follows the flow faithfully, it will be possible to determine the flow velocity in the control volume. Although the exact route of the particle movement through the control volume can not be determined by the LDA technique, the dimensions of the control volume are small (0.19 mm x 0.71 mm with the present optical arrangement) and velocities of

different particles are treated as the flow velocity in the centre of control volume.

An extensive description of the principles and practice of LDA is beyond the scope of the present investigation, as it has been given by Durst et al (1981), Drain (1980) and others. Only the components and considerations particularly relevant to the present LDA system are given below. More detailed considerations of the application of LDA to stirred vessel flows can be found in Yianneskis (1982a), Yianneskis et al (1987) and Calabrese and Stoots (1989).

2 6.1 Optical arrangement

A 10 mW Helium Neon laser was employed in the LDA measurements. The laser beam diameter was adjusted to 0.80 mm by means of an aperture wheel placed in front of the laser. The laser beam was focused onto a diffraction grating by a plano-convex lens of focal length f_1 = 200 mm. The diffraction grating (Technisch Physische Dienst [tno-th] model H) had three tracks of chemically etched radial lines. The upper track had the highest number of lines (n = 16384) and was used for splitting and frequency shifting of the beams.

The grating was coupled to the shaft of a small D.C. motor rotating at a speed of N_g = 3000 rpm. As a result, a frequency shift of $F_s = \pm$ 1.6384 MHz was provided by the first order beams. Considering the highest measured velocity (at the tip of the impeller) which was V = 1.2 m/s and a turbulence level of 50%, this frequency shift was adequate to resolve the ambiguity in the direction of the flow throughout the tank.

The first order beams were used to generate the control volume by means of two plano-convex lenses of focal lengths $f_2 = f_3 = 300$ mm. The beams were first collimated and then were focused onto the measurement point as shown in Figure 2.22. The half angle of intersection of the beams in the air was 5.9°. The beams were blocked at the exit from the test section and the scattered laser light from the control volume was focused by a zoom lens of $f_4 = 80$ - 200 mm to a pinhole ($d_{ph} = 0.5$ mm) located in front of a photomultiplier tube (EMI 9817B).

2.6 2 Alignment of the optical system

As mentioned in section 2.2, the test section could be traversed in three directions. The optical benches were fixed and the laser beam was aligned to the optical bench with a pinhole moving along the optical bench. The test section base was adjusted to be horizontal and it was ensured that the side wall of the trough (facing the laser) was perpendicular to the laser beam by rotating the test section around the z axis. Both adjustments were made by coinciding the reflected beam from the trough to the incident one passing through the pinhole in front of the laser. A sheet of paper was attached to the side wall of the trough in front of the laser beam. Two lines, one horizontal and one vertical and intersecting each other at the laser spot were drawn on the sheet. In introducing any optical component the position of this spot for the incident beam or the zero order diffracted beam (after the grating was introduced) was kept constant by adjustment of the component being introduced.

The reflection of the incident or the zero-order diffracted beam from the component was also adjusted to pass through the pinhole in front of the laser. The alignment was made while the grating unit was rotating. In the

alignment of the grating unit the different orders of the diffracted beams were made to lie along the horizontal line drawn on the sheet for the radial and tangential velocity measurements, and along the vertical line for the axial velocity measurements. The incident beams at the control volume were projected to a screen 3 m away by a mirror in order to measure the half angle of the intersecting beams accurately.

2 6.3 Positioning of the control volume

The position of control volume was determined through an iterative computer program considering the principles of Snell's law for the refraction of the laser beams passing from one medium to another. The program calculated the traverse of compound table in two directions (X and Y) to move the control volume from a reference point (r = 147 mm, $\theta = -90^{\circ}$) to the point of measurement. The calculation allowed for the presence of the trough, the cylinder and the baffles in all possible beam orientations. The program also calculated the velocimeter conversion factor at each location.

In order to locate the control volume on the reference point the test section was moved along and perpendicular to the optical axis until the beams intersected with the shaft symmetrically on either side. Then the test section was moved in the direction of optical axis until the intersection of the beams was observed in the inner wall of the vessel. The accuracy of the movement of the compound table in both directions was 0.05 mm.

The positional error in the control volume location was estimated to be 0.5 mm along the optical axis and 0.25 mm in the direction perpendicular

to the optical axis. The z co-ordinate (elevation) of the control volume was measured by a moving micrometer mounted in front of a ruler fixed on to the trough. In order to minimise the positional error in the z direction the elevations of the upper and the lower impellers were selected as reference points for the measurement locations at the top and bottom half of the vessel respectively.

2.6.4 Beam orientations for the measurements of the U, V and W velocity components

The orientation of the beams for axial, radial and tangential velocities are shown schematically in Figure 2.23. In this Figure the laser beams are shown by dashed-line arrows, the velocities are shown by solid-line arrows and the directions of the rig movement for the measurement of each velocity component (at different location in $\theta = 0^{\circ}$ r-z plane) are shown by the lines with arrows at both ends.

All the measurements were carried out at the $\theta = 0^{\circ}$ r-z plane (half way between two baffles). The collection of the scattered light by the photomultiplier was performed on-axis for the measurements of the axial and radial velocities in all locations and for the measurements of the tangential velocities in the locations below the lower impeller (Figure 2.23 (a) and (b)).

As the employed LDA system could only operate in forward scattered mode due to low power of laser used, direct measurements of W in the locations above the lower impeller (close to the impeller or shaft) were not possible. At these locations measurements were carried out in directions 45° or 22.5° to the radial direction with impeller rotating in

both directions. The measured velocities in these directions were a combination of radial and tangential velocities and the procedure of calculating W and w is given by Yianneskis (1982a). It must be noted that these measurement were carried out in the $\theta = 0^{\circ}$ r-z plane as shown in Figure 2.23 (c).

2.6.5 Signal processing system

The frequency counting technique was employed for the determination of the mean and rms velocities from the photomultiplier output. The procedure of signal processing by counter has been described in detail by Suen (1992) and only a brief description is given here.

The signal from the photomultiplier was filtered by a low pass passive filter (5 MHz) for noise removal and by a high pass variable active filter in the range of 0.1 - 1 MHz (Krohn-Hite model 3200) for eradication of the pedestal. The signal was then fed simultaneously to a frequency counter (Imperial College design FS4) and a two-channel storage oscilloscope (Tektronix model 5111). An Apple II microcomputer, interfaced to the counter, was programmed to control the counting procedure. If the amplitude of a Doppler burst exceeded a pre-defined threshold level, the counter would generate an amplitude validation pulse.

The frequencies of the amplitude-validated Doppler bursts would be considered by the counter for the measurement of ensemble-averaged velocity. The number of cycles within every amplitude-validated Doppler burst could be selected (8 or 16) for a final (frequency) validation of the Doppler burst before a frequency measurement was made by the counter.

The Doppler frequency in every burst (with an amplitude higher than the threshold level) was calculated from the comparison of the first 5 (or 10) and of the first 8 (or 16) cycles. If two frequencies were similar to within a pre-set tolerance, (0% - 1.6%), then the burst frequency was taken into account for the ensemble-averaged velocity measurements.

In order to monitor the signal quality, the lower level of filtering and the appropriateness of the amplitude validation/trigger level, the band-pass filtered Doppler signals were fed to Channel 1 of the oscilloscope, while the counter amplitude validation pulses were fed to Channel 2. By addition of the two Channels the validated Doppler bursts could be monitored and signal quality was checked all times. The filtered signal, counter amplitude validation pulses and the validated Doppler bursts as displayed on the oscilloscope, are shown in Figure 2.24.

In order to have acceptable statistical accuracy for each measurement, 2000 Doppler bursts were captured for the determination of the mean and rms velocities. Measurements were performed over 360° of impeller revolution and thus in the impeller region the results are influenced by the periodicity of the flow. Each measurement was repeated to establish the repeatability of the results. The number of repetitions varied, depending on the relative magnitudes of the mean and rms velocities, the location in the vessel, etc. In general, measurements were repeated from 1-5 times.

2.6.6 Validation of the results and experimental errors

In order to assess the accuracy of the measurements, the radial mean and rms velocities generated by a Rushton impeller (d = T/3, C = T/3, t = 3.3

mm) were measured in the vicinity of the impeller (at r = 51 mm). These profiles were compared with those obtained by Yianneskis (1982a) and the results are presented in normalised form in Chapter 3, Figure 3.36. The comparison shows an excellent agreement.

However, several parameters could contribute to the experimental error. The main parameters affecting experimental accuracy and precision are: the location of the control volume, impeller speed, threshold level for validating of Doppler bursts, seeding, frequency shifting, velocity bias effect, velocity gradient broadening and statistical errors.

Uncertainty in locating the control volume depends on the accuracy of the traversing mechanism, the dimensions of control volume and also on the accuracy of the procedure with which the operator positions the control volume at a reference point. As mentioned before, the accuracies of the traversing tables were 0.05 mm in the X and Y directions and 0.25 mm in the Z direction. However, extreme care was taken in locating the control volume in the impeller elevation which was used as a reference point to minimise positioning errors.

The impeller speed was displayed during all the measurements. As a result of mounting the flywheel the speed fluctuation was very small (around ± 0.5 rpm). The fluctuation was monitored constantly during the experiments and any measurement with a higher speed fluctuation was rejected. The fluctuation in the rotational speed of the grating unit was ± 10 rpm (0.3% of the nominal velocity).

The quality of the Doppler bursts was monitored continuously on the oscilloscope. In the setting of the threshold level for the Doppler burst

amplitude validation, care was taken not to allow any noise to affect the counter measurements and also not to reduce the data rate. In most of the measurements impurities suspended in the water were sufficient to obtain a good signal to noise ratio and data rate and whenever necessary a few drops of diluted milk were added to the liquid in the vessel until an adequate number of Doppler bursts was observed on the oscilloscope, i.e. significant drop-out was avoided. When it was found that the bursts were superimposed (indicating the presence of more than one particle in the control volume at a time) the water in the vessel was changed in order to reduce the data rate.

The rate of particle arrivals to the control volume can be in direct proportion with the particle velocity. This will result in a higher calculated average velocity (Mclaughlin and Tiederman, 1973). Many workers have tried to introduce some correction methods. Weighting of the velocity data from individual particles with respect to their residence time was suggested by Hoesel and Rodi (1977). Durao and Whitelaw (1975) proposed random sampling of the measured velocities obtained by individual particles after storing the data obtained by all the particles. A similar approach can be a reduction in the number of particles which would result in the randomising of the time intervals between the measurements (Drain 1980). The latter two methods require longer measurement times and they do not eradicate the error.

A suitable method to cancel out this type of error confidently has not been devised as yet, particularly for three-dimensional flows. In the present flow where turbulence intensities are high, velocity bias errors are expected to be low and thus bias correction methods are not expected

to improve significantly the accuracy of the results (see also Yianneskis, 1982b)

Velocity gradient broadening occurs when the control volume is located in positions where the velocity gradient is steep. At these locations the particles moving through different parts of the control volume will have different velocities. The variation of mean velocities within the control volume may also result in a skewed frequency distribution. In the present work the highest velocity gradient occurred in the vicinity of the Rushton impeller in the z direction and the above effect was minimised as the smaller dimension of the control volume was oriented in this direction.

The number of data points for measurements of the ensamble-averaged mean and rms velocities in the counter can also result in an experimental error. This statistical error may be estimated from the equations suggested by Yanta (1973). For a sample size of 2000 measurements the error in the mean velocity with a turbulence intensity of 50% is calculated to be 1.5% with a confidence level of 95%. With the same degree of confidence, the statistical error for the rms volcity is 3%.

However, no correction was made for the measured velocities in this thesis. Employing the same counter and a very similar optical system Suen (1992) estimated that the overall errors in the mean and rms velocities were 5% and 10% respectively. This estimation for the measurements in the present work was confirmed by the day to day repeatability of the measurements and by comparison with measurements made by others.

2.7 Closure

The aforementioned error sources introduce uncertainties which are small enough not to have any significant quantitative, and definitely not qualitative, effect on the measurements of power, mixing time, mean velocity and turbulence presented in the following three chapters.

The detailed mean and rms velocity and kinetic energy of turbulence distributions presented in the following text were determined from a large number of data obtained throughout the vessel (at around 250 locations, with average spacing between locations of around 4 mm). The density of the grid of measurement locations employed was non-uniform: more data were obtained in regions of steep velocity gradients in order to minimise interpolation errors and less data in regions of relatively uniform velocity variation, in order to minimise the measurement time. The latter regions were in the bulk of the vessel where the velocity gradients are very small and negligible interpolation and velocity-gradient related errors are expected.

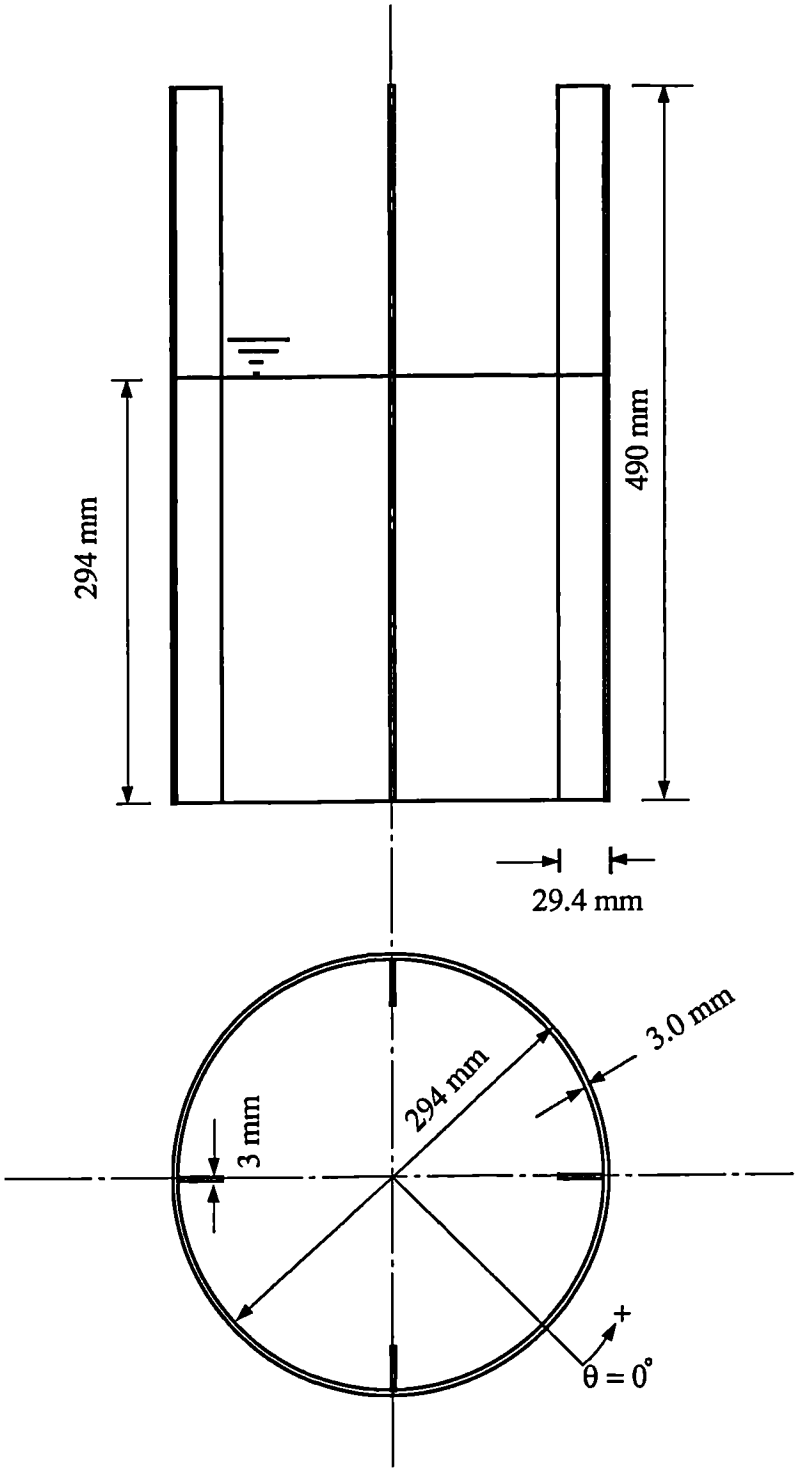

Figure 2.1. The dimensions of the vessel.

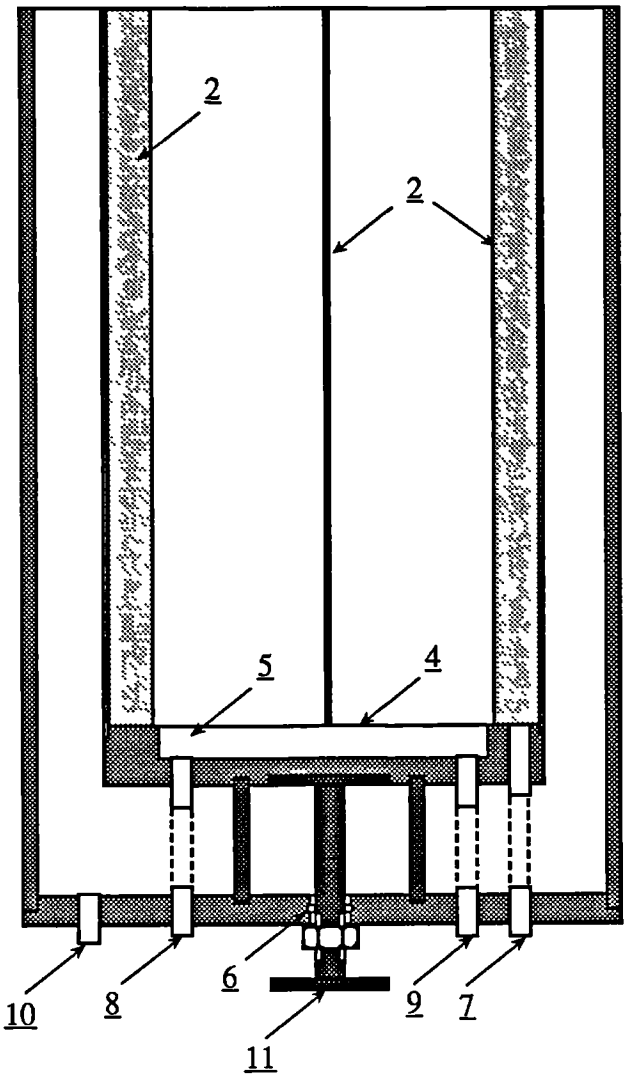

1 - Vessel
2 - Baffles
3 - Trough
4 - Heat Exchanger cover
5 - Heat Exchanger
6 - O ring
7 - Vessel drain
8 - Heat Exchanger inlet
9 - Heat Exchanger outlet
10- Trough drain
11- Vessel rotating device
Scale 1:5

(a)

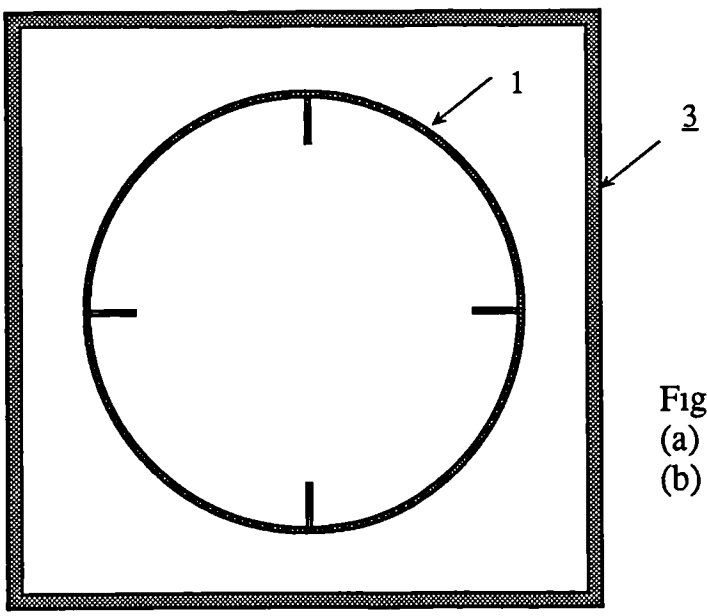

(b)

Figure 2.2. Mixing vessel;
(a) Vertical cross section,
(b) Horizontal cross section.

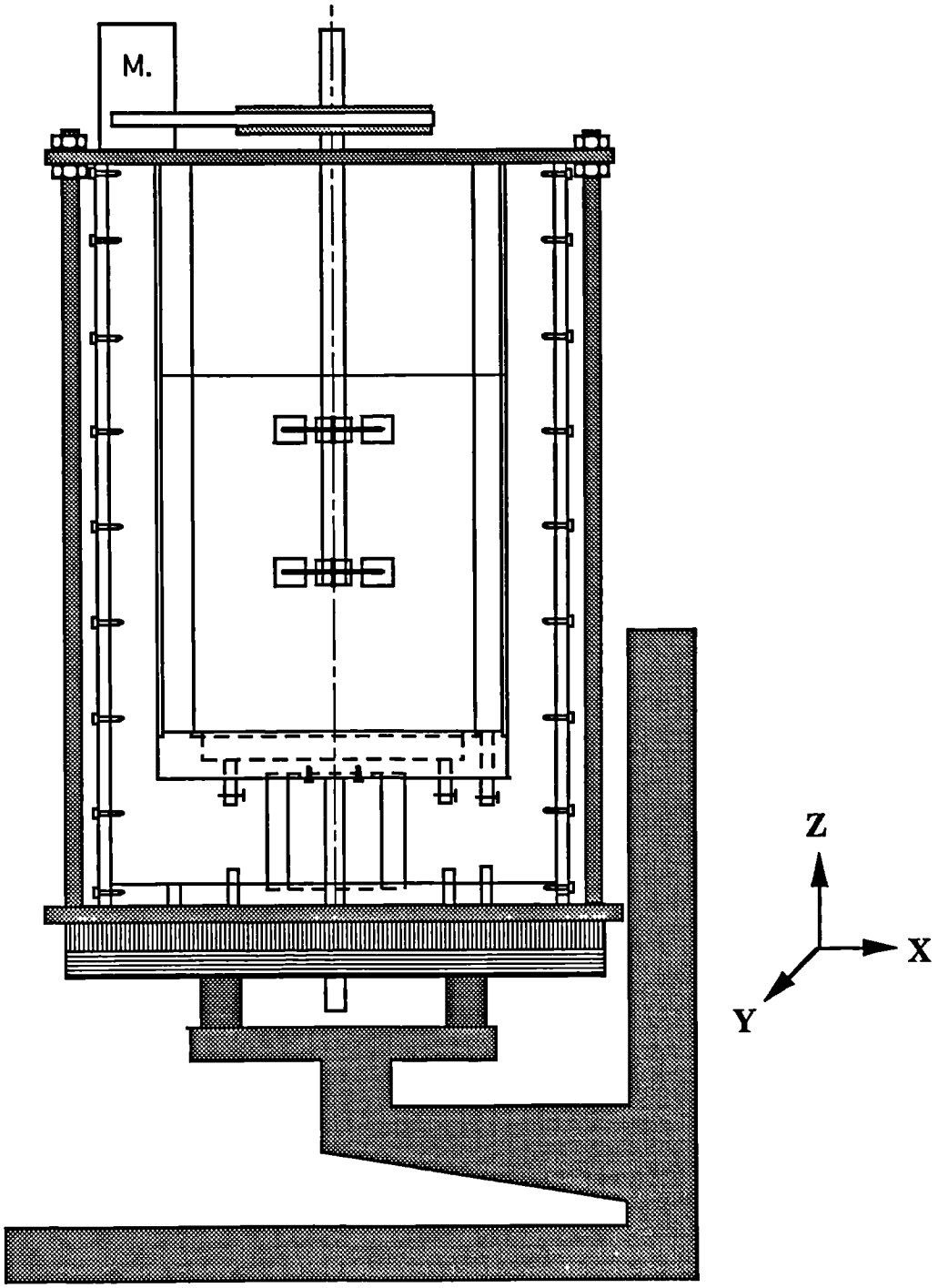

Figure 2.3. Schematic diagram of the test section.

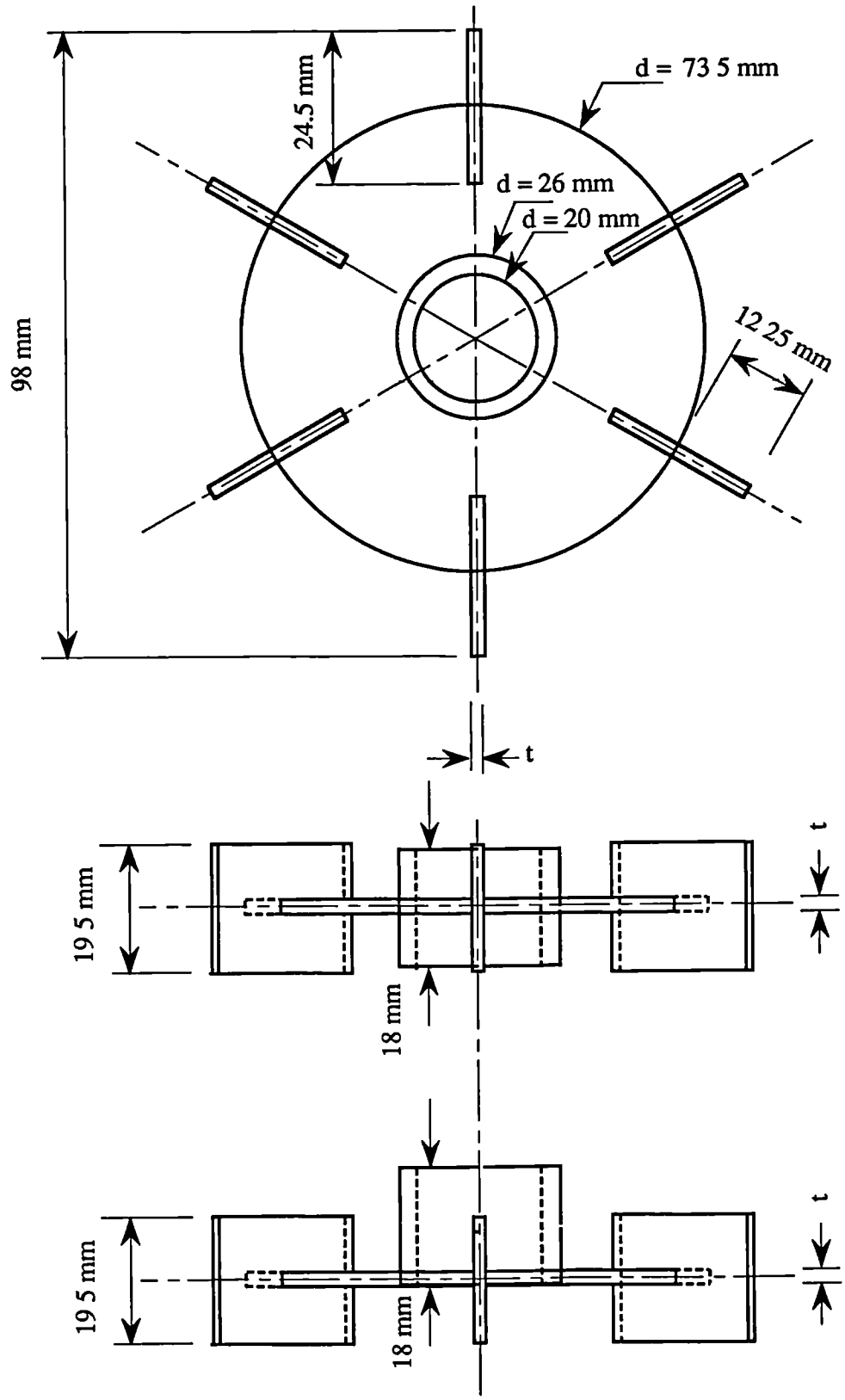

Figure 2.4. Rushton impeller geometry

t = 0.8, 1.65, 2.0, 3.3 mm

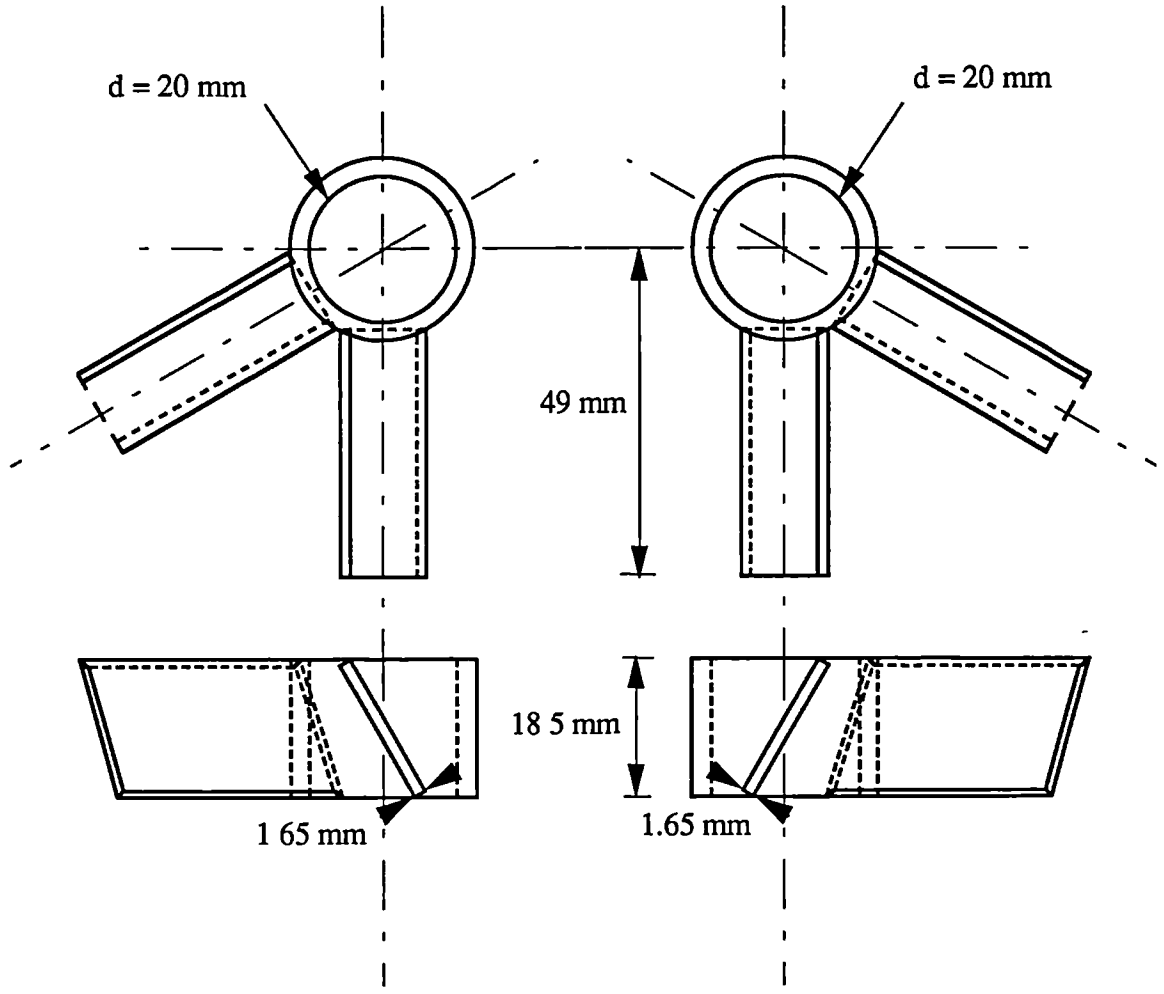

Figure 2.5. Pitched blade impellers

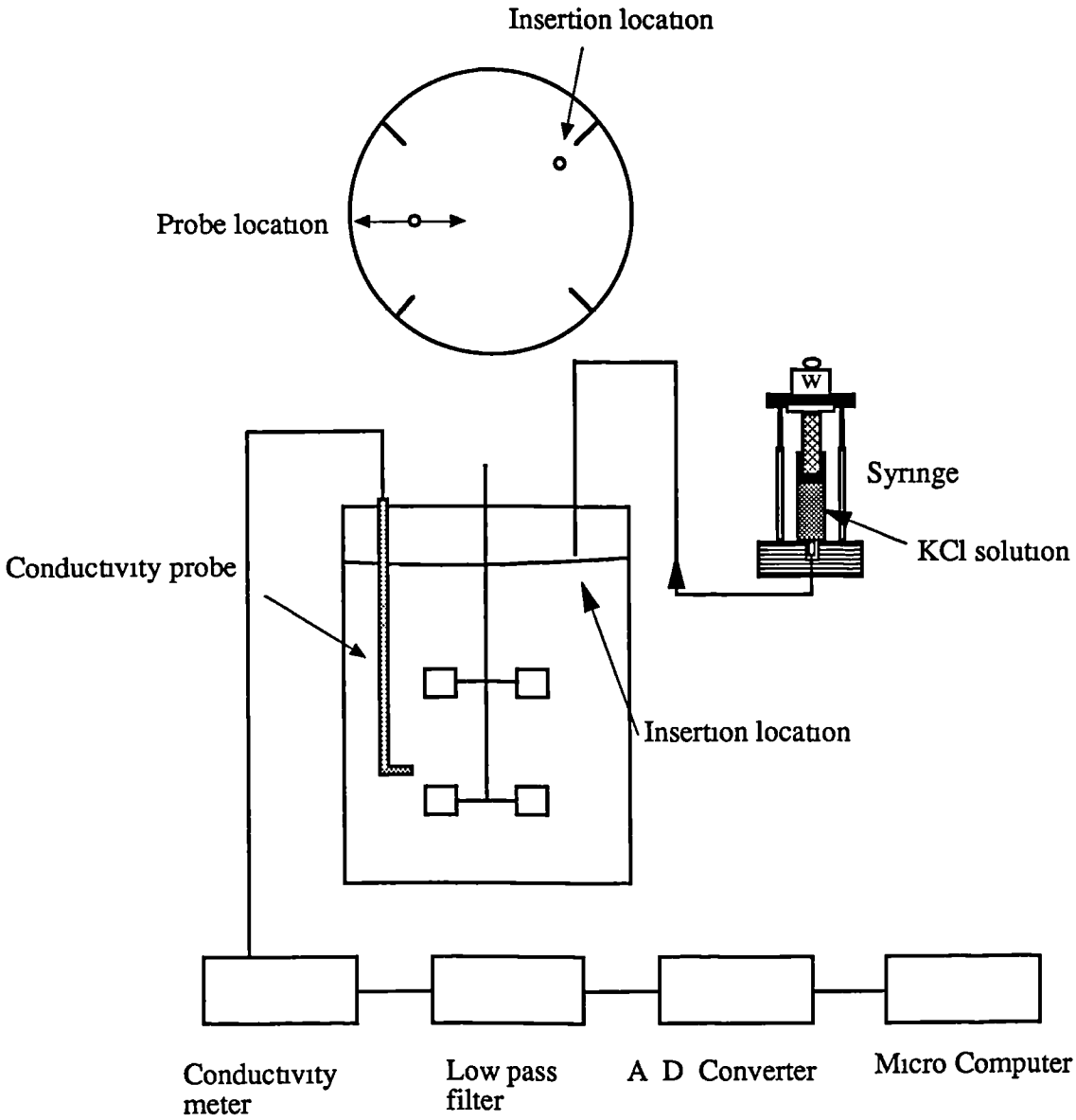

Figure 2.6. Conductivity measurement arrangement

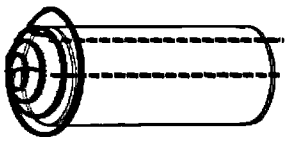

Figure 2.7. The conductivity probe

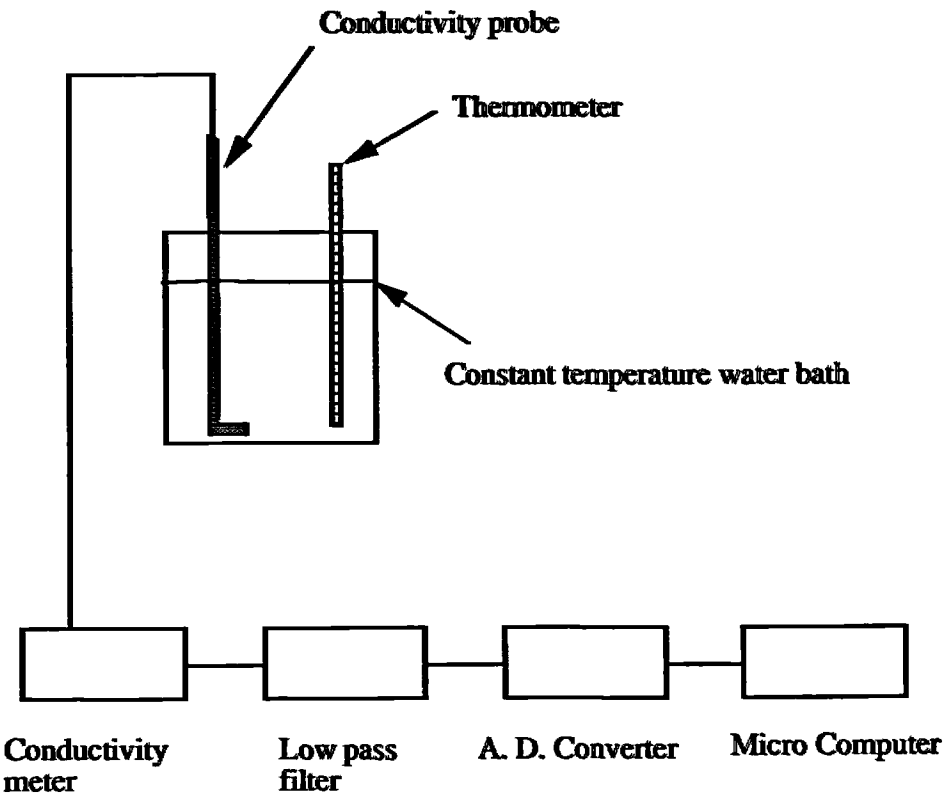

Figure 2.8. Probe calibration arrangement

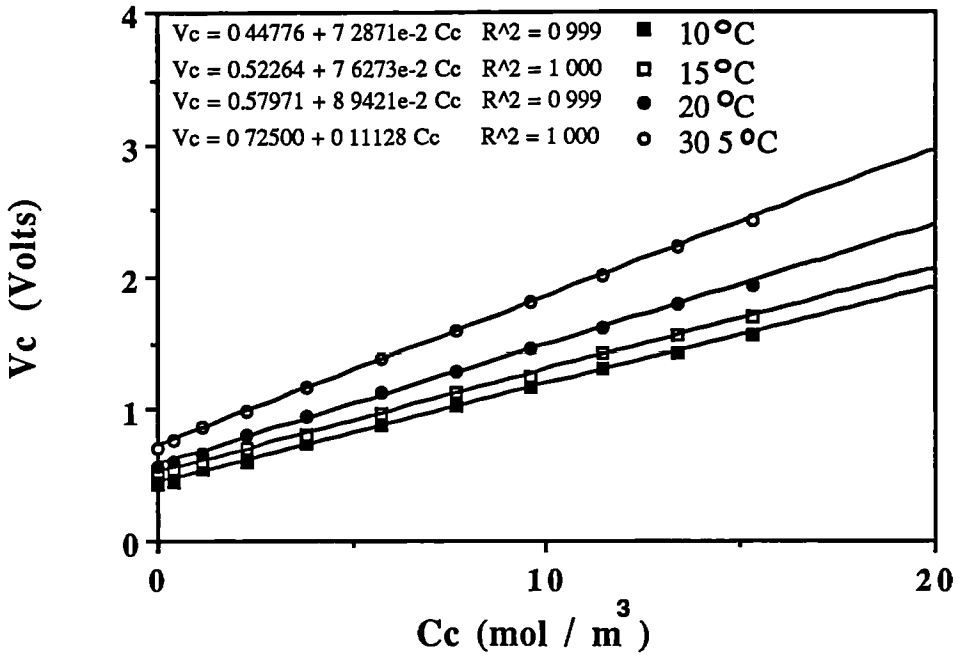

Figure 2.9. Conductivity probe calibration; variation of voltage with concentration.

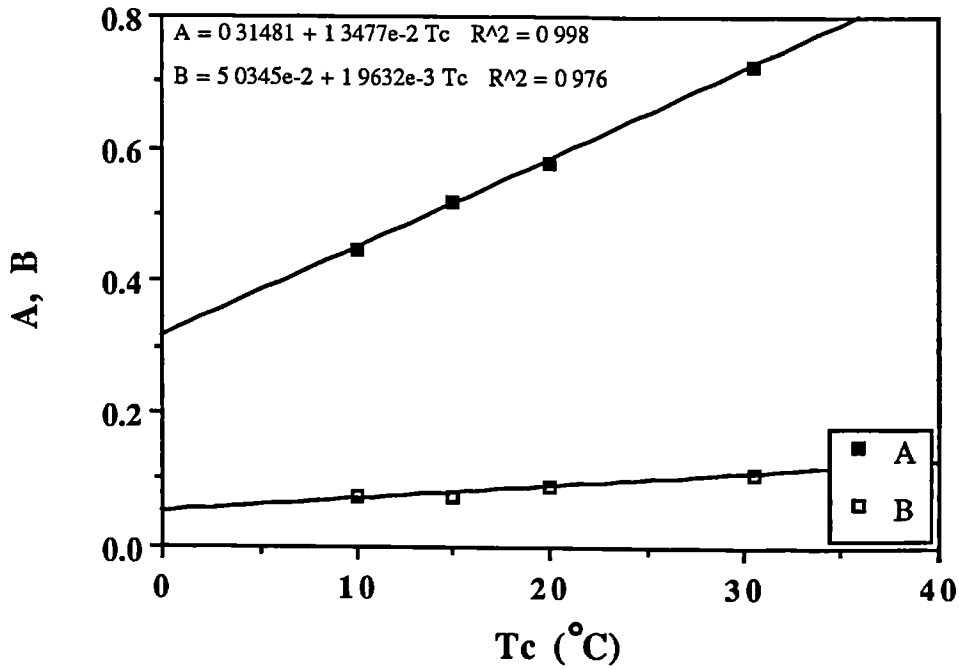

Figure 2.10. Variation of calibration constants A and B with temperature in the conductivity probe calibration equation.

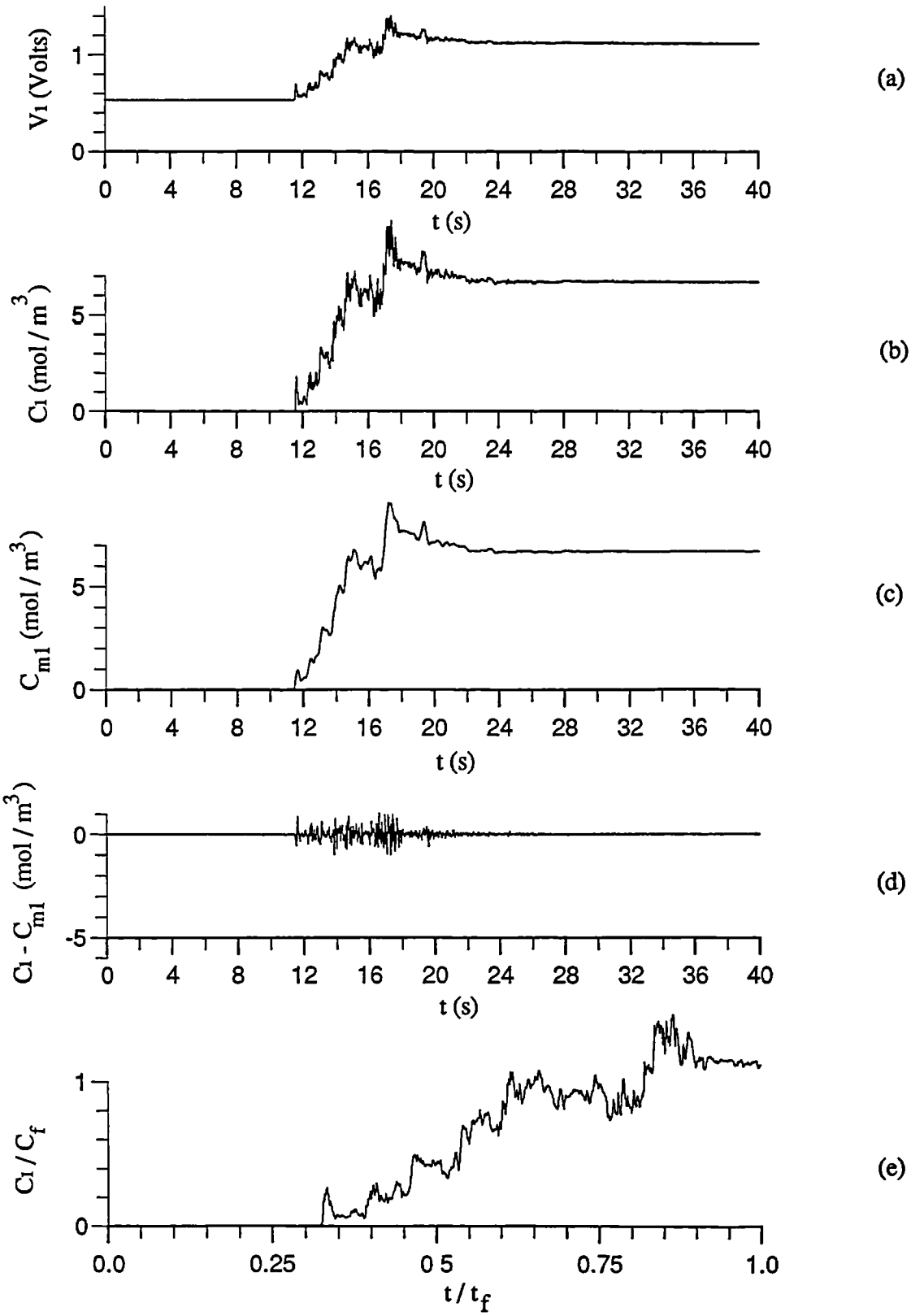

Figure 2.11. Characteristic voltage (a), concentration (b), mean concentration (c), concentration flutuation (d), and normalized concentration (e) variations; Parallel flow pattern: C1 = T/4, C2 = T/2, z = T/2, r = 80 mm.

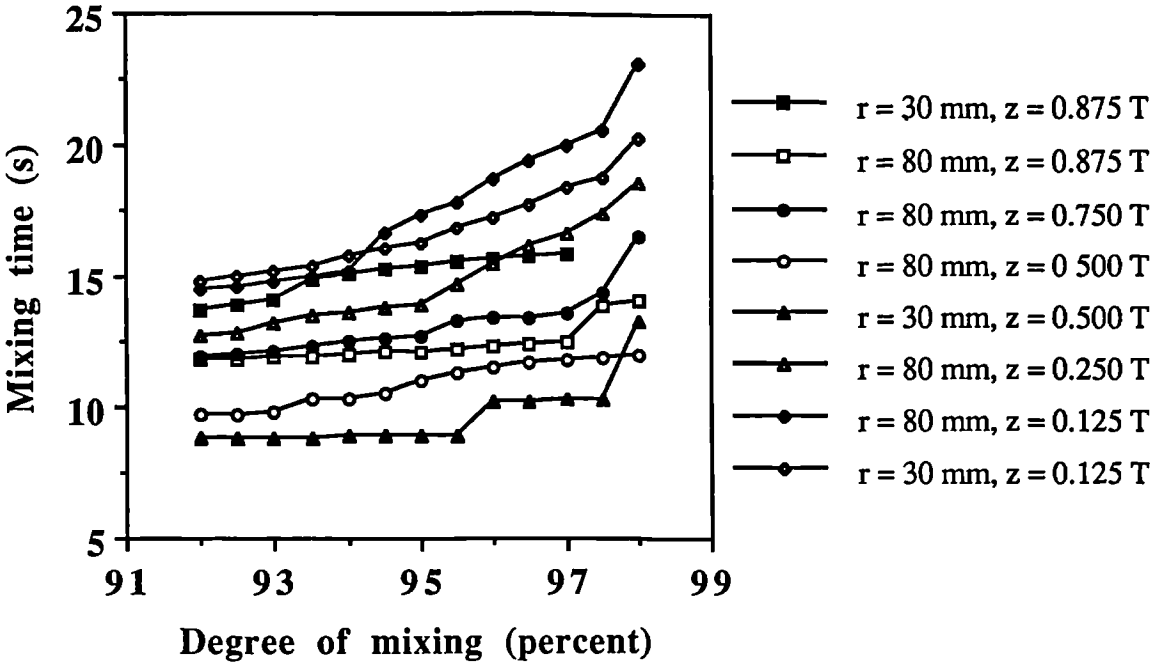

Figure 2.12. The variation of mixing time with degree of mixing; C1 = T/4, C2 = T/2, N = 200 rpm, insertion time 6.5 s.

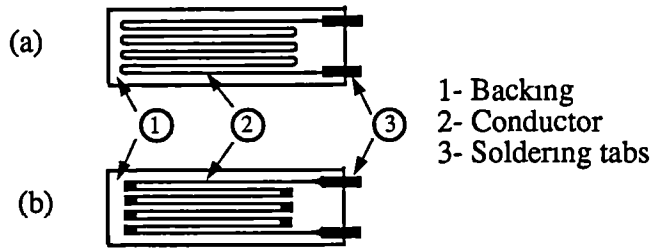

Figure 2.13. Typical wire (a) and foil (b) strain gauges

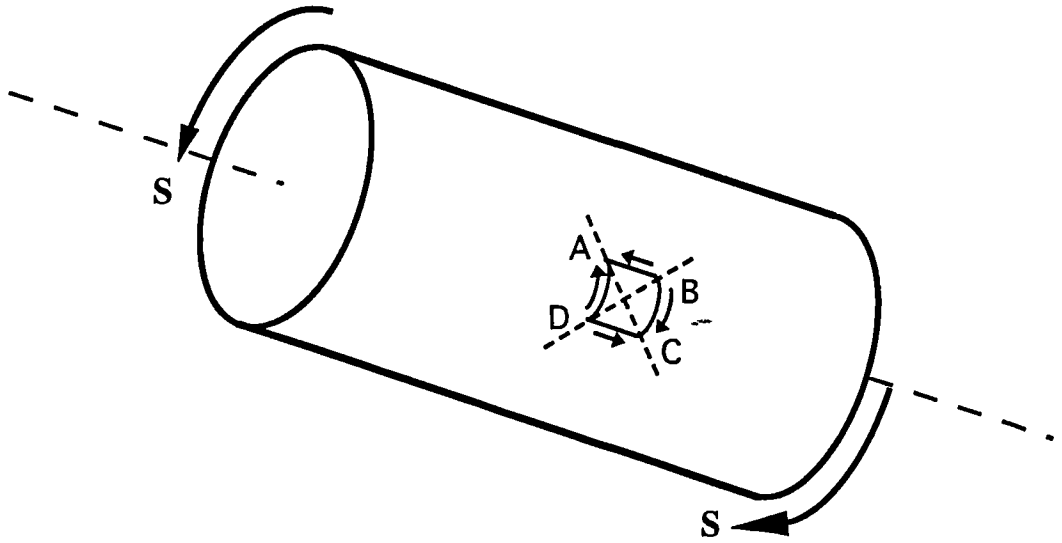

Figure 2.14. The shaft under an applied torsion of S.

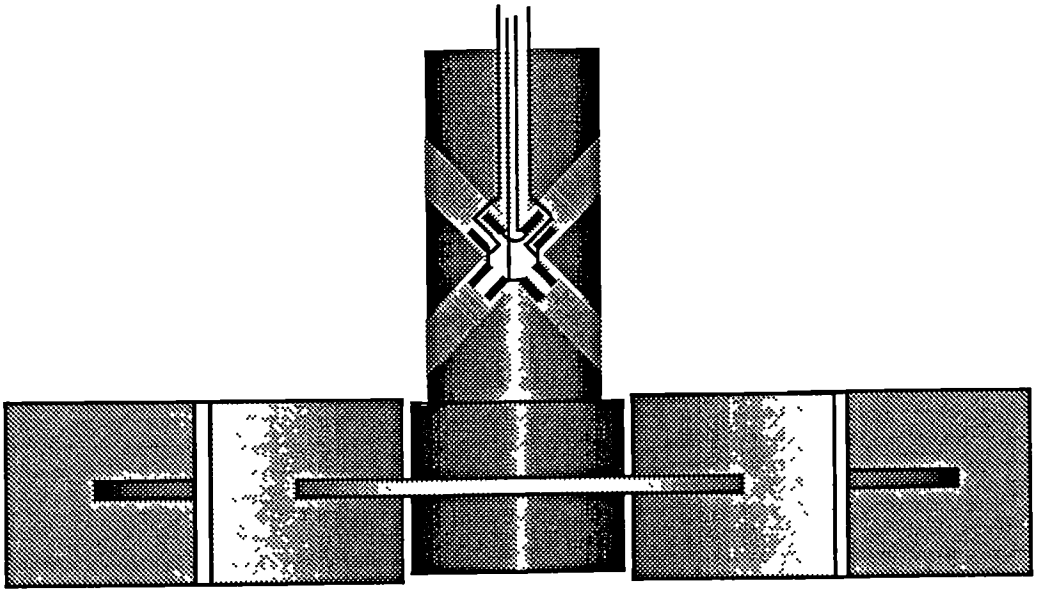

Figure 2.15 The Wheatstone bridge installed on the shaft.

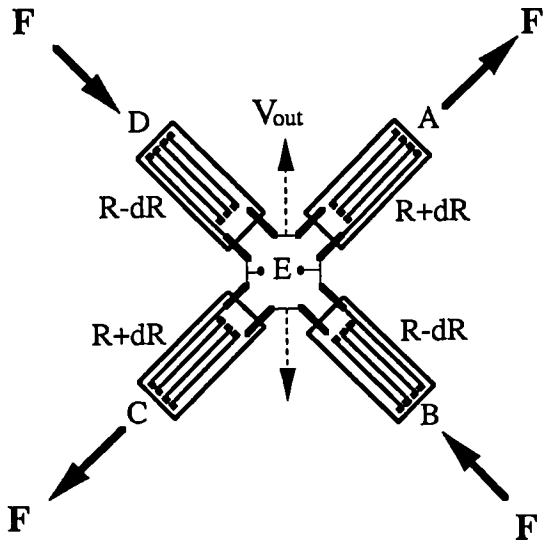

Figure 2. 16. Wheatstone bridge under torsion

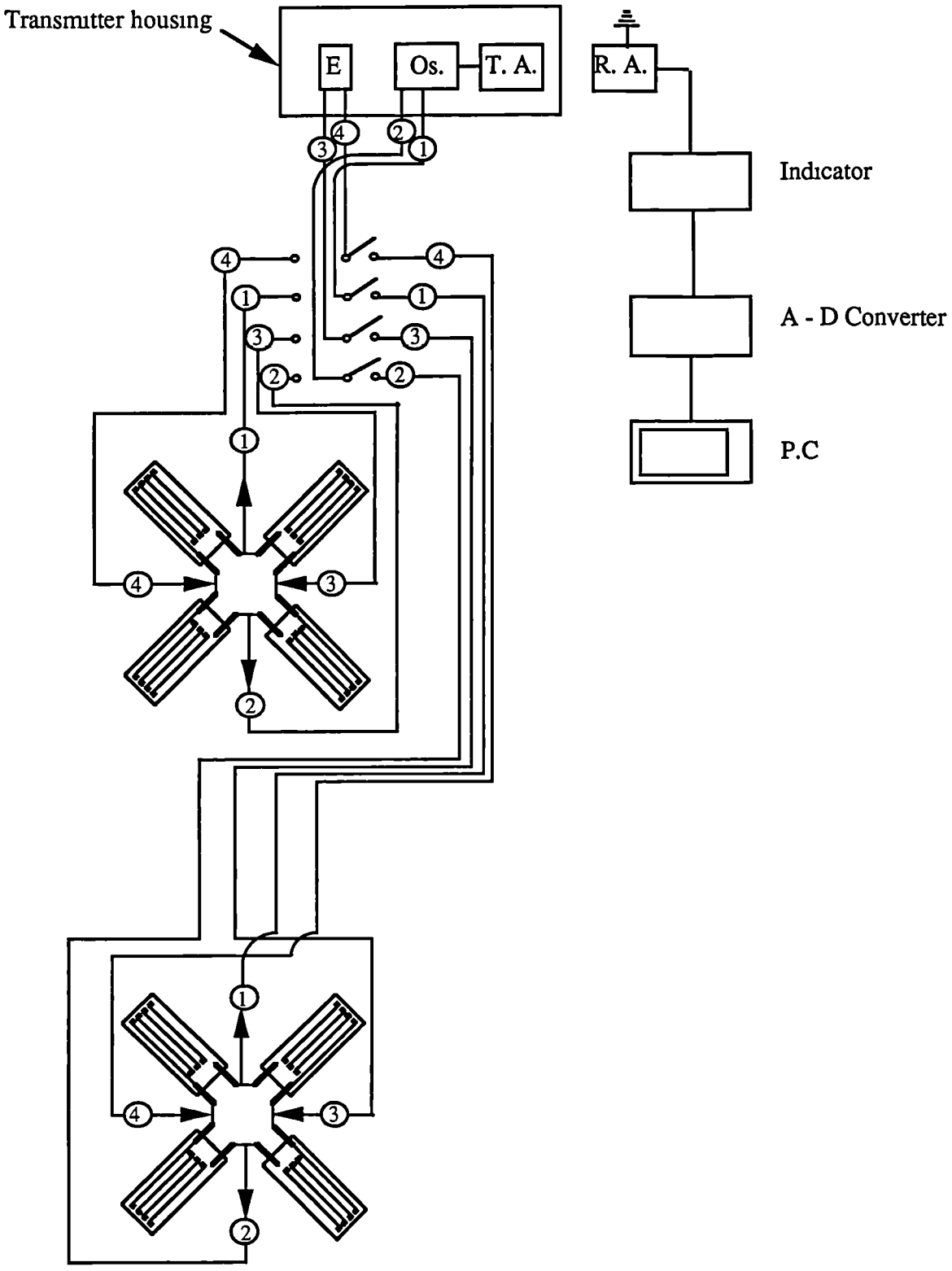

Figure 2.17. Electrical circuitry of telemetric system with strain gauges.

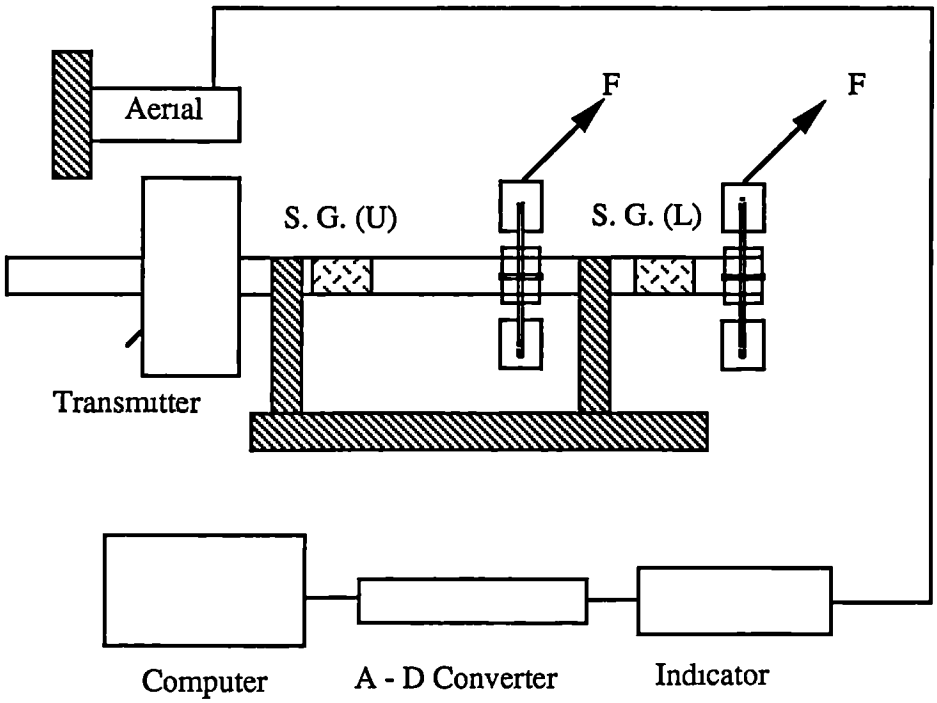

Figure 2.18. Experimental set-up for strain gauge calibration

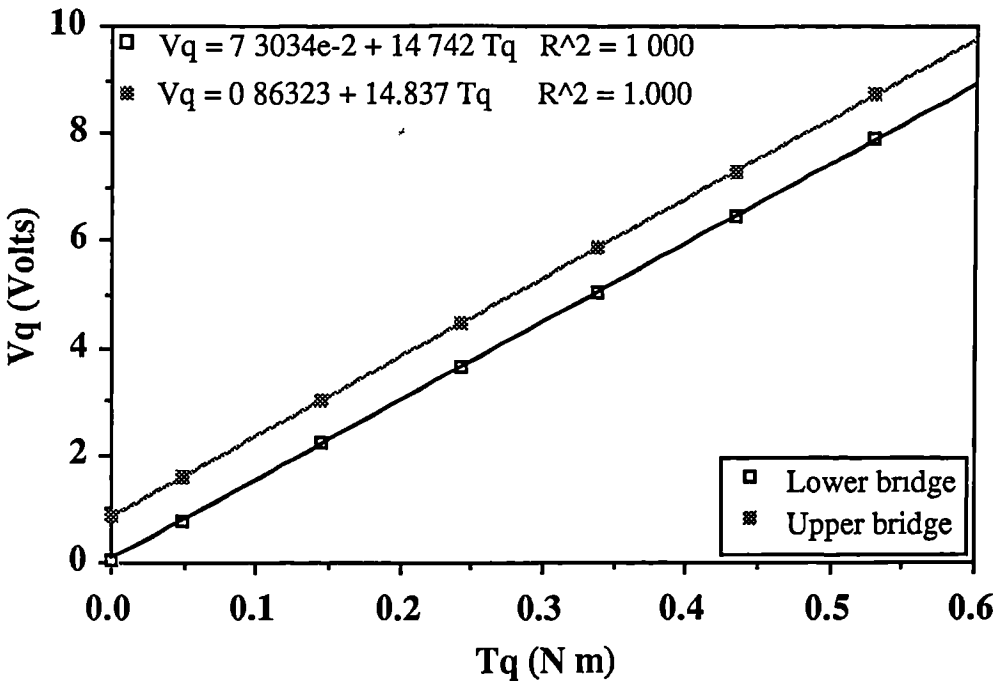

Figure 2.19. Calibration of strain gauge bridges

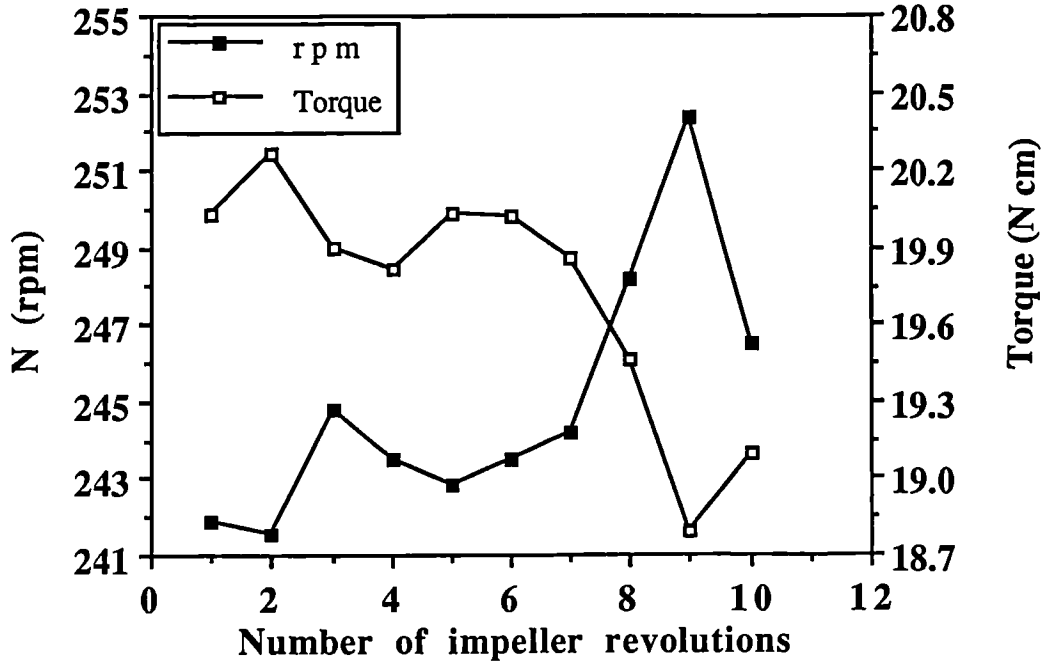

Figure 2.20 (a). A typical time history of torque and impeller speed.

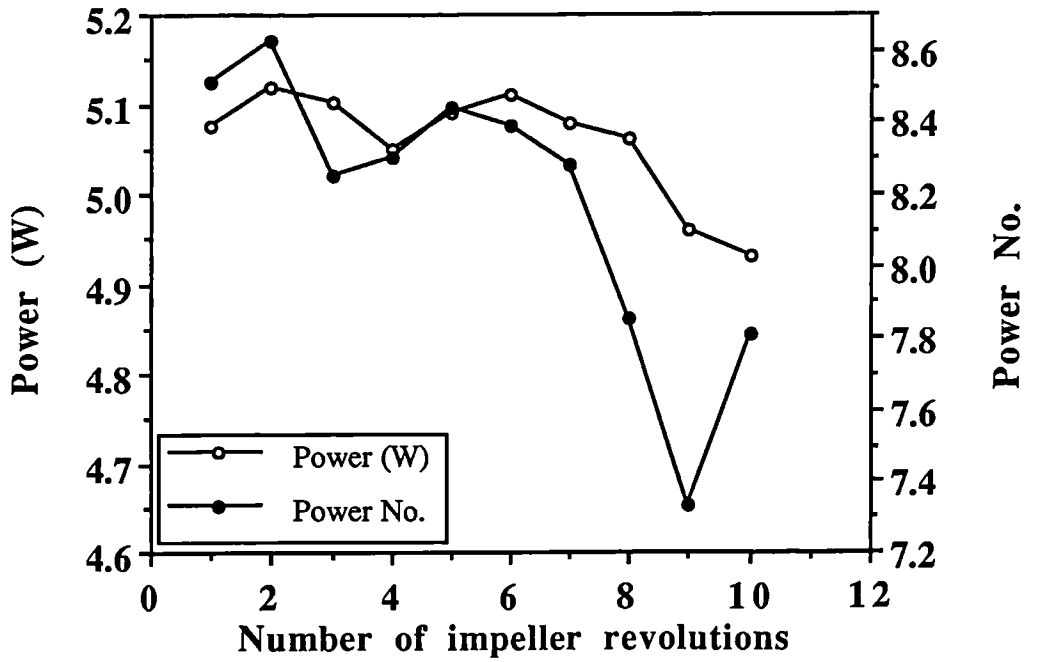

Figure 2.20 (b). A typical time history of power and power number.

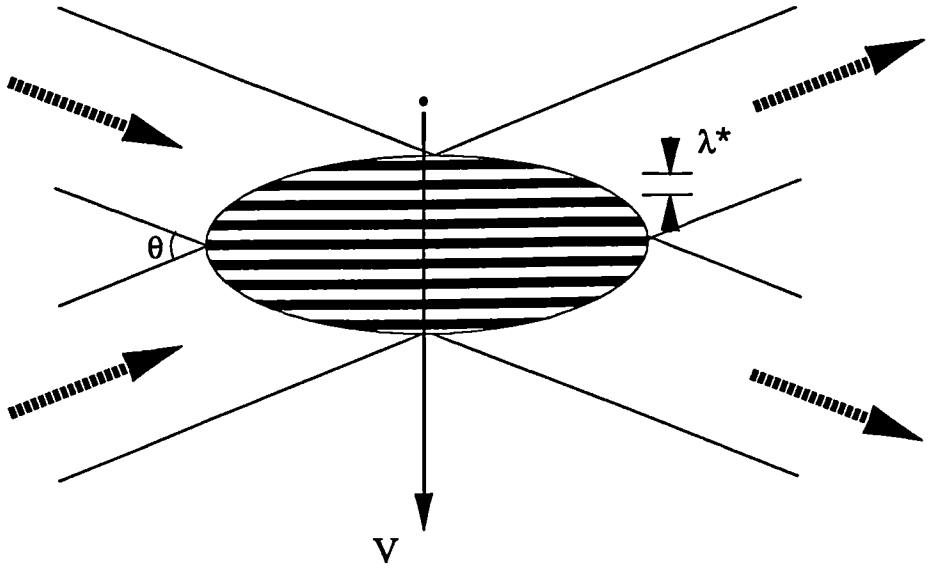

Figure 2.21. The fringe pattern formed as a result of beams intersection.

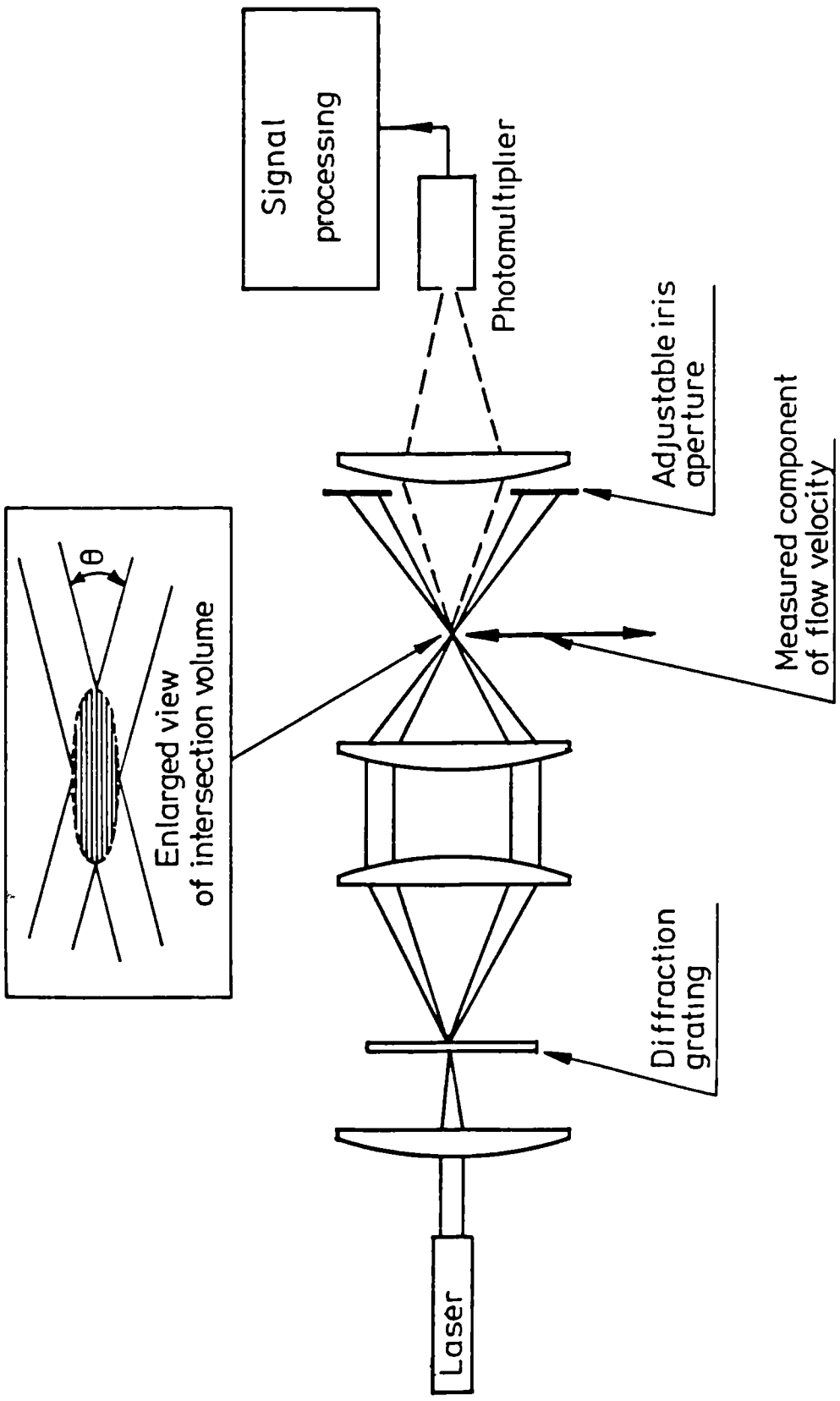

Figure 2.22. General outline of optical arrangement of laser-Doppler anemometer.

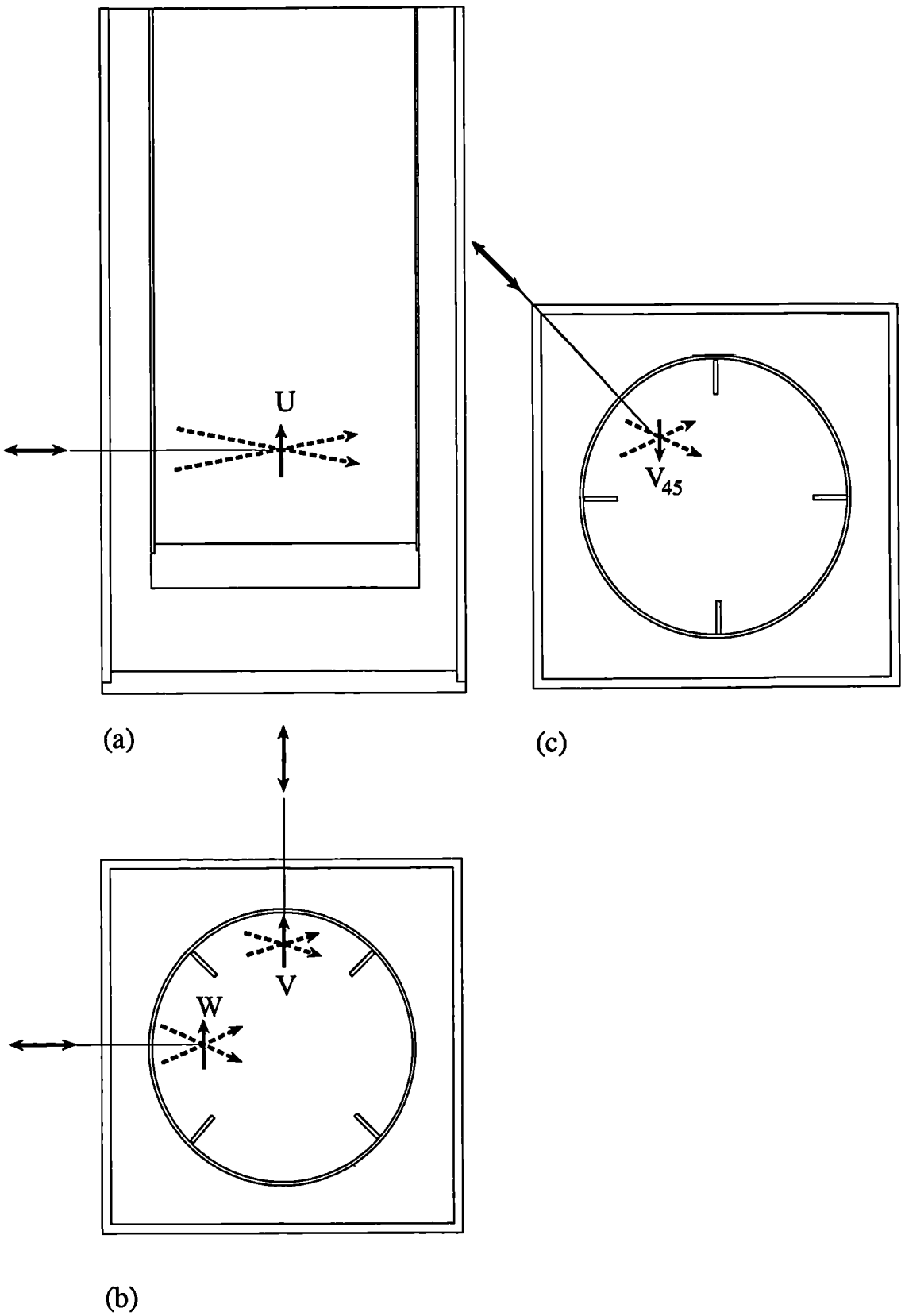

Figure 2.23. Beam orientations for measurements of U, V, W and V_{45} velocities.

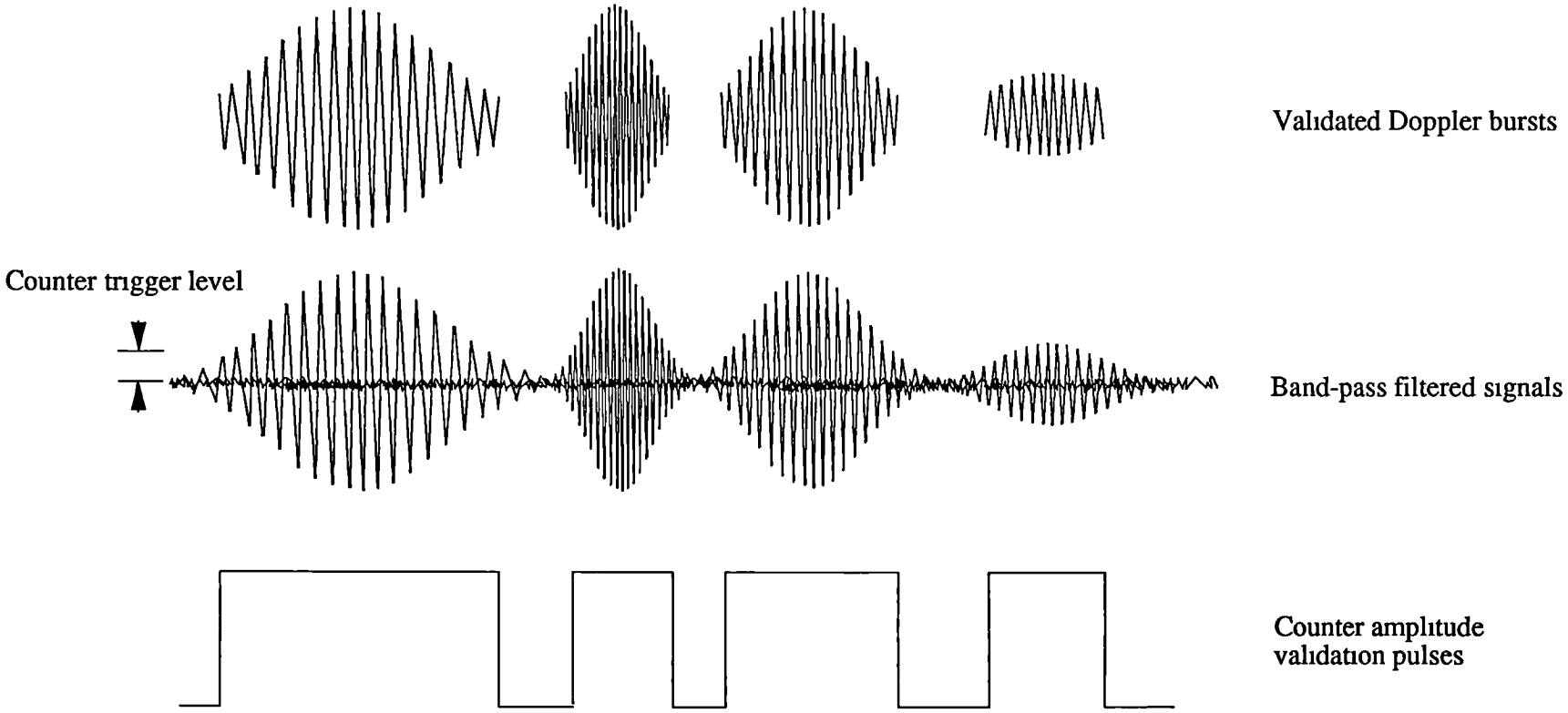
Validated Doppler bursts
Counter trigger level
Band-pass filtered signals
Counter amplitude validation pulses

Figure 2.24

CHAPTER 3

MIXING CHARACTERISTICS OF VESSELS STIRRED BY TWO RUSHTON IMPELLERS

3.1 Introduction

An experimental investigation of the flow patterns, power consumption, velocity characteristics and mixing times in a stirred tank agitated by two Rushton impellers is described in this chapter. The Rushton impellers employed in these investigations had a symmetrical hub, a diameter d = T/3 and an impeller thickness t = 1.65 mm. In order to differentiate between those flow effects produced by the interaction between the two impellers and those resulting from the shape of the impeller, some measurements were obtained with a single Rushton impeller (d = T/3, t = 1.65 and/or 3.3 mm). The majority of the observations and measurements were carried out in the $\theta = 0^{\circ}$ r-z plane. The effects of various parameters were studied. The impeller rotational speed was varied from 60 to 300 rpm.

More attention was paid to the effect of impeller spacing variation which resulted in changes of flow pattern and variations in power consumption and mixing time. In the flow visualisation investigations the liquid level in the vessel was varied from T to 1.5 T and the impeller clearances C_1 and C_2 were varied from 0.15 T to 0.4 T, and 0.25 T to 0.5 T respectively.

The results of the flow visualisation revealed a complex flow pattern in two-impeller systems and three stable and four unstable flow patterns were identified. Power measurements were carried out for the three

stable flow patterns and the power numbers were found to be dependent on the impeller spacings. The power number of the lower impeller differed from that of the upper one in some cases. At a liquid height of H = T, the interaction of the two impeller streams resulted in a fluctuating torque, impeller rotational speed and consequently power number for all impeller spacings. The instability of the flow pattern for some spacing combinations intensified these fluctuations, causing a higher fluctuation level in the power number of the impellers.

The stable flow patterns with H = T were quantified by detailed measurements obtained by laser-Doppler anemometry. The three components of the ensemble-averaged mean and rms velocities were measured over 360° of impeller rotation and the distribution of turbulence kinetic energy in the vessel was quantified. The weighted average value of the turbulence kinetic energy in the vessel was calculated and found to be different for the three stable flow patterns. Using the conductivity technique, the effect of the stability or instability of the flow pattern on mixing time was investigated and the results provided useful information for process design purposes. The flywheel was attached to the shaft for all the measurements and observations for minimisation of the impeller speed fluctuation; some power measurements were performed without the flywheel in order to investigate the fluctuating power characteristics.

3.2 Flow visualisation

3.2.1 Single Rushton impeller

The flow pattern induced by a single Rushton impeller was determined using the laser light-sheet technique described in section 2.3 and is shown

schematically in Figure 3.1. It confirms the results of many workers (for example Nouri, 1988), and the following points may be deduced from the observations:

a) The impeller stream generated by the impeller produces two ring vortices, one above and one below the impeller. The centres of these vortices are located close to the impeller and the vessel wall.

b) Moving the impeller towards the vessel bottom, results in an inclination of the impeller stream towards the free surface. This inclination increases with decreasing impeller clearance from the bottom of the vessel and the velocities in the lower vortex increase while those in the upper one decrease. The impeller stream inclination to the horizontal is almost zero when the impeller is located at the centre of the vessel.

c) A whirlpool-type of vortex is present near the free surface of the liquid with a local direction of rotation opposite to that of the impeller. The vortex precesses with the bulk of the flow in the same direction as the rotation of the shaft. This whirlpool is responsible for the surface aeration at higher Reynolds numbers, in agreement with the findings of Greaves and Kobbacy (1981).

e) Two helical vortices, one on either side of the impeller stream, exist behind each baffle.

3.2.2 Two Rushton impellers

The effects of impeller spacing, liquid height and impeller rotational speed on the flow patterns were investigated and a large number of photographs and video recordings of the flow patterns were made. As the

flow in most cases was strongly three-dimensional, particularly in impeller regions the photographs taken do not illustrate the flow patterns clearly. The particles did not stay in the plane of illumination long enough to form sizeable streaks during the exposure time of photographs. However, the video recordings were observed with care. This video film is held in the Mechanical Engineering Department of King's College London and can be viewed on request. In this investigation three stable and four unstable combinations of these three flow patterns were observed. The stable flow patterns are named below according to the directions of the impeller streams which result from the shape of the impellers, the interaction of the two impeller streams and/or by the re-direction of the lower impeller stream due to the proximity of the bottom of the vessel.

Each visualisation test was carried out for at least twenty minutes and the observation commenced with the start of the motor driving the impeller. At the start of the motor the impeller streams for all the cases studied, i.e. with different C_1, C_2 and H, were horizontal and each impeller stream formed two ring vortices. If this flow pattern lasted for at least twenty minutes, it was concluded that the pattern was stable and termed 'parallel'. If during the observation period the impeller streams were directed towards each other or the lower stream was directed downwards after the start of the observation and the pattern lasted for at least twenty minutes, it was concluded that the flow was stable and the flow pattern was termed 'merging' or 'diverging' respectively.

If the change of the direction of the impeller streams occurred more than once in twenty minutes or it occurred ten minutes or more after the start of the motor, the flow pattern was concluded to be unstable and again it

was named on the basis of the combinations of the impeller stream directions resulting from the flow pattern changes. Each test was repeated at least 2-4 times to establish the repeatability of the flow pattern.

Fig. 3.2(a) shows a schematic diagram of the flow pattern induced by two Rushton impellers located far enough from each other to operate independently. The impeller streams show almost no inclination to the horizontal, similar to the case described above with a single impeller located in the middle of the vessel. Four ring vortices were observed, one above the upper impeller, two between the impellers and one below the lower impeller. The most crucial parameters for this flow pattern are the clearances C_1 and C_2. With a liquid height of H = T, C_2 must be greater than 0.385 T and C_1 must be not less than 0.20 T for this flow pattern to be maintained at an impeller speed of N = 260 rpm. This flow is termed the parallel flow pattern hereafter.

Crozier (1989) studied the flow in a 2:1 aspect ratio stirred tank using an impeller spacing of C_2 = T between two impellers. Crozier found that the flow streams produced by each of the two impellers did not appear to be affected by the presence of the other impeller. The flow pattern was very similar to the 'parallel' one revealed by the present investigation.

Figure 3.2(b) shows the second stable flow pattern observed in which the impeller streams are directed towards each other. In this case two strong ring vortices are generated, one in the upper part and the other in the lower part of the vessel. Two smaller and less clearly defined vortices could be observed as shown in this Figure. However, the flow in the region between the impellers essentially rotates around the shaft in an almost solid-body type of rotation. As for the case of the parallel flow

pattern, C_2 and C_1 are the crucial parameters for this flow regime. With a liquid height of H = T, C_2 must be less than 0.385 T and C_1 must be bigger than 0.17 T for this pattern to be maintained at an impeller speed of N = 260 rpm. This flow is termed the merging flow pattern in the following text. With the impeller spacings $C_1 = C_2 = T/3$, Kuboi and Nienow (1982) reported a similar flow pattern in a gassed unit of larger scale.

The effect of C_1 on the flow pattern is shown in Figure 3.2(c). The lower impeller stream is in this case directed towards the vessel bottom while the upper impeller is pumping horizontally. With this flow pattern in the vessel roughly two-thirds of the bulk flow are mixed primarily by the upper impeller. Once again four ring vortices are observable but the one under the lower impeller is not well defined and it is small in size in comparison with the others. This flow is termed the diverging flow pattern and is present in the vessel when C_1 is less than 0.18T with C_2 is greater than 0.385T at N = 260 rpm.

In the merging and diverging flow patterns a decrease in clearance C_2 for the former and in clearance C_1 for the latter pattern, shortens the time at the start of the experiment during which the flow pattern is parallel.

The effect of the impeller spacings and liquid height on the flow pattern at the impeller speed (N) of 260 rpm has been summarised in Figs. 3.3 - 3.7. In these Figures the observations made from flow visualisation experiments are presented as plots of H/T (varying from 1.0 to 1.5) against C_1/T (varying from 0.12 to 0.4), for five values of C_2/T; 0.35, 0.365, 0.375, 0.385 and 0.4. The different stable and/or unstable flow patterns observed are denoted by different symbols in these plots and the

(H/T - C_1/T) regions in which the various flow patterns are present, are separated by solid lines.

Figure 3.3 shows the variation of the flow pattern for C_2 = 0.35 T. Merging flow pattern occurs in the majority of the (H/T - C_1/T) regions in this Figure. A small region at the top right corner of this Figure can be seen in which the flow is unstable, changing from merging to parallel flow pattern and vice versa. The flow at lower impeller clearances of (C_1/T) less than 0.16 is stable and diverging for all the liquid height in the vessel except for H = T and C_1 = 0.15 T for which the flow is unstable, varying between the merging and diverging flow patterns.

In Figure 3.4 the impeller spacing between two impellers has been increased to C_2 = 0.365 T and six different flow patterns can be observed. Comparing this Figure with Figure 3.3 it can be seen that an increase of C_2 from 0.35 T to 0.365 T (i.e. by 4.5 mm) has resulted in a major change in the regions where the different flow patterns occur. A new region is present at the top right corner of Figure 3.4 where the flow is parallel. The parallel-merging instability region has moved towards the bottom left corner of the Figure and the merging flow pattern region has decreased in size. The region of merging-diverging instability has extended towards higher values of liquid height in the vessel and is now present at slightly higher C_1/T values. With C_2 = 0.365 T an unstable regime involving a transition between all the three stable flow patterns was also observed with the lower clearance of C_1 = 0.18 T and liquid height of H = 1.1 T. As this Figure suggests the changes in the flow pattern due to the variation of the lower impeller clearance C_1 for values around C_1 = 0.17 T are quite complex; different flow patterns are

observed even for very small changes of C_1 and it is often impractical, if not impossible, to distinguish between them.

Figure 3.5 shows the variation of the flow patterns for a clearance between the impellers C_2 = 0.375 T. Very detailed observations were made at this impeller spacing as the flow visualisation observations shown in this Figure were the first to be carried out and the hereto unknown complexity of the flow pattern variation revealed by this experiment prompted the extension of the investigations to different values of C_2. As shown in this Figure, a growth of the parallel flow pattern region and a displacement of the parallel-merging instability region, both towards the bottom left corner of the Figure can be seen by comparison with Figure 3.4. The stable merging flow pattern region is limited to lower liquid levels in the vessel. Similarly to C_2 = 0.365T, Figure 3.4, the flow pattern is extremely sensitive to the change in C_1 at around C_1 = 0.18 T.

The flow patterns obtained at C_2 = 0.385 T are presented in Figure 3.6 in which the merging flow pattern region has vanished and a movement of the flow regime regions towards the bottom left corner of the graph similar to those observed earlier has occurred for the parallel flow pattern region. This region is confined by the separation lines of the flow patterns to the region where $C_1 > 0.19$ T and $H > 1.05$ T. As this Figure shows, at C_1 = 0.18 T the liquid level in the tank effectively determines the type of the flow pattern in the vessel. At this impeller clearance the parallel-diverging instability occurs at higher H values ($H > 1.1$ T), while at H = T the instability is between the parallel and merging flow patterns and an unstable regime involving all the three types of the flow pattern was observed at H = 1.05 T.

Figure 3.7 presents the results of the flow visualisation performed with an impeller spacing of C_2 = 0.4 T. With this spacing only two types of flow patterns were observed, the parallel and diverging flows, depending on the lower impeller spacing which was above or below C_1 = 0.19 T respectively. No unstable flow patterns were observed in these tests.

In Figures 3.3 to 3.7, it is evident that an increase of C_2 and H results in more stable parallel flow patterns. The merging flow pattern region is very sensitive to a change in C_2 and similarly the stability of the diverging flow pattern depends critically on C_1.

Figure 3.8 shows the regions of different flow patterns obtained with an impeller rotational speed of N = 100 rpm. The clearance between the two impellers with this impeller speed was set at C_2 = 0.375 T which is the same as that of Figure 3.5. A comparison between these two Figures shows that at N = 100 rpm there is no stable merging flow pattern region, the parallel flow pattern region is limited to the top right corner of the Figure and around C_1 = 0.17 T the flow pattern is unstable, changing between parallel and diverging, while at N = 260 rpm the unstable flow in this region of the Figure varied between the merging and diverging flow patterns.

3.3 Power consumption

As mentioned in Chapter 2, the interaction of the impeller streams resulted in fluctuations of the impeller speed and torque for almost every impeller clearance. The mean and the fluctuation level of the power number were determined for the three stable (parallel, merging and diverging) and one unstable (parallel-merging) flow patterns. In order to

differentiate between the torque (and impeller speed) fluctuations as a result of interaction between the impeller streams and those fluctuations which maybe produced by the motor itself, torque measurements were also carried out for a single-impeller system (d = C = T/3 and t = 3.3 mm).

Power measurements were performed with and without a flywheel attached. The flywheel was used to minimise speed fluctuations in order to simulate the level of power number / torque and speed fluctuations in a mixing system with a powerful motor. Conversely, in the absence of the flywheel both speed and torque fluctuations were possible, as in many practical mixing systems. For all the power measurements the liquid height in the vessel was H = T.

3.3.1 Measurements without flywheel

Every measurement was repeated at least 2 - 3 times. For economy of presentation and also in order to avoid repetition, only characteristic results of these measurements are presented below, in Figures 3.9 to 3.16. In every Figure the variation of the torque (T_q), impeller rotational speed (N), consumed power (P) and power number (N_p) with time (or, equivalently, number of impeller revolution) are presented. For presentation purposes these parameters are grouped as N and T_q and as P and Np and plotted versus the number of impeller revolution in two separate graphs. However, all the variables in each impeller revolution were measured simultaneously.

Figure 3.9 shows the time history of N, T_q, P and Np for the single Rushton impeller. No clear correlation can be seen among the variations

of these four parameters. The maximum percentage fluctuations of the above parameters in this case are $(\delta N)_{max} / N = 0.6\%$, $(\delta T_q)_{max} / T_q = 1.4\%$, $(\delta Np)_{max} / P = 1.7\%$ and $(\delta Np)_{max} / Np = 2.3\%$.

Figure 3.10 shows the time history of the above parameters for both impellers (taken from the upper bridge) when the impeller streams are parallel. The variation of the speed and torque with time are opposite to each other, i.e. the higher the impeller speed the lower the torque, as might be expected. Levels of fluctuations which are higher than those for the single impeller are shown for all the parameters except for the consumed power. The maximum percentage fluctuation of the above parameters are $(\delta N)_{max} / N = 2.5\%$, $(\delta T_q)_{max} / T_q = 3.2\%$, $(\delta P)_{max} / P = 1.7\%$ and $(\delta Np)_{max} / Np = 8\%$. These values are 300%, 130%, 0.0% and 250% higher than those in the single-impeller system. It is interesting to note that the increase of the torque and speed fluctuations occurs without any increase in the power fluctuation level. However, the power fluctuations recorded in repetitions of the experiment were different and the 0% change in comparison with the single impeller noted above should not be taken as a definitive finding.

The variation of the above parameters with time for the lower impeller (lower bridge) is not the same as that for both impellers (upper bridge). As simultaneous measurements of the consumed power for the lower and the upper impeller were not possible and the two impellers continuously affect the torque characteristics of each other, the correlation between torque and speed for individual impellers could not be identified; Figure 3.11 shows the variation of the power characteristics of the lower impeller with the parallel flow pattern. Although these variations do not show any particular trend, the fluctuation levels for all the parameters

including the consumed power are higher than those of single-impeller system.

Measurements of the above mentioned parameters for two impellers in the merging flow pattern regime ($C_1 = C_2 = T/3$) are shown in Figure 3.12. The variations of T_q and N with time are similar to those when the impellers are located at $C_1 = T/4$ and $C_2 = T/2$ (parallel flow pattern). Although the fluctuation levels with the merging flow pattern shown are higher than those of the parallel flow pattern, however, as mentioned before these measurements could not be taken over a sufficiently long period of time in order to characterise the fluctuations in the power characteristics of the impellers in a statistically independent manner.

Figure 3.13 presents the time history of the impeller speed and lower impeller power characteristics for the merging flow pattern regime. The results were obtained with the lower bridge in identical conditions to those of Figure 3.12. These results are similar to the parallel flow case and particular trends can not be discerned between the variation in the impeller speed and the induced torque.

The results of the torque measurements for both impellers and for the lower impeller with diverging flow pattern in the vessel are shown in Figures 3.14 and 3.15 respectively. In contrast to the parallel and/or merging flow patterns the total required torque does not always vary inversely to the impeller speed. The reasons for this are not clear. It would be useful to obtain longer recordings of the speed/torque variation with the data acquisition system modified accordingly, in order to establish the exact nature of these variations. In addition the fluctuation

level of the parameters N, T_q, P and Np are in general smaller than the corresponding values with the parallel and the merging flow patterns.

With the parallel-merging unstable flow pattern in the vessel, particularly when the flow was in transition stage, the fluctuation level of the torque and the impeller speed was considerably higher than those with the stable flow patterns. The 'transition' stage where the flow changed from one pattern to another lasted longer than the duration of the experiments. Therefore, the coverage of the impeller speed and torque fluctuation with a single measurement was impossible. A number of measurements were made and attempts were made to take the measurements in the transition stage of the flow pattern.

Figure 3.16 shows the results of a typical measurement of the above parameters. Once again it indicates that the reverse proportionality between the impeller speed and the required torque is present except for the last cycle of the impeller rotation. The maximum percentage fluctuations of the impeller speed, required torque, consumed power and the power number are $(\delta N)_{max} / N = 4.4\%$, $(\delta T_q)_{max} / T_q = 7.5\%$, $(\delta P)_{max} / P = 4.5\%$, $(\delta Np)_{max} / Np = 15\%$ respectively. These values are roughly 100% higher than the corresponding values with the parallel flow pattern in the vessel.

3.3.2 Measurements with the flywheel

As mentioned in Chapter 2, some of the torque measurements were carried out at constant impeller speeds ($\delta N = \pm 0.5$ rpm) with the aid of a heavy flywheel coupled to the shaft. These measurements were performed over a longer period of time (40 seconds) in order to resolve

more of the torque fluctuations. The signals obtained were analysed and the fluctuation level of the power number in the form of rms (shown by $[rms]_{Np}$) was calculated by means of a specially written program run in the Vax main frame computer. The power numbers of the impellers forming unstable parallel-merging flow pattern could not be measured in the transient stage between the two flow patterns due to a significant change in impeller speed. However, the measurements were performed in two runs so that in each run the flow pattern did not change.

Figure 3.17 presents time histories of the power numbers obtained from the torque measurements of a single impeller (a) and of two impellers (b) to (e). The flow patterns with two impellers are; diverging flow pattern (b), merging flow pattern (c), parallel flow pattern (d) and parallel-merging unstable flow pattern (e). In Figures 17(b) to (d), the lower curve shows the power number of the lower impeller and the upper curve shows the total power number for both impellers. In Figure 3.17 (e) the upper curve of the total power number and the upper curve of the lower impeller power number have been obtained when the impellers generated a parallel flow pattern and the other two sets of the power number time histories have been obtained when the impellers generated a merging flow pattern, i.e. the power numbers with a parallel flow pattern measured were always higher than when the impellers produced a merging flow pattern. It must be noted that the measurements for the lower impeller and both impellers are not simultaneous as the telemetric torque measurement system employed had only one channel.

From the results shown in Figure 3.17 the variation of the single impeller power number was found to be around $(\delta Np)_{max} / Np = 3.7\%$ which is not very different from that obtained without any flywheel on the shaft

(2.3%). As Figures 3.17 (b) to (e) indicate, the variations of the power numbers for the lower impeller (lower curve) and/or both impellers (upper curve) are considerably higher than the corresponding values obtained when no flywheel was used. The maximum percentage variation of the power numbers for every flow pattern is typically 25% except for the lower impeller with the diverging flow pattern for which a value of 12.5% was obtained. The maximum percentage variation of the power number with each of the two different flow patterns in the unstable flow regime was also around 25%.

Torque measurements for the three stable flow patterns were performed at different impeller speeds and the mean values of the power numbers are presented in Figures 3.18 and 3.19 for the lower impeller and for the two impellers respectively. In the range of impeller speed N = 100 - 250 rpm the variation of Np was very small. The highest total power number (Np = 10) was measured with the parallel flow pattern in the vessel at N = 250 rpm and the lowest total power number (Np = 8) was obtained with the merging flow pattern at N = 100 rpm. The power number of the upper impeller (determined by subtracting the Np for the lower impeller from the Np for both impellers) was highest Np = 5.3 with the diverging flow pattern. With the merging and diverging flow patterns the lower impeller power numbers were almost the same (Np = 4.1).

Effect of C_2 on the mean and rms values of the power numbers, N = 250 rpm

With the lower impeller located at C_1 = T/4, power measurements were performed with various impeller spacings between the two impellers. The mean and rms values of these measurements are presented in Figure 3.20 for the lower impeller and Figure 3.21 for both impellers.

Figure 3.20 indicates a slight drop on the mean power number as the impeller spacing increases from C_2 = 0.25T to C_2 = 0.35T after which the mean power number starts increasing. A step rise of the mean power number can be seen at the impeller spacing C_2 = 0.385T where the flow pattern is unstable. In general the fluctuation level, $[rms]_{Np}$, increases with increasing impeller spacing and the two values at C_2 = 0.385T have been obtained with the two different patterns of the unstable flow. The rms values are about 0.15 - 0.22 and the corresponding range of power number fluctuation, i.e. the range of $\pm$ 3.5 x $[rms]_{Np}$, is around 25% of the mean value).

Figure 3.21 shows that the total power number of the touching impellers (C_2 = 0.068T) is Np = 6.6. This is around 18% higher than the power number obtained for single impeller, (see Figure 4.1, Chapter 4). This percentage increase is lower than that reported by Hudcova et al (1989) which was 30%. This variation is expected to be due to the different liquid heights used in the present investigation (H = T) and by Hudcova et al (H = 2T) as the liquid level above the impeller influences the power number (Bader 1986).

Figure 3.21 also indicates that the mean total power number has increased by 25% as C_2 has increased from 0.068T (touching impellers) to 0.25T. In the spacings between C_2 = 0.25T to C_2 = 0.385T, for which the flow pattern is always merging, an almost constant value has been obtained for the total mean power number (Np = 8.3). Similarly with the parallel flow pattern (C_2 > 0.385T), the total mean power number does not change much with C_2. Similar to the results obtained for the lower impeller

Figure 3.21 shows a nearly linear increase of $[rms]_{Np}$ as the clearance between the two impellers increases.

The intensity of the fluctuation {i.e. the normalised value $[rms]_{Np}$ / Np obtained from the results of Figures 3.20 and 3.21} is shown together with the mean values of the power numbers in Figures 3.22 and 3.23 for the lower impeller and two impellers respectively. The intensity of fluctuation is a useful parameter as it allows a relative assessment of the mean and rms variation through a single value. Both Figures show that the fluctuation intensity increases with the spacing between the impellers up to $C_2 = 0.385T$ after which the fluctuation intensity drops.

Effect of misalignment of the impellers blades

With a merging flow pattern in the vessel ($C_1 = C_2 = T/4$), torque measurements were carried out with the impellers located with 30° misalignment in their blades and the Np and $[rms]_{Np}$ values were compared with the corresponding values obtained with aligned blades. These comparisons are shown in Figures 3.24 and 3.25 for the Np and $[rms]_{Np}$ respectively. No difference can be seen in the mean values and the rms values are only slightly smaller (by around 5%) when the impellers blades are misaligned.

3.4 Mixing time studies

Employing the conductivity technique outlined in Chapter 2 mixing time measurements were carried out with the probe located at different parts of the vessel as shown in Figure 3.26. In particular, the effect of instability of the flow pattern on the mixing time was investigated. The

measurements were performed with stable parallel, stable merging and unstable parallel-merging flow patterns. It is interesting to look at the shape of the concentration traces obtained at different parts of the vessel and with different flow patterns before presenting the quantitative results of the measurements.

3.4.1 Concentration traces

Approximately 400 conductivity measurements were performed. The analysis of the data from a typical obtained trace was described in Chapter 2 (shown in Figure 2.11). As inclusion of all these results in the thesis is not possible, only three typical traces obtained at locations with different flow conditions will be presented and the effect of the flow on the concentration fluctuations will be discussed. These three traces were obtained with parallel and merging flow patterns and the first trace is presented in two Figures considering the two types of mean concentration, $C_{m1}(t)$ and $C_{m2}(t)$, to obtain the concentration fluctuations as discussed in Sections 2.4.2 and 2.4.3.

The time history of the voltage (or concentration) variation shown in Figure 3.27(a) (or Figure 3.27(b)), is the same as that presented in Figure 3.28(a) (or Figure 3.28(b) respectively). This trace was obtained from the measurement carried out with the parallel flow pattern with the probe located at the boundaries of the two middle ring vortices ($z = T/2$, $r = 80$ mm and $\theta = 0^{\circ}$).

Generally in Figure 3.27(b) two types of fluctuation can be observed, one due to the passage of tracer parcels through the probe (with higher fluctuation levels and lower frequencies), and the other one due to the

passage of small tracer-containing eddies through the probe (with smaller fluctuation levels and higher frequencies). As the mixing process approaches completion, the fluctuations due to the parcel passages decay considerably. This is due to the breakage of the big parcels into small ones as the process proceeds. The time intervals between the peaks shown in Figure 3.27(b) indicate the residence times of tracer fluid parcels in the ring vortices. The time intervals between these peaks vary considerably more than those recorded by Holmes et al (1964) with one impeller in the vessel. This can be expected as the number of ring vortices and the intensity of circulation is higher in the two-impeller system.

Figures 3.27(c) and 3.28(c) show the variation with time of the mean concentrations C_{m1} and C_{m2} respectively. Figures 3.27(d) and 3.28(d) present the time history of the concentration fluctuation with respect to the corresponding mean concentration history. An attempt was made to correlate the concentration rms values obtained from these fluctuation levels to the local mean and/or rms velocities but not particular trend was found. However, the concentration fluctuation shown in Figure 3.27(d) demonstrates only the second type of fluctuation mentioned earlier. Figure 3.27(e), the same as Figure 3.28(e), shows the concentration history in normalised form from the start of insertion to the time that the mixing is completed to the degree of mixing as discussed in Section 2.4.3, Chapter 2.

The concentration recording of Figure 3.27 or 3.28 was obtained in the 'bulk flow' region of the vessel and can be compared with one obtained in the impeller stream under identical conditions, which is presented in Figures 3.29(a) - (e). Although the concentration fluctuation for both

traces is quite random, some distinctions can be made between them. It can be seen that in Figure 3.29(b) the concentration fluctuation level in the impeller stream is significantly higher 3 seconds after the start of the insertion. The instantaneous concentration level reaches almost 1.2 times the final concentration, indicating a direct crossing of the impeller stream by a parcel of concentrated tracer. This does not in general happen in the bulk flow where the fluctuations are smaller. The fluctuation frequency in Figure 3.29 is higher in comparison with that of Figure 3.28; this result is expected to be due to the higher velocity and consequently smaller mixing time scales in the impeller stream.

Similarly, the concentration traces shown in Figures 3.28 and 3.30, which were recorded at the same location but with different impeller clearances and therefore flow patterns, may be compared to determine the significance of the change in C_2 which has resulted in a change of flow pattern from parallel to merging. The point of measurement with the merging flow pattern is in the meeting region of the two inclined impeller streams while with the parallel flow pattern this point lies in the boundaries of the two middle vortices as discussed in the flow visualisation section 3.2.2. The concentration fluctuation level with the merging flow pattern is significantly higher than that of Figure 3.28. It is even higher than that of the trace obtained in the impeller stream with the parallel flow pattern (Figure 3.29). From this Figure it may be concluded that a significant amount of the inserted tracer is forced to move directly to this region during the insertion and this may explain a relatively shorter mixing time obtained in the merging flow pattern in comparison with the parallel one as will be discussed later.

3.4.2 Mixing time results

Single Rushton impeller

Measurements of mixing time were obtained with a single Rushton impeller to allow comparisons with the results of two Rushton impellers, as discussed in detail in the following Chapter.

The Rushton impeller employed for these measurements (d = T/3 and t = 1.65 mm) was located at a clearance of C = T/3 from the base of the vessel and was rotating at a speed of N = 200 rpm. The tracer was inserted at r = 75 mm, $\theta = -135^{\circ}$ on the free surface. The insertion time was 5 ± 0.5 seconds and measurements were carried out for five different probe locations at $\theta = 0^{\circ}$ r-z plane. One location was in the impeller stream, two in the lower ring vortex and two in the upper ring vortex as shown in Figure 3.26(a). The average mixing time obtained from these measurements was around 12.8 seconds.

Double Rushton impeller

Figures 3.31 to 3.33 show the effect of impeller spacing on the local mixing time.

In all of these Figures the symmetry of the impeller locations with respect to the liquid level in the vessel, H, was maintained, i.e. $C_1 = C_3$, and the spacing between two impellers was changed to vary the flow pattern. The tracer insertion time in all the experiments was 6.5 ± 0.5 seconds. The mixing time measurements were carried out at the same plane as that of the flow visualisation observations ($\theta = 0^{\circ}$) at the eight locations shown in Figure 3.26 (b).

Figure 3.31 shows the results of the measurements at three different locations, points 2, 5 and 8 in Figure 3.26 (b), in parallel, merging and unstable parallel-merging flow patterns. With the merging flow pattern, C_2 = T/3, almost identical mixing times were obtained for all the three locations. However, with the parallel flow pattern, C_2 = T/2, a significantly higher (by around 30%) value of mixing time was obtained at the lowest of these three locations. This difference may indicate that an amount of tracer is trapped in the upper ring vortices of the parallel flow pattern during the measurement. From the flow visualisation experiments described earlier it may be expected that the mixing across the vortices generated by each impeller is less vigorous with parallel impeller streams than with merging streams. This Figure also shows that the variation of the mixing time with impeller spacing C_2 is almost the same for all the results obtained at these three locations. The increase in the mixing time with the unstable flow pattern is evident, particularly when compared with the merging flow pattern.

Figure 3.32 shows the mixing times obtained at two locations, at impellers elevations at r = 80 mm (locations 3 and 6 in Figure 3.26-b). These two locations are in the impeller streams when the flow pattern is parallel and in the 'bulk flow' when the flow pattern is merging. The rise of the mixing time when the flow pattern becomes unstable (i.e. for C_2/T = 0.385) is more clear from this Figure. Similarly to the results shown in Figure 3.31, a shorter mixing time occurs for merging flow pattern. The mixing times with the parallel flow pattern in general have values between those with the merging and the unstable flow patterns.

The results at the locations with the same elevations as of those shown in Figure 3.31 but at a radius of r = 30 mm are presented in Figure 3.33. In this Figure the shortest mixing times are shown to be obtained at the mid height of the vessel (i.e. at $z = C_1 + C_2/2$ in all the impeller spacings (C_2). This is similar to the results presented in Figure 3.31. Also the variation of the mixing time with the impeller spacing between the two impellers is similar to that of the measurements obtained in the other locations.

From the above discussion the following conclusion may be drawn: The increase in mixing time when the flow pattern becomes unstable, i.e. for $C_2 = 0.385T$ is evident from almost all of the graphs. Shorter mixing times were obtained with the merging flow pattern which is likely to be due to the directions of the impeller streams resulting in the tracer to be drawn rapidly to the lower part of the vessel. In this way the inserted solution is dispersed quickly and also the liquid contained in the vessel is circulated more frequently. The mixing time for the parallel flow pattern has in general values between those for the unstable and those for the merging flows. The lowest mixing time for all the spacings was recorded at the centre of the vessel, at z = T/2 and r = 30 mm. The variation of the local mixing time from point to point is significantly lower in the merging flow pattern in comparison with those of parallel and unstable flow pattern.

The mean mixing time over the whole of the vessel obtained from recordings at eight points (see Figure 3.26-b) is presented in Figure 3.34. The variation of the mixing time with C_2/T is similar to the local results and confirms the above findings. This last result shows clearly the effect of flow pattern on the mixing time and is therefore useful for mixing

process design as it indicates the clearances which result in unstable flows and should be avoided.

In the mixing literature, many investigators have used a pulse injection to study mixing times. In the present work different insertion times were used. However, the variation of mixing time with insertion time was found to be linear as shown in Figure 3.35. The measurements in this Figure were obtained with the parallel and merging flow patterns and each measurement was repeated 3 to 4 times. Both curves show a linear variation of mixing time with insertion time and the mixing times are longer when the flow pattern is parallel, as might be expected from the above results.

The results of the flow visualisation, power consumption and mixing time measurements presented in preceding sections have indicated clearly that significant variations in mixing performance occur with relatively small alterations of the impeller spacings. The lowest total power consumption and shortest overall mixing time are present with the merging flow pattern. This is clearly the desirable regime for minimising blending time. In contrast, the unstable flow regimes at the transition from merging to parallel flow patterns are the least efficient in terms of mixing time and should be avoided in process design, unless, of course, they meet specific process requirements. On the other hand, when high power consumption per unit volume is desirable for mixing, a parallel flow regime may be preferable.

The above findings indicate clearly the need for more experimentation in vessels with H > T with 2 or 3 impellers, to establish the flow patterns and mixing time and Np variations for such geometries. In addition as the

majority of the above parameters has provided information about quantities averaged over the whole fluid volume in the tank, it would be useful to determine the differences from one location to another. For this purpose the distribution of the mean flow and turbulence in the tank was investigated and is described in the following section.

3.5 Velocity and turbulence distribution

3.5.1 Single Rushton impeller

In order to compare the measurements with already published data and to verify the accuracy of the LDA technique employed, the radial mean and rms velocities were measured in the impeller stream of a single Rushton impeller with a diameter of d = T/3 and a thickness of t = 3.3 mm located at a clearance of C = T/3 from the vessel base. The measurements were carried out at the $\theta = 0^{\circ}$ r-z plane and a radius of r = 51 mm with an impeller speed of N = 250 rpm.

The results were normalised by the impeller tip speed ($V_{tip} = \pi N d$) and are shown in Figure 3.36. It can be seen that they are in good agreement with the data obtained by Yianneskis (1982a). This Figure also indicates the upward inclination of the impeller stream which was observed in the flow visualisation. The maximum radial mean velocity was measured at 1 mm above the impeller elevation and valued at $V = 0.71\ V_{tip}$. This value was higher with thinner impellers as will be discussed in Chapter 4.

In this Figure three small peaks can be seen in the normalised rms velocity profile. The middle peak is likely to be due to broadening effects as the measurements were carried out over 360° of impeller rotation. The

variation of the rms values in the measurement locations was from $0.19V_{tip}$ at 1 mm below the lower edge of the impeller blade to 0.34 V_{tip} at the impeller elevation.

3.5.2 Comparison between single and double impeller system

In order to compare the performance of a Rushton impeller in both single- and two-impeller agitation systems, LDA measurements were made with a single Rushton impeller located at a clearance of C = T/4 from the base of the vessel and with two impellers in the parallel flow regime. For the latter the Rushton impellers were located with clearances of C_1 = T/4 and C_2 = T/2. In this way the location of the lower impeller is the same as that for the single impeller system. The Rushton impellers employed in these comparative measurements had a diameter d = T/3 and a thickness t = 1.65 mm.

The measurements were carried out at the $\theta = 0^{\circ}$ r-z plane and at r = 51, 70 and 85 mm in the impeller stream with an impeller speed of N = 250 rpm. These measurements are presented in Figures 3.37 to 3.39 for the radial mean velocities and in Figures 3.40 to 3.42 for the radial rms velocities. In these Figures the elevation of each impeller in both the single- and two-impeller systems was taken as the origin of the axial co-ordinate of the measurement locations (z') and z' is positive for the locations above the impeller elevation. Figure 3.37 shows the radial components of the mean velocities obtained at r = 51 mm (2 mm away from the impeller tip). The velocity profiles generated by the lower and the upper impeller in the two-impeller system are almost identical but differ from that produced by the single impeller. The velocities measured at the upper half of the single impeller are typically 15% higher than

those measured at similar locations of the upper and/or the lower impeller.

The lower velocities produced by the two Rushton impellers are probably due to the fact that roughly half of the impeller stream issued by each impeller is redirected, by the vessel wall, towards the other impeller and restricts the flow generated by the other impeller to some extent. The above results indicate that in a single-impeller system the flow number which is given by:

$$F_l = \frac{\int_{-h/2}^{+h/2} V \, dz'}{N d^3} \qquad (3.1)$$

is higher and the impeller stream is inclined upwards. The former finding is discussed further in the following Chapter. The latter finding was observed in the results of the flow visualisation and is in agreement with the observations reported by Yianneskis et al (1987).

The distinction between the radial velocity profiles obtained for a single- and a two-impeller system is clearer from the measurements presented in Figures 3.38 and 3.39 which were carried out at radii of r = 70 and 85 mm respectively. A small inclination of the single impeller stream towards the free surface can be observed for the single-impeller system, while there is a slight inclination of the lower and no inclination of the upper impeller stream in the two-impeller system. The maximum mean velocities measured at these radii are higher with the single impeller as was the case at r = 51 mm.

Figure 3.40 shows a comparison of the rms velocity profiles measured in the three impeller streams at r = 51 mm. The velocities measured in

every location are almost the same as the differences are within the experimental error. However, in the two-impeller system the upper impeller appears to generate slightly higher turbulence levels than the lower one. The skewness of the rms velocity profile produced by the single impeller can be expected to be due to the inclination of the impeller stream and the correspondingly different locations of the associated velocity gradients. This skewness is shown more clearly in the results of the measurements presented in Figure 3.41 which are obtained at a radius of r = 70 mm. Also from this Figure the skewness of the lower impeller rms profile can be noted in comparison to profile for the upper impeller.

Figure 3.42 compares the rms velocities obtained by the single and by the lower and the upper impellers at a radius of r = 85 mm. At this radius the rms velocities obtained with the single impeller are slightly lower than those obtained by the other two impellers probably due to the influence of the impeller streams on each other in the two impeller-system, as mentioned earlier.

3.5.3 Mean and rms velocity distributions with two Rushton impellers

Detailed LDA measurements were carried out to quantify the three stable flow patterns identified by the flow visualisation results. In order to be sure about the stability of every flow pattern studied, the impeller spacings for all the flow patterns were selected as far away as possible from the critical values. These spacings were; C_1 = T/4 and C_2 = T/2 for the parallel, $C_1 = C_2$ = T/3 for the merging, C_1 = 0.15T and C_2 = T/2 for the diverging flow patterns. Seven radial positions r = 20, 51, 70, 85, 115, 130 and 140 mm were selected for the measurement locations and in

the impeller region small intervals of 1-2 mm were chosen along the z-axis. The measurements were made with two Rushton impellers with symmetrical hubs, diameter d = T/3 and impeller thickness t = 1.65 mm. All the measurements were carried out with an impeller rotational speed of N = 250 rpm in the $\theta = 0^{\circ}$ r-z plane.

The axial, radial and tangential components of the mean and rms velocities with the three different stable flow patterns are presented in Figures 3.43 - 3.60. For comparative purposes the velocity scales in all these Figures were chosen to be identical. Positive mean velocities indicate velocities in the upward direction for the axial component, towards the vessel wall for the radial component and in the direction of the impeller rotation for the tangential component.

Parallel flow pattern

Figures 3.43 - 3.48 show the three components of the mean and rms velocity profiles with the parallel flow pattern in the vessel. The profiles of the axial components of mean velocities are presented in Figure 3.43. They show near zero values at a height of z = 150 mm. These locations lie in the boundary of the two middle vortices observed in the flow visualisation. The measured mean velocities in the impeller stream and close to the impeller, also have near zero values. Away from the impeller, positive and negative mean velocity values were obtained in the upper and lower side of each of the impeller streams respectively, indicating the spreading of the flow away from the impeller region in both streams.

At a radius of around 112 mm in the bulk flow the axial velocities change sign. This indicates the radial locations of the centres of the vortices. Higher velocities occur along the vessel wall in comparison with the flow along the shaft and the inner part of the vessel. These higher velocities are associated with the re-direction of the impeller stream into wall jets along the vessel perimeter.

Figure 3.44 shows the distribution of the rms velocities in the vessel with this flow pattern. Higher turbulence levels can be seen in both the impeller streams in the vicinity of the impeller, partly due to the larger velocity gradients and the periodicity of the flow in those regions. The measured values show that the turbulence levels generated by the upper impeller are slightly higher than those produced by the lower impeller. It must be noted, however, that these differences are generally small and in many locations well within the experimental error.

Figure 3.45 shows the distribution of the radial mean velocities in the vessel for the parallel flow pattern. The spread of the impeller stream generated by each impeller is clearer from this Figure. The maximum velocities which occur at the impeller elevations decrease linearly with increasing radius of the measurement point. This linear variation can be described by the equation,

$$V = 1.34 - 8.86\, r \qquad (3.2)$$

where V is in m/s and r in meters. The measured velocities at a radius of r = 20 mm are small but negative. At all other radii positive values are found in the impeller stream and negative values in the bulk flow. Large negative values of the mean velocity were measured at elevations of around z = 11, 150 and 270 mm and at radii of r = 85 and 115 mm, as

might be expected as these measurement locations lie in the boundaries of the ring vortices.

As mentioned earlier, from the interpolation of the results in Figure 3.43 zero axial mean velocities were obtained at a radius of around r = 112 mm. On the other hand, Figure 3.45 indicates that at this radius the mean radial velocities change sign at elevations z = 40, 105, 185 and 250 mm. Therefore the centres of the four ring vortices are expected to be at these locations.

The corresponding rms values for the mean velocities shown in Figure 3.45 are presented in Figure 3.46. Higher rms values can be seen in the vicinity of the impeller streams: higher values are encountered at r = 51, 70 and 85 mm. The lowest rms values were measured at elevations of z = 11, 150 and 270 mm and in radii greater than r = 85 mm. These regions lie in the boundaries of the vortices where there is relatively little turbulence present.

As described in Chapter 2, direct measurement of the tangential mean and rms velocity components was not possible at small radii due to the optical access limitations or significant beam refraction by the baffles. For this reason, the tangential components were obtained from two measurements. Therefore, the experimental error is expected to be larger and as a result there is some scatter in the mean and rms velocity profiles presented in Figures 3.47 and 3.48 respectively. Comparison of Figures 3.45 and 3.47 shows that the tangential component of the mean velocity at the tip of the impellers is higher (by about 10%) than the radial component. This is in agreement with the findings of Yianneskis (1982a) for a single-impeller system.

The velocity profiles at r = 51 mm show more spread for the tangential component, in agreement with the findings of Cooper and Wolf (1968) for a single-impeller system. In addition, although the tangential component in the impeller streams decays quickly with increasing distance from the impeller tip, higher values of tangential mean velocities were measured in the vicinity of the wall in comparison with the radial component. As can be seen from Figure 3.47 almost all the measured values are positive indicating that the mean flow direction is the same as the impeller rotational direction at all measurement locations. This might be expected to be the result of the presence of the two impellers: in contrast Yianneskis (1982a) found that with a single Rushton impeller there were some regions of counter-rotating flow, especially below the impeller.

Similar to the tangential mean velocity results the measured rms values in Figure 3.48 show higher values in the impeller vicinity. Comparing this Figure with the corresponding radial rms velocities, the tangential rms values at the mid height of the vessel and in the vicinity of the shaft are lower than the radial ones. The reverse occurs at the same height near the vessel wall.

Merging flow pattern

The three components of the mean velocities and turbulence levels measured with this flow pattern are presented in Figures 3.49 - 3.54. Figure 3.49 shows that high axial mean velocities occur above the lower impeller and below the upper impeller, at a radius of r = 70 mm. The peaks in the velocity profiles are found nearer the vessel wall as the

impeller streams approach each other. Similarly to the results obtained with the parallel flow pattern, higher velocities occur along the vessel wall in comparison with the flow around the shaft.

Zero axial mean velocities were measured at a height of z = 150 mm indicating the division of the flow field in the vessel: This indicates that two flow cells are found, one by the lower and one by the upper impeller. This was also the case with the parallel flow pattern. The flow direction changes at almost all elevations at a radius of around r = 115 mm. This is the point where the impeller streams meet at the central part of the vessel. The radii of the centres of the two ring vortices, one below the lower impeller and one above the upper impeller are also at r = 115 mm. In the region confined between the two impellers the axial mean velocities are very small and practically zero in some locations close to the upper impeller.

The axial rms velocities corresponding to the mean values shown in Figure 3.49 are presented in Figure 3.50. Higher levels can be observed in the impeller streams while there is little variation in the bulk flow: the rms profiles there are quite uniform. The maximum rms values were measured in the vicinity of the impellers, in the impeller stream. However, these values may be also associated with the periodicity of the flow and the trailing vortices behind the blades.

Figure 3.51 shows the profiles of the radial mean velocities with the merging flow pattern in the vessel. The maximum velocities were measured in the vicinity of both the impellers (r = 51 mm), at 4 mm above the lower impeller elevation and at the same distance below the upper impeller elevation. These velocities were almost equal and valued

at 0.82 m/s. The peaks of these profiles (occurring in the impeller streams) move towards each other as the flows move away from the impellers and the impeller streams merge. A small reverse flow exists immediately above the upper impeller and below the lower impeller and at a radius of r = 51 mm. The velocities in the bulk flow are much smaller than those obtained with the parallel flow pattern (Figure 3.45). The reverse flow (i.e. towards the shaft) between the impellers begins to form at a radius of less than 85 mm and causes the small and not well-defined vortices observed between the impellers in the flow visualisation.

Figure 3.52 shows the distribution of the radial rms velocities in the vessel with this flow pattern. In general the turbulence levels are slightly higher in the impeller stream (closer to the impellers) and lower in the bulk flow in comparison to the corresponding values with the parallel flow pattern in the vessel (presented in Figure 3.46).

The tangential mean and rms velocity profiles are presented in Figures 3.53 and 3.54 respectively. At a radius of r = 20 mm in the region between the two impellers, mean tangential velocities of around 0.5 m/s were measured. These mean velocities are considerably higher than the corresponding values measured with the parallel flow pattern in the vessel. The directions of the impeller streams are clearly indicated by the profiles. The rate of decay of the mean tangential velocities with increasing radius in the impeller streams, is almost the same as for the radial components, while this was not the case with the parallel flow pattern.

The profiles of tangential rms velocities show almost uniform values at radii greater than 115 mm (Figure 3.54). The turbulence levels in the

region above the upper impeller and at radii less than 70 mm are higher than the corresponding levels below the lower impeller. This is expected to be caused by the whirlpool-type vortex as occasionally the free-surface vortex crosses these measurement locations at regular intervals as it precesses around the shaft.

Diverging flow pattern

Figure 3.55 shows the distribution of the axial mean velocities with the diverging flow pattern in the vessel. As this Figure indicates the mean velocities are zero at a height of around z = 100 mm. This indicates the unequal division of the flow field in the vessel by the two impellers. At a radius of r = 115 mm the mean velocities change sign in all elevations. Relatively higher mean velocities were measured above and below the upper impeller in comparison with the velocity data measured in the same locations with respect to the upper impeller with the parallel flow pattern. The shape of the profiles under the lower impeller at radii of between 51 mm and 115 mm reveals the direction of the lower impeller stream towards the vessel bottom that was observed in the flow visualisation.

Figure 3.56 shows the axial rms velocity distribution in the vessel with this flow pattern. No significant difference exists in the bulk flow among the measured values. Slightly higher values of the axial components of turbulence level were measured at the vicinity of the lower impeller in comparison with those measured near the upper impeller.

The measurements of the radial mean and rms velocities are shown in Figures 3.57 and 3.58 respectively. Negative mean radial velocities are

found in the vicinity of the lower impeller at r = 51 mm, along the upper half of the impeller blade. These velocities are larger than those obtained at the edges of both impellers with the merging flow pattern (Figure 3.51).

Comparing Figures 3.55 and 3.57, the centres of the vortices, i.e. the locations where the mean velocities in r and z directions are both zero can be identified. The centre of the bigger vortex generated by the lower impeller lies around a point at r = 115 mm and z = 50 mm. The centre for the lower vortex of the upper impeller is around r = 115 mm and z = 150 mm while the corresponding location of the centre of the top vortex is around r = 115 mm and z = 235 mm. The existence of a smaller vortex immediately below the lower impeller, which was indeed observed in flow visualisation, is supported by the reverse flow occurring under the impeller at radii of r = 20 and 51 mm.

Figure 3.58 shows the distribution of the radial rms velocities and like that of the axial rms velocities, Figure 3.56, the v values are uniform everywhere except for the impeller streams. In comparison with the parallel flow pattern lower turbulence levels were measured in the bulk flow in the diverging flow case.

Finally the tangential mean and rms velocity distributions are presented in Figures 3.59 and 3.60 respectively. The mean tangential velocities measured between the impellers show that this pattern is the only one, among the three quantified flow patterns, in which some negative tangential mean velocities are present in the flow. The reverse flow occurs in the region around r = 85 mm and z = 120 mm. The flow under the lower impeller is highly rotational, with a typical mean velocity value

of around 0.5 m/s. The highest value for the mean velocity was measured in the vicinity of the upper impeller at z = 192 mm and is valued at 1.08 m/s. This is 15% higher than the highest value measured in the lower impeller vicinity. Again little variation can be found in the bulk of the flow from the measurements of tangential rms velocity results presented in Figure 3.60 other than in the impeller stream profiles.

3.5.4 Velocity vectors

The axial and radial mean velocities presented in Figures 3.43 and 3.45 for the parallel flow pattern, Figures 3.49 and 3.51 for the merging flow pattern and Figures 3.55 and 3.57 for the diverging flow patterns, have been plotted as velocity vectors in the $\theta = 0^{\circ}$ r-z plane and are presented in Figures 3.61, 3.62 and 3.65 for the parallel, merging and diverging flow patterns respectively. In order to have a clear presentation of the results some of the velocity vectors, particularly in impeller streams, have been deleted and for comparative purposes the velocity scales for all the flow patterns were chosen to be the same. The velocities with the merging flow pattern are also shown in three-dimensional form $(\vec{U} + \vec{V} + \vec{W})$ in Figure 3.63. The same velocities in the impeller region are presented in larger scale in Figure 3.64.

The three-dimensional vectors were plotted in order to help visualise better the flow pattern in the vessel. The rectangular cross section vectors help indicate, by means of the perspective of the three-dimensional arrow body and tip, the turning of the flow in a direction perpendicular to the plane of measurement. The magnitude and direction of the tangential velocity component for the merging flow pattern can be clearly assessed from the orientation of the vectors in Figures 3.63 and 3.64.

From the velocity vectors shown in Figure 3.61 (parallel flow pattern) the entrainment from both sides of the impeller streams can be seen at radii between 51 and 85 mm. The flow entrainment to the impeller streams forming the merging flow pattern (Figure 3.62) occurs only from the upper side of the upper impeller stream and the lower side of the lower impeller stream at the same radii as for the parallel flow pattern. In the case of the diverging flow pattern (Figure 3.65) the flow entrainment to the upper impeller stream is similar to that of the parallel impeller streams (Figure 3.61) but with a higher rate. The flow entrainment for the lower impeller stream of the diverging flow pattern occurs only from the upper side of the stream.

Comparing the flow in the impeller streams for the parallel and merging flow patterns (Figures 3.61 and 3.62), although the mean velocity values near the impellers have not changed significantly, the mean velocities in the rest of the streams away from the impellers, are smaller with the merging flow pattern, by around 50%. This is also true for the radial velocity components in the bulk flow except in the vicinity of the wall. It must be noted, however, that the tangential velocities in the bulk flow surrounding the impellers were much higher with the merging flow pattern than the corresponding velocities in the parallel flow pattern. In Figure 3.62 the nearly-linear impeller stream paths and also the meeting point of the impeller streams for the merging flow pattern can be seen.

Similarly the inclination of the lower impeller stream in the diverging flow pattern can be clearly observed in Figure 3.65. The flow in the vicinity of the impeller at the top half height of the impeller blade is directed towards the vessel axis. The impeller stream is directed towards

the vessel base at an average angle of around 30° to the horizontal in the impeller vicinity and at 60° to the horizontal close to the vessel bottom. The impeller stream flow meets the bottom of the vessel at around r = 70 mm.

The diverging flow pattern might be usefully employed in practical situations where lifting of solids from the vessel bottom is required. The sweeping action of the lower impeller stream should be beneficial in this respect and small values of the C_1 clearance should be employed for such purposes.

The flow of the upper impeller stream in this case is similar to the impeller stream of the parallel flow pattern except for a slight increase of the mean velocities measured with the diverging flow pattern. This may be expected due to the weaker interaction between the impeller streams of the diverging flow pattern. The division of the flow field in the vessel by the two impellers into two cells discussed earlier is more prominent in this case. The vortices observed in the flow visualisation for all the stable patterns have been confirmed by the velocity vectors presented above (Figures 3.61 to 3.65).

3.5.5 Turbulence level and kinetic energy contour plots

In order to aid the interpretation of the results, the turbulence components measured in all the three stable flow patterns have been plotted in contour form in Figures 3.66 3.67 and 3.68 (for the parallel, merging and diverging flow patterns respectively). In every Figure a, b and c indicate the axial, radial and tangential component of the rms velocities respectively.

In Figure 3.66 (parallel flow pattern) rms values of above 0.3 m/s can be seen for all the three components in the impeller stream close to the impeller. The width of the axial component distribution in which higher rms values were measured (Figure 3.66-a), is greater than the corresponding radial one (Figure 3.66-b). This higher rms area is limited to a smaller region for the tangential component (Figure 3.66-c) then for the radial component.

Close to the vessel wall and near the middle of the vessel the axial contours show higher values of around 0.18 m/s compared with values below 0.1 m/s in the radial component distribution. The three components of the rms velocities measured at the centre of the r-z plane are similar, typically around 0.16 m/s. The axial rms velocities measured in the region between the impellers and at r = 51 mm are typically 0.1 m/s which is lower than the other two components.

Figure 3.67 shows distributions of the three components of the rms velocities measured with the merging flow pattern in the vessel. Rms values of above 0.3 m/s are again shown in the impeller streams close to the impellers. At the point where the impeller streams meet, the values of radial and tangential rms components are almost the same, around 0.17 m/s. The axial component values at the same locations have however significantly higher values, around 0.27 m/s.

There are similarities in the distribution of the rms velocities in the bulk flow between the radial and tangential components; higher values of rms velocities, typically 0.16 m/s, occur close to the shaft and lower values, typically 0.1 m/s, close to the wall. The reverse happens with the

distribution of the axial rms component with relatively lower values of u near the shaft.

In the region below the lower impeller a maximum of around 0.2 m/s was measured for the radial component and a minimum of 0.1 m/s for the axial component. There is little difference between the radial and tangential components in the flow between the impellers and these velocities are typically around 0.14 m/s. This value is comparable to the axial component which is around 0.12 m/s.

The distributions of the three rms velocity components with the diverging flow pattern in the vessel are presented in Figures 3.68(a - c). At first glance significantly lower axial rms velocity values of less than 0.1 m/s can be seen in the bulk flow of this flow pattern compared with the other two cases (parallel and merging flow patterns). In the lower part of the vessel close to the wall (z = 110 mm) the radial and tangential rms velocities are around 0.1 m/s which is about 60% of the axial component.

In the region above the upper impeller there is little variation between the shaft and the wall, where both u and v are typically 0.1 m/s. The tangential rms velocities measured in these locations are only a little different from the axial and radial velocities. In the locations close to the shaft at z greater than 200 mm, w was slightly higher, around 0.14 m/s, while close to the vessel w is similar to the axial and radial component values. The maximum rms velocity component measured in the region between the impellers was the tangential one, valued at about 0.18 m/s and the minimum in this region was measured in the axial component, which was less than 0.1 m/s.

Comparing the radial rms velocity contours in the Figure 3.68-b with that of parallel flow pattern (Figure 3.66-b), the difference between the length and width of the higher rms velocity regions in the impeller stream of the upper impeller can be noticed. This region is longer and thinner with the diverging flow pattern, as was the case with the mean velocity results. As mentioned before this is likely to be due to the direction of the impeller streams in the two flow patterns and therefore the weaker interaction between the impeller streams in the diverging flow pattern.

From a comparison of these Figures (3.66 to 3.68) it may be concluded that, on average, higher values of turbulence levels are found in the impeller regions for the merging flow pattern in comparison with the parallel flow pattern while in the bulk flow the reverse occurs. With the diverging flow pattern the turbulence levels are significantly lower than the values with the other two patterns, particularly for the axial and radial components.

Figures 3.66 - 3.68 indicate clearly that the turbulence with all three flow patterns is anisotropic. Although the distributions of u, v and w are similar in the vicinity of the impellers, there are differences in the magnitude and/or distribution of the three turbulence levels there as well. An assumption of isotropy in the impeller stream should therefore be used only as an approximation. As a result, predictions of the flow employing turbulence models which assume isotropic turbulence might not represent accurately the flow characteristics.

Figures 3.69 to 3.71 show the distribution of the turbulence kinetic energy for the three flow patterns in the same order as above. The turbulence kinetic energy is given by:

$$k = \frac{1}{2}(u^2 + v^2 + w^2) \qquad (3.3)$$

A comparison of the turbulence kinetic energy generated with the three flow patterns can be made very clearly from these Figures. As expected from the rms velocity contours presented above the maximum turbulence kinetic energy occurs in the impeller streams with all flow patterns. In general, the variation of the k, measured in the bulk flow of the parallel flow pattern is more than that of the merging flow patterns, (i.e. steeper gradients of k in the bulk flow of the parallel flow pattern). This variation is the smallest with the diverging flow pattern in comparison to the other two patterns.

In the parallel flow pattern shown in Figure 3 69, the lowest turbulence kinetic energy levels are around 0.02 m^2/s^2 and are found near the wall and the free surface and bottom of the vessel. k in these regions is at least ten times lower than those in the vicinity of the impellers.

Comparing Figure 3.70 with 3.69 significantly lower values of turbulence kinetic energy, (typically 30% less) are shown in the bulk flow of the merging flow pattern. In the bulk flow of the diverging flow pattern (Figure 3.71) the kinetic energies have smaller values than the other two flow patterns. In Figure 3.70 the kinetic energy levels obtained in the region between the impellers show steep gradients of k. In the part of the vessel below the lower impeller, the highest k values were

measured with the diverging flow and the lowest with the merging flow pattern.

In contrast to the merging and diverging flow patterns, parallel flow results in a more uniform distribution of high k regions throughout the vessel. In the region around r = 50 mm close to the free surface, the highest turbulence kinetic energy was obtained with merging flow pattern, albeit that the highest position of the upper impeller was that with the parallel flow pattern. This may be related to the direction of the upper impeller stream in the merging flow pattern which may act so as to intensify the helical vortex on the free surface.

The weighted average values of the kinetic energy, over the whole of the vessel were determined by calculating area-weighted averages of k values shown in Figures 3.69 to 3.71. They were 4.69×10^{-2}, 4.29×10^{-2} and 3.53×10^{-2} for the parallel, merging and diverging flow patterns respectively.

The mean flow vectors and the turbulence kinetic energy distributions presented above for the three flow patterns indicate the significant variations in the local macromixing and micromixing that may be encountered with different impeller spacings. Appropriate positioning of the impellers could be beneficial for:

More uniform blending throughout the vessel (parallel flow);
More intense mixing near the middle of the vessel (merging flow);
Solids suspension and lifting off the vessel bottom (diverging flow).

The turbulence distributions with all three flow patterns can be considered to be only approximately isotropic in some parts of the

impeller stream regions but are anisotropic in some parts of the bulk flows and of impeller streams. As the average turbulence energy with the parallel flow pattern is 9% and 33% higher than the merging and diverging flow patterns respectively, parallel flow impeller spacings might be preferable for most mixing operations where high turbulence levels are required for most efficient blending and/or chemical reactions.

3.6 Closure

The measurements presented in this Chapter have provided useful insights in to the mixing processes with stable flows produced by two impellers. However, due to the presence of unstable flow regimes at some spacing combinations care should be exerted in process design to avoid such spacings.

Each of the three impeller spacing combinations that result in the three stable flow patterns has different power consumption and mean flow and turbulence distribution characteristics that could be beneficial for specific mixing processes. Similarly, the parallel and merging flow patterns result in different mixing times.

The results of this chapter do not indicate that any of the three flow patterns is preferable in all respects for mixing purposes: for example, although lower mixing times and power consumption were measured for the merging flow, the levels of k were also lower compared with the parallel flow pattern. The choice of dual-impeller spacings in practice must therefore be made based on the requirement of the particular mixing operation to be performed.

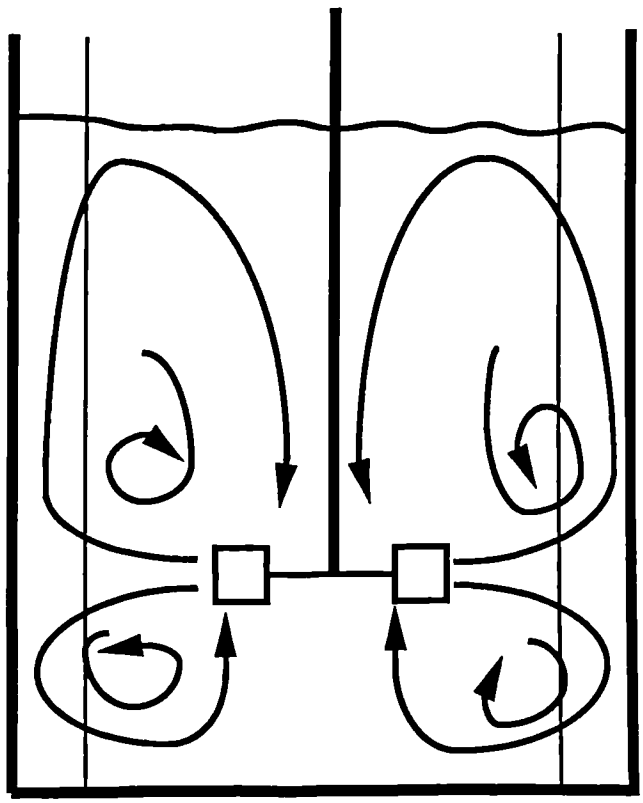

Figure 3.1. Schematic diagram of flow pattern in stirred tank agitated by single Rushton impeller.

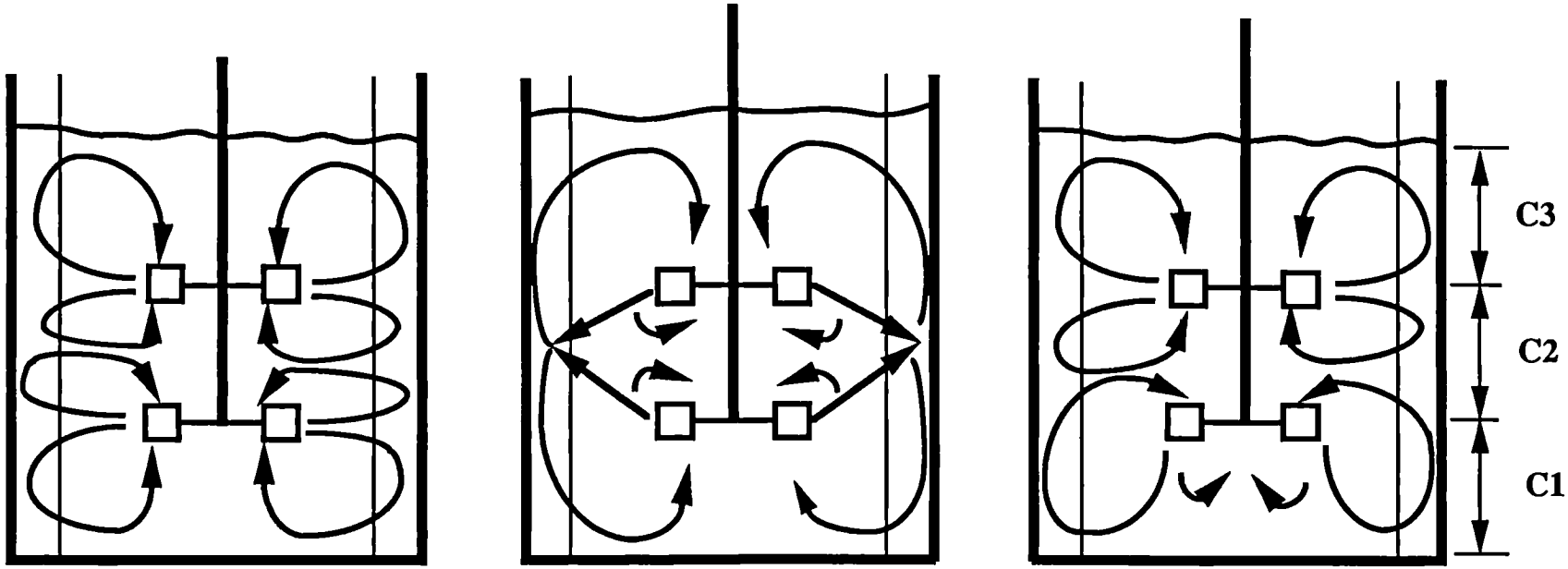

(a) Parallel streams (b) Merging streams (c) Diverging streams

Figure 3.2. Schematic diagram of flow patterns with two Rushton turbines

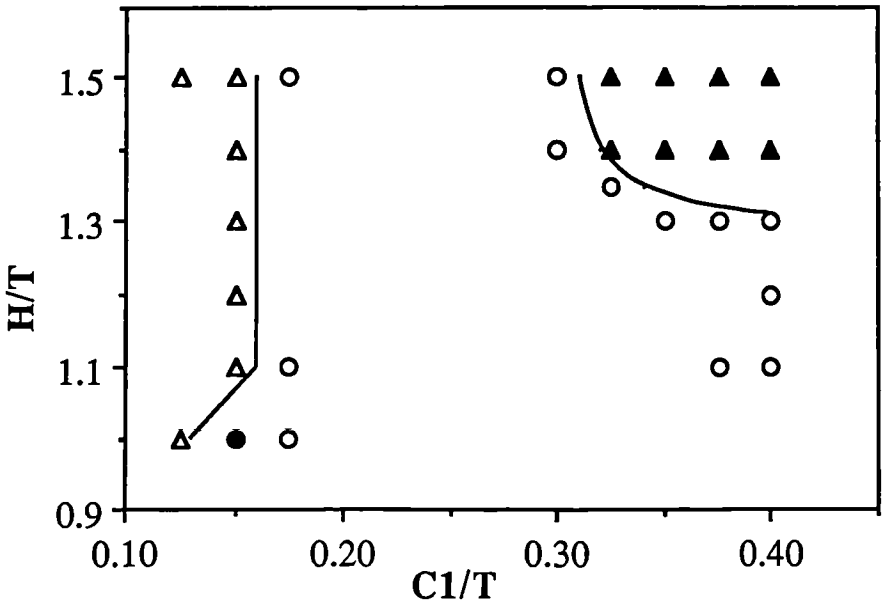

Figure 3.3. Effect of C1 and H on flow patterns; C2 = 0.35T, N = 260 rpm.

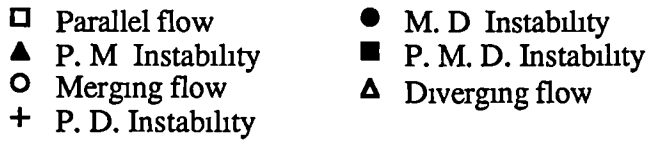

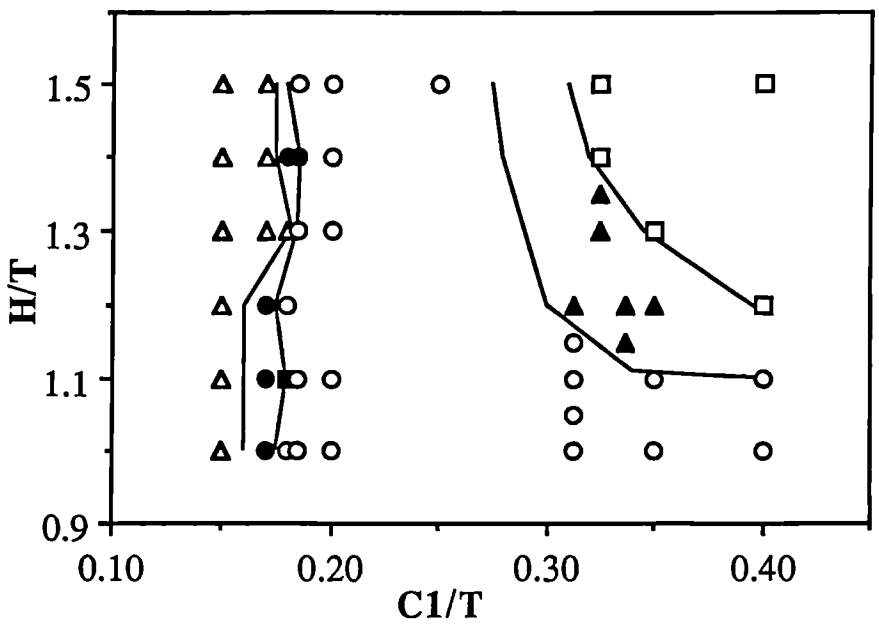

Figure 3.4. Effect of C1 and H on the flow patterns; C2 = 0.365 T, N = 260 rpm.

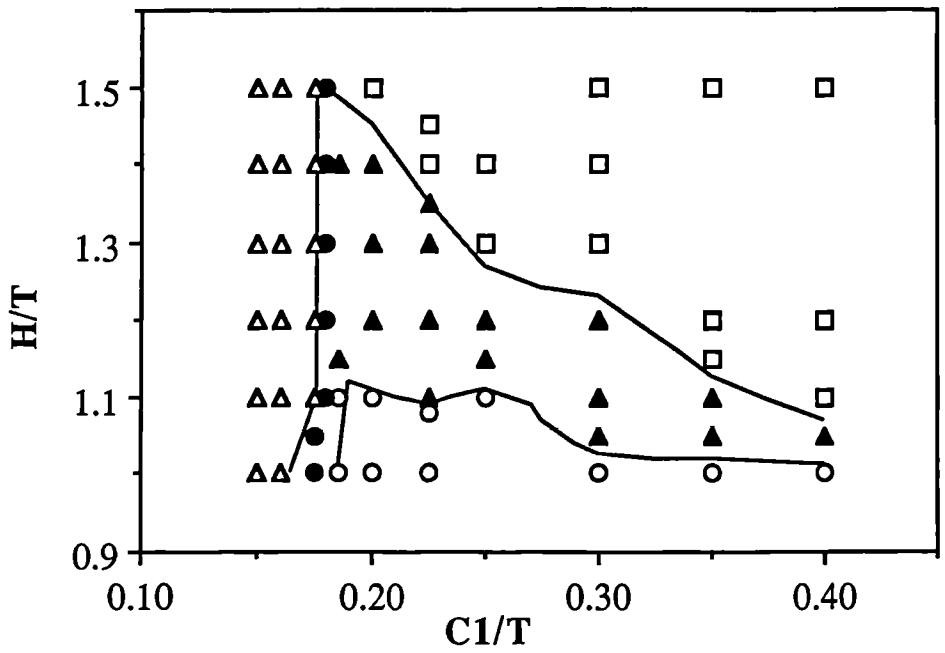

Figure 3.5. Effect of C1 and H on flow patterns;
C2 = 0.375 T, N = 260 rpm.

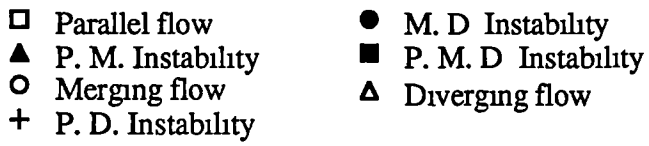

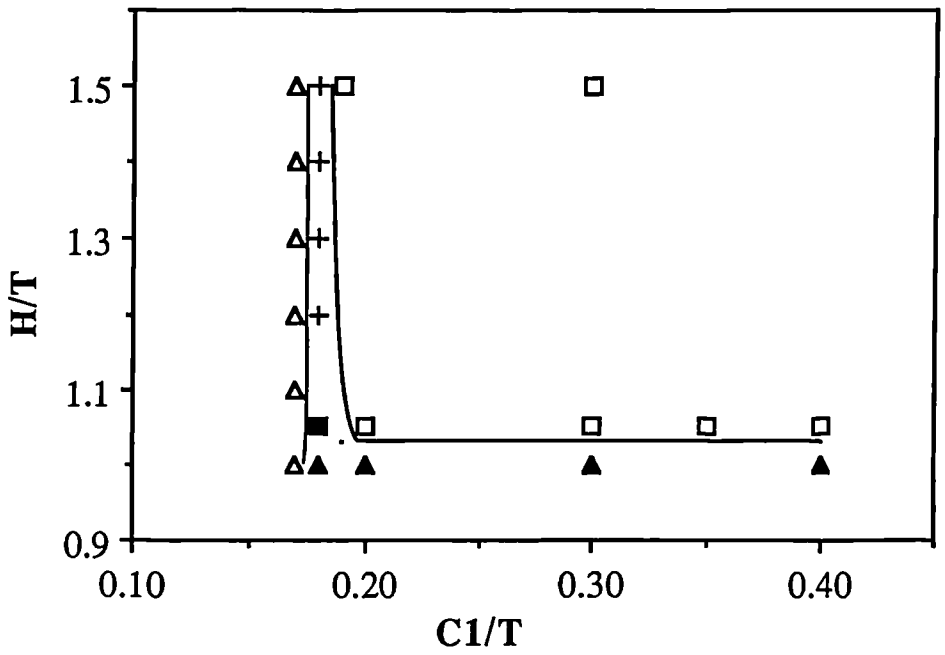

Figure 3.6. Effect of C1 and H on flow patterns;
C2 = 0.385 T, N = 260 rpm.

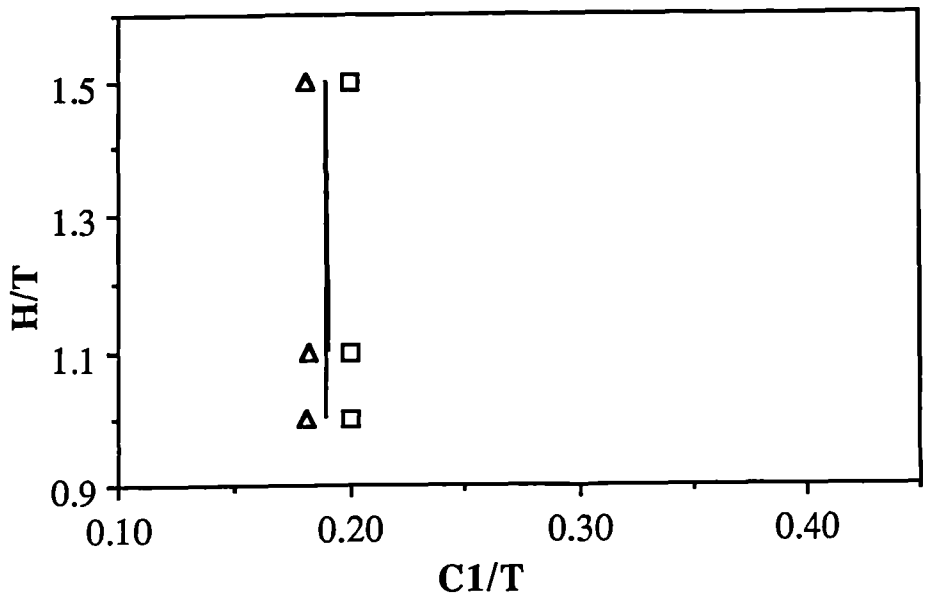

Figure 3.7. Effect of C1 and H on flow patterns;
C2 = 0.4 T, N = 260 rpm.

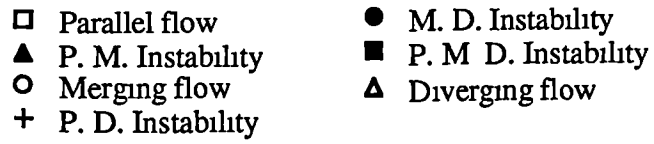

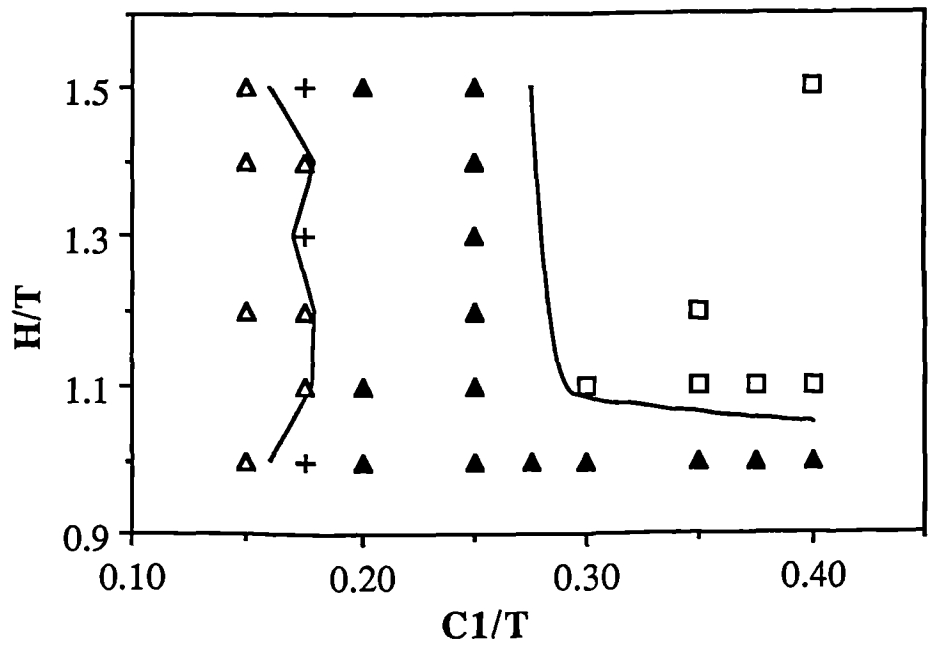

Figure 3.8. Effect of C1 and H on flow patterns;
C2 = 0.375 T, N = 100 rpm.

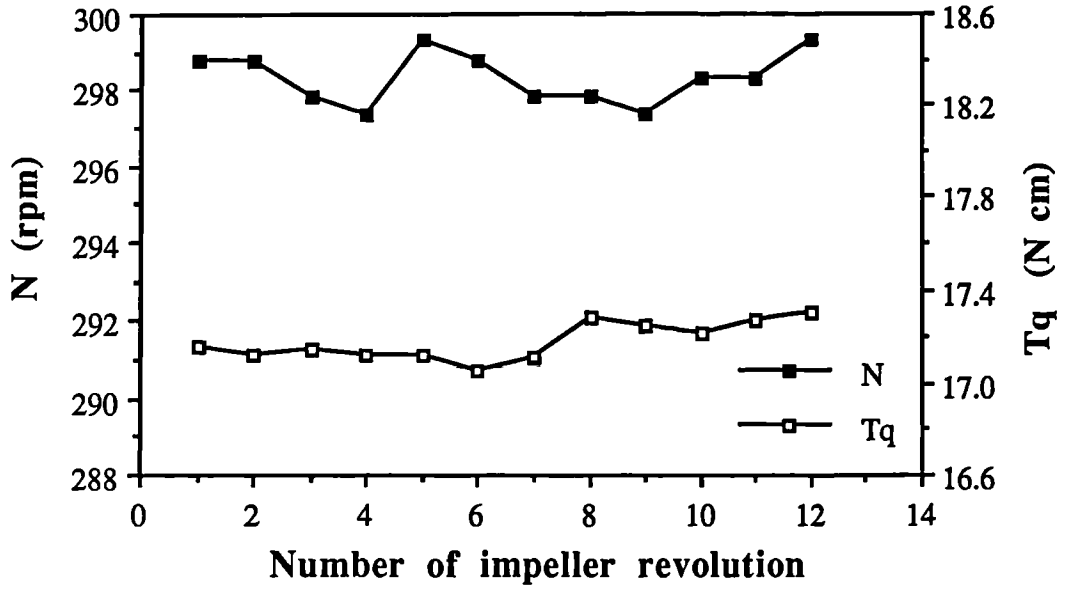

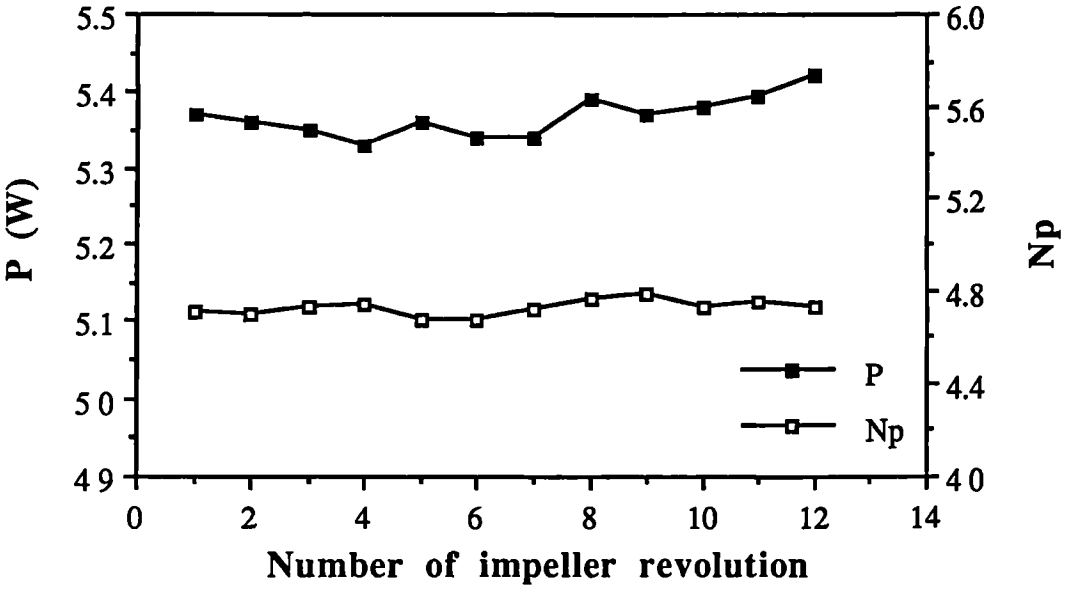

Figure 3.9. Variation of speed and power characteristics of single Rushton impeller; C = T/3, d = T/3 and t = 3.3 mm.

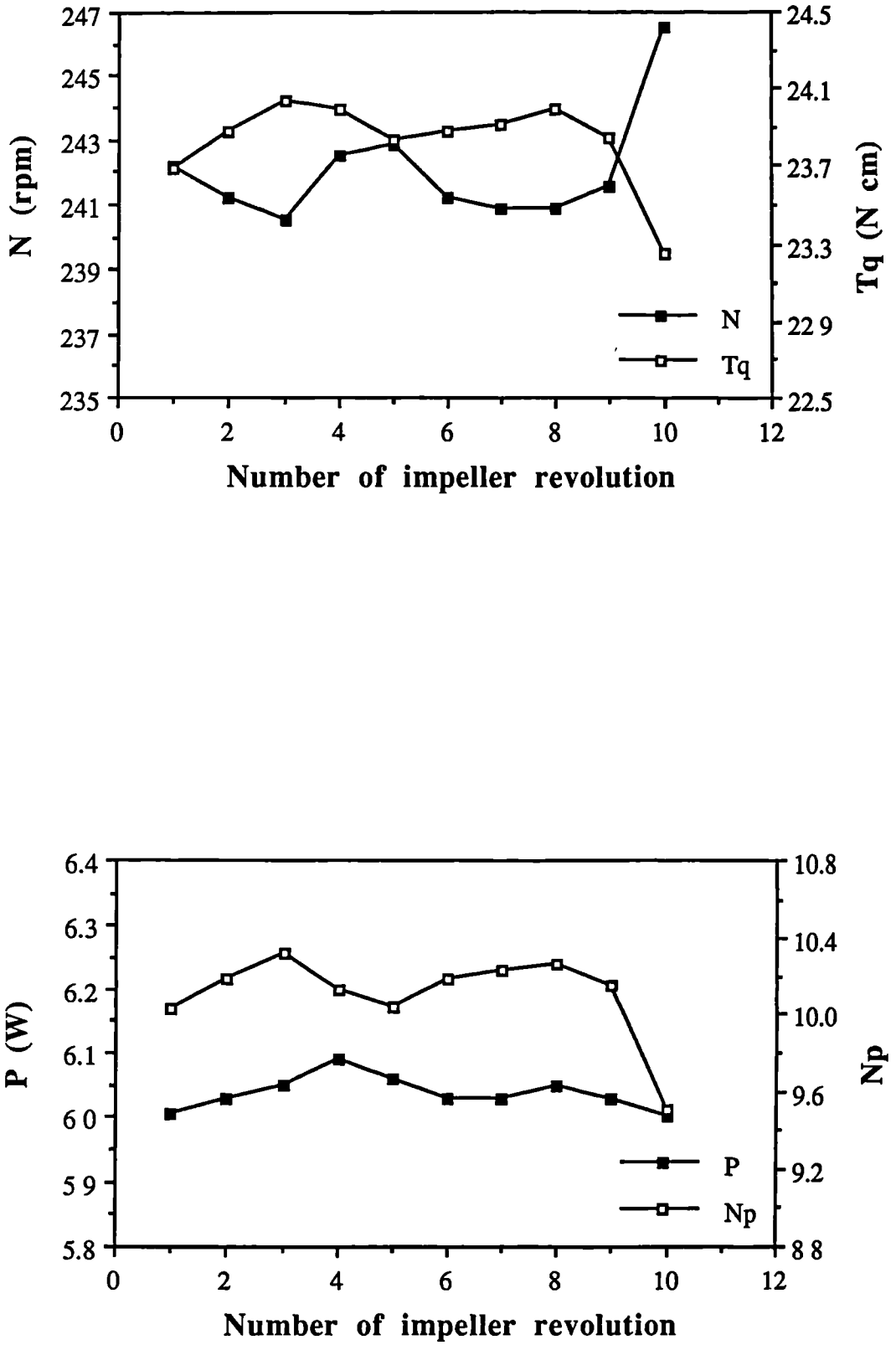

Figure 3.10. Variation of speed and total power characteristics of two Rushton impellers from cycle to cycle of impeller rotation; C1 = T/4, C2 = T/2 and t = 1.65 mm.

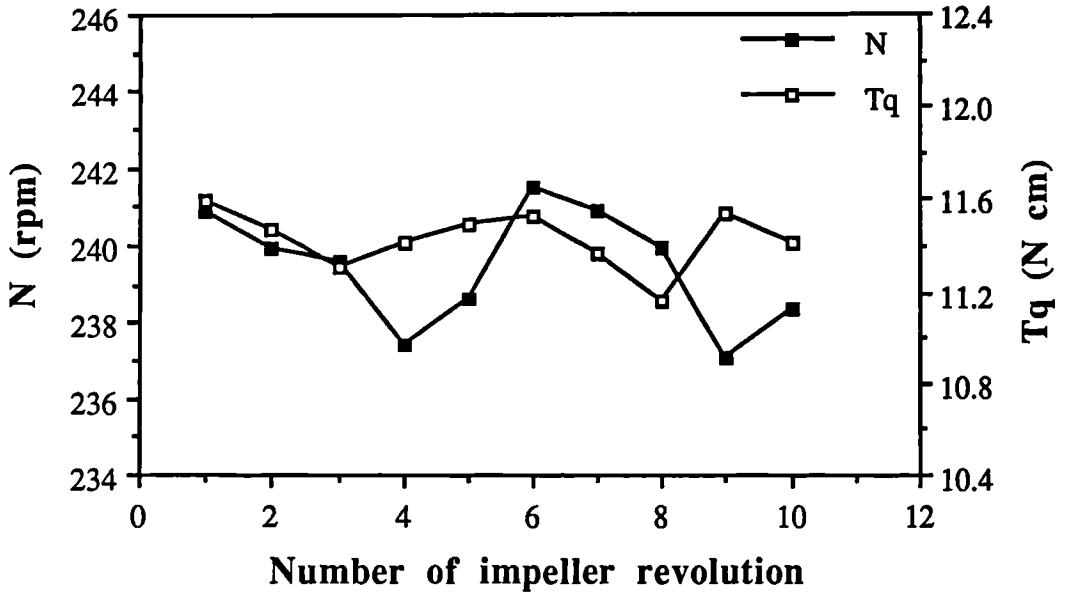

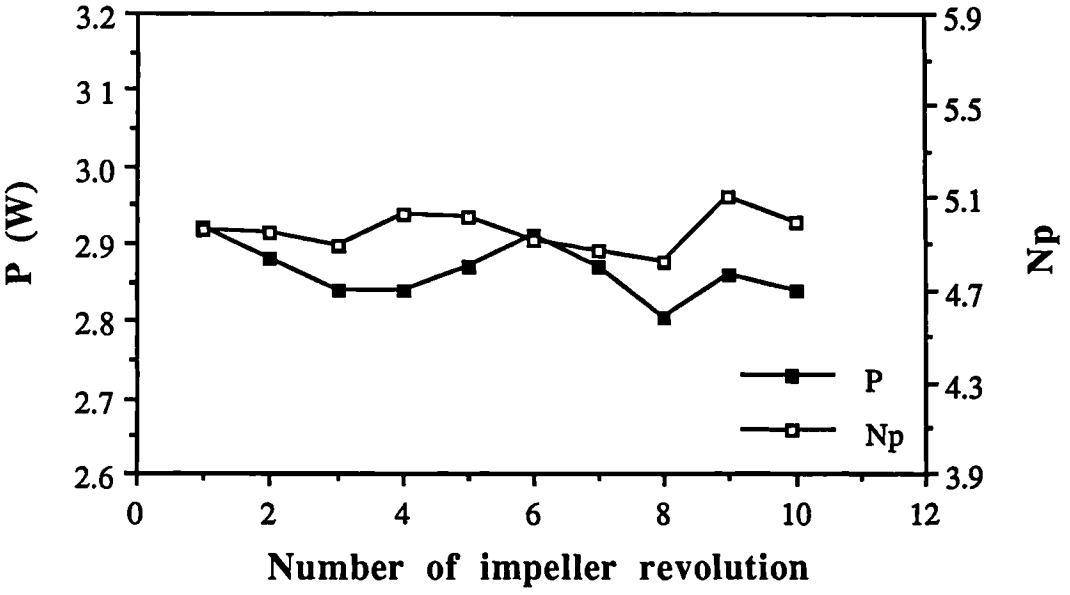

Figure 3.11. Variation of speed and power characteristics of lower impeller from cycle to cycle of impeller rotation; C1 = T/4, C2 = T/2 and t = 1.65 mm.

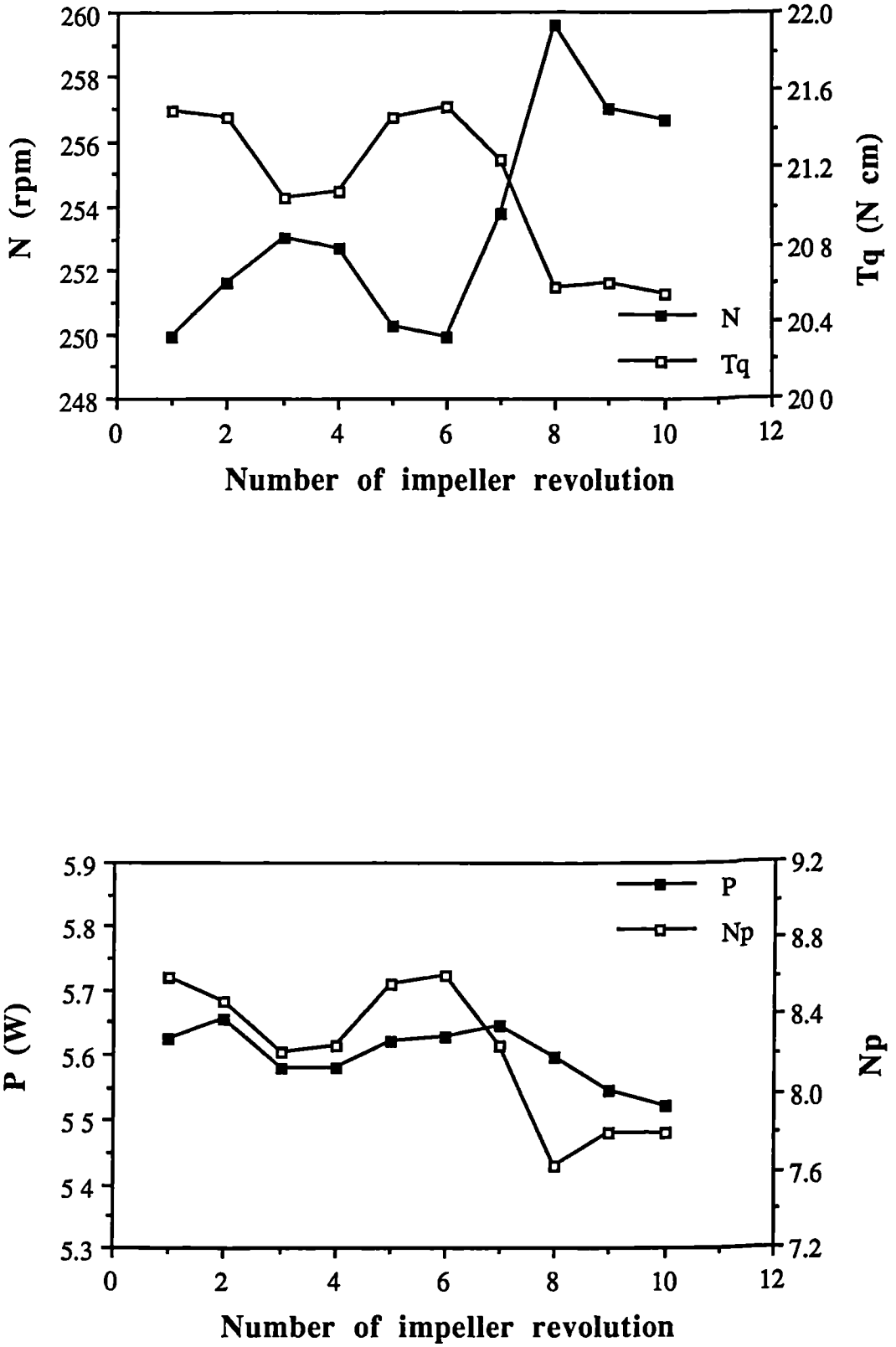

Figure 3.12. Variation of speed and total power characteristics of two Rushton impellers from cycle to cycle of impeller rotation; C1 = C2 = T/3 and t = 1.65 mm.

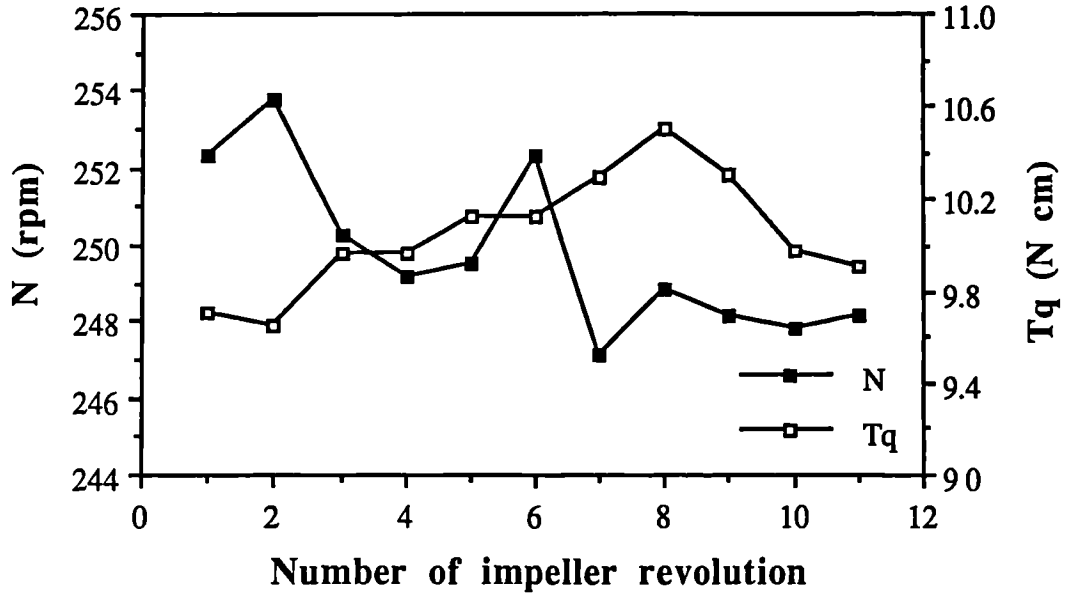

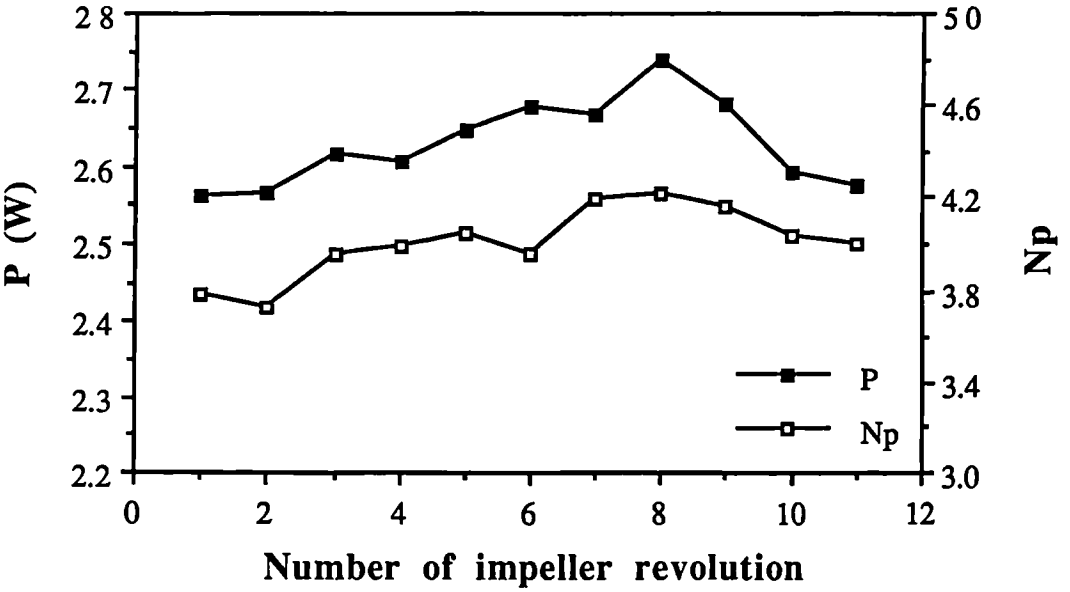

Figure 3.13. Variation of speed and power characteristics of lower impeller from cycle to cycle of impeller rotation; C1 = C2 = T/3 and t = 1.65 mm.

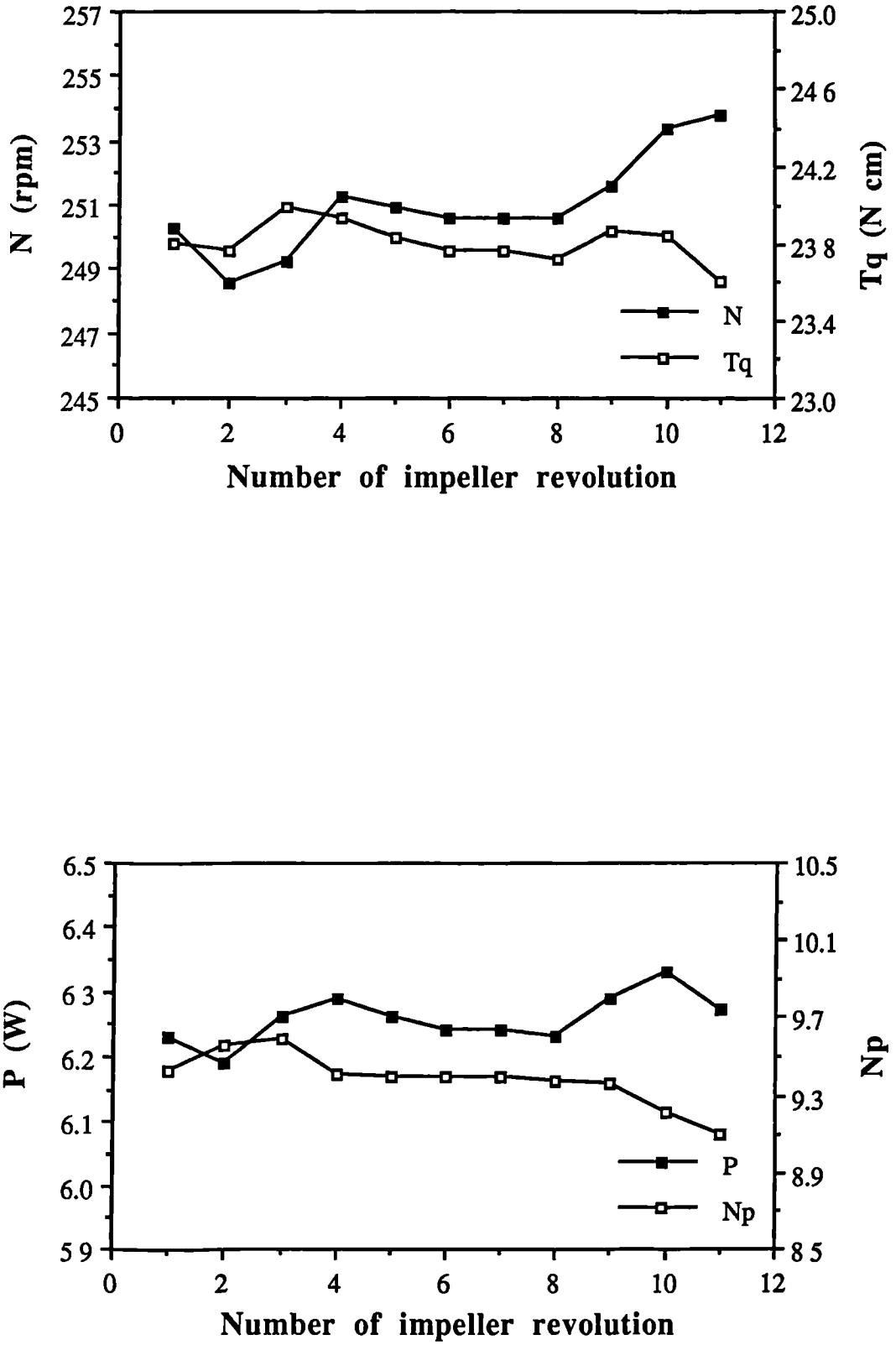

Figure 3.14. Variation of speed and total power characteristics of two Rushton impellers from cycle to cycle of impeller rotation; C1 = 0.15T, C2 = T/2 and t = 1.65 mm.

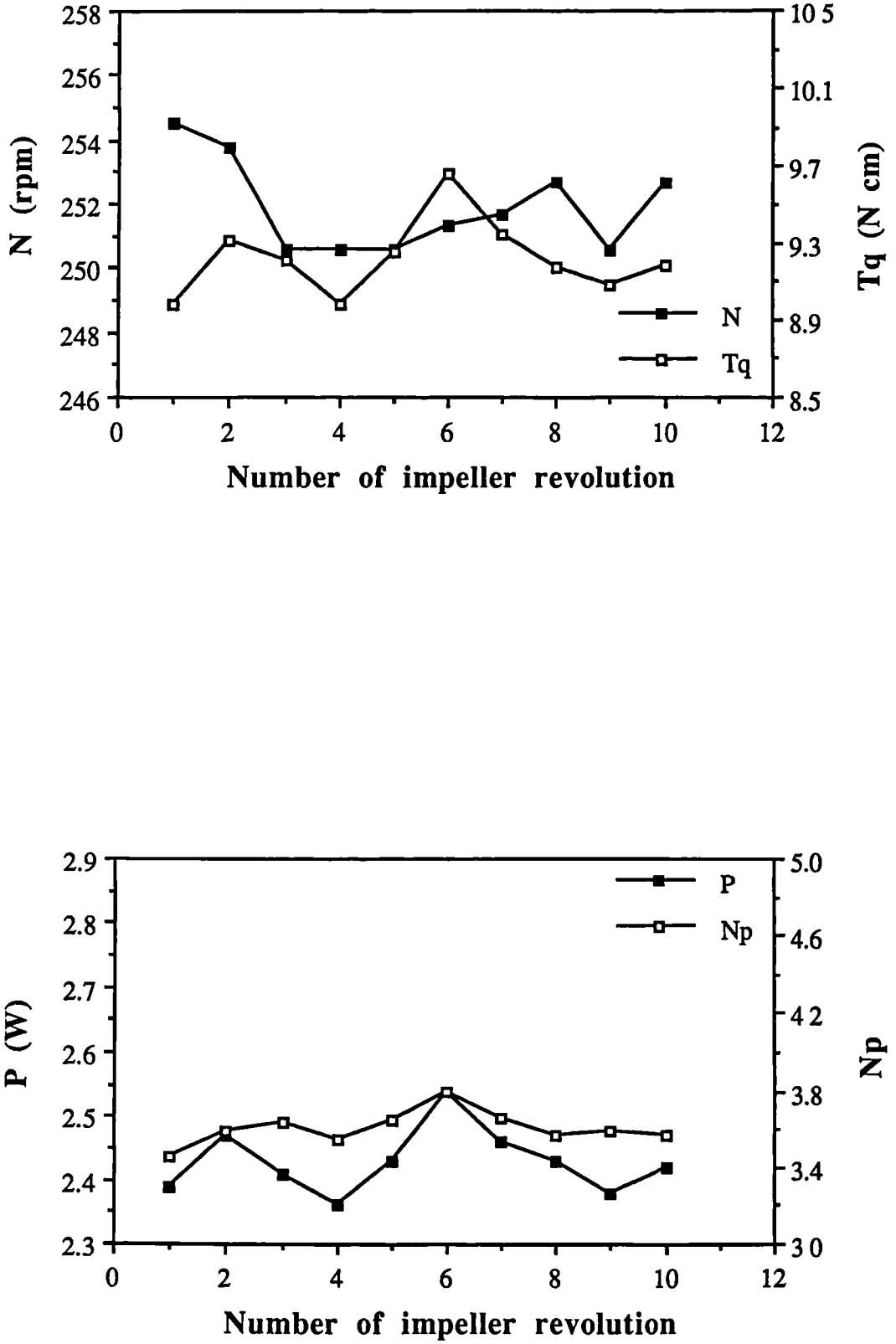

Figure 3.15. Variation of speed and power characteristics of lower impeller from cycle to cycle of impeller rotation; C1 = 0.15T, C2 = T/2 and t = 1.65 mm.

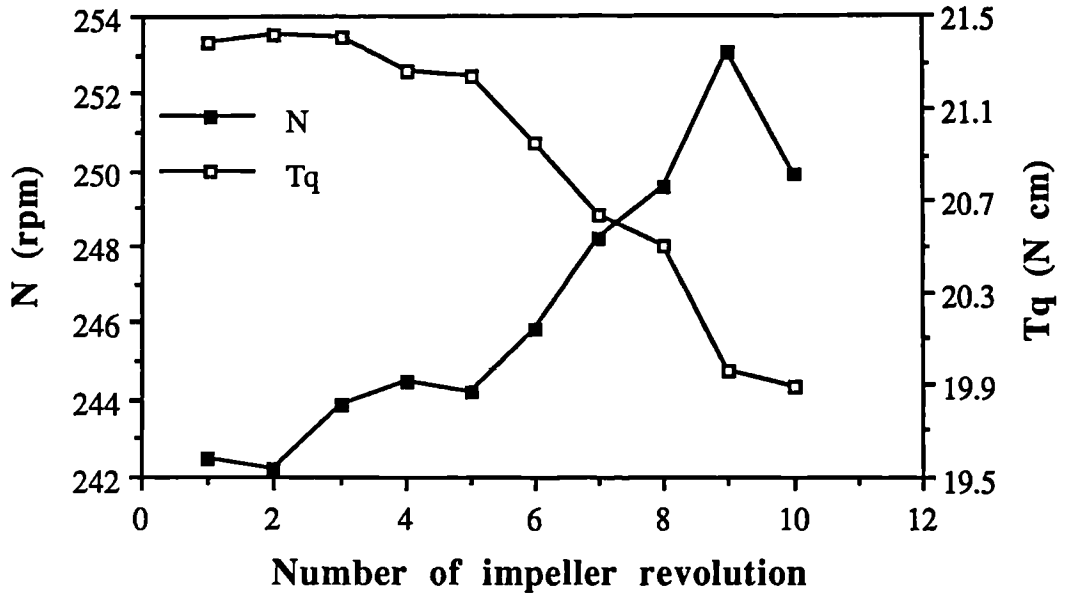

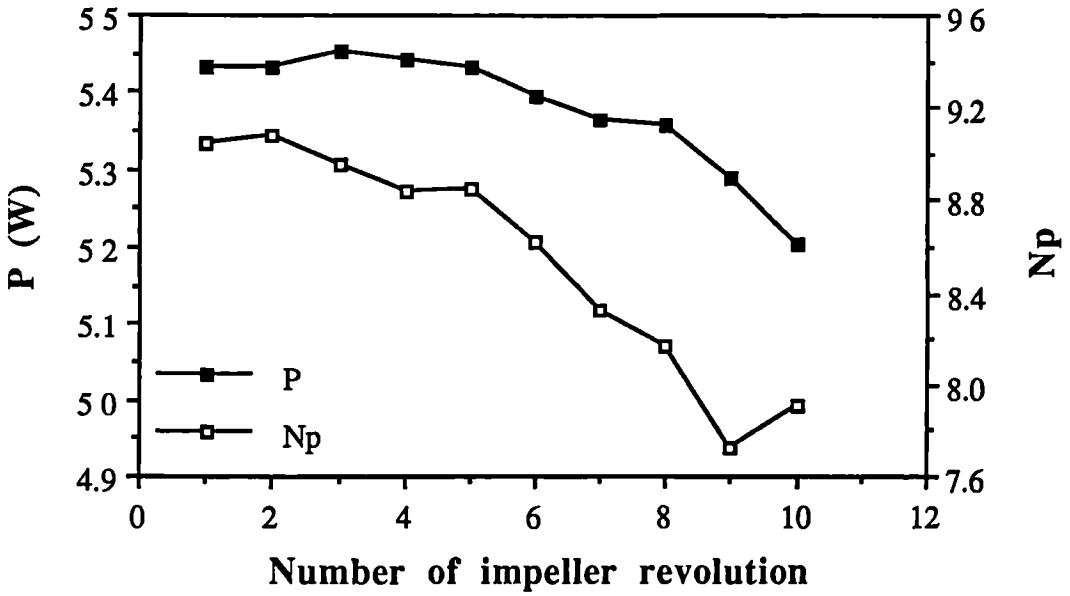

Figure 3.16. Variation of speed and total power characteristics of two Rushton impellers from cycle to cycle of impeller rotation; C1 = C3, C2 = 0.385T and t = 1.65 mm.

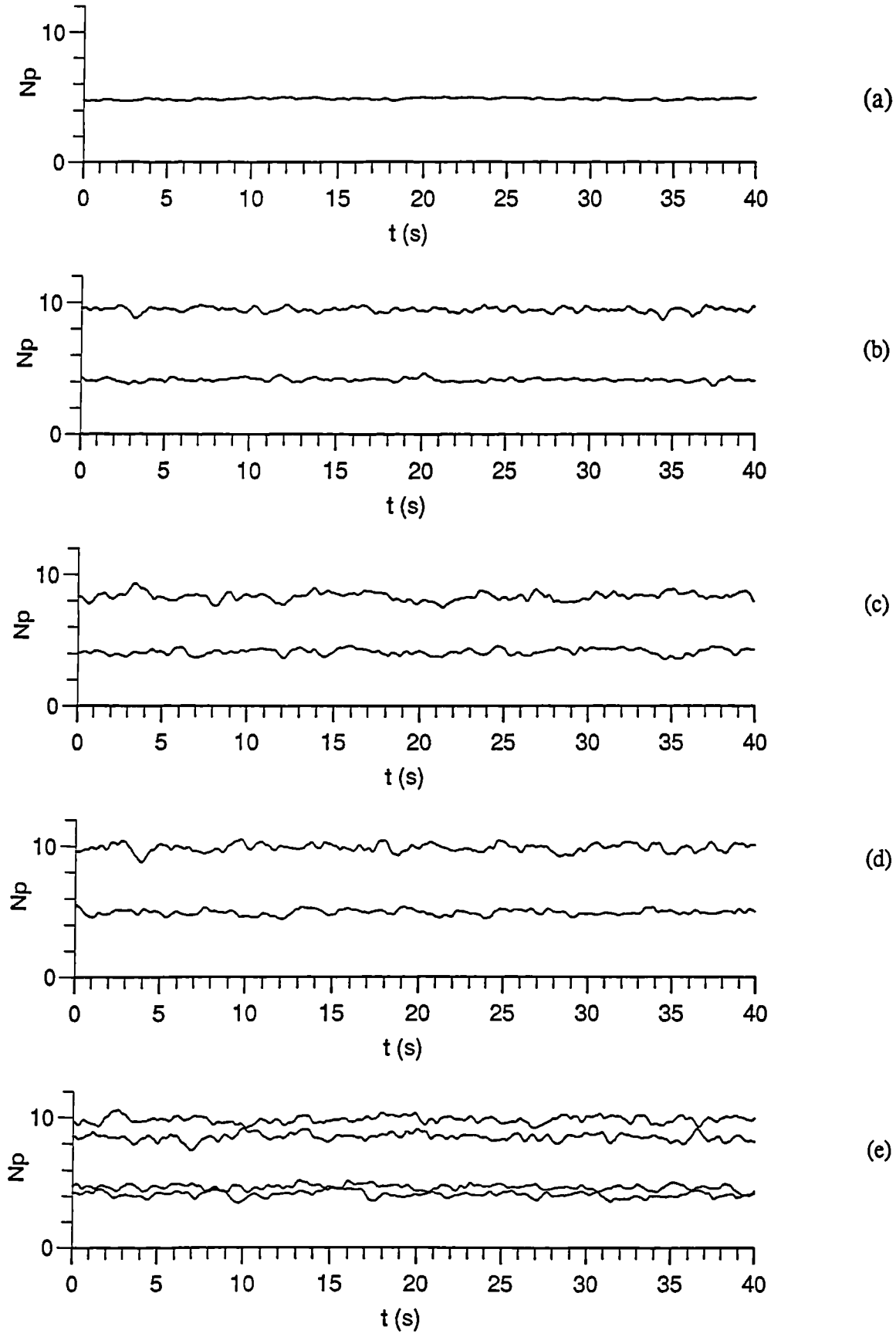

Figure 3.17. Time history of d = T/3 impeller(s) power number: (a) single impeller, C = T/3; (b) - (e) two impellers producing respectively diverging, merging, parallel and parallel-merging flow patterns; the impeller thickness is 3 3 and 1.65 mm for the single and the two-impeller systems respectively.

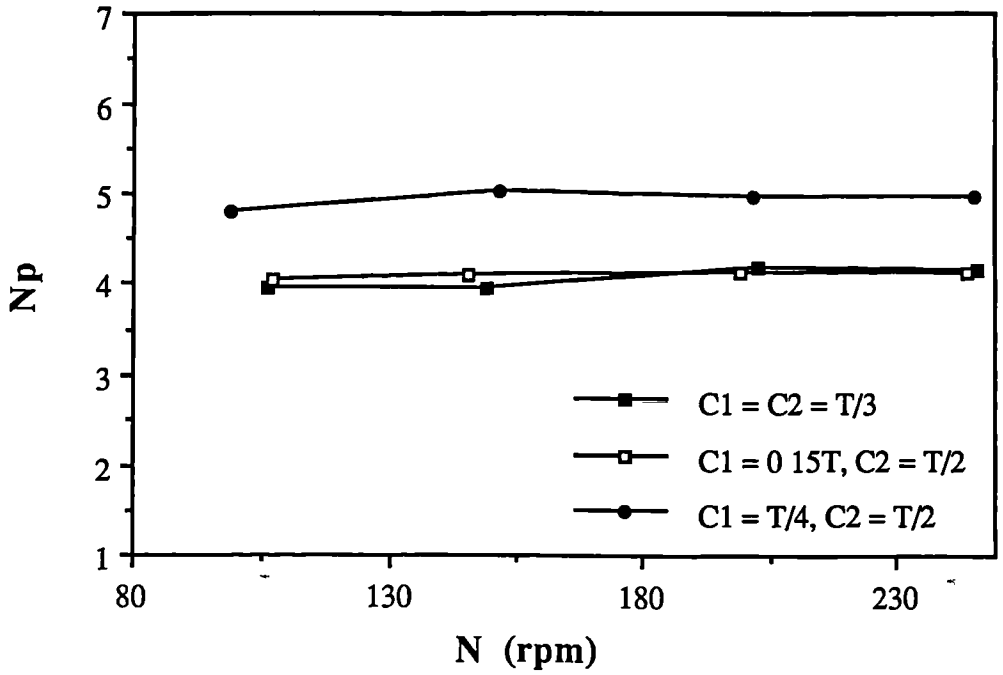

Figure 3.18. Effect of impeller spacing on the power number, lower impeller.

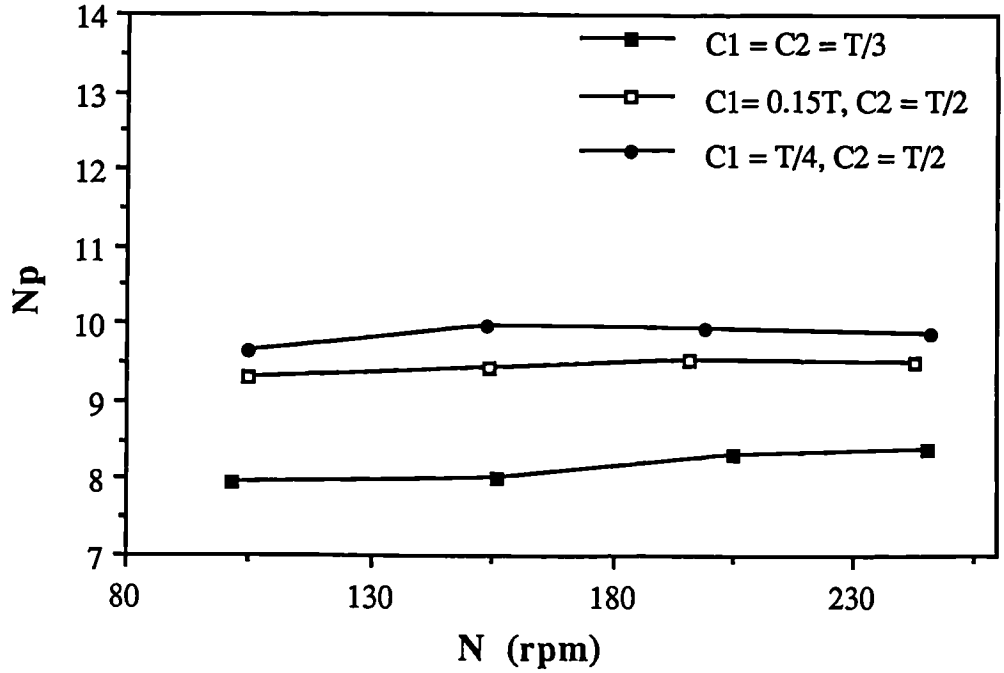

Figure 3.19. Effect of impeller spacing on power number, two impellers.

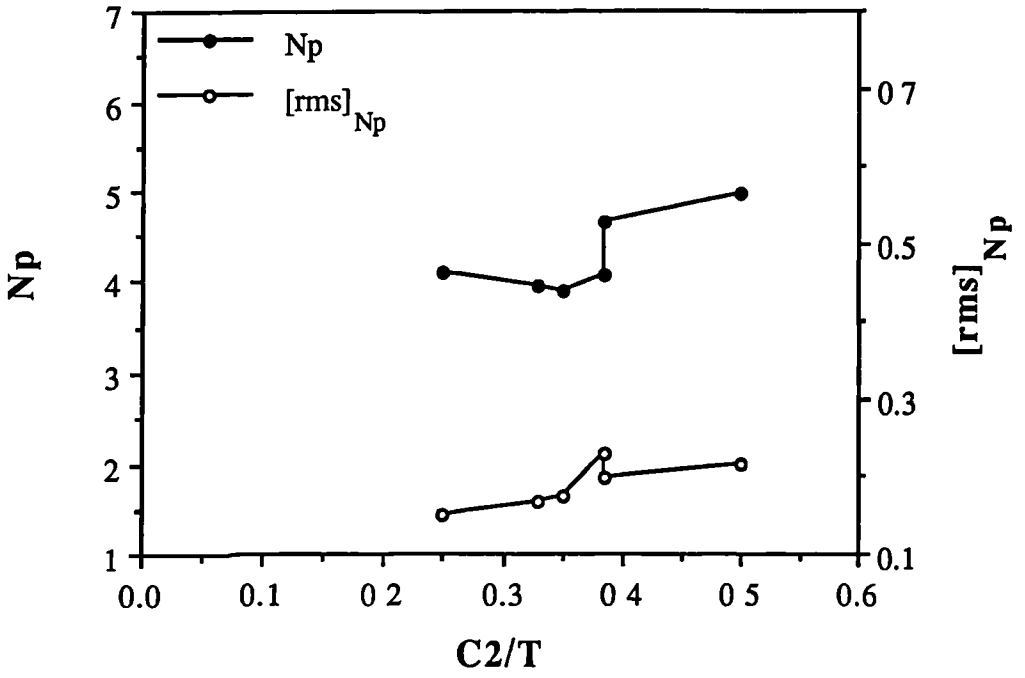

Figure 3.20. Effect of impeller spacing on power number and power number fluctuation, lower impeller, C1 = T/4, t = 1.65 mm, H = T.

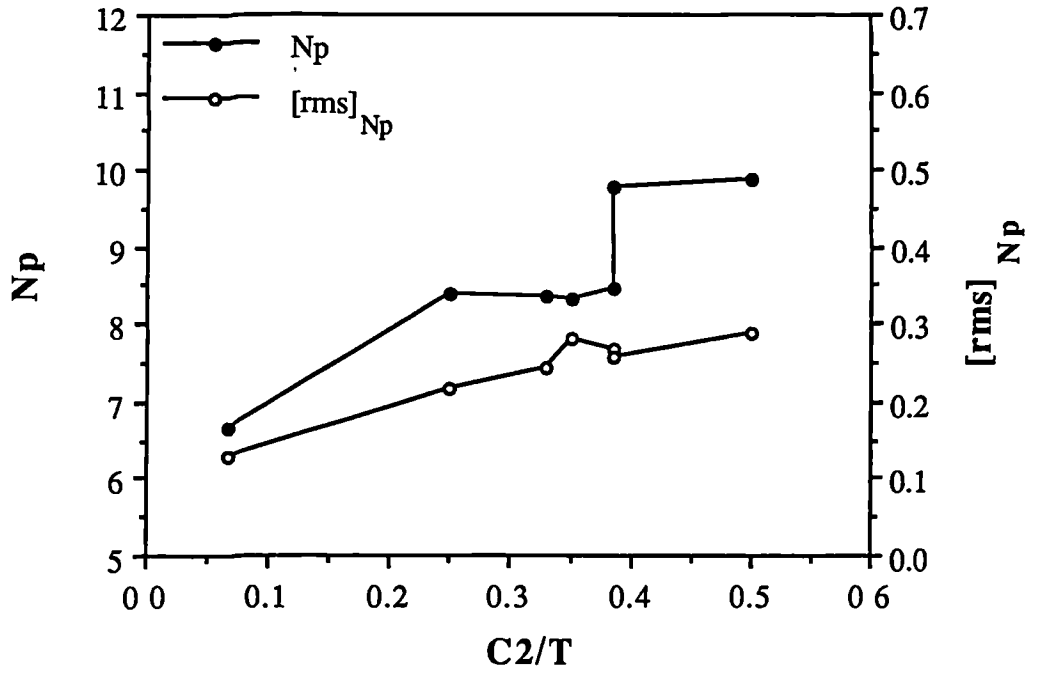

Figure 3.21. Effect of impeller spacing on power number and power number fluctuation, two impellers, C1 = T/4, t = 1.65 mm, H = T.

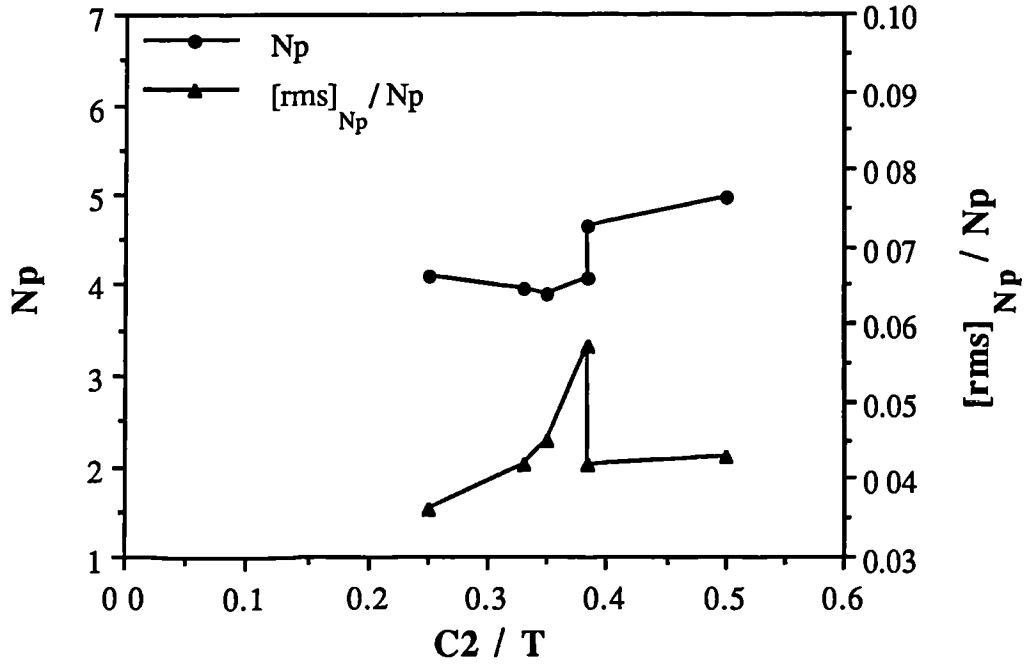

Figure 3.22. Effect of impeller spacing on Np and $[rms]_{Np}$, lower impeller, C1 = T/4, t = 1.65 mm, H = T.

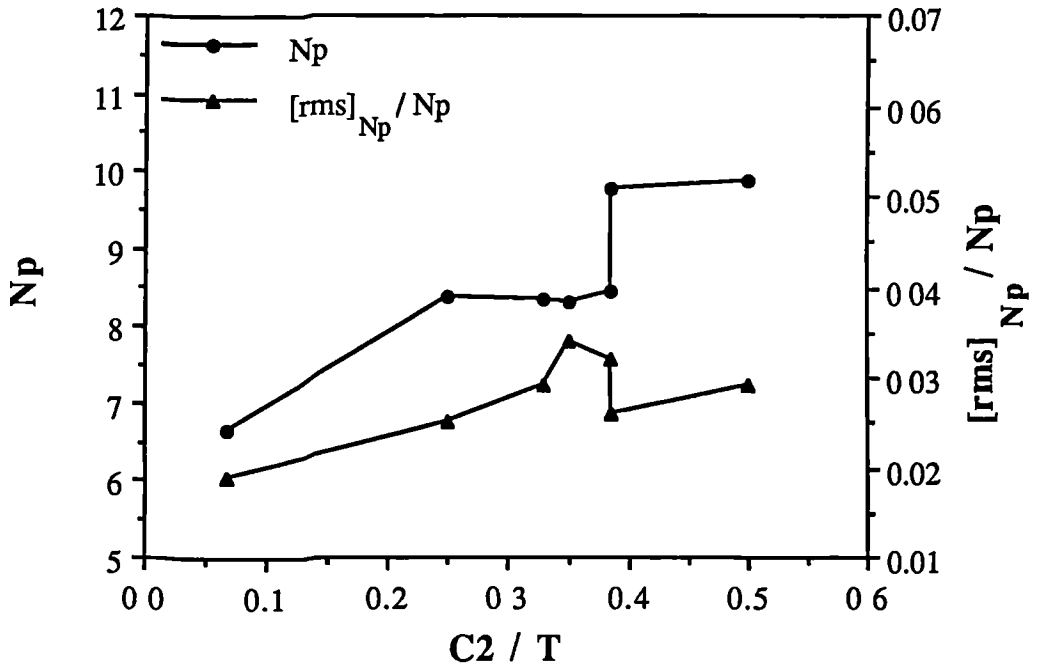

Figure 3.23. Effect of impeller spacing on Np and $[rms]_{Np}$, two impellers, C1 = T/4, t = 1.65 mm, H = T.

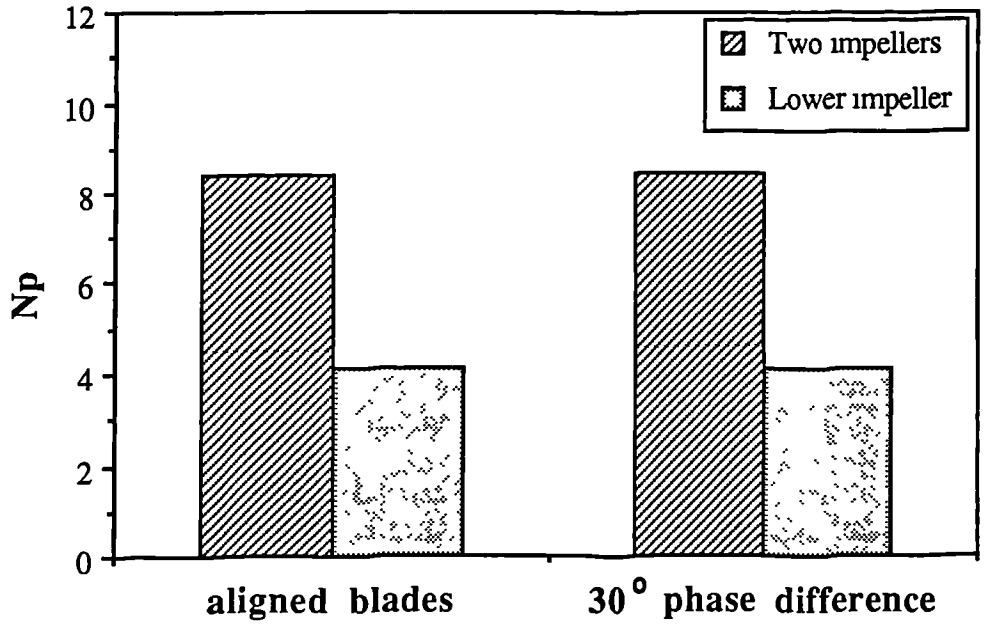

Figure 3.24. Effect of impeller blades alignment on power number, C1 = C2 = T/4, t = 1.65 mm.

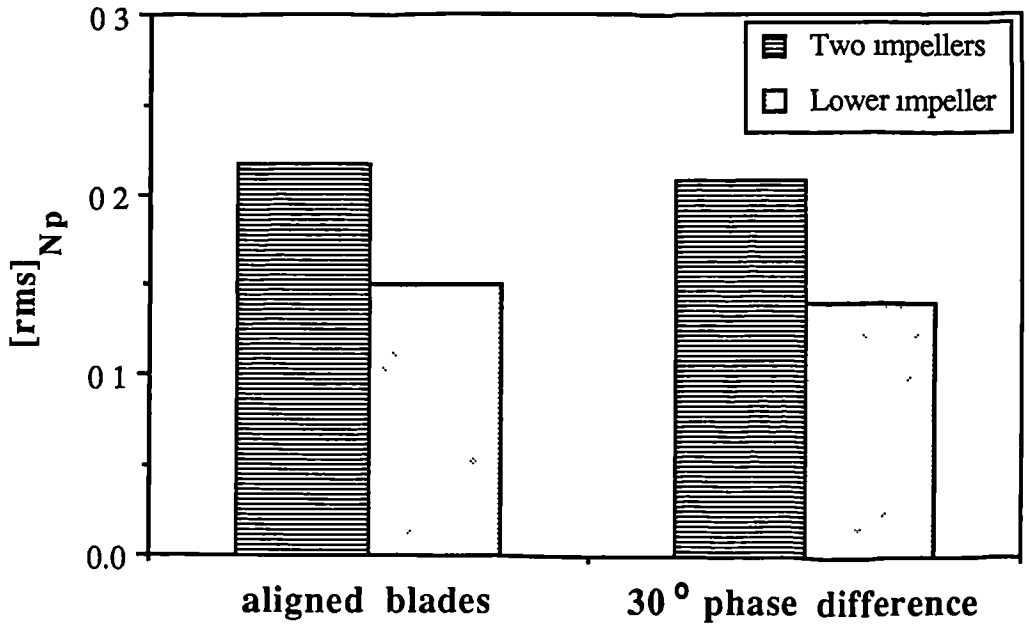

Figure 3.25. Effect of impeller blades alignment on the fluctuation of power number, C1 = C2 = T/4, t = 1.65 mm.

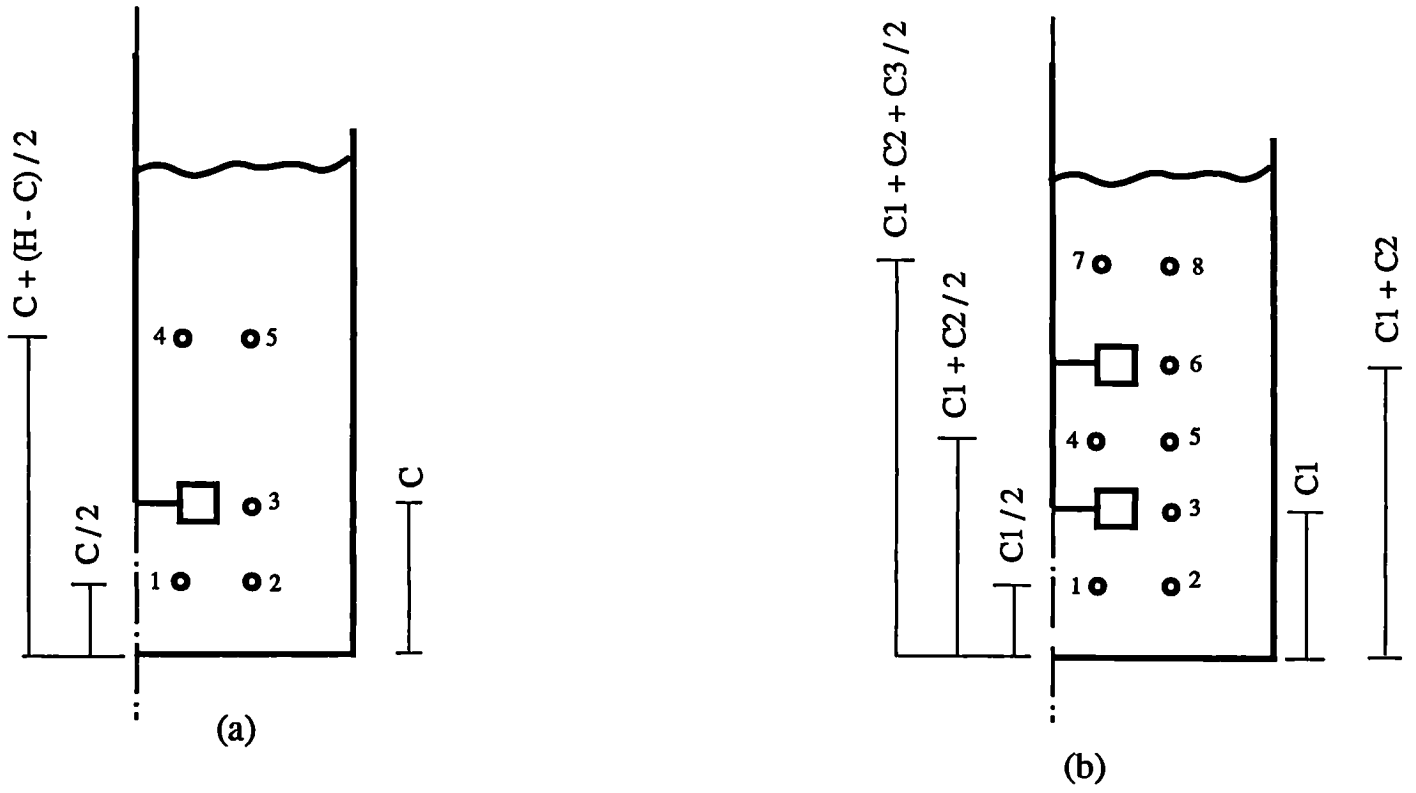

Figure 3.26. Probe locations, $\theta = 0^{\circ}$, r = 30 and 80 mm;
(a) Single-impeller system,
(b) Two-impeller system.

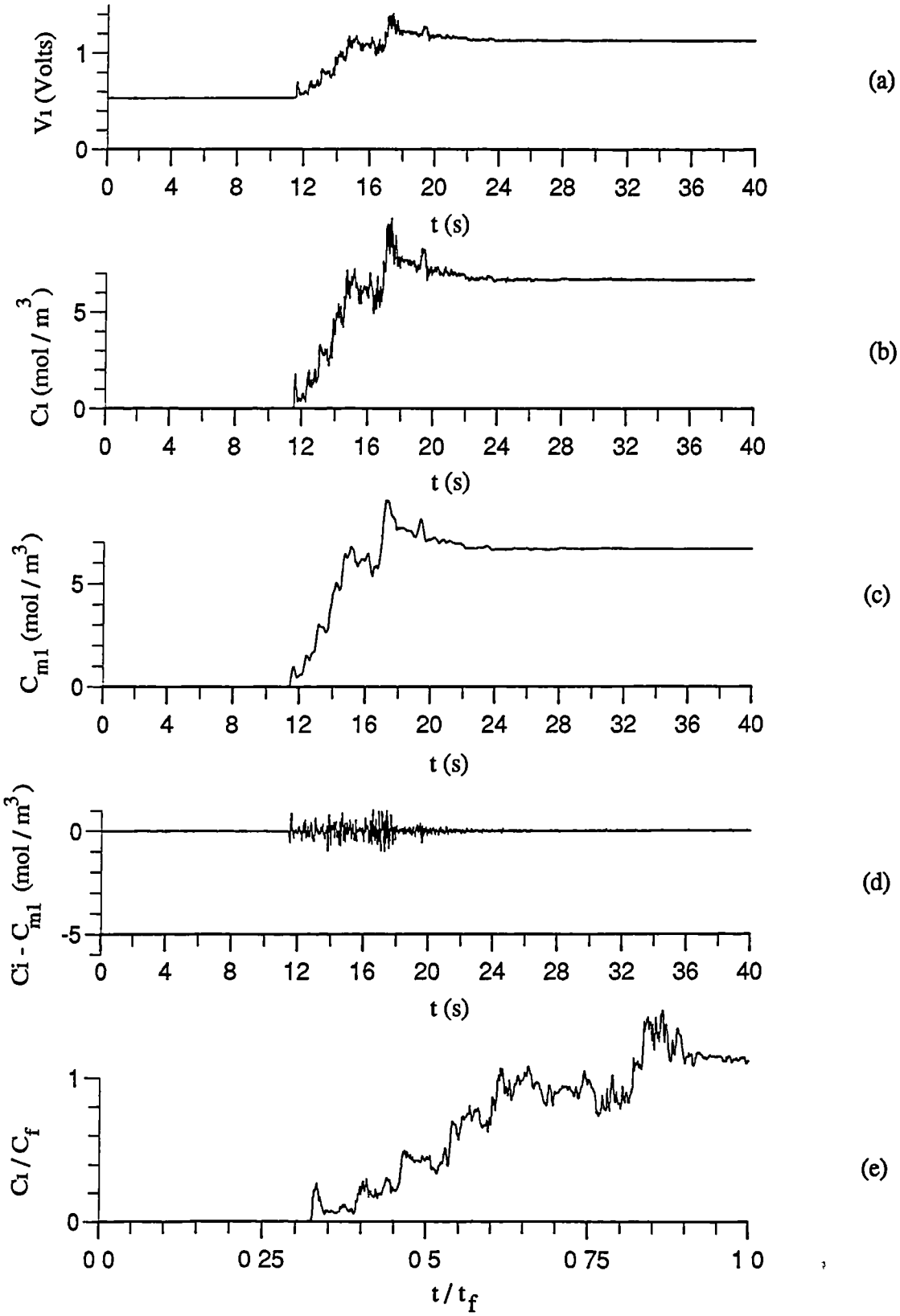

Figure 3.27. Characteristic voltage (a), concentration (b), mean concentration (c), concentration flutuation (d), and normalized concentration (e) variations; Parrallel flow pattern: C1 = T/4, C2 = T/2, z = T/2, r = 80 mm.

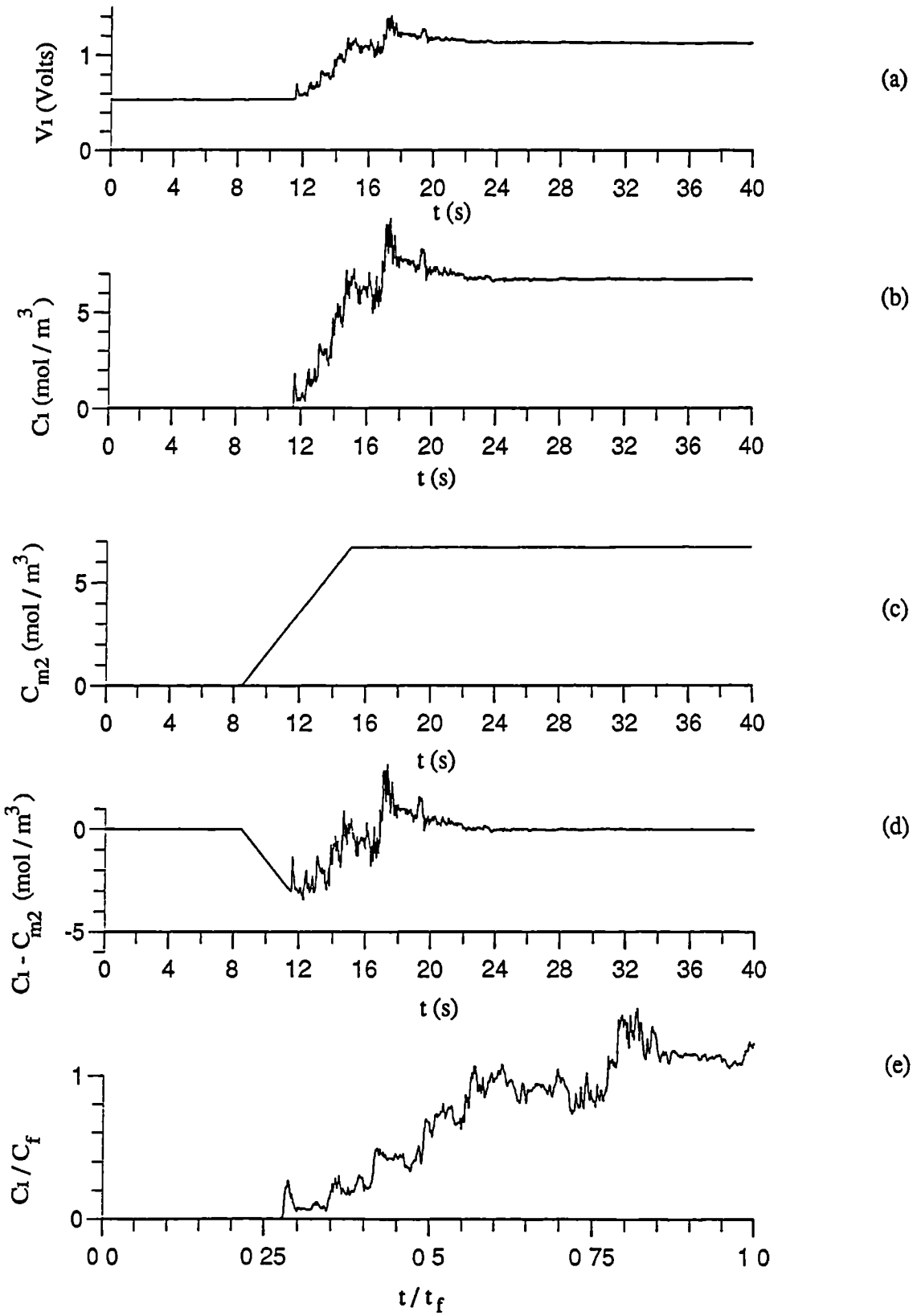

Fig 3.28. Characteristic voltage (a), concentration (b), mean concentration (c), concentration flutuation (d), and normalized concentration (e) variations; Parallel flow pattern: C1 = T / 4, C2 = T / 2, z = T / 2, r = 80 mm.

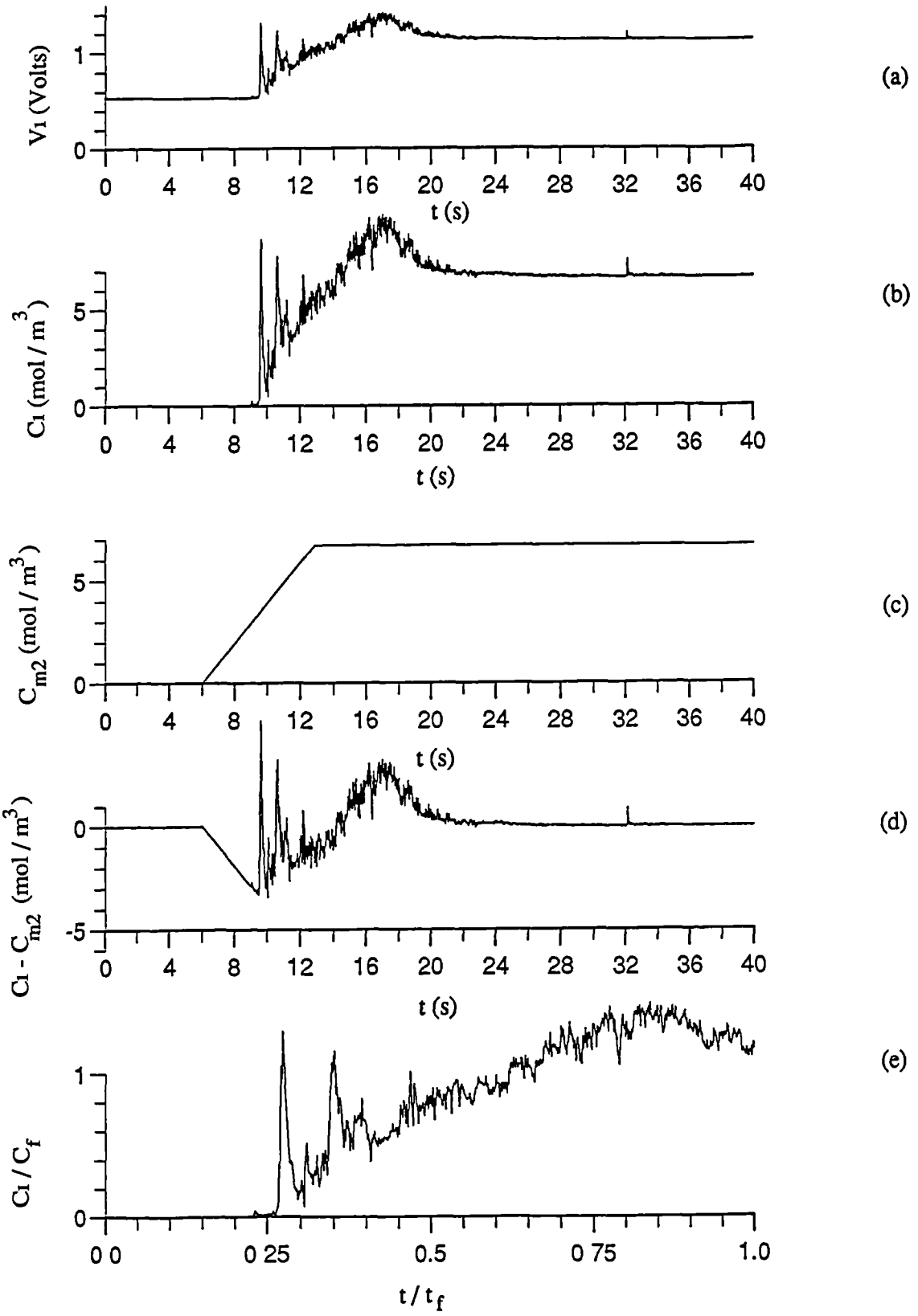

Fig 3.29. Characteristic voltage (a), concentration (b), mean concentration (c), concentration flutuation (d), and normalized concentration (e) variations; Parallel flow pattern: C1 = T/4, C2 = T/2, z = 3T / 4, r = 80 mm.

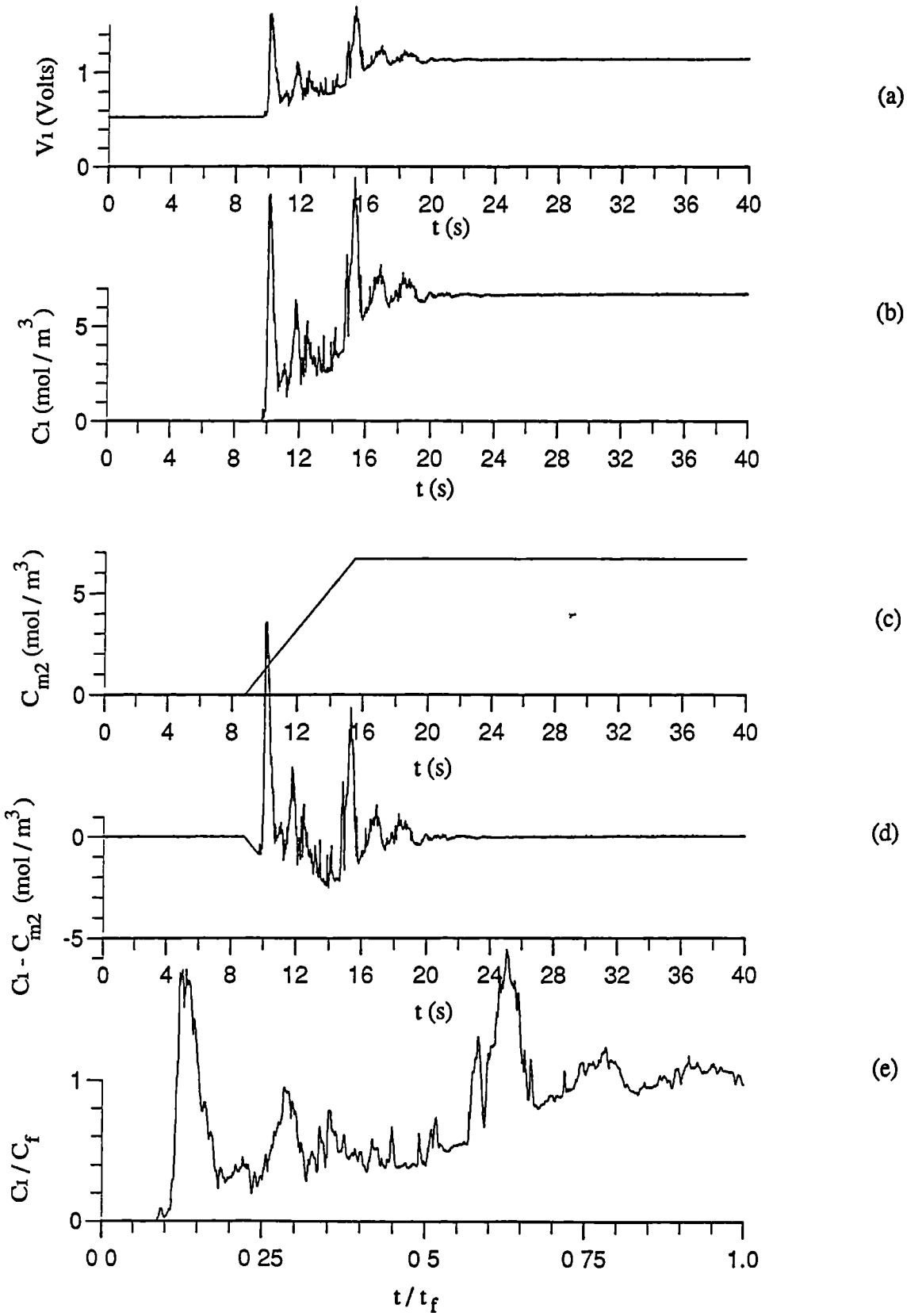

Fig 3.30. Characteristic voltage (a), concentration (b), mean concentration (c), concentration flutuation (d), and normalized concentration (e) variations; Merging flow pattern: C1 = C2 = T / 3, z = T / 2, r = 80 mm.

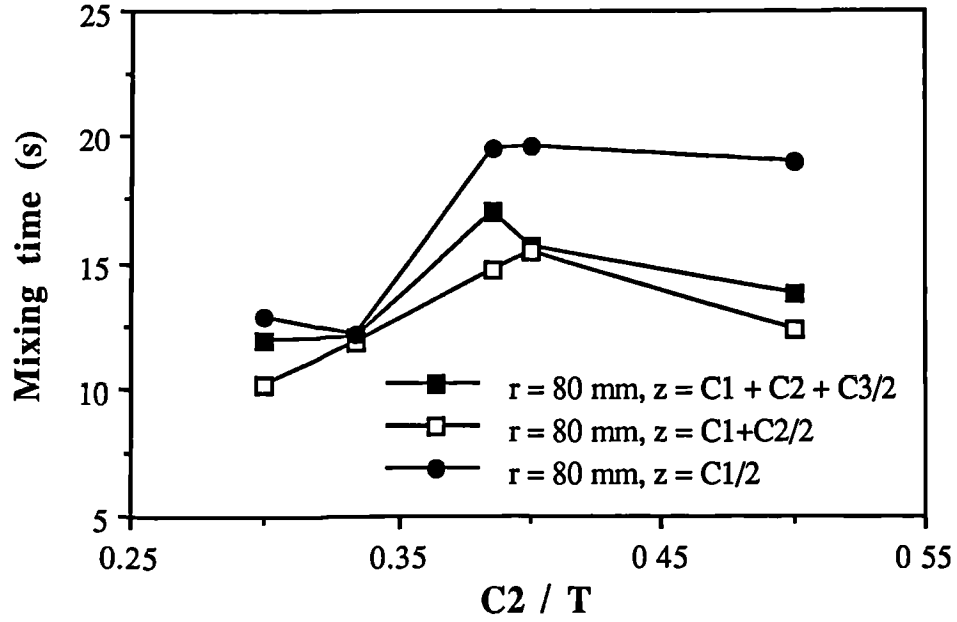

Figure 3.31. The effect of impeller spacing on local mixing time; N = 200 rpm, insertion time = 6.5 s, tracer volume = 50 cc.

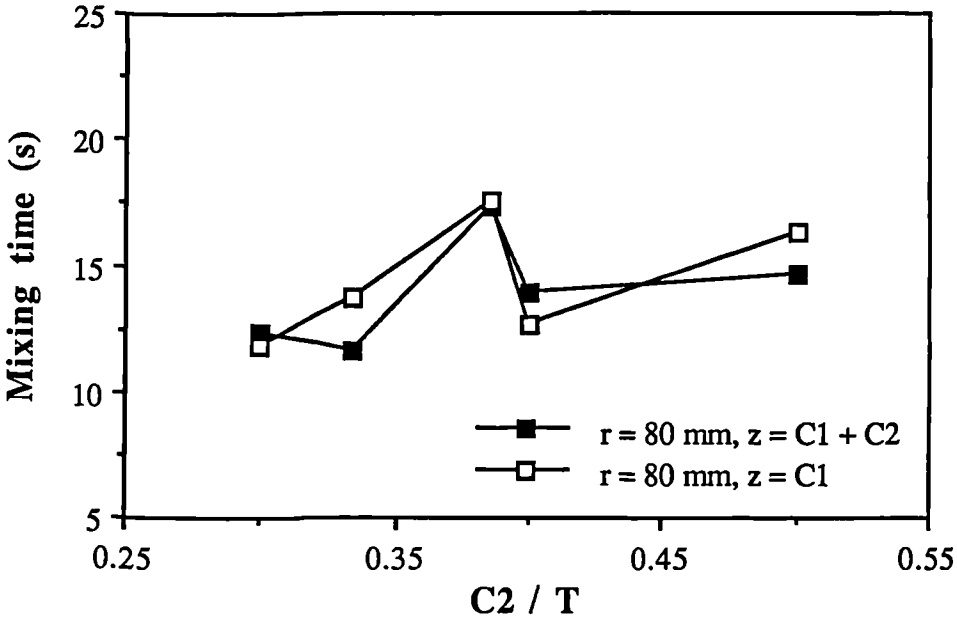

Figure 3.32. The effect of impeller spacing on local mixing time; N = 200 rpm, insertion time = 6.5 s, tracer volume = 50 cc.

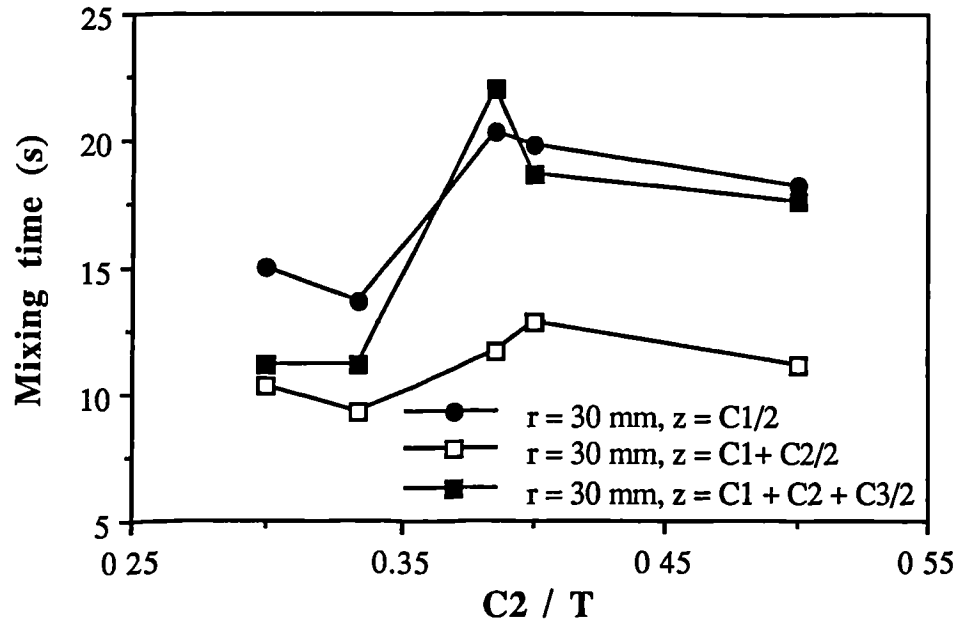

Figure 3.33. The effect of impeller spacing on local mixing time: N = 200 rpm, insertion time = 6.5 s, tracer volume = 50 cc.

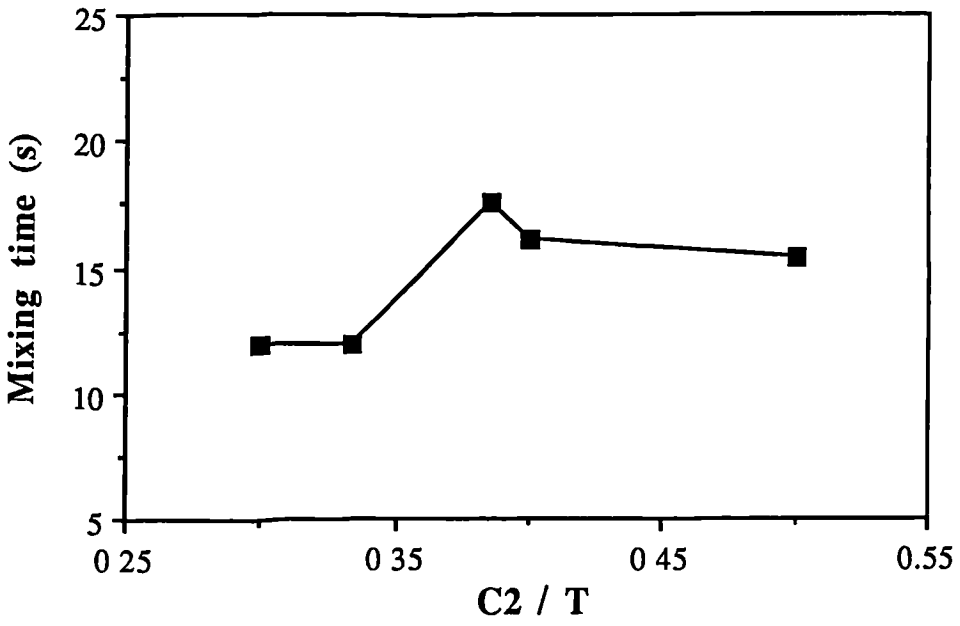

Figure 3.34. The effect of impeller spacing on mixing time averaged at 8 points: N = 200 rpm, insertion time = 6.5 s, tracer volume = 50 cc.

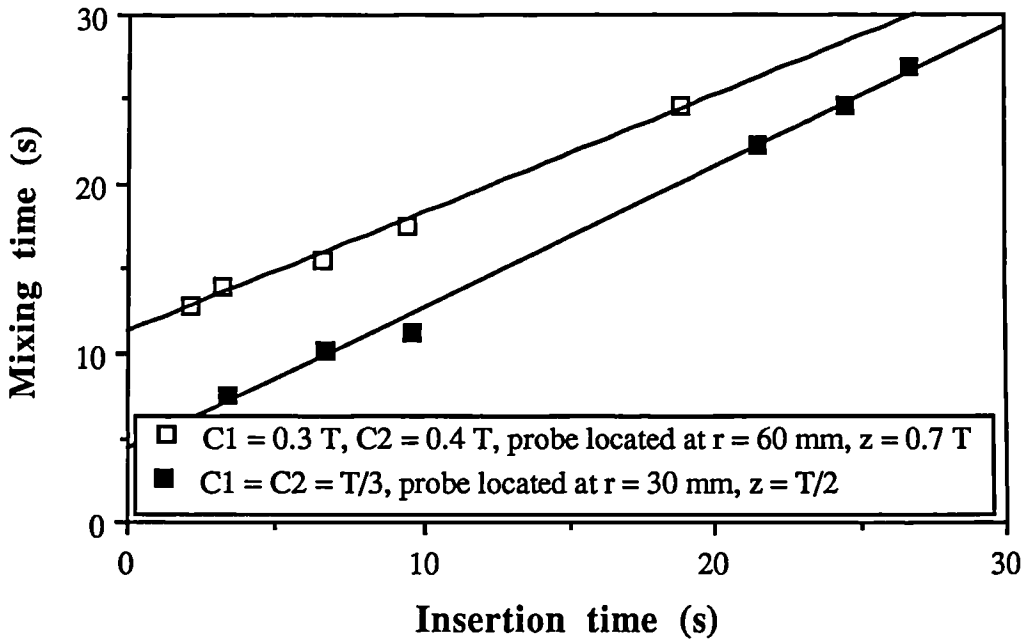

Figure 3.35. The effect of insertion time on mixing time; N = 200 rpm, tracer volume = 50 cc.

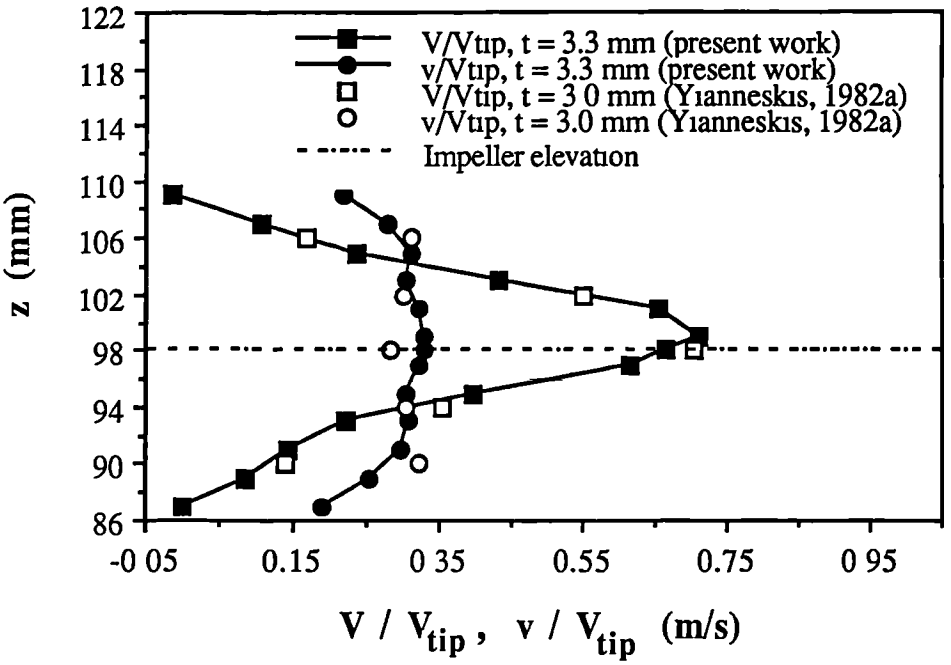

Figure 3.36. Normalized radial mean and rms velocity profiles in the impeller stream; C = T/3, r = 51 mm, theta = 0°.

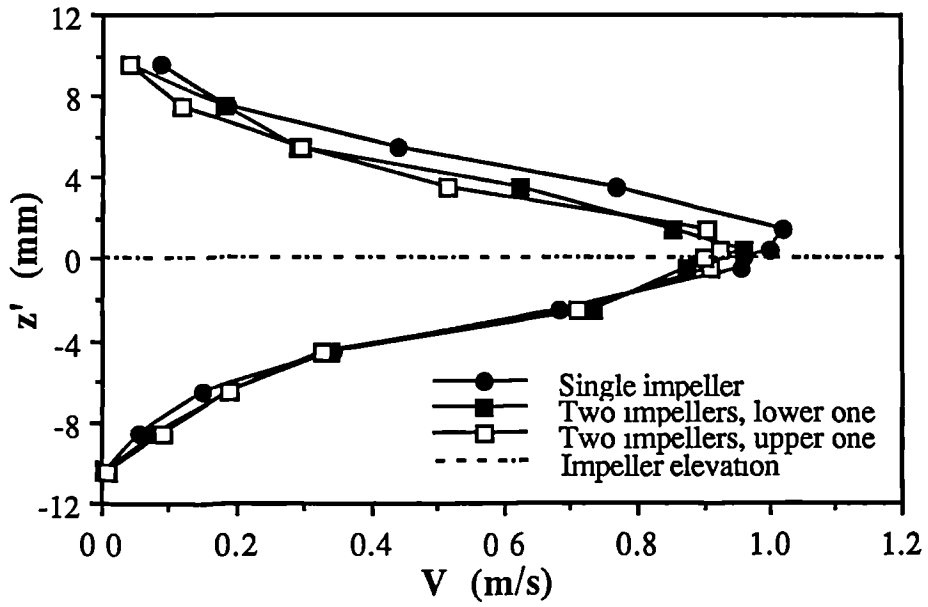

Figure 3.37. Comparison of radial mean velocities in the impeller stream between single- and double-impeller systems;
C = C1 = T/4, C2 = T/2, N = 250 rpm, r = 51 mm, theta = 0°.

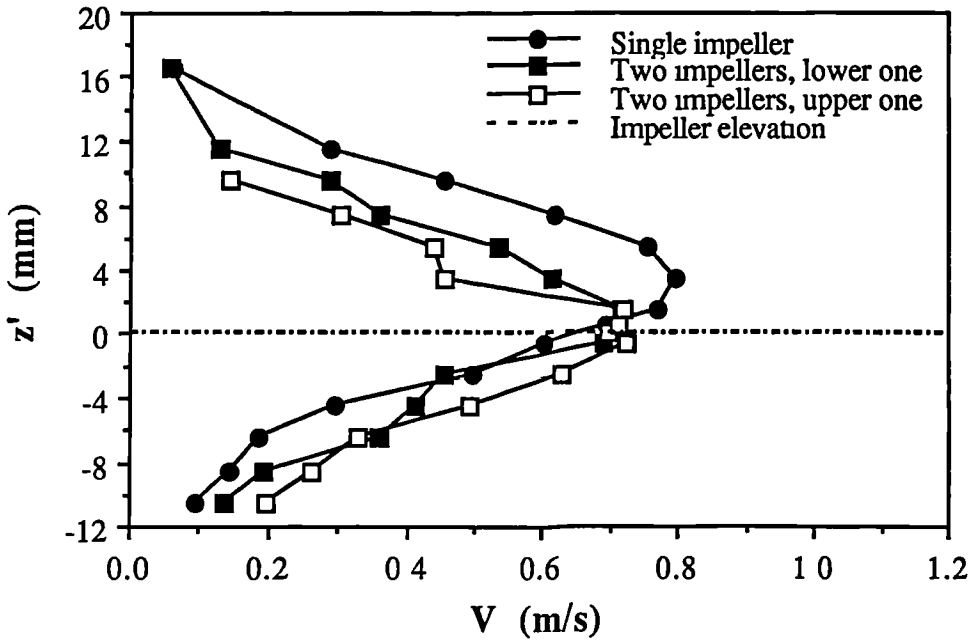

Figure 3.38. Comparison of radial mean velocity in the impeller stream between single- and double-impeller systems.
C = C1 = T/4, C2 = T/2, N = 250 rpm, r = 70 mm, theta = 0 °.

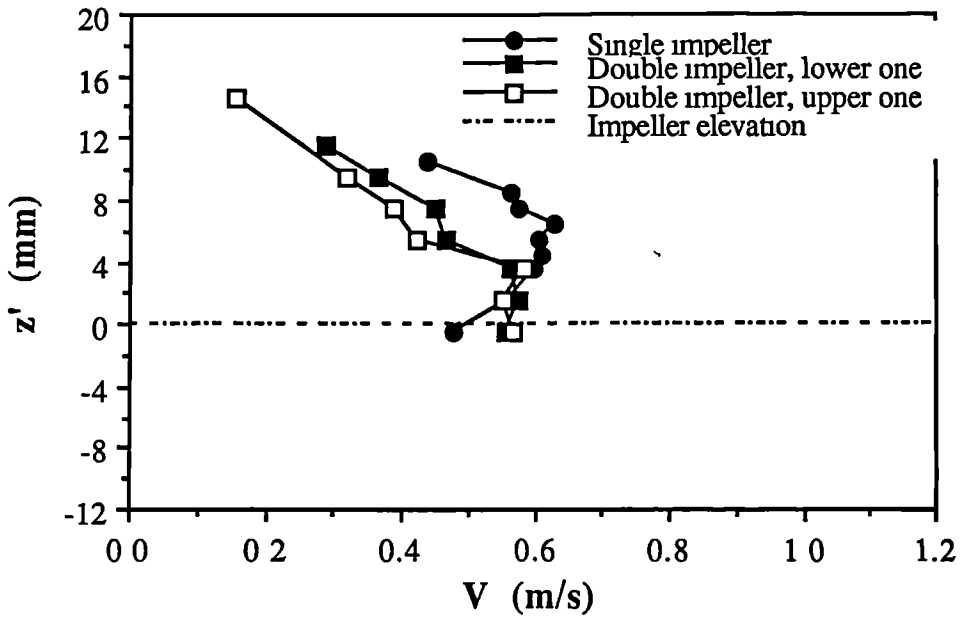

Figure 3.39. Comparison of the radial mean velocities in the impeller stream between single- and double-impeller systems;
C = C1 = T/4, C2 = T/2, N = 250 rpm, r = 85 mm, theta = 0° .

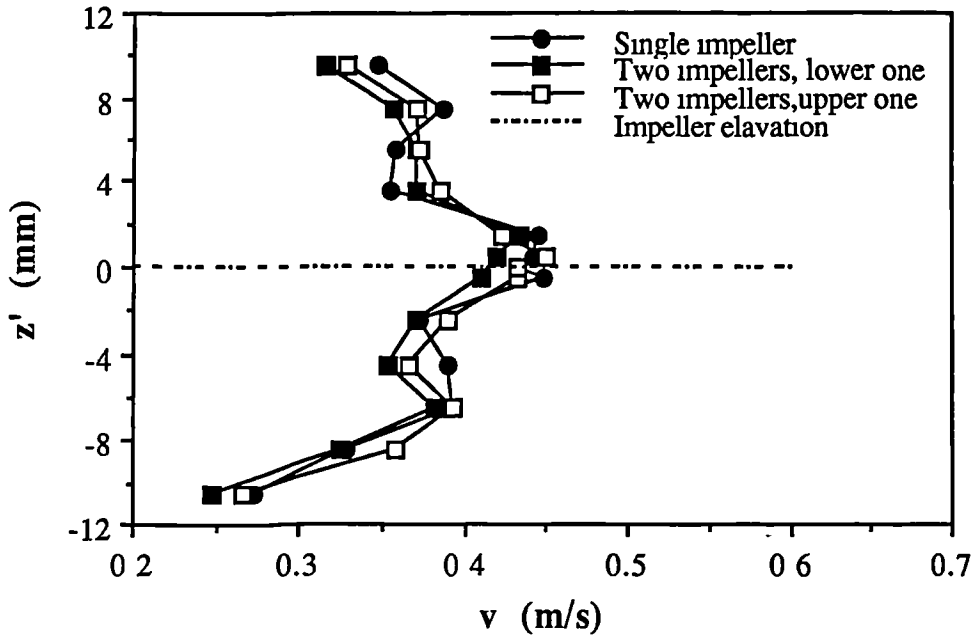

Figure 3.40. Comparison of radial rms velocities in the impeller stream between single- and double-impeller systems;
C = C1 = T/4, C2 = T/2, N = 250 rpm, r = 51 mm, theta = 0°.

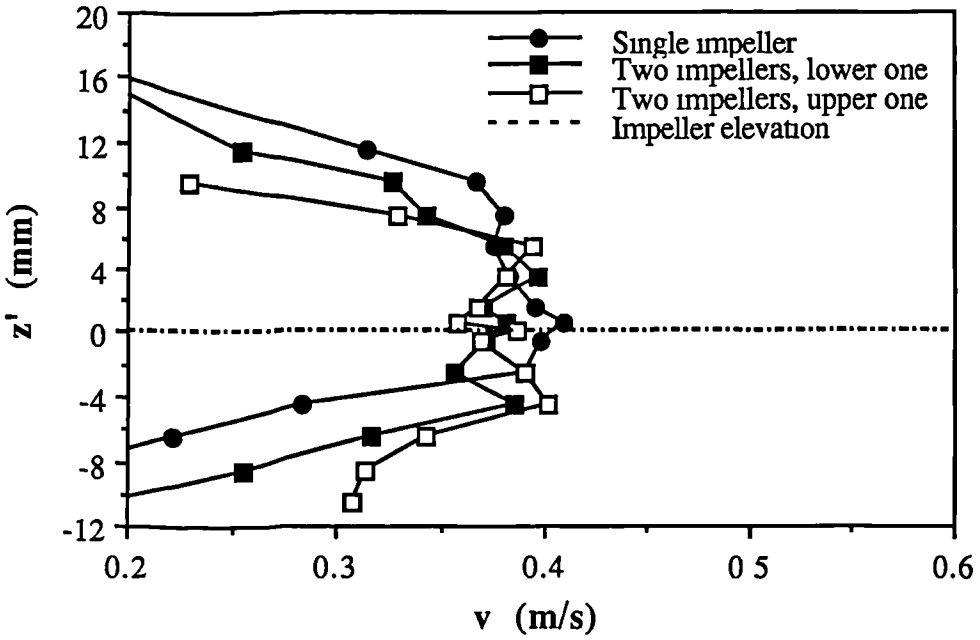

Figure 3.41. Comparison of radial rms velocities in the impeller stream between single and double impeller systems;
C = C1 = T/4, C2 = T/2, N = 250 rpm, r = 70 mm, theta = 0°.

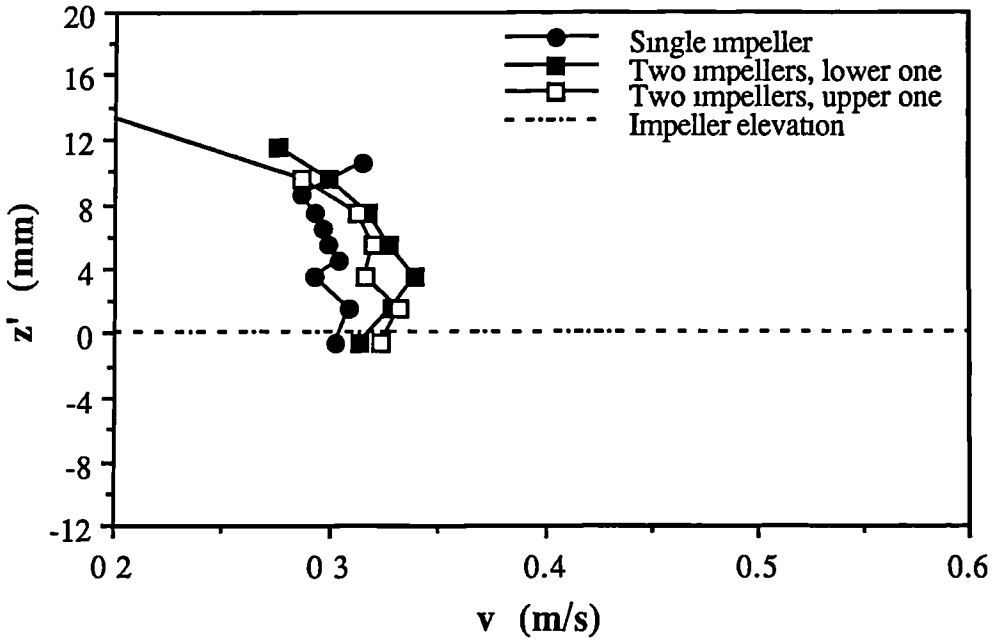

Figure 3.42. Comparison of radial rms velocities in the impeller stream between single and double impeller systems;
C = C1 = T/4, C2 = T/2, N = 250 rpm, r = 85 mm, theta = 0°.

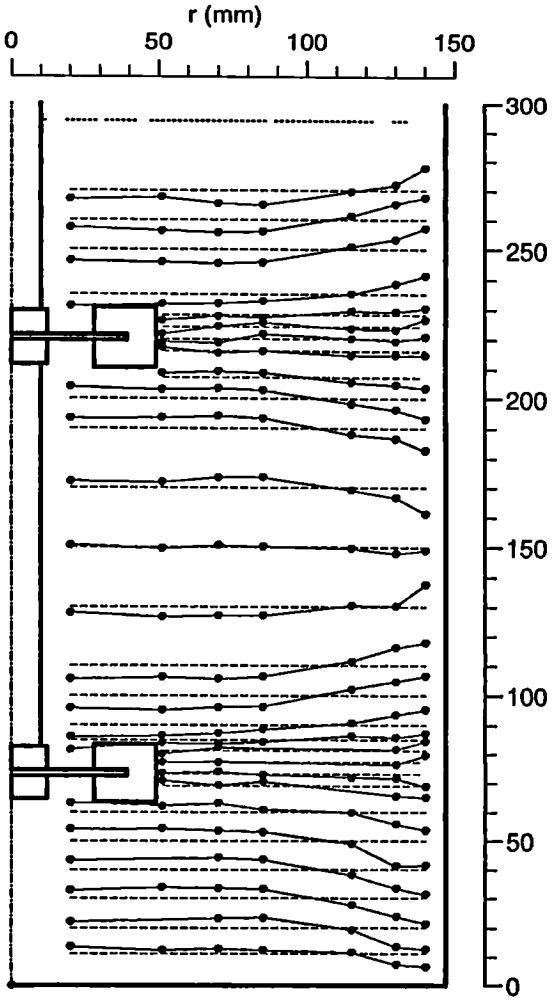

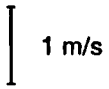

Figure 3.43. Axial mean velocity profiles, C1 = T/4, C2 = T/2.

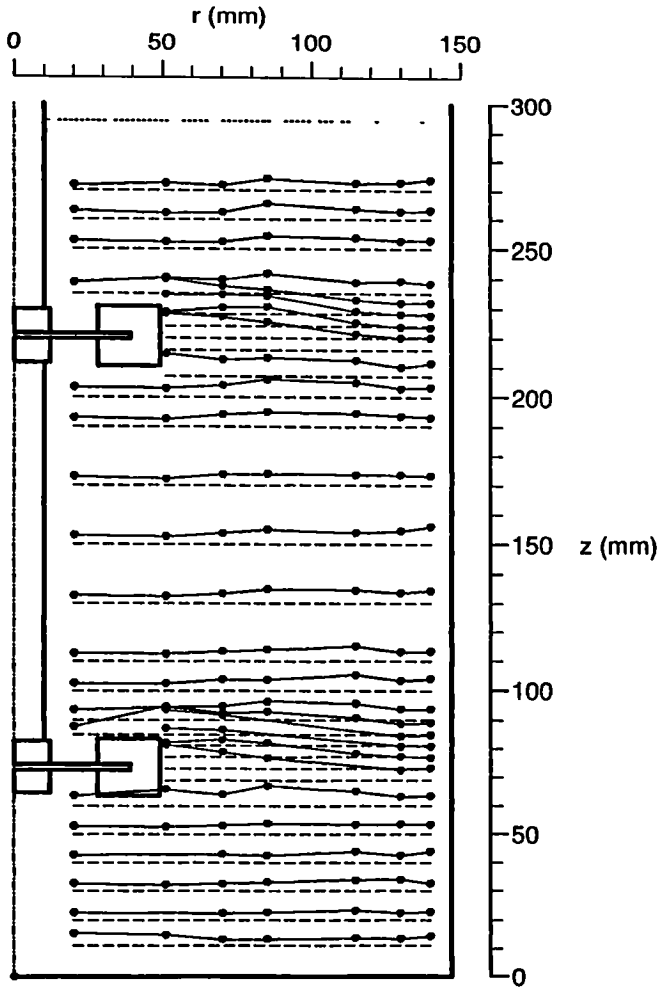

Figure 3.44. Axial rms velocity profiles, C1 = T/4, C2 = T/2.

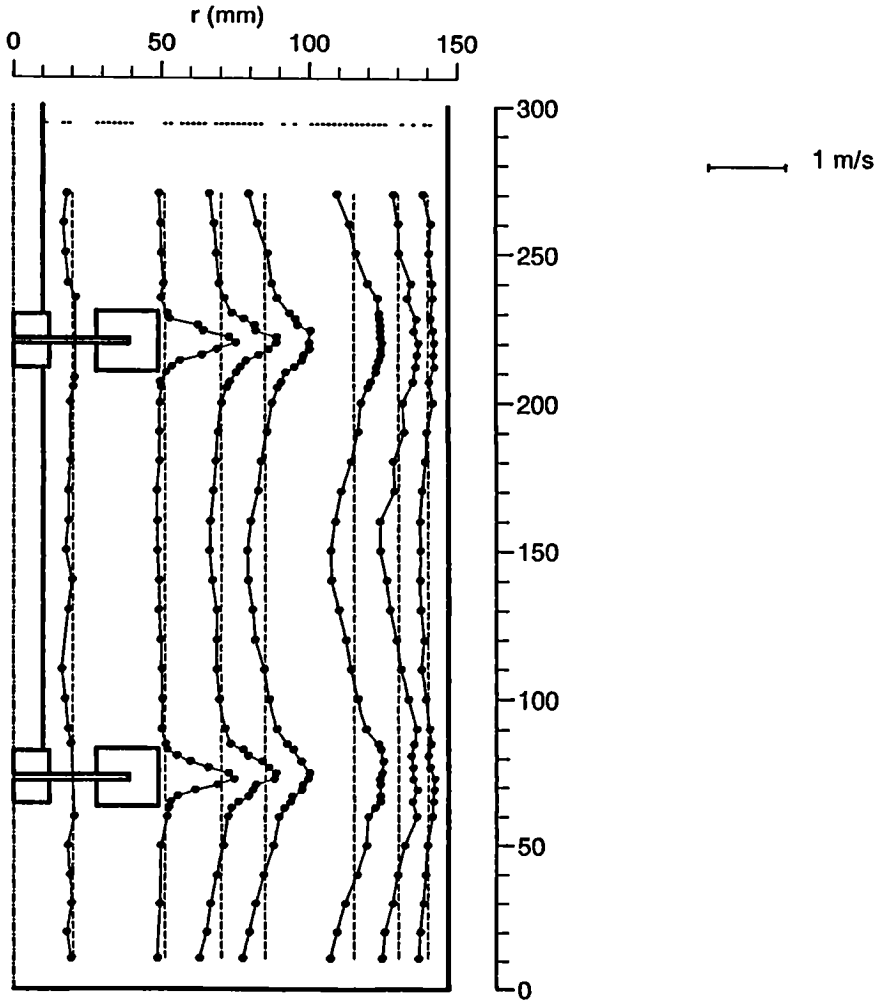

Figure 3 45. Radial mean velocity profiles, C1 = T/4, C2 = T/2.

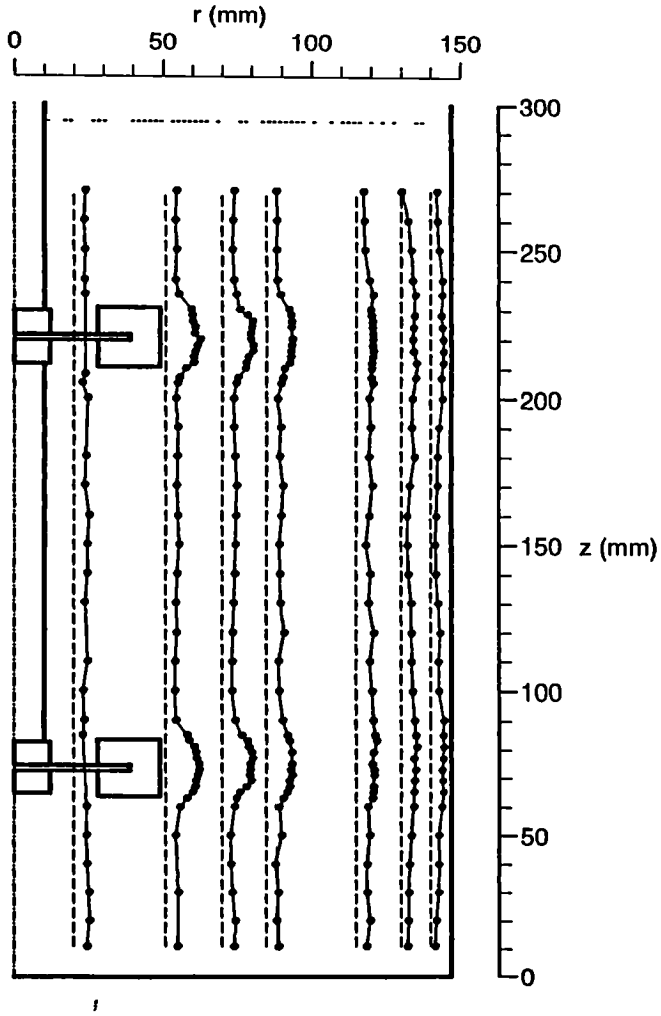

Figure 3.46. Radial rms velocity profiles, C1 = T/4, C2 = T/2.

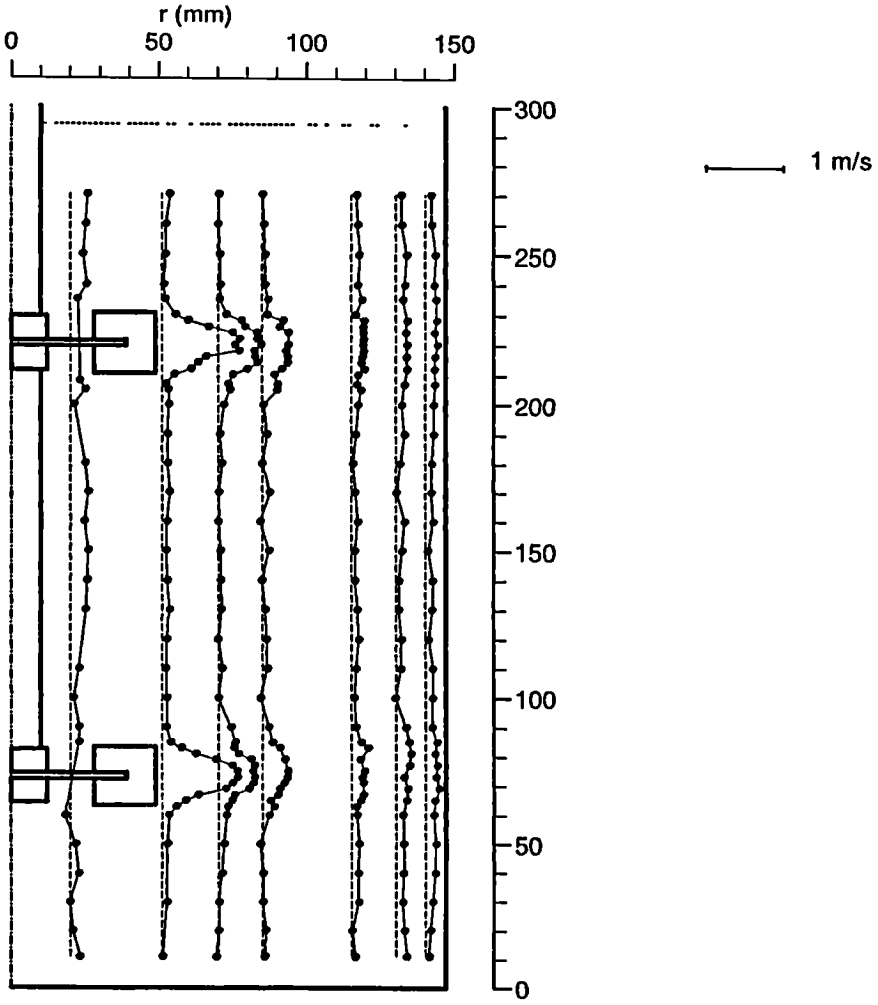

Figure 3.47. Tangential mean velocity profiles, C1 = T/4, C2 = T/2.

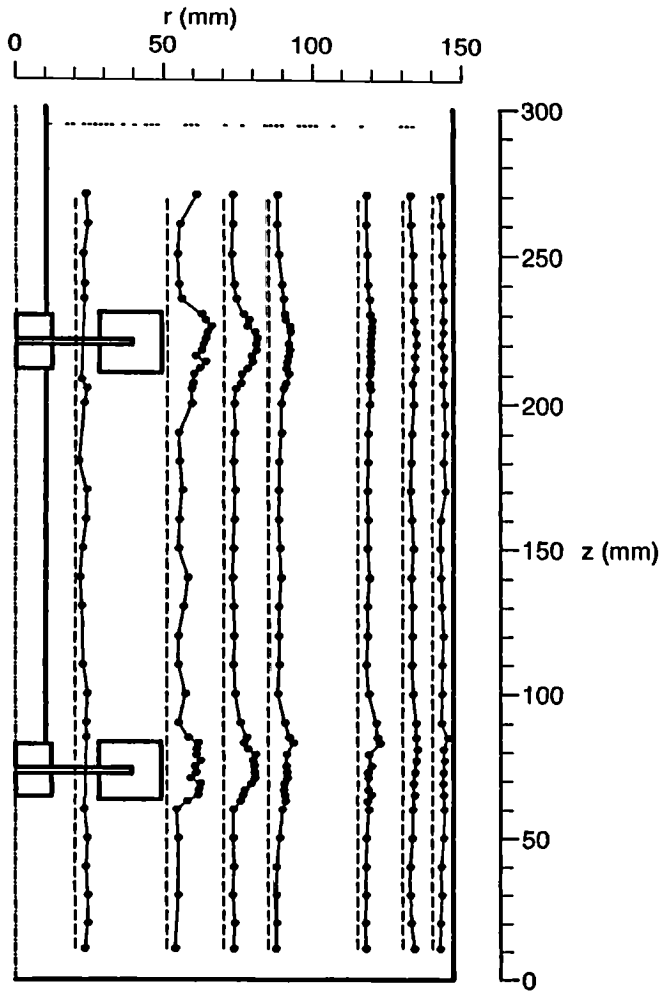

Figure 3.48. Tangential rms velocity profiles, C1 = T/4, C2 = T/2.

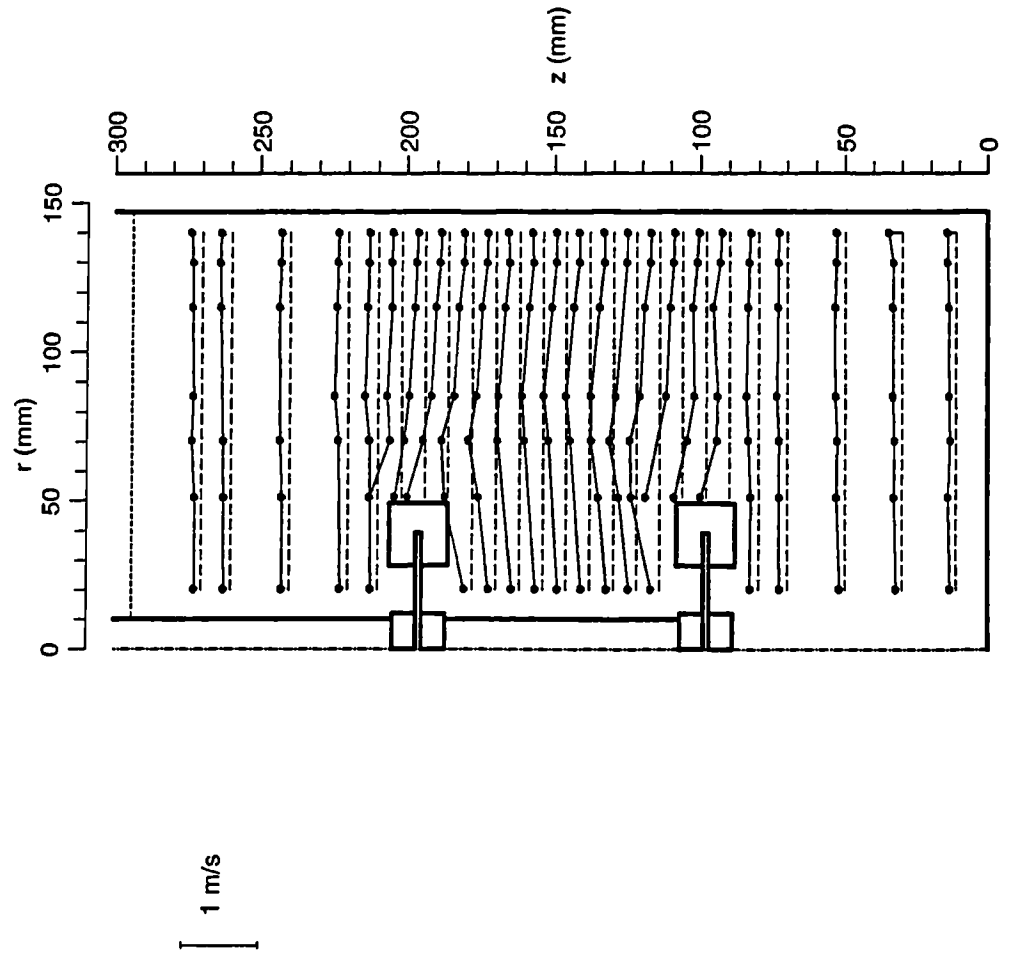

Figure 3.50. Axial rms velocity profiles; C1 = C2 = T/3.

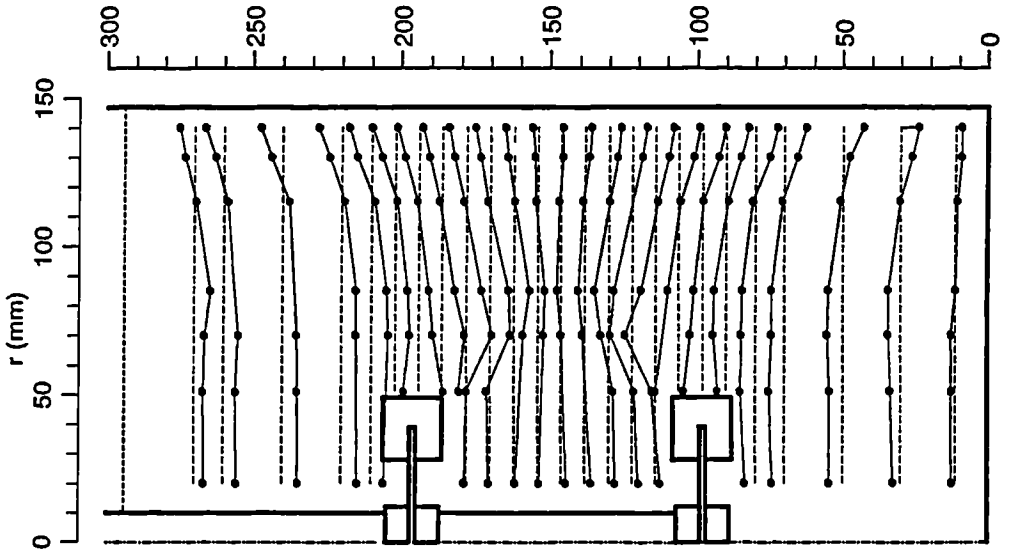

Figure 3.49. Axial mean velocity profiles; C1 = C2 = T/3.

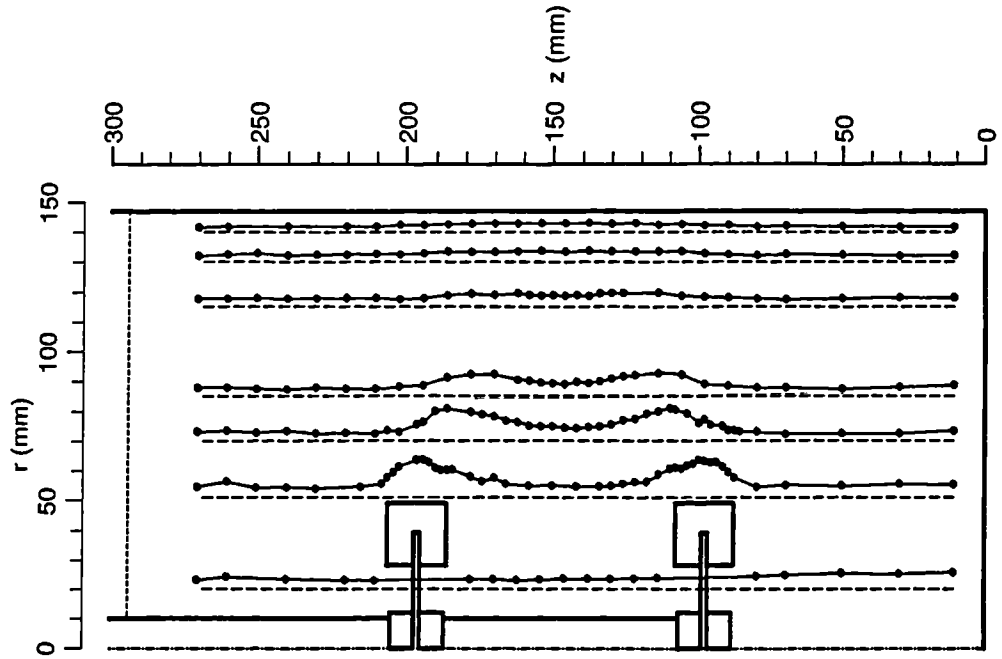

Figure 3 52. Radial rms velocity profiles; C1 = C2 = T/3.

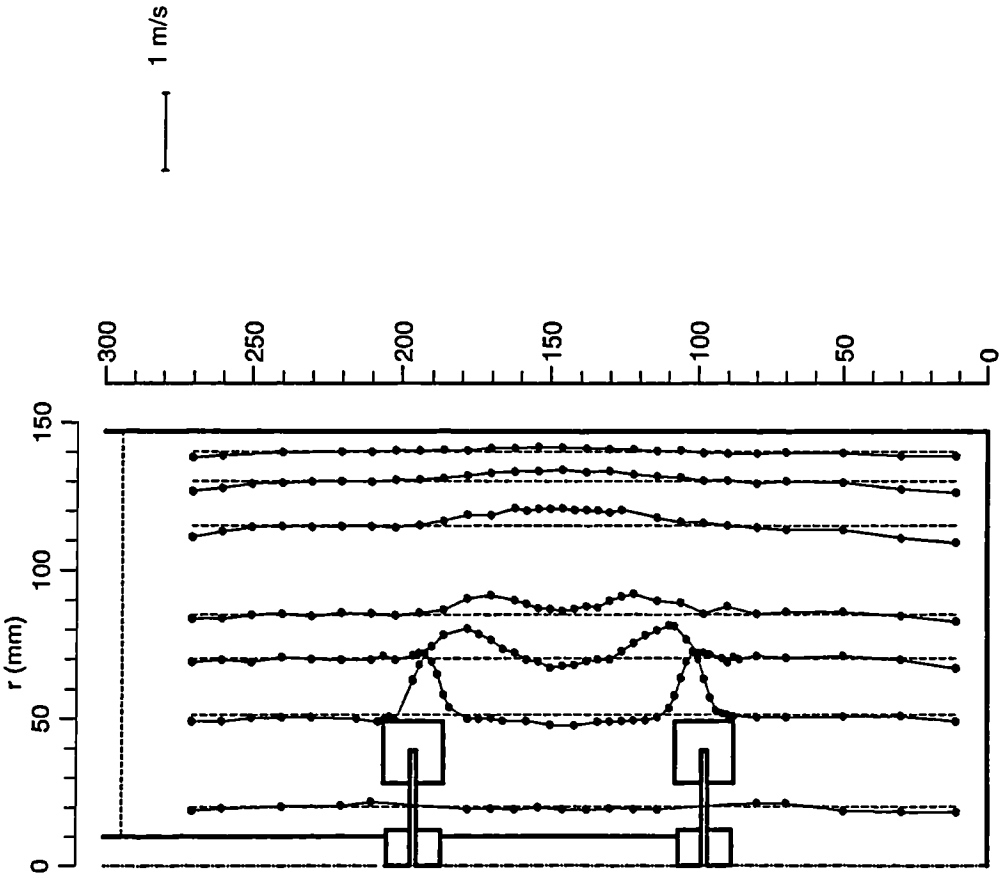

Figure 3.51. Radial mean velocity profiles; C1 = C2 = T/3.

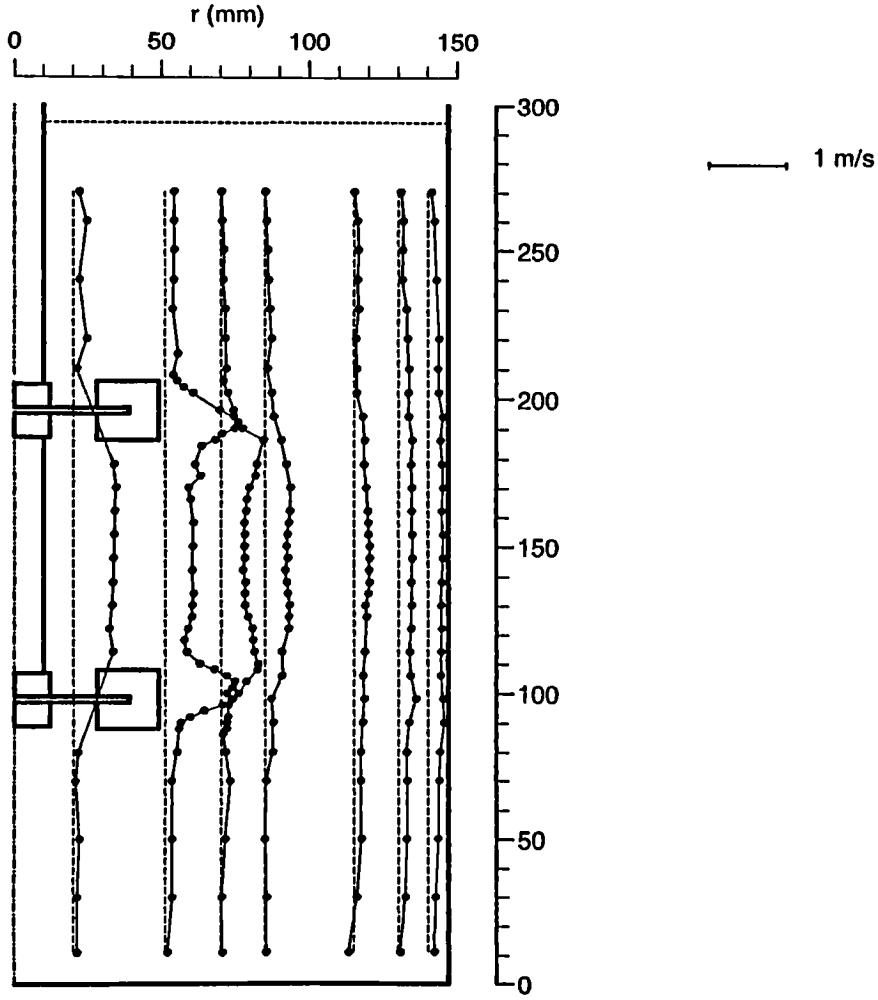

Figure 3.53. Tangential mean velocity profiles, C1 = C2 = T/3.

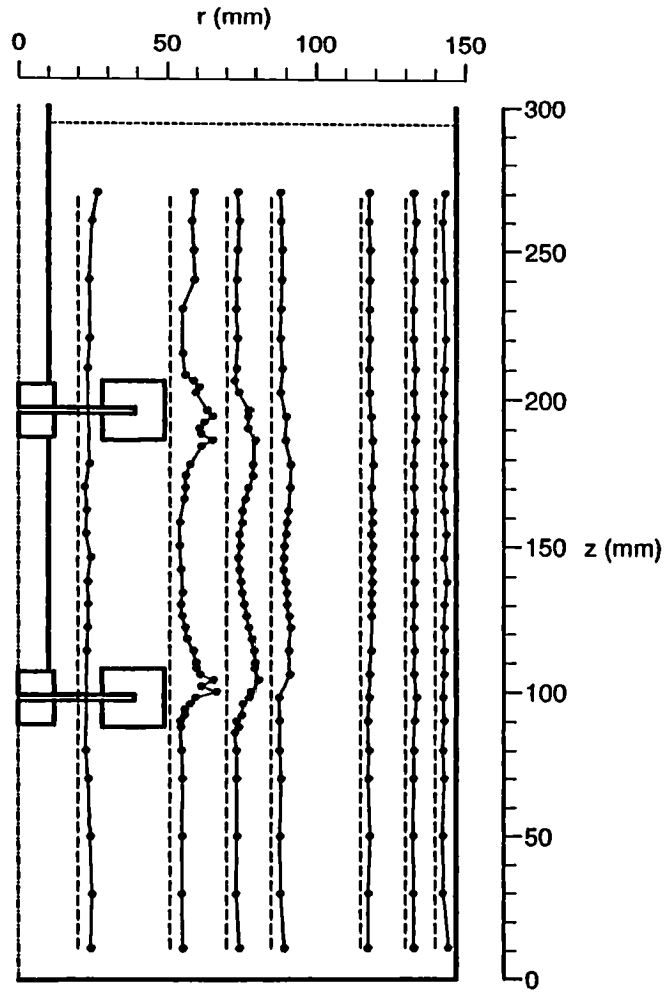

Figure 3 54. Tangential rms velocity profiles; C1 = C2 = T/3.

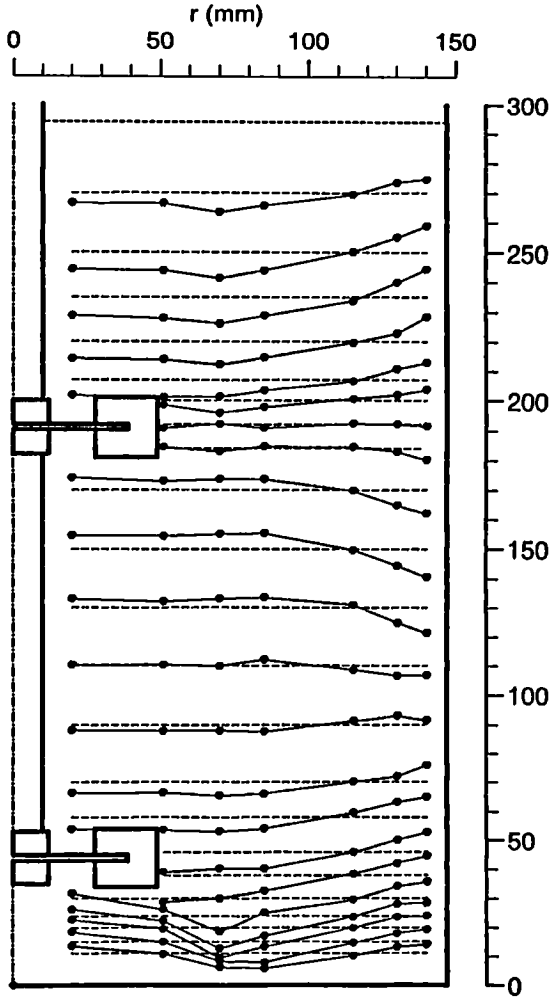

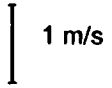

Figure 3 55. Axial mean velocity profiles; C1 = 0.15T, C2 = T/2

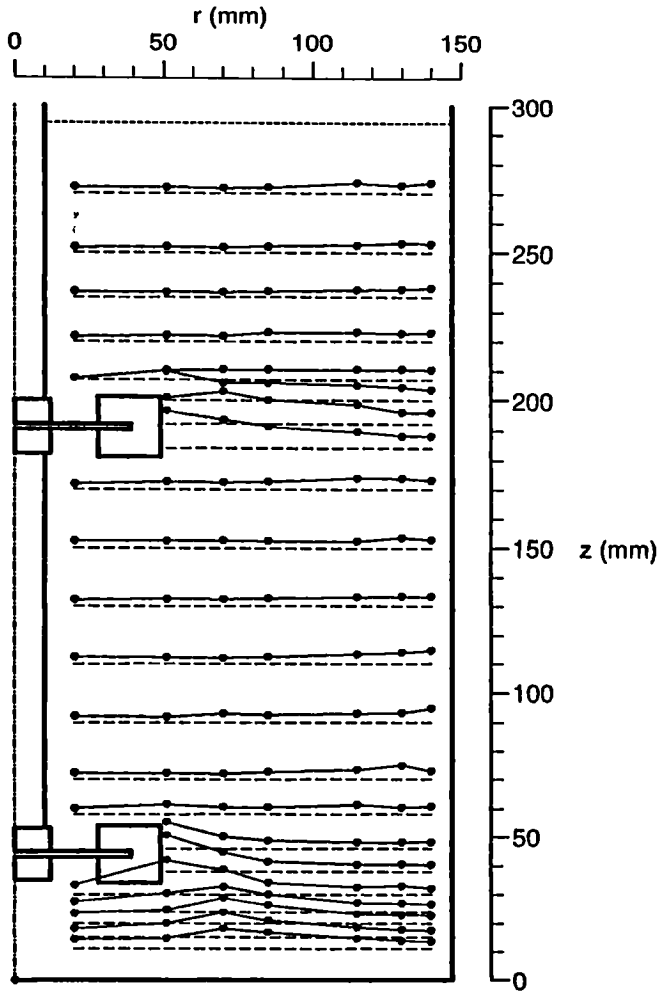

Figure 3.56. Axial rms velocity profiles; C1 = 0.15T, C2 = T/2.

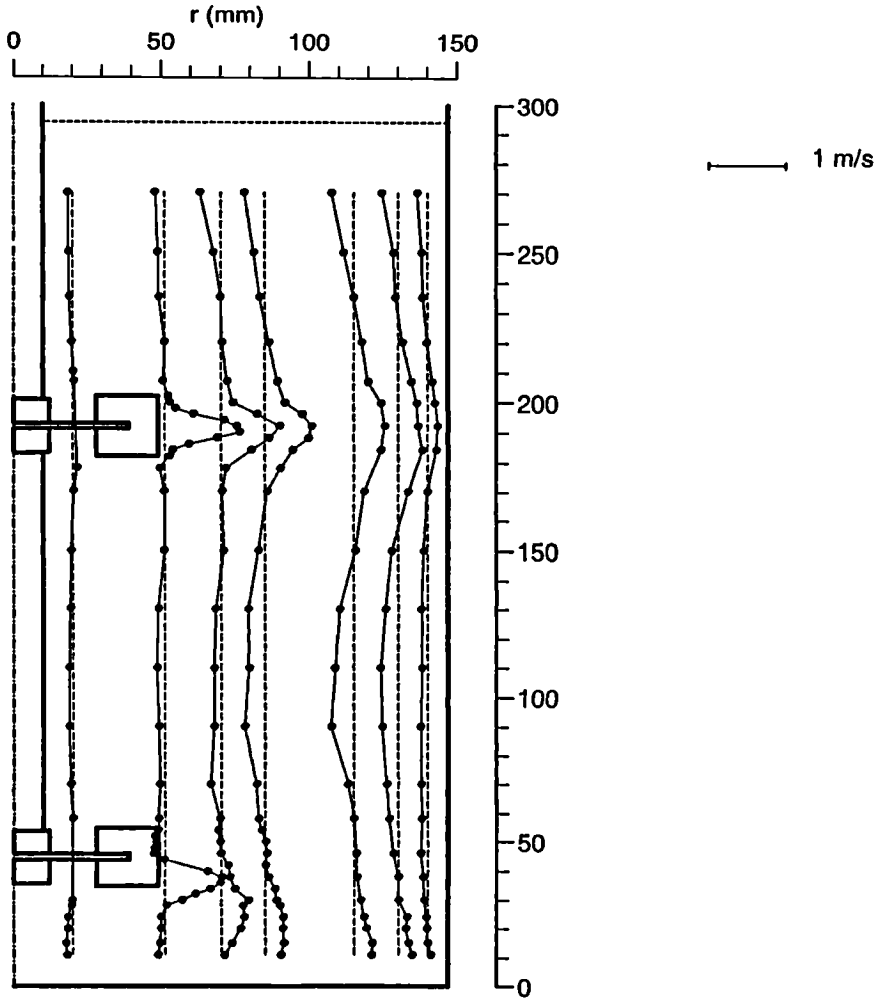

Figure 3.57. Radial mean velocity profiles; C1 = 0.15T, C2 = T/2.

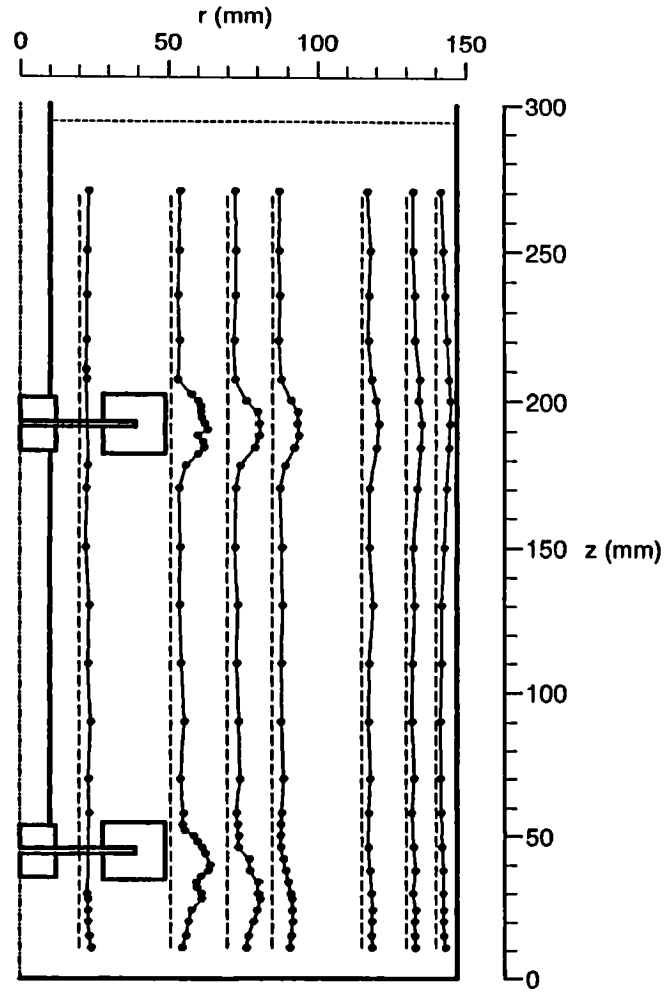

Figure 3.58. Radial rms velocity profiles; C1 = 0.15T, C2 = T/2.

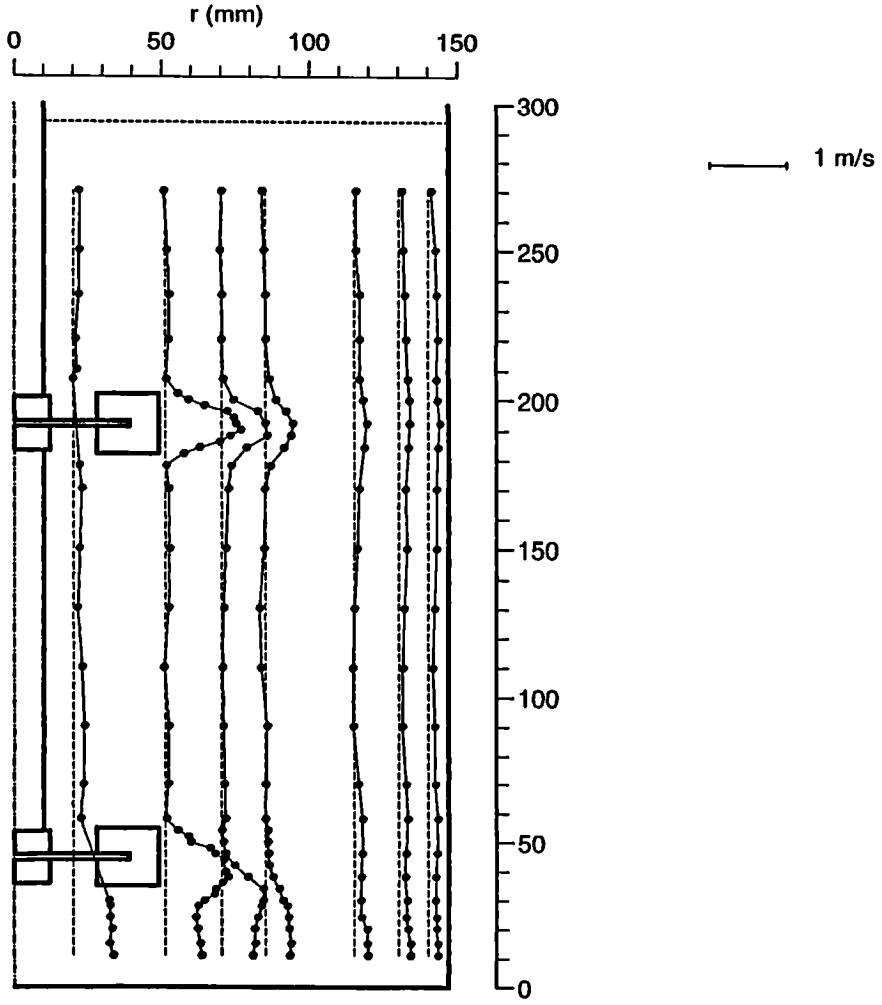

Figure 3.59. Tangential mean velocity profiles; C1 = 0.15T, C2 = T/2.

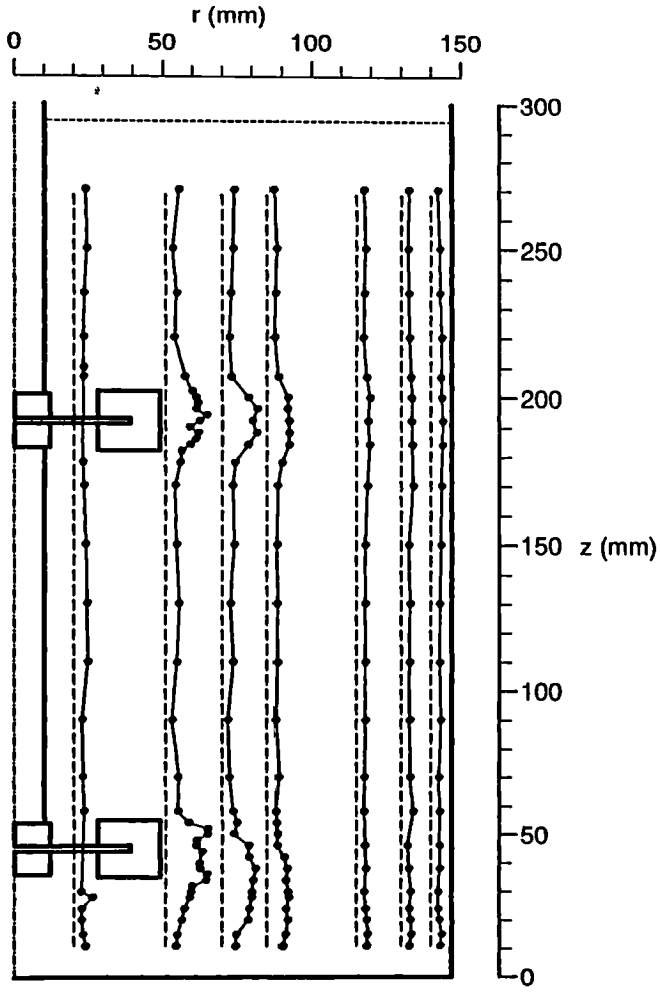

Figure 3 60. Tangential rms velocity profiles; C1 = 0.15T, C2 = T/2.

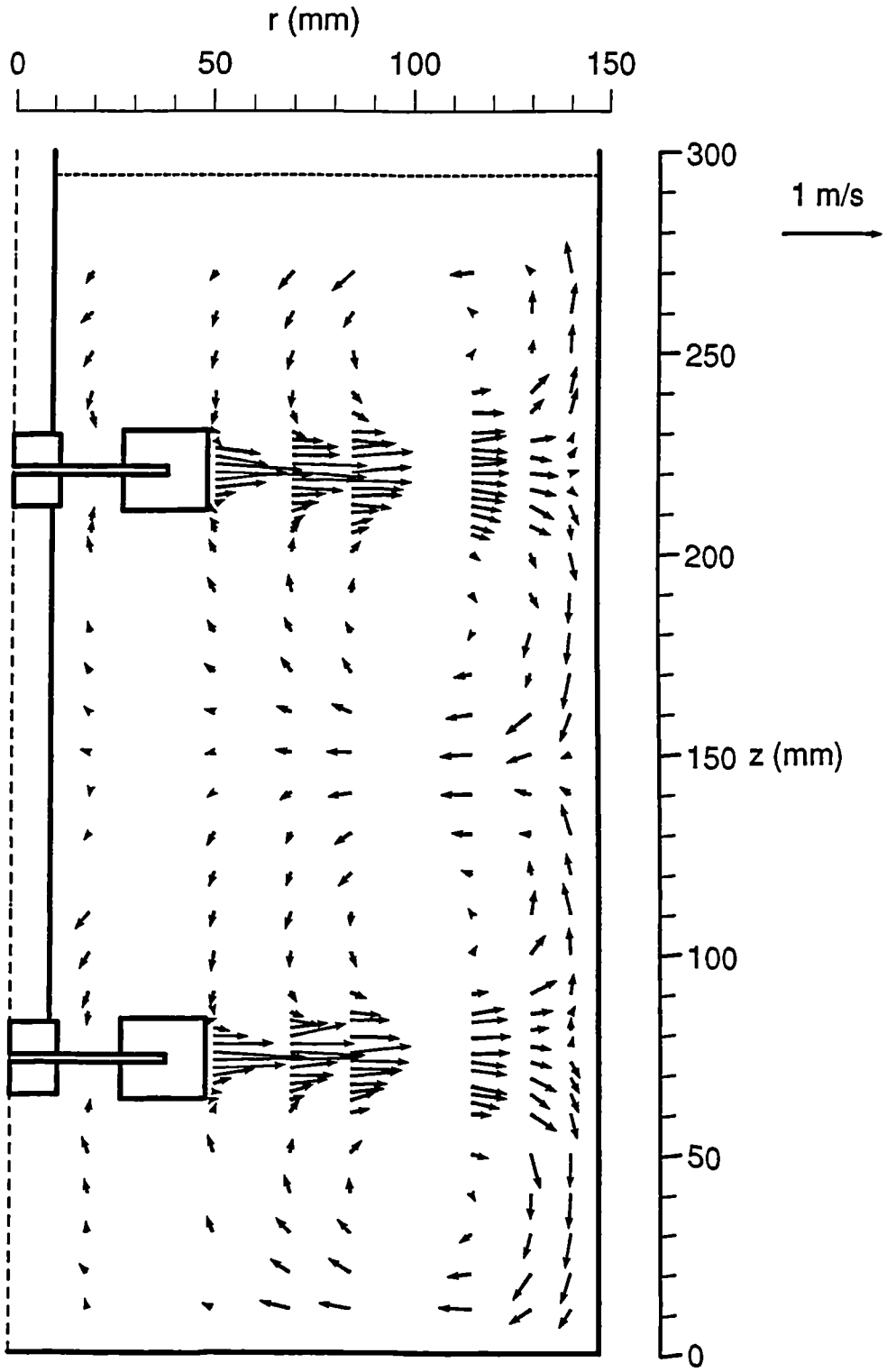

Figure 3.61. Velocity vectors in $\theta = 0^{\circ}$ r-z plane; C1 = T/4, C2 = T/2.

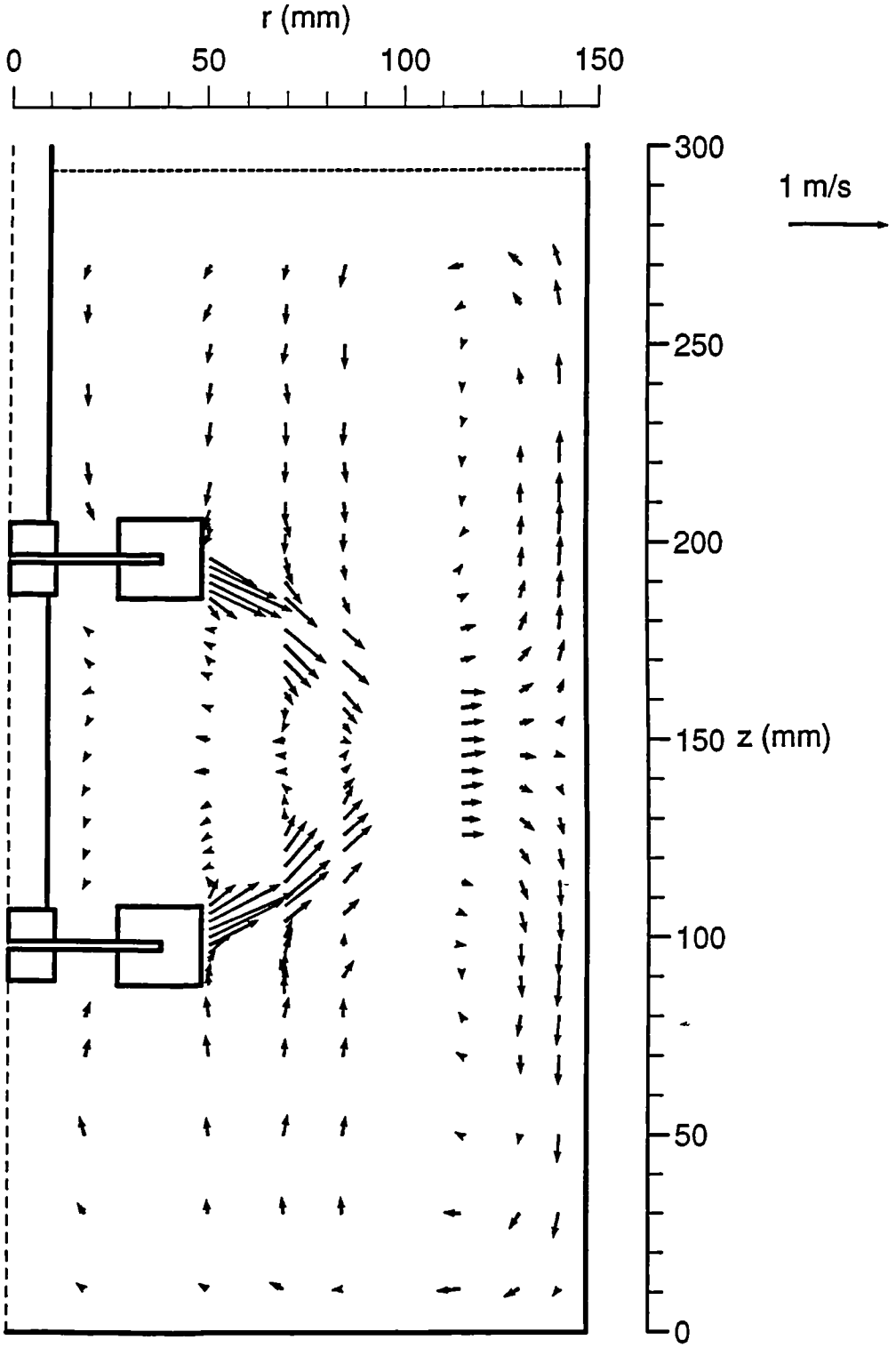

Figure 3.62. Velocity vectors in $\theta = 0^{\circ}$ r-z plane; C1 = C2 = T/3.

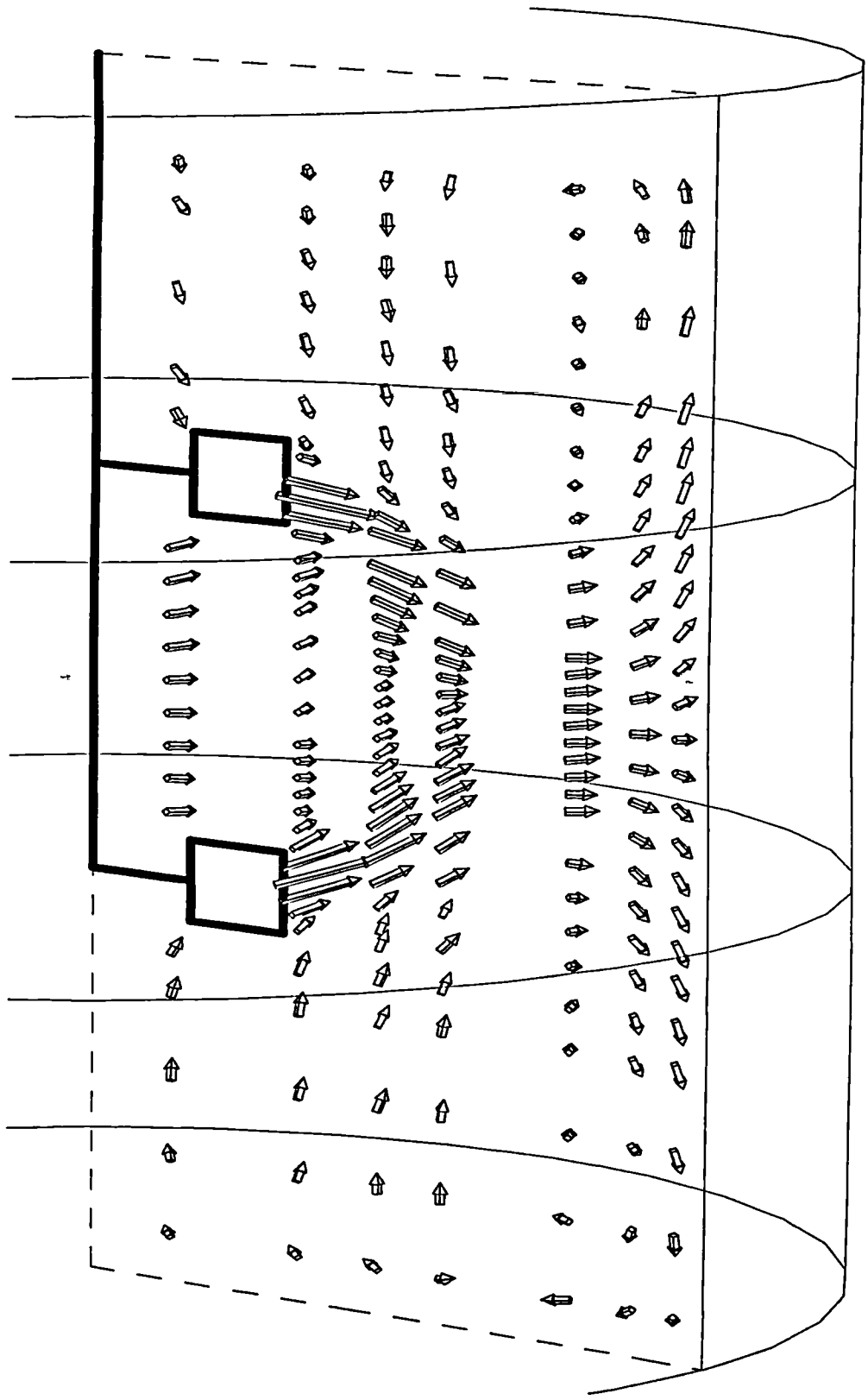

Figure 3.63. Three-dimentional velocity vectors in $\theta = 0^{\circ}$ r-z plane;
C1 = C2 = T/3.

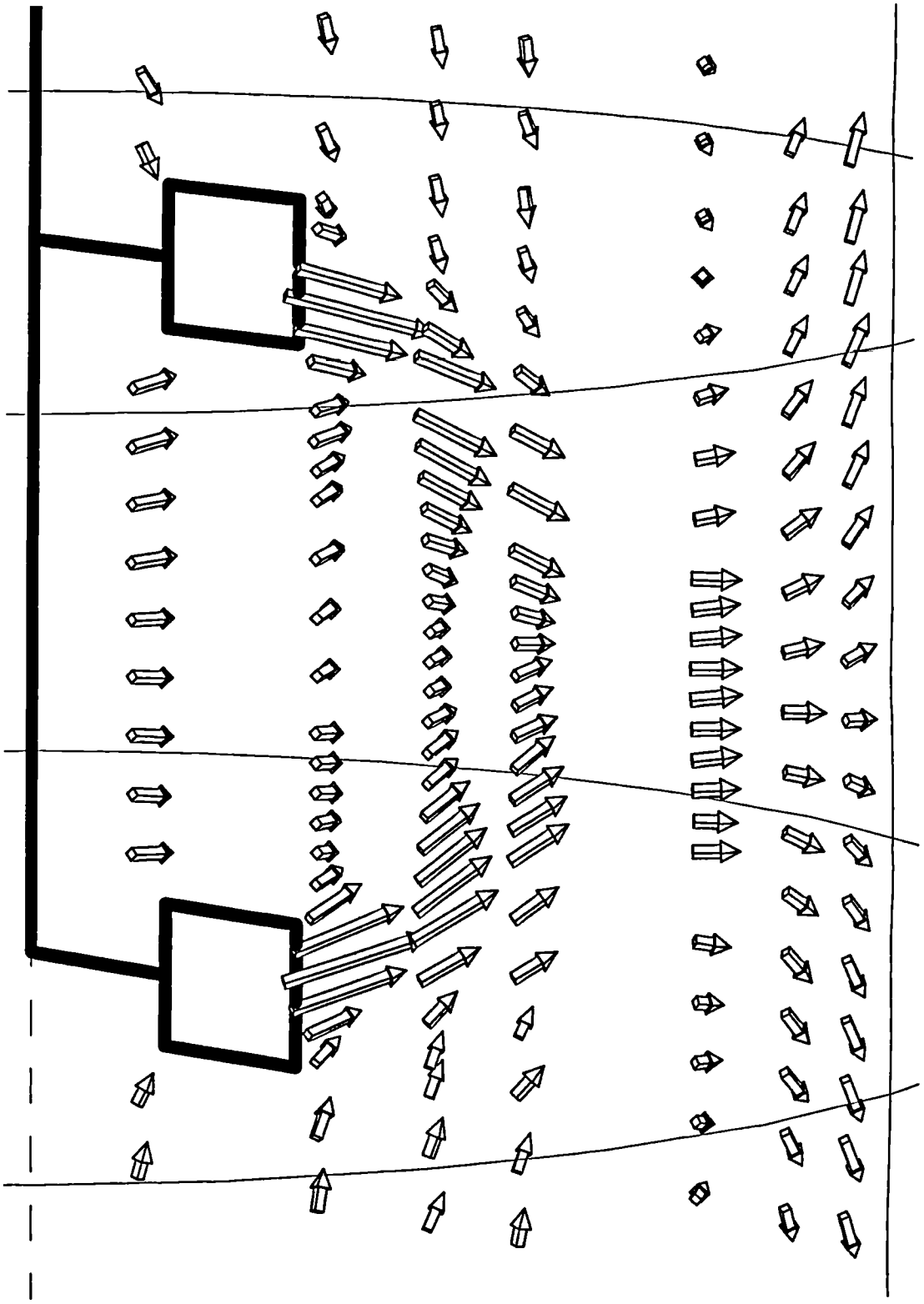

Figure 3.64. Three-dimentional velocity vectors in $\theta = 0^{\circ}$ r-z plane; impellers region, C1 = C2 = T/3.

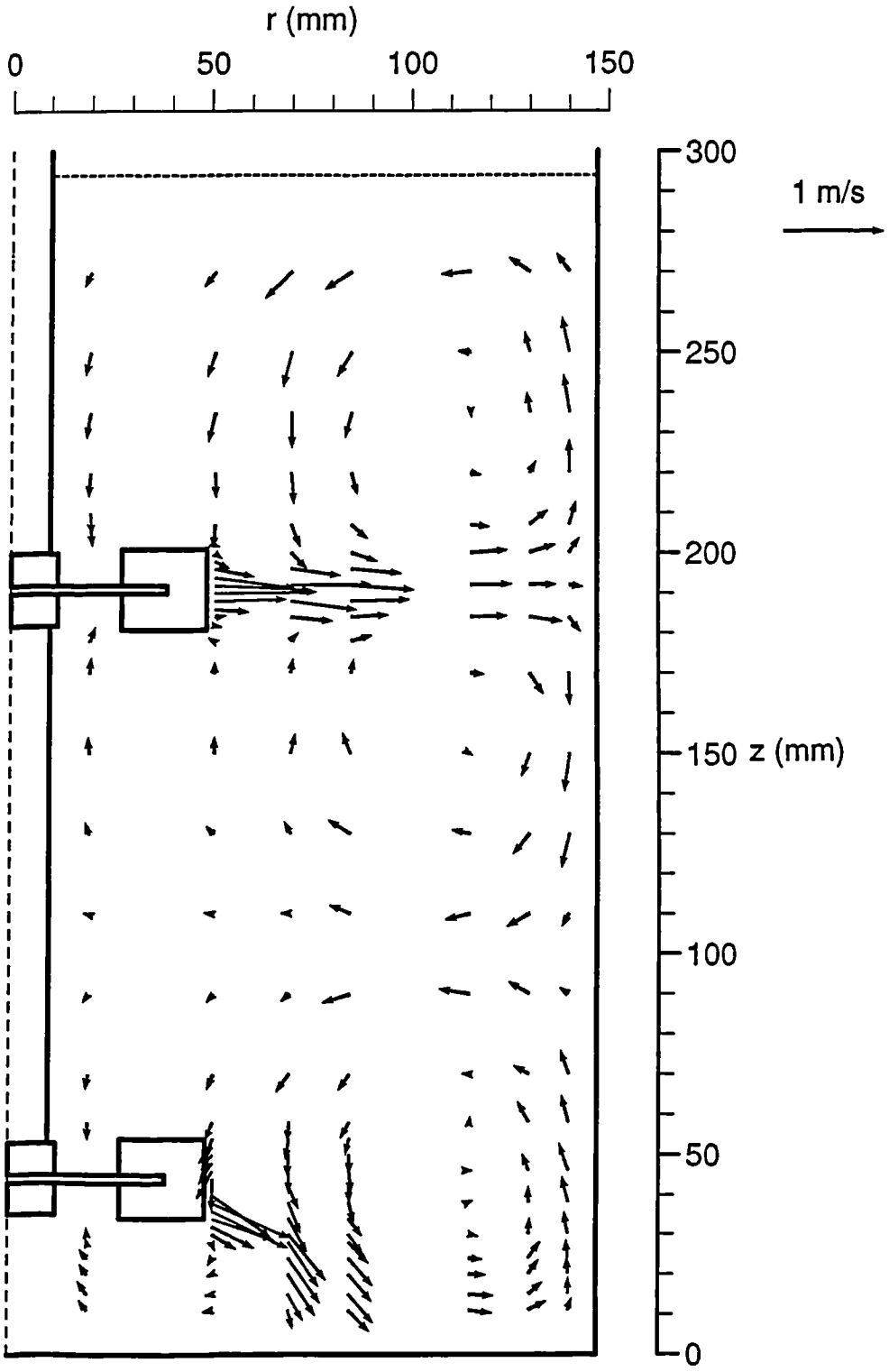

Figure 3.65. Velocity vectors in $\theta = 0^{\circ}$ r-z plane; C1 = 0.15T, C2 = T/2.

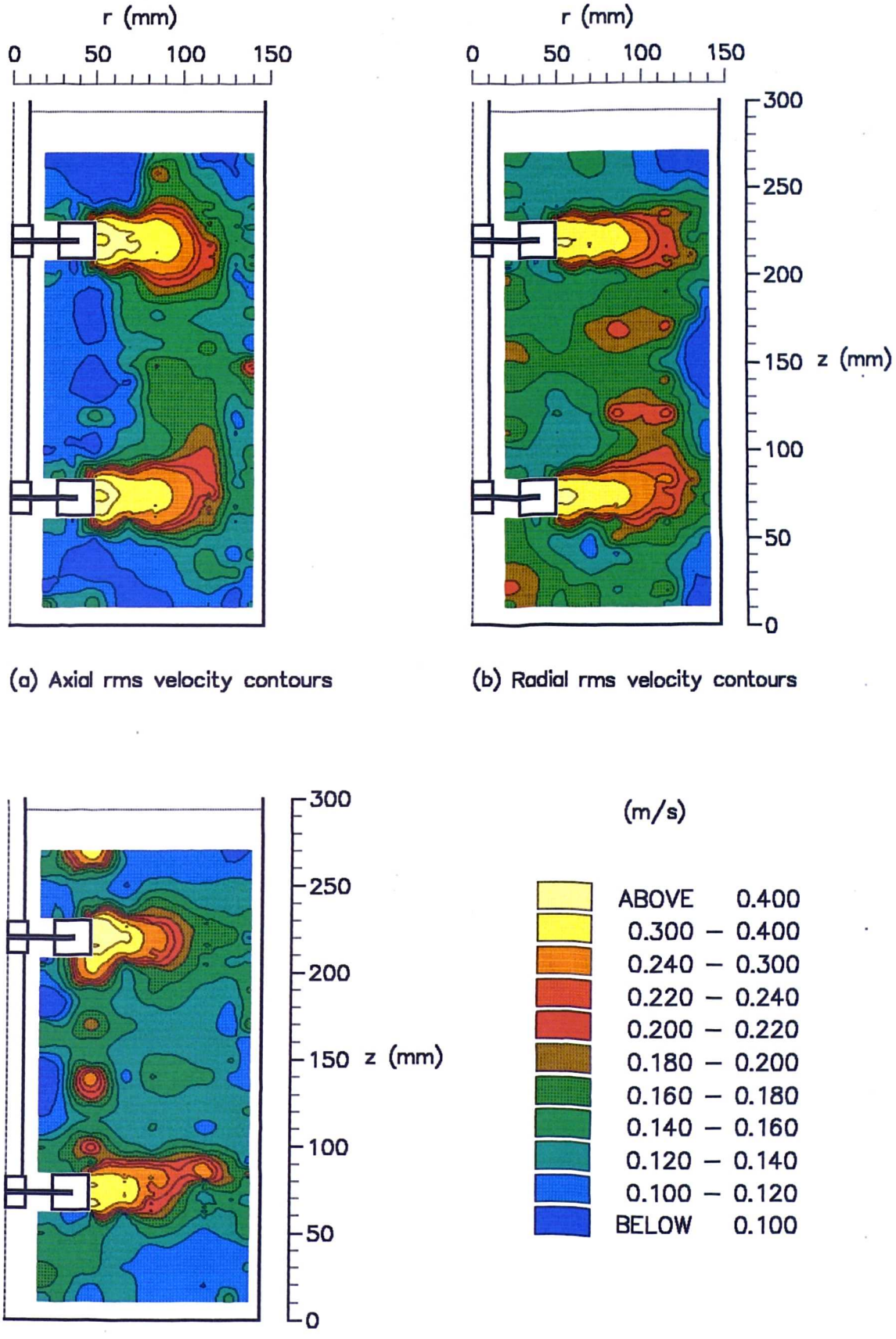

Figure 3.66. Rms velocity contours in $\theta = 0^{\circ}$ r-z plane; C1 = T/4, C2 = T/2.

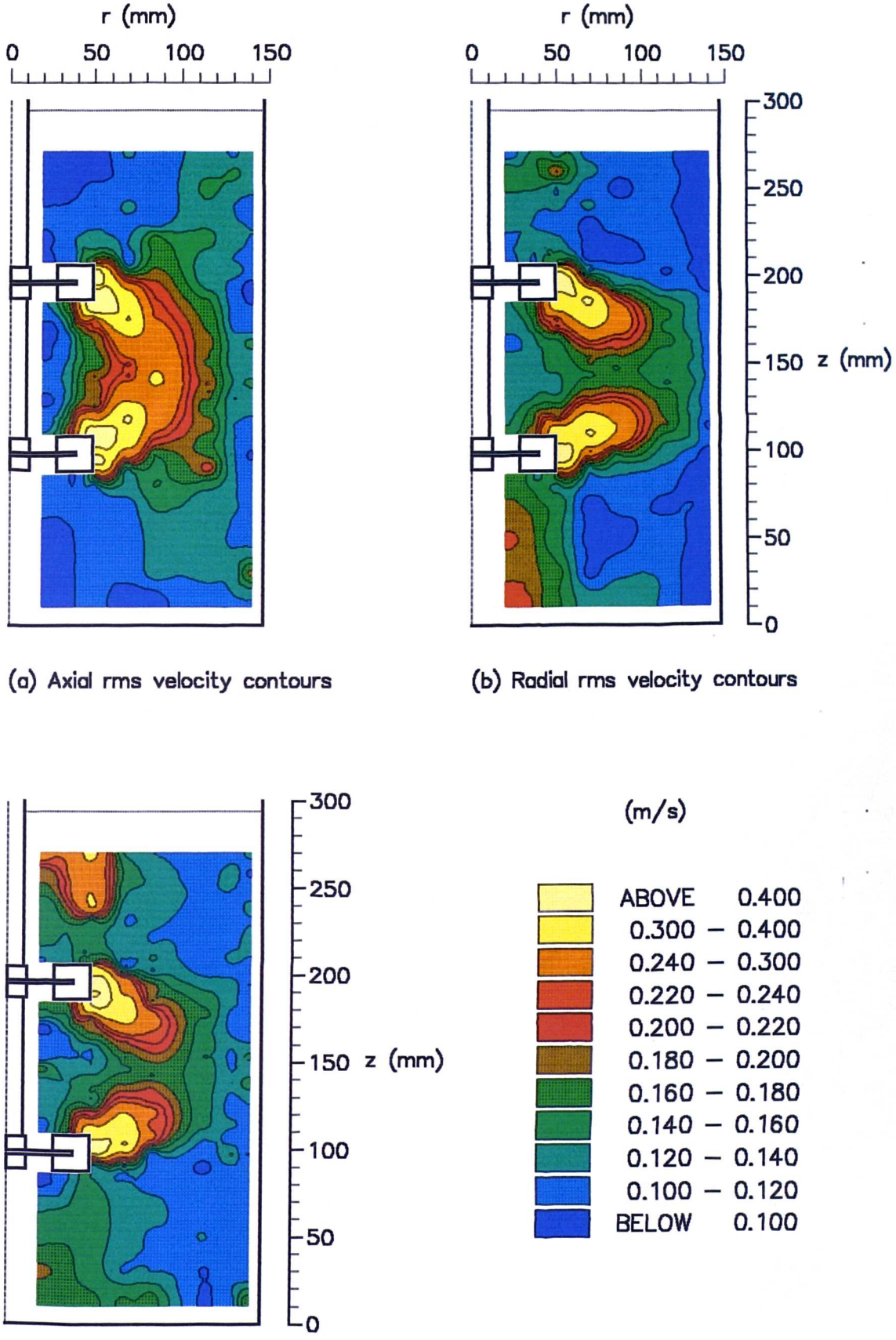

Figure 3.67. Rms velocity contours in $\theta = 0^{\circ}$ r-z plane; C1 = C2 = T/3.

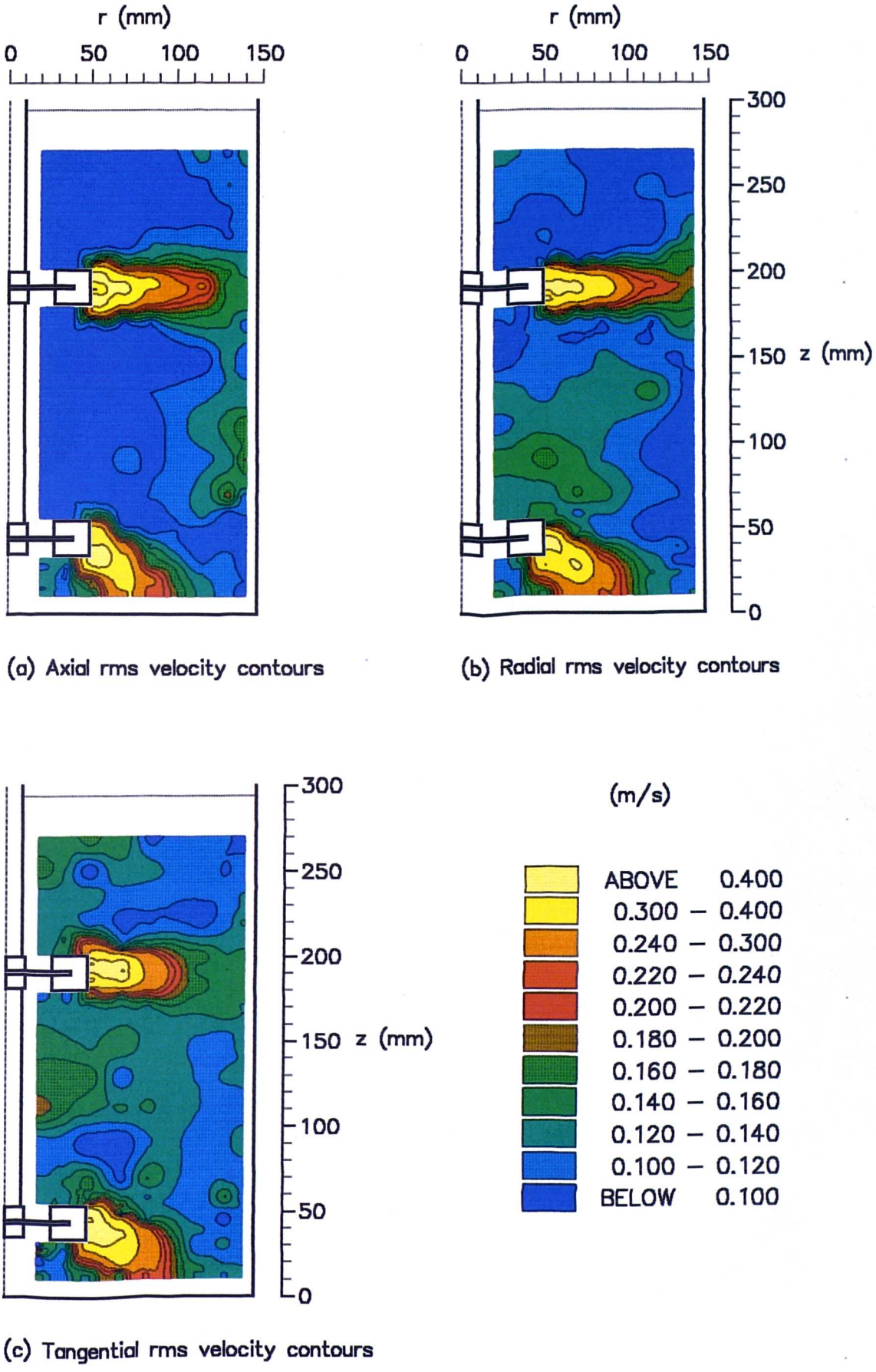

Figure 3.68. Rms velocity contours in $\theta = 0^{\circ}$ r-z plane; C1 = 0.15T, C2 = T/2.

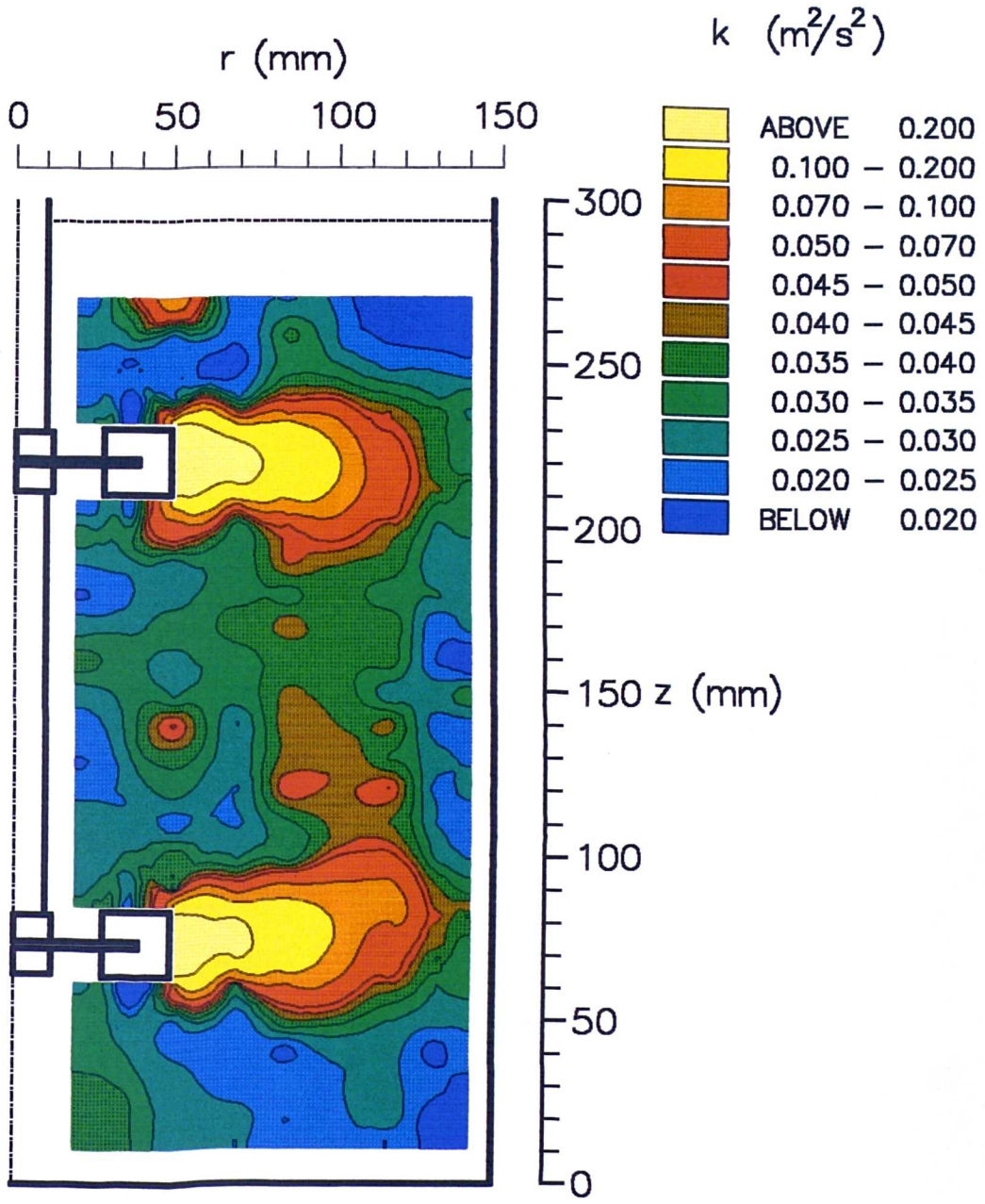

Figure 3.69. Turbulence kinetic energy contours in $\theta = 0^{\circ}$ r-z plane: C1 = T/4, C2 = T/2.

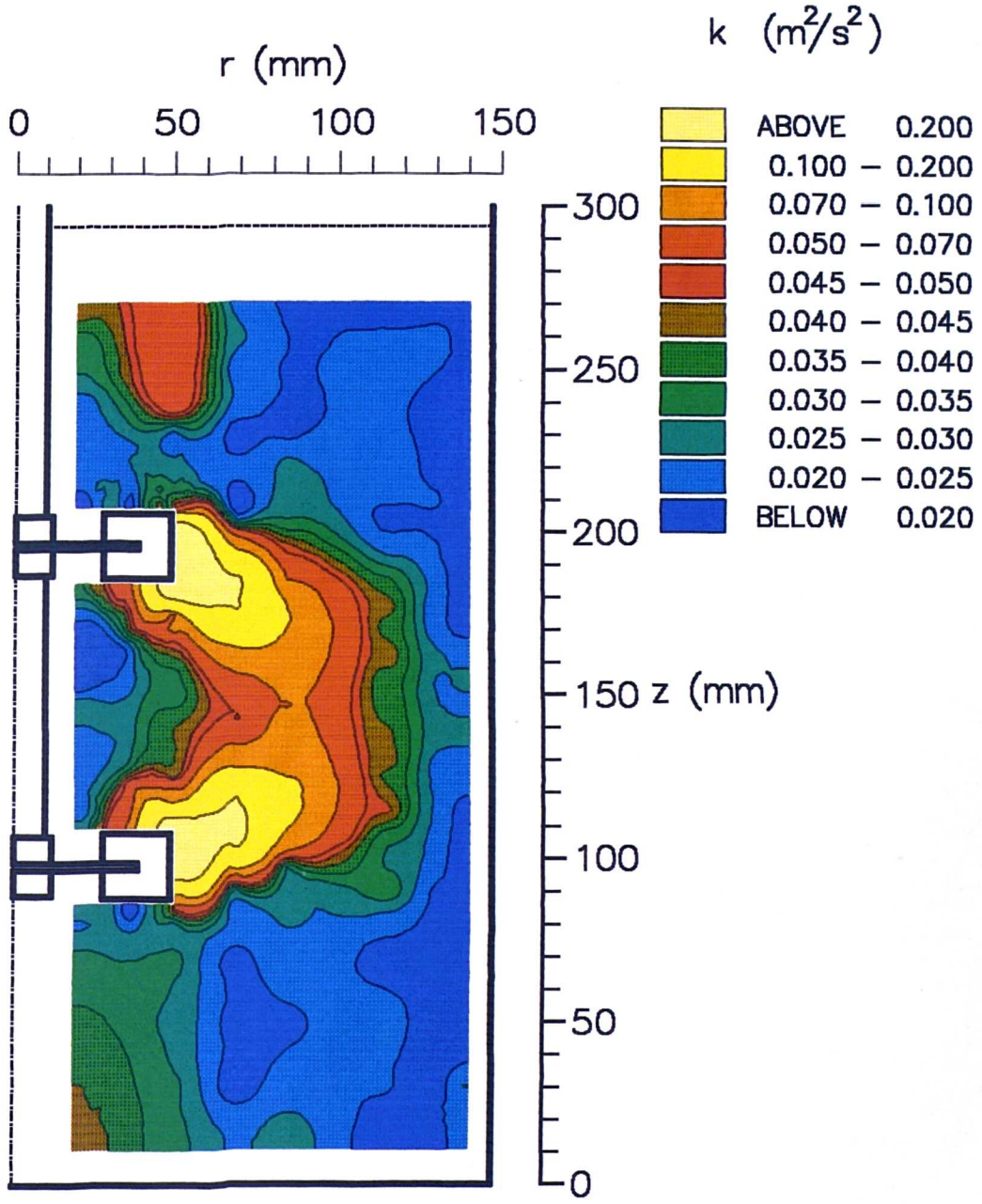

Figure 3.70. Turbulence kinetic energy contours in $\theta = 0^{\circ}$ r-z plane: C1 = C2 = T/3.

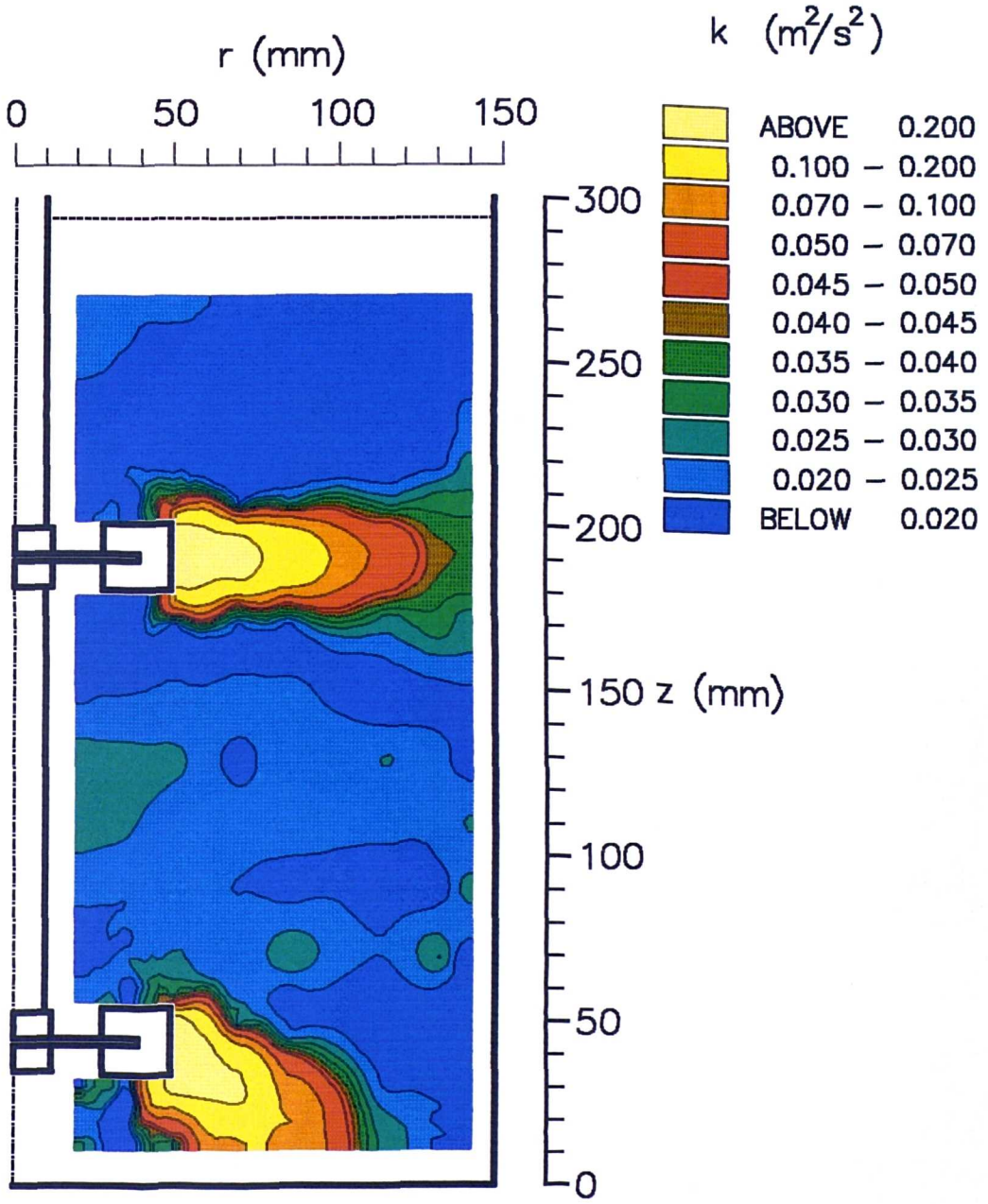

Turbulence kinetic energy contours, C1 = 0.15T, C2 = T/2.

Figure 3.71

CHAPTER 4

EFFECTS OF IMPELLER ROTATIONAL SPEED, DIAMETER AND BLADE THICKNESS ON FLUID MIXING WITH RUSHTON IMPELLERS

4.1 Introduction

This chapter describes the results of an experimental investigation concerned with the effect of impeller geometry and Reynolds number on the power consumption, mixing time, and the distribution of the mean and rms velocities in the impeller region of the stirred vessel. The experiments were carried out for both single and double Rushton impeller configurations and comparisons were made between the two.

The range of impeller rotational speeds investigated was 60 to 350 rpm. In the case of the two-impeller system the maximum speed was limited to 250 rpm in order to avoid air entrainment into the liquid from the free surface.

The variation of the power consumption with the above mentioned parameters was investigated by performing extensive and accurate torque measurements employing the telemetric device. The measurements were carried out with a flywheel attached to the shaft and only the mean values of the power numbers are presented. These results are useful for process design purposes. In addition they are important because they can be used as a reference for power consumption investigations in gassed units, using the approach which has been reported by many workers, (see, for example, Nienow and Lilly, 1979 and Bruijn et al 1974).

All the axial and radial velocities were measured over 360° of impeller revolution at the $\theta = 0^{\circ}$ r-z plane. The velocity measurements revealed a distinct effect of the impeller blade thickness on the velocity distribution in the impeller streams. They are also of benefit in removing the ambiguities inherent in the literature regarding the effect of the Reynolds number on the velocity field in the impeller stream and bulk flow of agitated tanks.

4.2 Effect of blade thickness and impeller size

As previously mentioned in Chapter 2, the impeller blade thickness for each impeller used in this project was equal to the disc thickness and both of these parameters are termed impeller thickness in the following text.

For the investigation of the effect of the impeller thickness (t), four Rushton impellers with impeller thicknesses of t = 0.8, 1.65, 2.0 and 3.3 mm were employed. All of these impellers had identical diameters, d = T/3. One Rushton impeller with t = 2.0 mm and d = 0.4T was also used in this investigation to determine the effect of the impeller size on the mixing characteristics when either the impeller thickness to diameter ratio ($\frac{t}{d}$) or the impeller thickness remains constant.

4.2.1 Power consumption

Figure 4.1 shows the results of the variation of power number obtained by the single Rushton impellers with different thicknesses at various Reynolds numbers. All the impellers involved in the above measurements had a diameter of T/3 and they were located at a clearance of C = T/3 from the bottom of the vessel. A significant increase of power number with decreasing impeller thickness is evident from this Figure. The increase of

power number is in agreement with the findings of Nienow and Miles (1971) who measured a smaller power number with an impeller with a thicker disk. The difference between the power numbers obtained by the t = 0.8 and 3.3 mm impellers (Figure 4.1) is around 1.5, i.e. an increase of around 35%. This difference is almost constant in every Reynolds number. The results also indicate an increase of power number with a rise in Reynolds number in the range of Re studied. This is particularly noticeable in the lower Reynolds numbers. The increase in Np with increasing Re is around 0.7 for all the impellers with different thicknesses.

Torque measurements were also carried out with the d = 0.4T impeller. The power numbers obtained from these measurements were compared with those measured with the smaller diameter (d = T/3) impeller but with the same impeller thickness-to-diameter ratio. This comparison is given in Figure 4.2. As can be seen from this Figure, the power number is only slightly higher with the smaller impeller. This difference is around 0.3 in the lower Reynolds numbers and decreases to 0.1 for Re's above 50000. It can be therefore concluded that t/d is an appropriate ratio to characterise impeller thickness effects. This finding is in agreement with the conclusions of Bujalski et al (1986).

In order to compare the power consumption in single- and two-impeller systems, torque measurements were carried out with the d = T/3 and t = 1.65 mm Rushton impeller located at a clearance of C = T/4. The power numbers obtained from these measurements at different Reynolds numbers were compared with those recorded for the lower impeller with the parallel flow pattern in the vessel (C_1 = T/4, C_2 = T/2). Thus the clearances C and C_1 is the same in both tests. A comparison of the two sets results is given in Figure 4.3. As this Figure indicates, the power number

obtained for the single impeller is higher (by around 7%) than that achieved for the lower impeller with the parallel flow pattern. The lower Np in the two-impeller case may be expected to be due to the interaction of the impeller streams in the parallel flow pattern, but more extensive experiments would be required to establish the reasons for the differences observed.

The power numbers obtained for impellers with different thicknesses were compared with that measured by Yianneskis (1982a). The average power numbers ($\overline{N_p}$), at different Reynolds numbers in the turbulent regime, were also calculated for all the d = T/3 impellers and compared with the ($\overline{N_p}$) prediction reported by Bujalski et al (1986). The results of these comparisons are shown in Figure 4.4. This Figure indicates that the present results are in very good agreement with the measurements of Yianneskis. A slight deviation of the present results with Bujalski et al's prediction can be observed with the t = 1.65 and 2 mm impellers. It must be noted that the accuracy of the predictions reported by Bujalski et al was 3% and the deviation of the present results from those predictions is not more than 3%. Therefore it can be expected that the present results are in good agreement with the equation formulated by Bujalski et al for the prediction of $\overline{N_p}$.

4.2.2 Mixing time

The experiments performed to investigate the effect of impeller thickness, t, and impeller diameter, d, on the overall mixing time were carried out with the Rushton impeller located at a clearance of C = T/3 from the bottom of the vessel. The impeller rotational speed was 200 rpm for the measurements with the d = T/3 impellers and 165 rpm with the d = 0.4T

impeller. The rotational speed was varied in order to maintain the impeller tip speed constant for both cases.

Mixing time measurements were carried out at five different probe locations: one in the impeller stream, two in the upper ring vortex and two in the lower ring vortex as shown in Chapter 3, Figure 3.26-a. The tracer insertion time (t_{in}) in all these experiments was 5.5 ± 0.5 seconds.

The results of the above investigation are shown in Figure 4.5. They indicate that with the small impellers (d = T/3) a comparatively shorter mixing time (10.89 s) is obtained with the thinnest impeller (t = 0.8 mm) while for the 1.65 and 3.3 mm impeller thicknesses the values are nearly identical (12.84 and 12.83 s respectively). The results also show a significant decrease of mixing time (by around 30%) when the d = 0.4T impeller was used. It must be noted that this decrease was obtained albeit the impeller thickness to diameter ratio was the same with impellers 'c'.

For comparison purposes the overall mixing time for a downward pumping pitched blade impeller is shown in this Figure as well. This mixing time is around 25% less than that obtained with the Rushton impeller with the same impeller diameter and thickness.

The mixing time obtained with the t = 1.65 mm Rushton impeller may be compared to the mixing times obtained in the two-impeller system presented in Chapter 3, Figure 3.34. The comparison indicates that a single impeller results in a mixing time almost equal to that obtained with two impellers producing the merging flow pattern.

4.2.3 Mean and rms velocity distribution in the vicinity of a single impeller

Three impellers with thicknesses of 0.8, 2.0 and 3.3 mm were employed for this part of the investigation. Detailed LDA measurements were carried out in the impeller stream at three radii: r = 51, 70 and 85 mm. The impeller rotational speed was 250 rpm and the clearance of the impeller from the bottom of the vessel was C = T/3 in all the experiments.

Figure 4.6 shows the radial mean velocities measured in the vicinity of the impellers (r = 51 mm) with different thicknesses. A significant increase of the mean velocities with decreasing impeller thickness can be observed in the region around the impeller elevation. However, at the locations above and below this region there is little variation in the velocities as the impeller thickness changes. The difference between the maximum mean velocities measured with the t = 0.8 mm and t = 3.3 mm impellers is about 0.2 m/s, i.e. around 20% higher with the thinner impeller.

Figure 4.7 shows the radial rms velocities corresponding to the mean values presented in Figure 4.6. Comparatively, the rms velocity profiles obtained with the thicker impellers are more uniform as might be expected due to the smaller gradients of the corresponding mean velocity profiles obtained with the thicker impeller (see Figure 4.6). Again the maximum difference in the rms velocity data occurred around the impeller elevation (z = 98 mm). The rms values measured with the impeller of thickness t = 0.8 mm were 20% higher than those with t = 3.3 mm.

At a radius of r = 70 mm (Figure 4.8), maximum radial mean velocities of 0.92 m/s for the t = 0.8 mm impeller and 0.73 m/s for the t = 3.3 mm impeller were measured. The percentage difference of these velocities are almost the same as that obtained at a radius of r = 51 mm. The region

where the three profiles are different is now wider than that of Figure 4.6. This is a result of the velocity profiles becoming less steep with increasing radius, (as also observed by Sachs and Rushton - 1954) and the spreads of the impeller streams away from the impeller tip can therefore also be different.

Figure 4.9 shows the profiles of the radial rms velocities obtained at a radius of r = 70 mm. It indicates a non-linear increase of the rms velocities with decreasing impeller thickness. Typically 25% higher rms velocities have been measured with the t = 0.8 mm impeller in comparison with those obtained with the other two impellers. The maximum measured rms velocity changed from 0.47 m/s to 0.34 m/s with a change in impeller thickness from 0.8 mm to 3.3 mm.

In order to investigate the effect of the impeller thickness on the inclination of the impeller stream to the horizontal and also on the decay of the radial velocity values in the impeller stream, measurements were made at locations further away from the impeller tip in the impeller stream. These measurements, which were carried out at a radius of 85 mm, are presented in Figures 4.10 and 4.11 for the radial mean and rms velocities respectively. The velocity profiles shown in these Figures were obtained with only two impellers, one of 0.8 and one of 3.3 mm thickness.

In Figure 4.10 a slightly higher mean velocity (by about 0.08 m/s) is evident at the impeller elevation region with the t = 0.8 mm impeller. A small change in the inclination of the impeller stream can also be observed; the impeller stream generated by the t = 3.3 mm impeller is more inclined to the horizontal direction as indicated by the different elevation of the peaks in the profiles (at approximately z = 103 mm, compared with z = 101 mm for the thinner impeller). By comparison of the velocity data

shown in this Figure with those presented in Figures 4.6 (r = 51 mm) and 4.8 (r = 70 mm), it can be seen that the change in the radial mean velocity as a result of the variation in the impeller thickness decays with increasing distance from the impeller tip.

The effect of t on the centreline mean velocities in the vicinity of the impeller and also on the decay of these velocities with increasing radius as reported by Mahmoudi and Yianneskis (1993) require a modification in the correlation proposed by van der Molen and van Maanen, (1978) as it is evident that the impeller thickness must be taken into consideration in that correlation.

Differences between rms profiles obtained with different impeller thicknesses are present at r = 85 mm (Figure 4.11); comparison between these results with those shown in Figure 4.7 (r = 51 mm) indicates that the difference between the rms velocities, measured with the t = 0.8 and t = 3.3 mm impellers, is slightly higher at r = 85 mm. This is probably due to the presence of the trailing vortices and the associated more pronounced periodicity of the flow in this region with the t = 0.8 mm impeller. The periodicity of the flow results in a broadening of the ensemble-averaged rms velocity measurements made over 360° of shaft rotation as confirmed recently by Yianneskis and Whitelaw (1993).

Employing a t = 3 mm and d = T/3 impeller, Yianneskis et al (1987) found that the trailing vortices behind the impeller blades persist up to a radius of 69 mm. They also suggested that the trailing vortices brake up at r = 98 mm. Therefore it is likely that the rms velocities measured with t = 3.3 mm (present work) at r = 70 and 85 mm are comparatively less affected by the periodicity of the flow. It can be expected that the trailing vortices generated by t = 0.8 mm impeller maintain their identity for a longer

distance away from the impeller tip as van der Molen and van Maanen (1978) measured higher peak-to-peak values of axial periodic velocity component in the vicinity of an impeller with thinner blades.

However, the results of radial rms velocities in the impeller stream (Figures 4.7, 4.9 and 4.11) suggest the need for a more detailed investigation of the effect of impeller thickness on the trailing vortices behind the blades. This is particularly significant as these vortices have an important role on gas dispersion or coalescence, (Rennie and Valentine - 1968, van't Riet and Smith - 1973) and on power consumption (Nienow and Wisdom - 1974).

In order to investigate the effect of the impeller thickness on the flow in the impeller 'suction' regions above and below the blades, axial mean and rms velocity measurements were carried out. The measurements were made at two elevations: 5 mm below the lower edge and 5 mm above the upper edge of the impeller blades. Measurements could not be obtained closer to the impeller due to optical access limitations. The velocity profiles measured along the upper and the lower edge of the impeller are presented in Figures 4.12 and 4.13 respectively.

In both these Figures it is shown that, in general, the mean axial velocities increase with decreasing impeller thickness (positive velocities indicate motion in the upward direction). This trend is similar to that of the radial mean velocities presented in Figure 4.6. The increase in the axial mean velocities, as the impeller thickness decreases, is small but consistent along most of the impeller blade length.

One exception to this trend is indicated in Figure 4.12 at radii above 46 mm. In this region the trend is reversed (the velocities are higher with

thicker impellers). This is probably due to the measurements being associated with the strength of the trailing vortices as mentioned previously, i.e. the trailing vortices may extend further into the measurement locations with the t = 0.8 mm impeller. Elsewhere above the impeller blades, at locations with radii smaller than 45 mm and bigger than 30 mm (Figure 4.12), higher velocities were measured with thinner impellers.

Below the impeller at the same radii (Figure 4.13) the velocities do not vary with impeller thickness as much. The different variation of the mean velocities with impeller thickness above and below the impeller might be expected as the streams generated by all the impellers are inclined slightly upward and the flow into the impeller from above is not the same to that from below. In addition, the stronger flows generated by thinner impeller may not affect the bottom ring vortex to the same degree as the top one. This cannot be determined from the present results and merits further investigation.

The rms velocity profiles corresponding to the mean velocities shown in Figures, 4.12 and 4.13, are presented in Figures 4.14 and 4.15 respectively. In these Figures the variations of the rms velocities with impeller thickness are shown to be negligible except that at the locations with radii greater than 25 mm and above the impeller the rms velocities are noticeably higher with the t = 0.8 mm impeller. Again, this increase might be attributable to the change in the strength or the direction of the axis of the trailing vortices as a result of change in the impeller thickness.

The variation of the axial mean and rms velocities in the impeller stream with impeller thickness was also investigated. The measurements were carried out at two elevations: 2 mm above the upper edge and 2 mm below

the lower edge of the impeller in the impeller stream. Figures 4.16 and 4.17 show these measurements at the upper and lower side of the impeller stream respectively. Again in these Figures positive velocities indicate motion in the upward direction. At the upper edge of the impeller stream, (Figure 4.16), the results in all locations show flow entrainment to the impeller streams generated by the t = 2 and 3.3 mm impellers. The entrainment is comparatively less for the t = 2 mm impeller. With the t = 0.8 mm impeller the results show flow away from the impeller stream at radii between 49 and 53 mm.

At z = 86 mm, i.e. on the lower side of the impeller, (Figure 4.17) flow entrainment into the stream is evident in all measurement locations and with all impellers. At radii between 49 and 53 mm, the axial mean velocities with the t = 0.8 mm impeller are small indicating that comparatively less flow entrainment to the impeller stream is generated by this impeller. The rms velocities corresponding to the mean values shown in Figure 4.16 and 4.17 are presented in Figures 4.18 and 4.19 respectively. In both Figures 4.18 and 4.19, it is shown that, in general, the rms velocities measured with thinner impellers are higher. In addition, in the locations closer to the impeller tip higher rms velocities have been recorded. These higher rms velocities might be expected to be caused primarily by the more intensive periodicity of the flow in the vicinity of the impeller. However, all the measurements in Figures 4.12 - 4.19 are influenced by the periodicity of the flow caused by the trailing vortices behind the blades. Therefore, as noted above the changes in the intensity and in the location of the axes of the trailing vortices as a result of a change in the impeller thickness require further investigation before making a definite and detailed conclusion on the effect of impeller thickness on the velocities in the vicinity of the impeller.

4 2.4 Combined effect of impeller size and thickness with a single impeller

Radial mean and rms velocity measurements were performed in the impeller stream of the Rushton impeller with the larger diameter (d = 0.4T, t = 2 mm). The impeller rotational speed in these measurements was 206 rpm. The change in the impeller speed was made in order to maintain the impeller tip speed the same as that of the small impeller (d = T/3 t = 1.65 mm) for comparison purposes.

The point r = 0 mm z = T/3 was taken as the origin of coordinates and the r-z coordinates of the measurement locations were normalised with the radius and the half-blade height of the impeller respectively. This normalisation was employed in accordance with the recommendations of Nouri et al (1987) to allow appropriate comparisons between impellers of different diameter. The new coordinates are denoted by r* and z*:

$$r^* = \frac{r}{d/2} \qquad z^* = \frac{z'}{h/2} \qquad (4.1)$$

The mean velocities measured in the impeller streams of both impellers with the same t/d and at a radius of r* = 1.04 are presented in Figure 4.20. Slightly higher values were obtained with the larger impeller coupled with a slight increase in the inclination of the impeller stream generated by the larger impeller. The increase in the angle of inclination is indicated by the higher velocities in the upper half of the profiles where a difference of around $0.07V_{tip}$ was measured.

The rms velocity profiles corresponding to those of the mean velocities shown in Figure 4.20 are presented in Figure 4.21. As this Figure indicates the differences between the rms velocities measured with the two impellers are small and within the experimental error.

Velocity measurements were also made at locations away from the impellers at r* = 1.428 in the impeller streams. Comparisons of these measurements are given in Figures 4.22 and 4.23 for the mean and rms velocities respectively. Figure 4.22 shows almost identical maximum velocities in both impeller streams indicating that the slight difference between the maximum mean velocities in the vicinity of the impellers, (see Figure 4.20), has decayed at r* = 1.428. However, it must be noted that in Figure 4.22 the upward shift of the mean velocity profile obtained with the larger impeller does not necessarily indicate a greater inclination of the impeller stream generated by this impeller: the measurement locations are closer to the vessel wall in the case of the larger impeller, as r* instead of r was kept constant for these profiles.

Figure 4.23 shows the radial rms velocities corresponding to the mean values presented in Figure 4.22. This Figure suggests negligible variations in the rms velocities with impeller size at a radius of r* = 1.428.

In order to study the effect of the impeller diameter on the flow induced by the impeller, the mean and rms velocities measured in the vicinity of the large impeller (d = 0.4T and t = 2 mm) at r* = 1.04 were compared with those measured with the small impeller but the same thickness (d = T/3 and t = 2 mm). These comparisons are given in Figures 4.24 and 4.25 for the mean and the rms velocities respectively. The slight increase of the mean velocities obtained in the upper-half of the profile for the larger impeller can be seen from Figure 4.24 which is similar to the case when the thickness-to-diameter ratio was the same (Figure 4.20). The differences between the rms velocities measured with these two impellers

(with the same t) are small and in general within the experimental error as was the case in Figure 4.21.

4.2.5 Mean and rms velocities in the impeller streams of two-impeller system

The significance of the impeller thickness, t, for the mean and rms velocity profiles in the impeller streams of the two-impeller system was examined. The investigation was carried out with the parallel and the merging flow patterns in the vessel. The impeller spacings used to obtain the stable parallel and the merging flow patterns were $C_1 = T/4$, $C_2 = T/2$ and $C_1 = C2 = T/3$ respectively. In every experiment the two impellers were of the same thickness which was either 0.8 mm or 3.3 mm. Radial velocity measurements were carried out at three radii (r = 51, 70 and 85 mm) in the impeller stream with an impeller rotational speed of 250 rpm. The results are presented in Figures 4.26 to 4.31 for the parallel flow pattern and in Figures 4.32 to 4.35 for the merging flow pattern. In all of these Figures the velocity profiles in the upper impeller stream are shown above the profiles obtained in the lower impeller stream.

Parallel flow pattern

Figure 4.26 shows the mean velocities in the upper and lower impeller streams and in the vicinity of the impellers (r = 51 mm). In the locations around both the upper and lower impeller elevations the velocities decrease (by up to 20%) as the thickness of impellers increase from 0.8 to 3.3 mm. This maximum reduction in the velocities is similar to that recorded in the elevation of the impellers with the same thicknesses in the single-impeller system (see Figure 4.6).

With the t = 3.3 mm impellers in the vessel the profiles of the mean velocities shown in Figure 4.26 indicate that the upper impeller stream is inclined slightly downward and the lower impeller stream is inclined slightly upward. However, Figure 4.26 does not show any inclination of the t = 0.8 mm impeller streams.

The radial rms velocities corresponding to the mean values shown in Figure 4.26, are presented in Figure 4.27. In this Figure it is shown that at locations around the impeller elevations relatively higher rms velocities were measured with thinner impellers. However, the increase of the rms velocities recorded in the lower impeller elevation (as a result of the decrease in the impeller thickness) is comparatively higher than that obtained in the upper impeller elevation.

The effect of impeller thickness on the variations of the radial mean and rms velocities in the impeller streams at a radius of 70 mm is shown in Figure 4.28. The results indicate that the variation in the mean velocities is similar to that shown in Figure 4.26 (r = 51 mm), i.e. higher velocities with thinner impellers around the impeller elevations. The results also confirm the slight downward and upward inclination of the upper and lower impeller streams generated by t = 3.3 impellers respectively, as mentioned earlier.

Profiles of the rms velocities corresponding to those of the mean values shown in Figure 4.28 are presented in Figure 4.29. A comparison between these profiles and those obtained at r = 51 mm (Figure 4.27) suggests that the increase of the rms velocities as a result of a decrease in the impeller thickness has not decayed with distance from the impeller tip. In fact, the regions where the rms velocities are different have extended in the z-direction which is probably due to the spread of the impeller streams with

distance from the tip of the impellers as mentioned earlier. Figure 4.29 also shows that the velocity differences in the lower impeller stream are slightly higher than those recorded in the upper impeller stream.

Velocity measurements were carried out at locations further away from the impeller, at r = 85 mm, in order to investigate the decay of the velocity differences with increasing radius due to the change in impeller thickness. These measurements are presented in Figure 4.30 for the mean and Figure 4.31 for the rms velocities respectively. At this radius there are only small differences between the mean velocities as the thickness of impellers change. This was expected as the impeller streams spread with distance from the impeller tip. In contrast, the comparisons of the rms velocities at r = 51, 70 and 85 mm (Figures 4.27, 4.29 and 4.31) suggest a more consistent influence of impeller thickness on the rms velocities at measurement locations further away from the impeller tip. This consistent influence was also found in the single-impeller system (Figures 4.7, 4.9 and 4.11). As mentioned before, it is likely that the rms velocities produced by thinner impellers are affected relatively more by a more pronounced periodicity of the flow.

Merging flow pattern

Employing the t = 0.8 and 3.3 mm impellers, radial mean and rms velocities were measured in both impeller streams at radii of 51 and 70 mm with the merging flow pattern in the vessel. Profiles of the mean velocities at a radius of r = 51 mm are shown in Figure 4.32. At the peaks of the profiles the mean velocities increase (by around 20%) as the thickness of impellers decreases.

Figure 4.33 shows the profiles of the rms velocities corresponding to those of mean values shown in Figure 4.32. Again, the influence of the impeller thickness is exhibited in this Figure as the profiles show higher rms values with thinner impellers. This Figure also indicates that there is no appreciable change in the inclination of the impeller streams due to the change in impeller thickness.

Measurements of the radial mean velocities at a radius of 70 mm are presented in Figure 4.34. Once again, the increase of the mean velocities due to the decrease in impeller thickness is evident from this Figure. The rms velocities corresponding to the mean values presented in Figure 4.34 are shown in Figure 4.35. It indicates the same trend of rms velocity variations with impeller thickness as that of Figure 4.33 except that the differences at r = 70 mm exist in the majority of the measurement locations, presumably due to the spread of the impeller streams.

4.2.6 Flow number

A more appropriate assessment of the flows in the impeller streams, generated by impellers with different geometry, can be made by employing the flow number (equation 3.1). Figure 4.36 shows the flow numbers obtained with impellers with different thicknesses and diameters employed in single- (C = T/3) and two-Rushton (C_1 = T/4, C_2 = T/2) impeller systems. In this Figure comparatively higher flow numbers are shown for the single-impeller systems with every impeller thickness. In both single- and two-impeller systems the flow number increases as the impeller thickness decreases. The highest flow number was obtained with the d = 0.4T impeller in the single-impeller system (F_l = 0.88) and the lowest value (F_l = 0.68) was obtained for the upper impeller in the two-

impeller system. The flow number of the lower impeller in two-impeller system was found to be slightly higher than that of the upper impeller. This is in agreement with that reported by Crozier (1989). The flow numbers obtained with the t = 3.3 mm impellers in the present work are nearly identical to those reported by Crozier in a tall tank (H = 2T) with an impeller separation of C_2 = T.

The effect of the geometry of Rushton impeller on the discharge performance can be determined from the correlation between the flow and power number. An efficient impeller for liquid homogenisation is one with higher discharge flow rate and lower power consumption as a higher discharge flow rate will result in a better circulation of the flow in the vessel and consequently a higher rate of macro-mixing will be achieved.

With a single-impeller system Sano and Usui (1985) correlated the flow and power numbers of Rushton impellers with diameters larger than 0.4T. The correlation was:

$$N_p = 6.6\, F_l^{134} \qquad (4.2)$$

In the present work the N_p and F_l obtained with the d = 0.4T impeller are well correlated by the above equation. With the d = T/3 impellers the Np obtained from the above equation (for the measured F_l) is smaller than the measured one. This difference increases with decreasing impeller thickness. However, the Np of the d = T/3 impellers with different t was found to be nearly proportional to the square of F_l which is in agreement with that reported by Hiroka and Ito (1975). The ratio F_l / Np can be compared for the impellers studied in the present investigation. For the d = T/3 impellers these ratios were 0.136, 0.146 and 0.156 for impeller thicknesses of 0.8, 2 and 3.3 mm respectively. For the d = 0.4T impeller

this ratio was 0.172. Considering both the significant decrease of mixing time and the comparatively higher value of F_l / Np for the larger impeller, this impeller is the most efficient one among those studied from the point of view of both energy and time saving.

The above comparison can not be easily applied to the two-Rushton impeller system as in such systems the impeller spacings play an important role and affect the flow interchange between the field of action of the two impellers.

4.3 Effect of impeller hub shape

The velocity and power characteristics of the Rushton impeller with an asymmetrical hub were investigated and the results were compared to those obtained for the impeller with symmetrical hub. This comparative study was undertaken as these two types of impellers were used by Yianneskis et al (1987) and Calabrese and Stoots (1989) and differences in the turbulence levels near the shaft were found with different hub designs. Both impellers (shown in Chapter 2, Figure 2.4) had a diameter of T/3 and a thickness of 1.65 mm. The investigation was carried out in a single-impeller system with the impeller located at C = T/3. The impeller speeds used were 100, 150, 200, 250, 300 and 350 rpm for the torque measurements and 250 rpm for the velocity measurements.

The comparison of the power numbers obtained for these two impellers is given in Figure 4.37. This Figure suggests nearly identical power numbers for the two impellers at all Reynolds numbers.

4.3.1 Radial mean and rms velocities

Figure 4.38 shows nearly identical mean velocity profiles for the two impellers at a radius of 51 mm. The rms velocities corresponding to the mean values shown in this Figure are presented in Figure 4.39. Although the rms velocities in the impeller elevation are indicated to be the same for both impellers, they differ by around 0.04 m/s at the locations half way between the impeller elevation and the upper and lower edges of the impeller. However, the differences are small and in most locations within the experimental error.

Radial velocity measurements were also made in locations away from the impeller, at r = 70 mm in the impeller stream. These measurements are shown in Figures 4.40 and 4.41 for the mean and rms velocities respectively. The comparison between the mean velocity profiles shows a slight upward shift of the profile generated by the impeller with symmetrical hub. In the corresponding rms velocities shown in Figure 4.41 there are no clear trends and the differences between the rms velocities are within the experimental error.

4.3.2 Axial mean and rms velocities

Axial mean and rms velocity measurements were performed at locations 5 mm above the upper edge and 5 mm below the lower edge of the impeller blades for both impellers. Figures 4.42 and 4.43 show the mean velocities obtained from these measurements above and below the impellers respectively (again positive velocities indicate motion in the upward direction). In both Figures it is shown that at radii smaller than r = 40 mm the mean velocities differ slightly with the type of impeller.

Above the impeller blades, as Figure 4.42 shows, at a radius of 32 mm the mean velocity is slightly higher with the impeller with asymmetrical hub while at radii smaller than 25 mm the velocities are higher with the impeller with symmetrical hub. Below the impeller (Figure 4.43) and at radii between 40 mm and 20 mm the velocities are higher with the impeller with symmetrical hub while at radii smaller than 20 mm the velocities are higher with the impeller with asymmetrical hub. Therefore, the variation of the axial mean velocities with the shape of the impeller hub below the impeller is in contrast to that above the impeller. However, it must be noted that in most of the locations the differences are small.

The rms velocities corresponding to the mean values shown in Figures 4.42 and 4.43 are presented in Figures 4.44 and 4.45 respectively. In general, at the locations above the impeller (Figure 4.44) the rms velocities are slightly higher (by around 0.05 m/s) with the impeller with the asymmetrical hub. The differences are almost negligible at radii smaller than r = 30 mm. Below the impeller (Figure 4.45) the differences in the rms velocities are also very small. However, at these locations and at radii greater than 35 mm the impeller with symmetrical hub has generated slightly higher rms velocities while at radii smaller than 25 mm the corresponding rms velocities are slightly lower.

Axial velocity measurements were also carried out in the impeller stream of these two impellers. The measurements were performed at elevations 2 mm above the upper edge and 2 mm below the lower edge of the impellers blades in the impeller stream. The mean velocities above and below the impeller streams are presented in Figures 4.46 and 4.47 respectively. There is little difference between the axial mean velocities obtained with these two impellers. However, the velocities obtained by the

impeller with the symmetrical hub are smaller in locations above the impeller and higher in locations below the impeller.

Figures 4.48 and 4.49 show the profiles of the rms velocities corresponding to those of the mean values presented in Figures 4.46 and 4.47 respectively. At every location above the impeller stream there is virtually no difference between the rms velocities produced by the two impellers (Figure 4.48). At the lower part of the impeller stream (Figure 4.49) the rms velocities do not change with the position of the impeller hub at radii greater than 53 mm while at radii smaller than r = 52 mm the rms velocities are slightly higher (by around 0.07 m/s) with the impeller with symmetrical hub. As there is no hub below the disk of the asymmetrical impeller, less turbulence might be expected to be generated there.

4.4 Effect of impeller speed

4.4.1 Flow visualisation

In the flow visualisation observations described in section 3.2.2 the significance of the variation of impeller speed (or, equivalently, the Reynolds number) on the flow patterns induced by two Rushton impellers at an impeller spacing of C_2 = 0.375T, was discussed by comparing Figures 3.5 and 3.8. It was shown that the 'flow pattern regions' in these Figures were affected as the impeller speed decreased from 260 to 100 rpm. For example at a liquid height of H = T and C_1 > 0.2T, the stable merging flow pattern changed to the unstable parallel-merging flow pattern with the above reduction in the impeller speed.

Further flow visualisation experiments (in the turbulent regime) showed that the effect of Reynolds number on the overall flow pattern is almost

negligible when the impeller spacings C_1 and C_2 are well away from the critical values which result in flow instabilities.

4.4.2 Mixing time

The mixing time experiments were performed at various impeller rotational speeds for the parallel and merging flow patterns with several tracer insertion times. Each experiment was repeated at least 2-3 times. Figure 4.50 shows the effect of the impeller rotational speed on the local mixing time for five different insertion times. These results were obtained with a stable parallel flow pattern. The mixing time in general decreases with increasing impeller speed as might be expected. However, an increase of the gradients can be noticed at the lower impeller speeds. Some scatter of the measured values can be seen in this graph. This might be expected due to the fact that the mixing time measured is a local one and the measurements have been repeated only three times.

Similar results were obtained for the mixing times in the merging flow pattern for three different insertion times and they are shown in Figure 4.51. The variation of mixing time with impeller rotational speed is similar to that of Figure 4.50. A comparison of Figures 4.51 and 4.50 shows that the merging flow pattern results in shorter mixing times. This was also the case for the average mixing time over the whole vessel (Figure 3.34, Chapter 3) and is probably due to the more rapid transport and subsequent dispersion of the tracer in the impeller regions in the case of the merging flow pattern. The higher k values in the middle of the vessel with the merging flow pattern, in comparison to those with the parallel flow pattern, as discussed in Chapter 3 (Figures 3.69 and 3.70), confirms the above argument. A comparison of Figures 4.50 and 4.51 also

indicates that the values obtained with the merging flow pattern show less scatter. A possible explanation for this effect may lie in the number of main ring vortices present in the flow, which is higher in the parallel flow pattern: the higher the number of ring vortices, the more likely it is for the tracer to get entrapped in a vortex and as a result there may be an increased chance of mixing time variations and this will be reflected in a poorer repeatability of the experiment.

Figure 4.52 shows the results of the effect of the impeller speed on the average mixing time in the parallel flow pattern. These results have been obtained from recordings at four locations (1, 2, 3 and 4 in Figure 3.26b) in the vessel and show an almost linear variation of the mixing time with impeller speed; also, significantly less scatter is evident in the results when they are compared with those of Figure 4.50. This Figure also indicates that the results obtained with the mixing time calculated as an average (with 92% to 98% degree of mixing) show less scatter than those calculated from a 95% degree of mixing and provide further justification for the use of the mixing time averaging definition employed in this work (see Section 2.4.4).

4.4.3 Mean velocity and rms profiles

In the present quantitative study of the effect of speed, extreme care was taken to avoid a change in the flow pattern due to the variation of the Reynolds number during the experiments. The impeller spacings were the same as those in the quantitative study described in Chapter 3 for the three different stable flow patterns.

Measurements were obtained for speeds of 100, 150, 200, 250 rpm and the radial mean and rms velocity results were normalised with the impeller tip

speed (V_{tip}). For ease of interpretation of the results, those obtained with the maximum and the minimum impeller speeds are presented below with symbols and solid lines while the rest of the results are shown with symbols only.

Parallel flow pattern

Figures 4.53 and 4.54 show the profiles of the normalised mean velocities obtained at the upper and lower impeller streams respectively. These measurements were carried out at a radius of r = 51 mm for four different impeller rotational speeds, or correspondingly, Reynolds numbers. The impeller spacings for the above measurements were C_1 = T/4 and C_2 = T/2, which result in a parallel flow pattern in the vessel.

An effect of the Reynolds number on the mean velocities is evident from the results presented in these Figures, albeit of small magnitude: higher impeller speeds resulted in higher normalised velocities. This is more evident at the impeller elevations: for example at z = 222 mm and z = 74 mm, the difference between the velocities measured at the maximum and minimum impeller speed is around $0.13V_{tip}$. This is significantly higher than the experimental error which is of the order of 0.01 to $0.05V_{tip}$ (Yianneskis 1982a).

Figures 4.55 and 4.56 show the normalised rms velocities corresponding to the mean velocities presented in Figures 4.53 and 4.54 respectively. In general, higher impeller speeds resulted in higher normalised rms velocities but the maximum magnitude of the difference between the rms velocities at different speeds does not exceed $0.07V_{tip}$. This is within the experimental error which is around 0.03 to $0.10V_{tip}$ for the rms velocity measurements Yianneskis (1982a). Therefore the variation of the rms

velocities with Reynolds number, is small and can not be resolved adequately with the present optical arrangement. A smaller control volume would improve the anemometer resolution, but the magnitude of the rms velocity differences is small and is not expected to affect process design to any significant extent.

Merging flow pattern

The normalised radial mean velocity profiles with the merging flow pattern are presented in Figures 4.57 and 4.58 for the upper and lower impeller streams respectively. These measurements were made around the maxima of the radial mean velocity profiles in the vicinity of the impeller and at a radius of r = 51 mm. The results show an almost identical angle of impeller stream inclination at the different impeller speeds. The variation of the velocities with impeller speed is practically the same as that for the parallel flow pattern.

The results of the normalised rms velocities corresponding to the mean velocities of Figures 4.57 and 4.58 are presented in Figures 4.59 and 4.60 respectively. These Figures indicate a lot of scatter particularly in the values obtained in the upper impeller stream. Although the maximum rms velocities in these profiles show slightly higher values at the higher impeller rotational speeds, the differences are in general small and within the experimental error.

In order to investigate the effect of the Reynolds number on the bulk flow and impeller stream directions, some LDA measurements were carried out in the locations away from the impellers at a radius of r = 85 mm. The results of the normalised radial mean and rms velocities obtained from these measurements are presented in Figures 4.61 and 4.62 respectively.

Figure 4.61 shows little difference between the values obtained at the impeller speeds of 200 and 250 rpm. However, in the lower impeller speeds the normalised velocity values decrease as the impeller speed decreases. The maximum difference occurs at the peak of the profiles and is around $0.12V_{tip}$.

Again the normalised rms velocities (Figure 4.62) are scattered and the differences are within the experimental error. Only the velocity profile measured at 100 rpm has a shape somewhat different from the others: the v/V_{tip} values are greater than those at the higher speeds near the middle of the impeller streams and around z = 145 mm.

Diverging flow pattern

The results of the effect of the Reynolds number on the normalised mean velocity profiles measured at a radius of r = 51 mm in the upper and lower impeller streams with the diverging pattern are presented in Figures 4.63 and 4.64 respectively. Once again the same trend as those with the parallel and the merging flow patterns is evident from these graphs. The normalised velocities are greater at the higher speeds in most locations. However, the increase in the normalised mean velocities due to the increase in impeller speed is small. This is an effect which may be partly due to the more extensive turbulent flow regime in the vessel at higher speeds. The corresponding normalised radial rms velocities of Figures 4.63 and 4.64 are presented in Figures 4.65 and 4.66 respectively. The profiles do not show any particular trend of rms velocity variation with impeller speed.

With the diverging flow pattern in the vessel the variations of radial mean velocities with impeller speed at the vicinity of the upper and lower impellers (r = 51 mm) are shown in Figure 4.67 and 4.68 respectively.

These measurements are the same as those in the lower part of the velocity profiles shown in Figures 4.63 and 4.64. Both Figures 4.67 and 4.68 show that the effect of impeller speed is not very significant. In addition, these Figures suggest that the velocity gradients are greater in measurement locations in high velocity regions.

In general, the variation of the mean and rms velocities with impeller speed are in agreement with the findings of Nouri et al (1987) in single impeller system. Nouri et al found similar normalised mean velocities at N = 150 and 300 rpm and somewhat smaller normalised mean velocities with a lower impeller speed (N = 50 rpm). However, in the measurements reported by Nouri et al the normalised mean velocities are slightly higher with N = 300 rpm in most of the locations; the small scale of the plots of Nouri et al does not allow differences to be distinguished very clearly. The small effect of the impeller speed on the normalised rms velocities reported above is also in agreement with that reported by Nouri et al.

4.5 Closure

The measurements presented in this Chapter quantified the effect of impeller blade thickness, diameter, speed and hub shape on the flows produced by single- and double- Rushton impeller configurations.

It is clear from the results presented in this Chapter, the differences obtained in some cases, as for example, the effect of t on N_p and F_l, are important. It was revealed that the discharge efficiency (F_l / Np) of the thicker impellers is slightly better than that of thinner impellers and from the point of view of energy and time saving large impellers are the most efficient ones. It was also revealed that the thinner impellers produce

higher rms velocities, in agreement with van der Molen and van Maanen (1978).

The increase of the mean velocity in the impeller stream by around 20% when the impeller thickness is decreased from 3.3 mm to 0.8 mm may be beneficial, but is accompanied by increased power consumption. Impeller selection must be made therefore by considering both circulation time / mixing time and power input requirements. In this respect, a F_l - N_p correlation might be appropriate for impeller selection for specific mixing tasks. Although the existing correlations can provide reasonable estimates, the present results indicate that a novel correlation allowing better for the effect of impeller thickness is required.

In other cases, e.g. in the variation of the normalised velocities with Reynolds number, the differences are small but not negligible. The effect of hub geometry also appeared to be very small. A number of consistent trends, however small have been revealed. These merit further investigation: a small improvement in impeller performance and consequently, in process efficiency, may provide significant benefits in terms of yield and selectivity as well as the associated financial savings. The scale of process operations is such that even a 1% improvement in process efficiency can yield substantial returns.

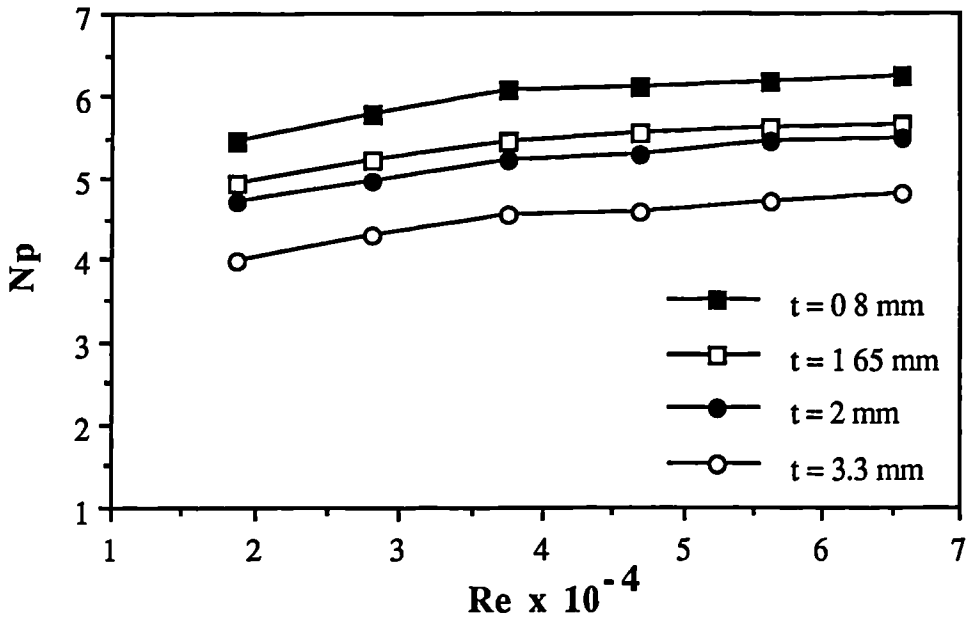

Figure 4.1. Effect of Reynolds number on power number of single Rushton impeller with different impeller thicknesses; d = T/3, C = T/3.

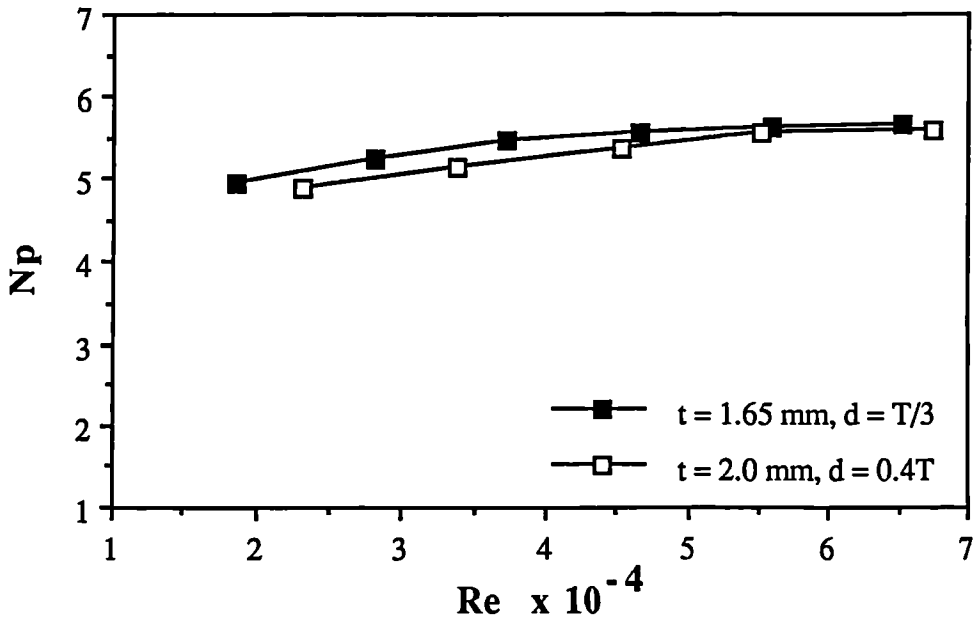

Figure 4.2. Effect of impeller size on the power number, t/d = constant, C = T/3.

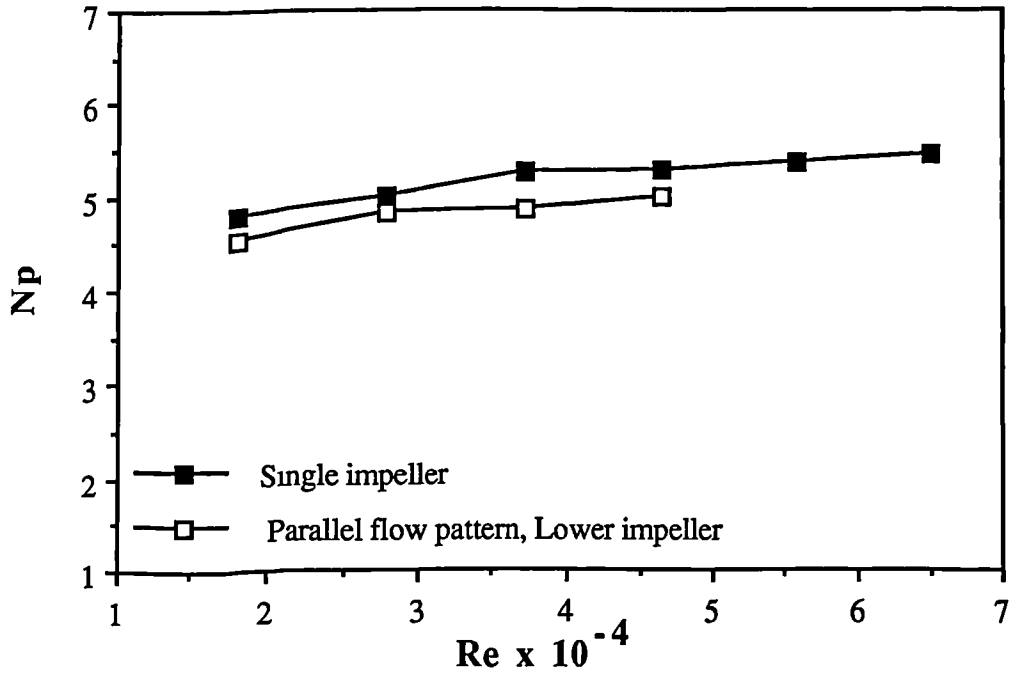

Figure 4.3. Comparison of power numbers between single and two impellers; C = C1 = T/4, C2 = T/2, t = 1.65 mm.

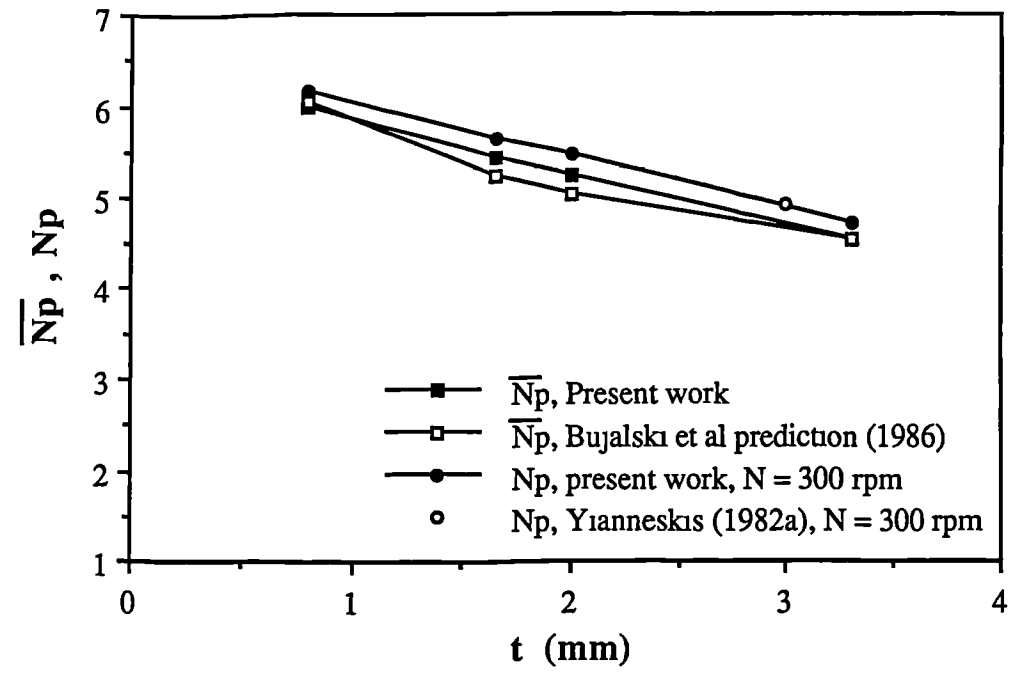

Figure 4.4. Effect of impeller blade thickness on the power number and average power number; single impeller, d = T/3, C = T/3.

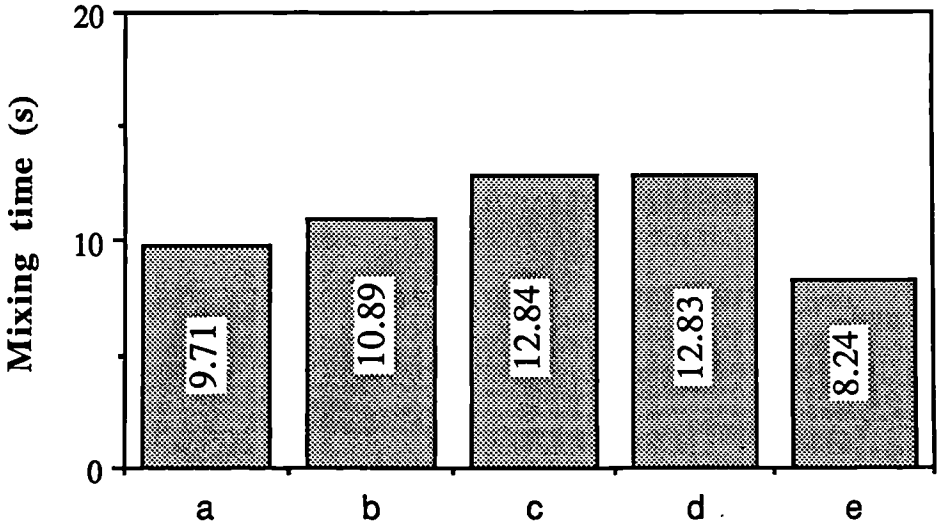

a: Pitched blade impeller, t = 1.65 mm, d = T/3
b: Rushton impeller, t = 0.8 mm, d = T/3
c: Rushton impeller, t = 1.65 mm, d = T/3
d: Rushton impeller, t = 3.3 mm, d = T/3
e: Rushton impeller, t = 2 mm, t/d same as for 'c'

Figure 4.5. Comparison of mixing time among single impellers.

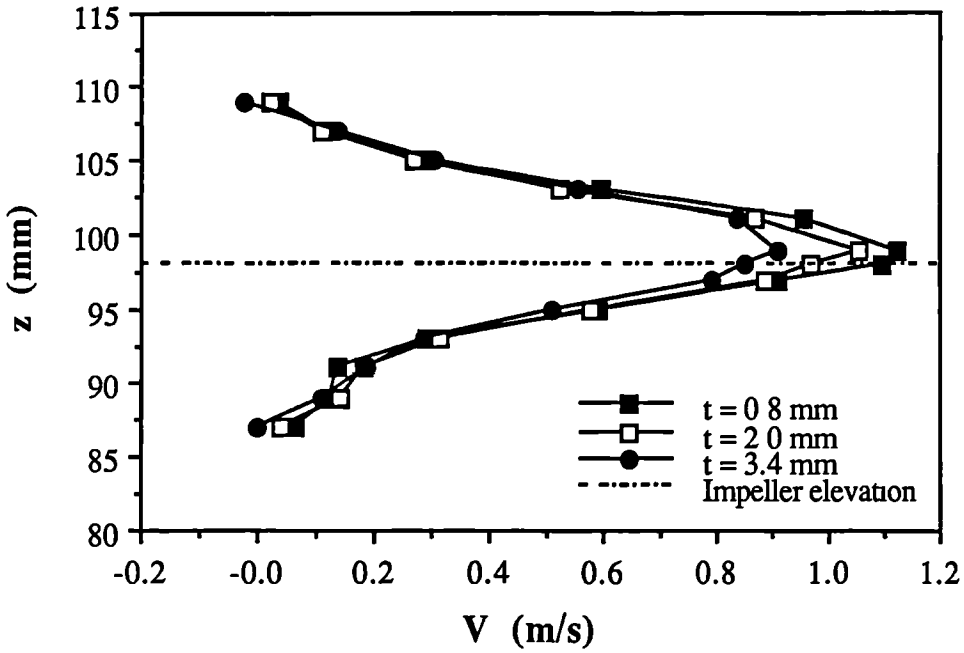

Figure 4.6. Effect of impeller blade thickness on the radial mean velocities in the impeller stream: Single Rushton impeller, C = T/3, N = 250 rpm, r = 51 mm, theta = 0°.

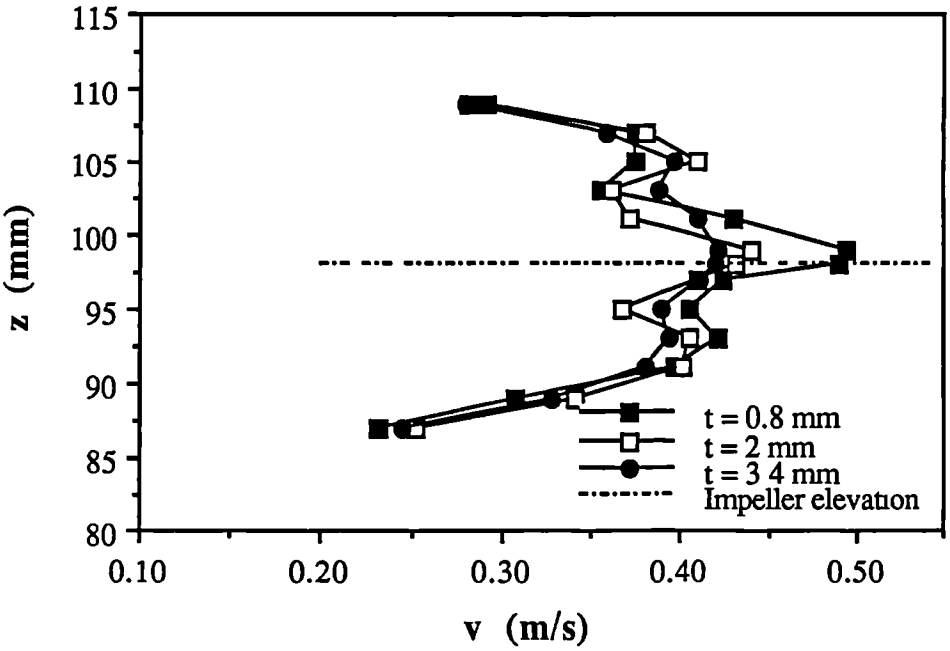

Figure 4.7. Effect of impeller blade thickness on the radial rms velocities in the impeller stream: Single Rushton impeller, C = T/3, N = 250 rpm, r = 51 mm, theta = 0°.

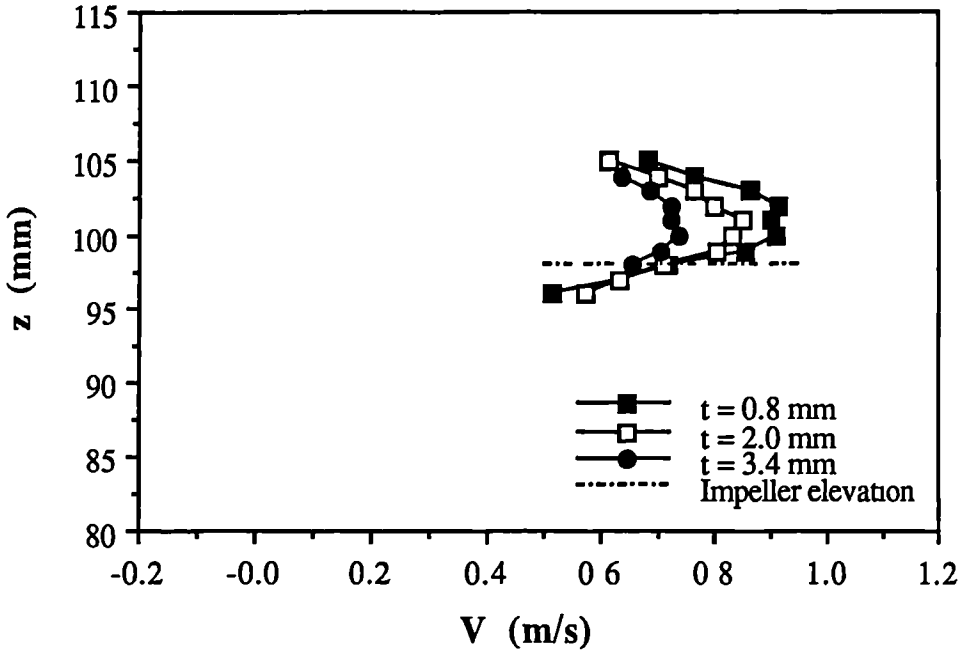

Figure 4.8. Effect of impeller blade thickness on the radial mean velocities in the impeller stream: Single Rushton impeller, C = T/3, N = 250 rpm, r = 70 mm, theta = 0 °.

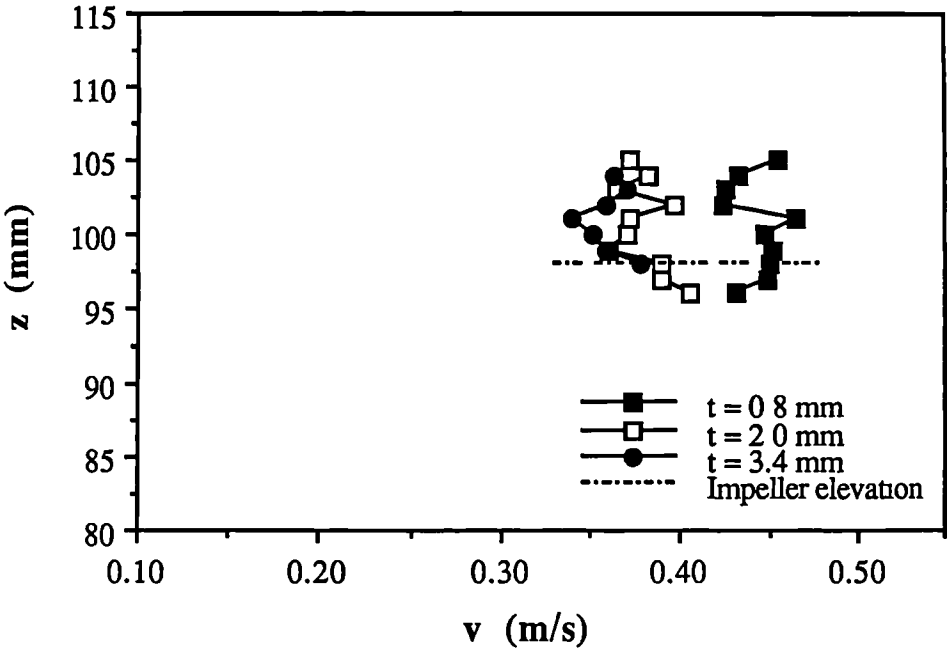

Figure 4.9. Effect of impeller blade thickness on the radial rms velocities in the impeller stream: Single Rushton impeller, C = T/3, N = 250 rpm, r = 70 mm, theta = 0°.

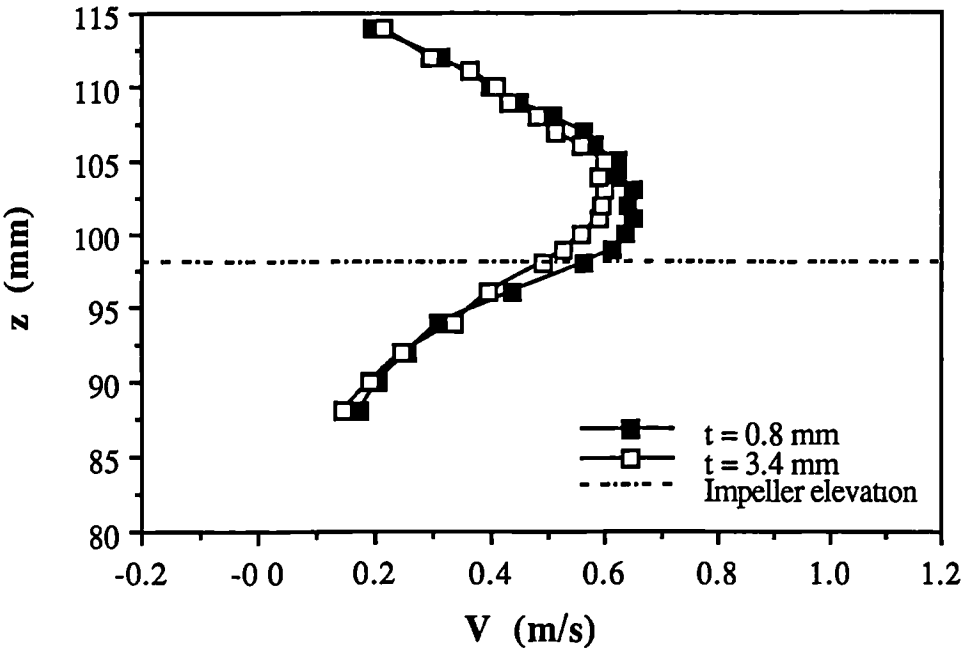

Figure 4.10. Effect of impeller thickness on the radial mean velocities in the impeller stream: Single Rushton impeller, C = T/3, N = 250 rpm, r = 85 mm, theta = 0°.

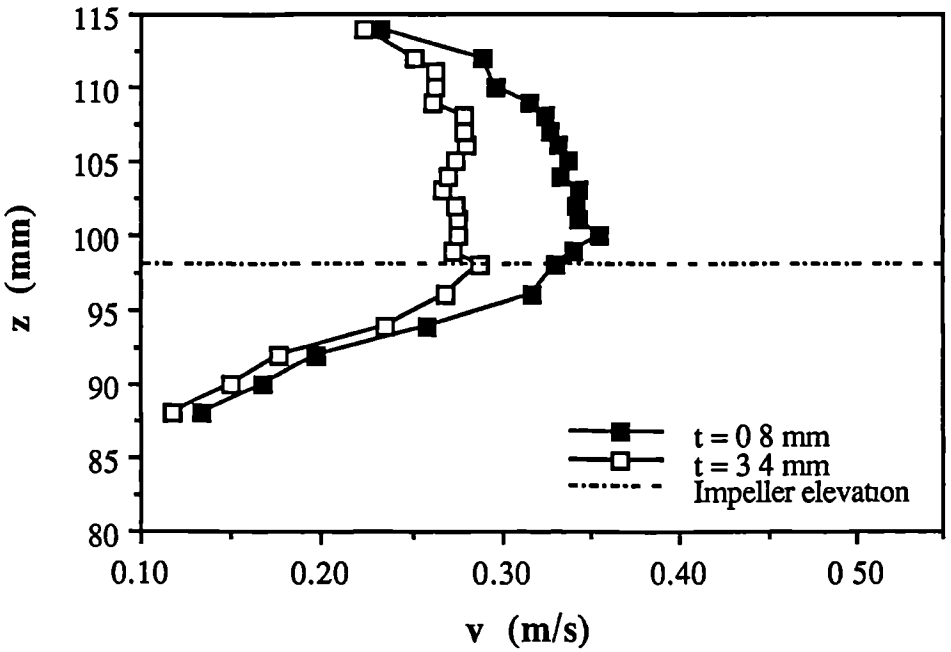

Figure 4.11. Effect of impeller thickness on the radial rms velocities in the impeller stream: Single Rushton turbine, C = T/3, N = 250 rpm, r = 85 mm, theta = 0°.

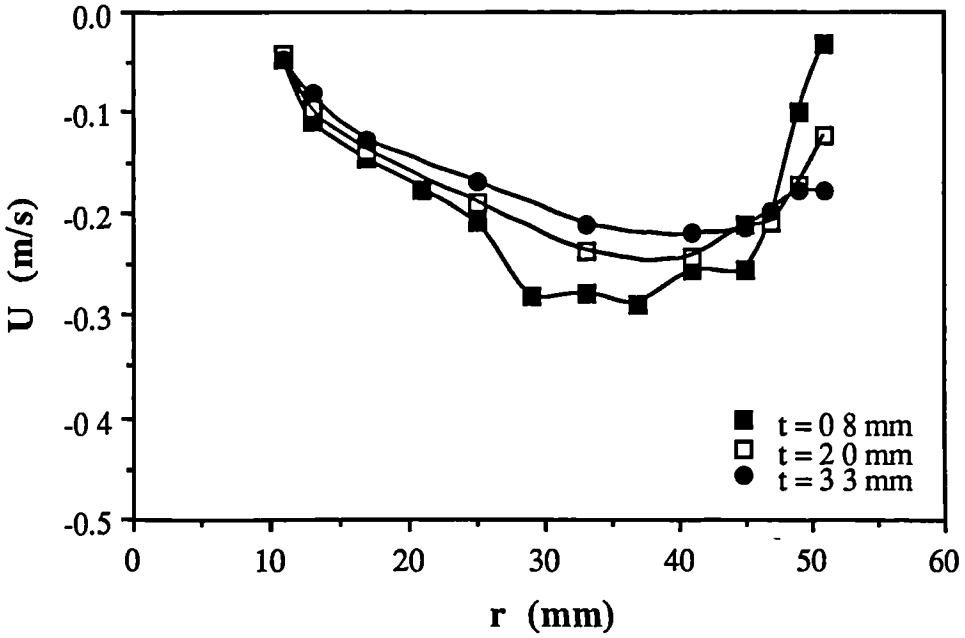

Figure 4.12. Effect of the impeller thickness on the axial mean velocities in the vicinity of the impeller: C = T/3, N = 250 rpm, z = 113 mm, theta = 0°.

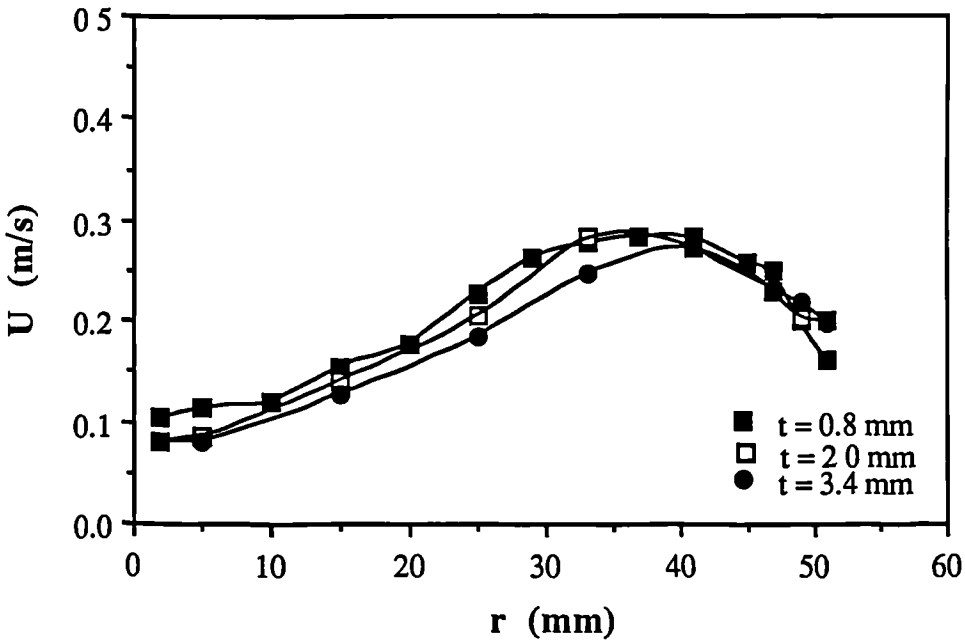

Figure 4.13. Effect of impeller thickness on the axial mean velocities in the vicinity of the impeller: C = T/3, N = 250 rpm, z = 83 mm, theta = 0°.

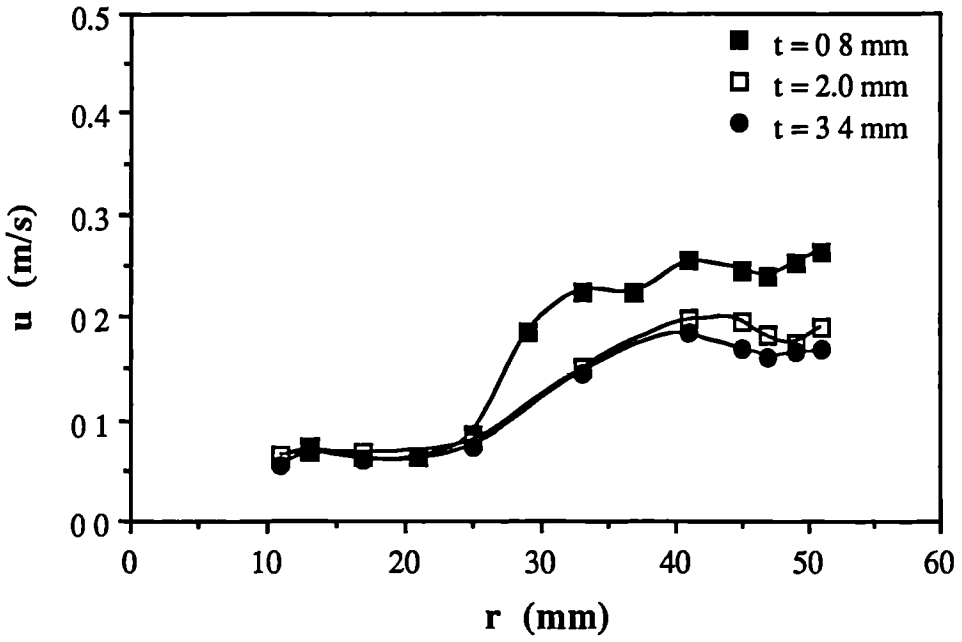

Figure 4.14. Effect of impeller thickness on the axial rms velocities in the vicinity of the impeller: C = T/3, N = 250 rpm, z = 113 mm, theta = 0°.

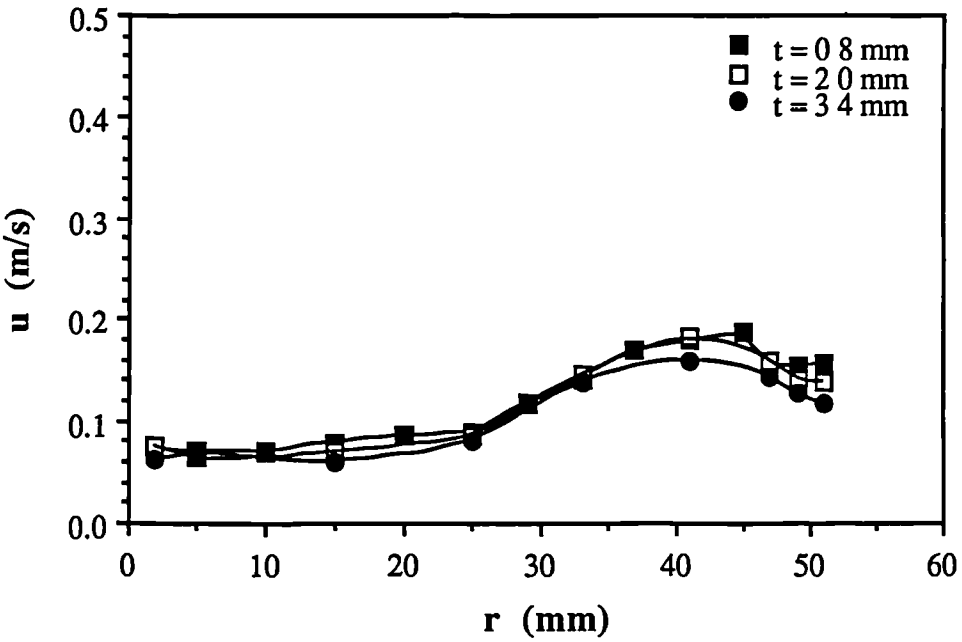

Figure 4.15. Effect of impeller thickness on the axial rms velocities in the vicinity of the impeller: C = T/3, N = 250 rpm, z = 83 mm, theta = 0°.

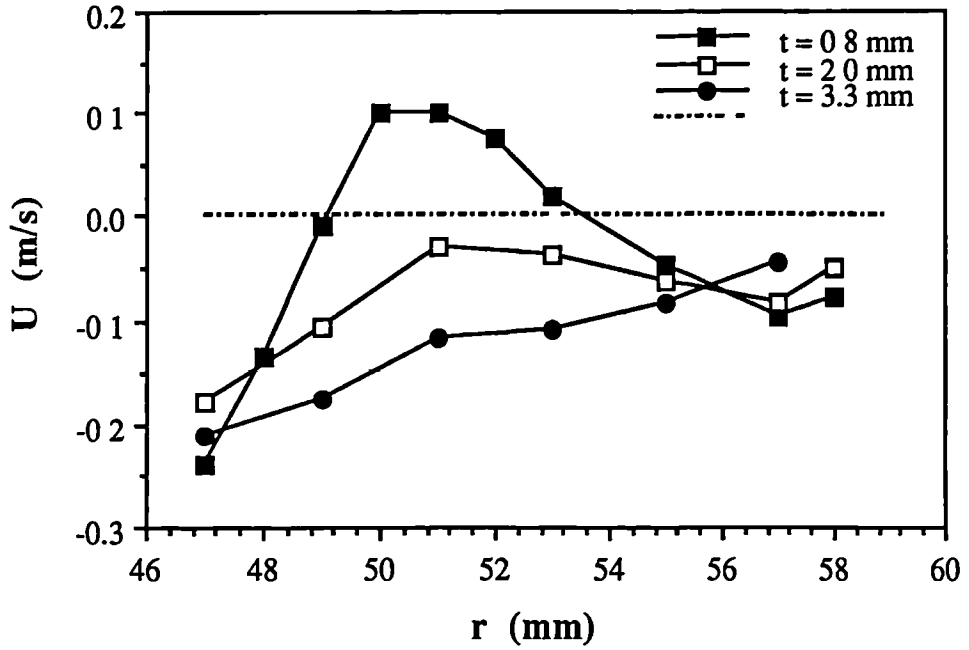

Figure 4.16. Effect of the impeller thickness on the the axial mean velocities in the impeller vicinity:
C = T/3, N = 250 rpm, z = 110 mm, theta = 0°.

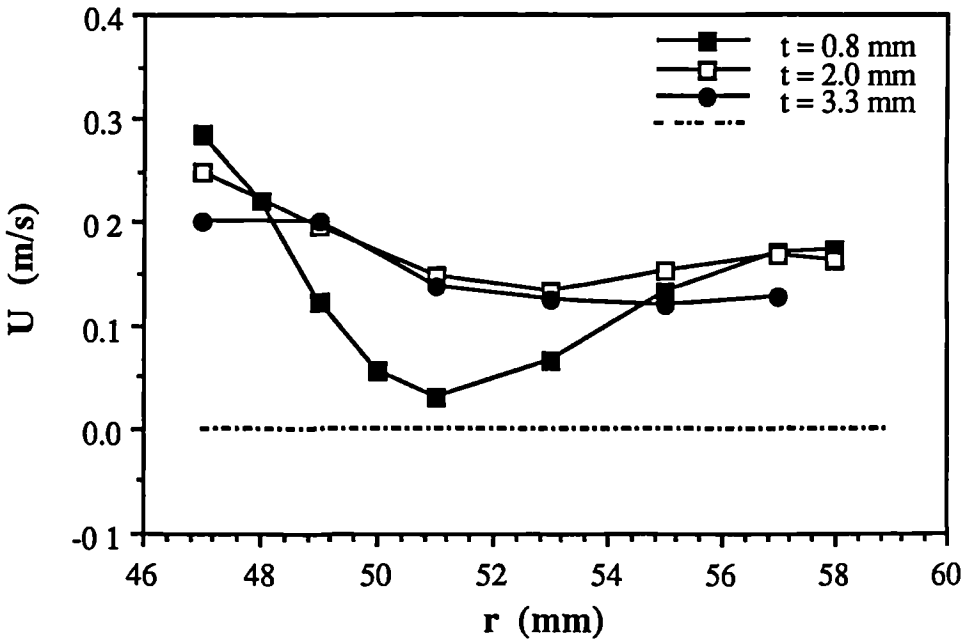

Figure 4.17. Effect of impeller thickness on the axial mean velocities in the impeller vicinity :
C = T/3, N = 250 rpm, z = 86 mm, theta = 0°.

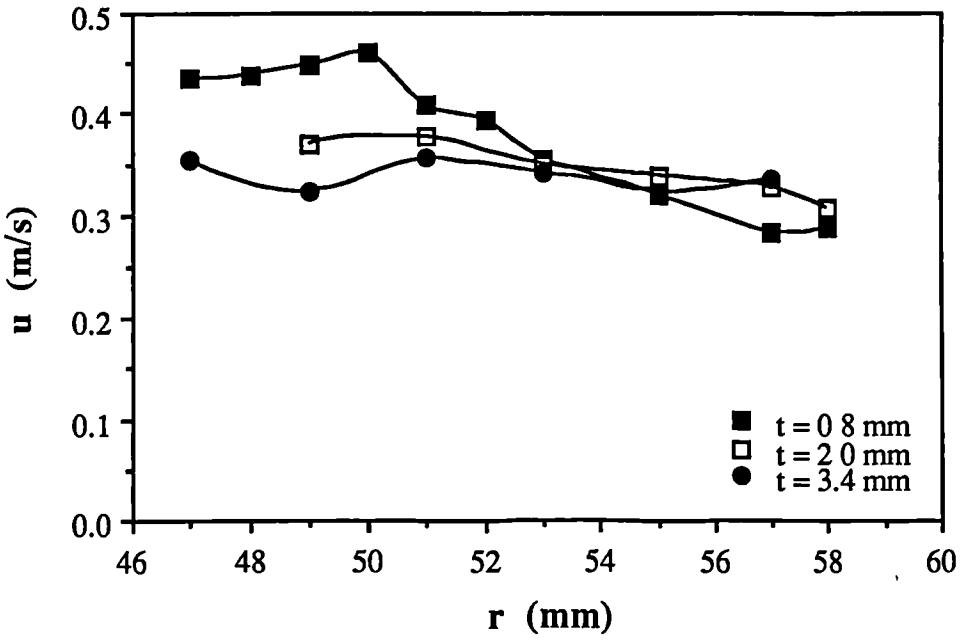

Figure 4.18. Effect of impeller thickness on the axial rms velocities in the impeller vicinity: C = T/3, N = 250 rpm, z = 110 mm, theta = 0°.

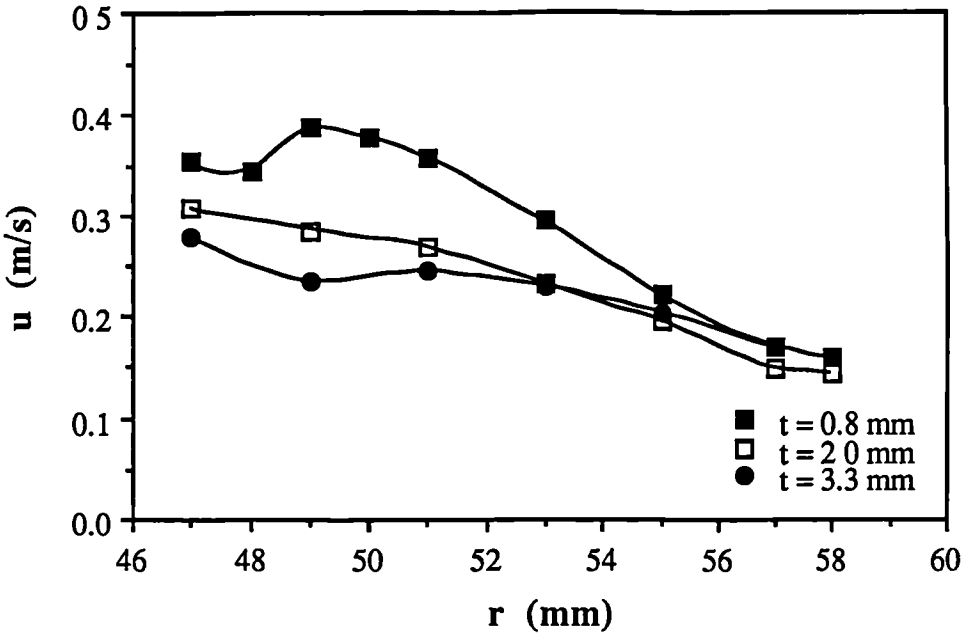

Figure 4.19. Effect of impeller thickness on the axial rms velocities in the impeller vicinity: C = T/3, N = 250 rpm, z = 86 mm, theta = 0°.

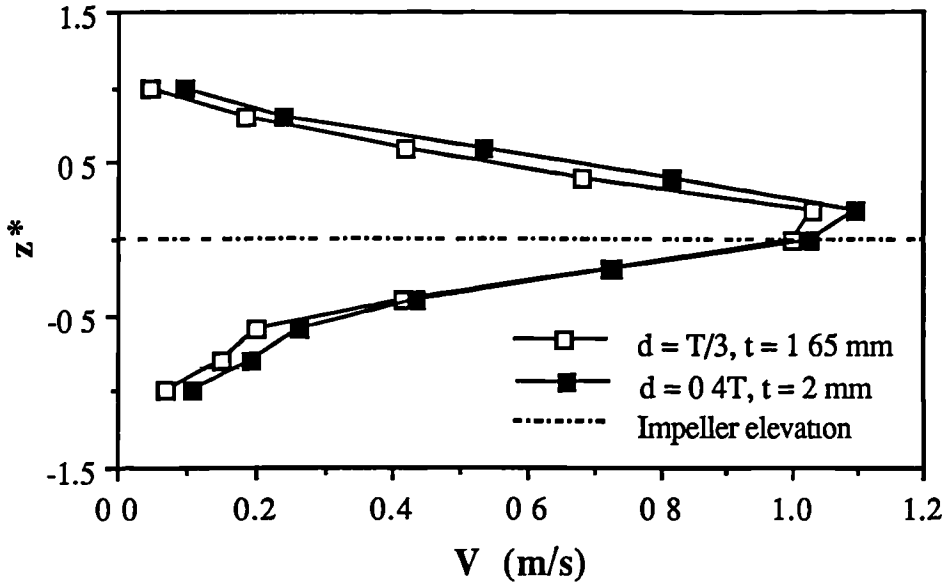

Figure 4.20. Effect of impeller size on the radial mean velocities at constant Reynolds number; C = T/3, t/d = constant, r* = 1.04, theta = 0°.

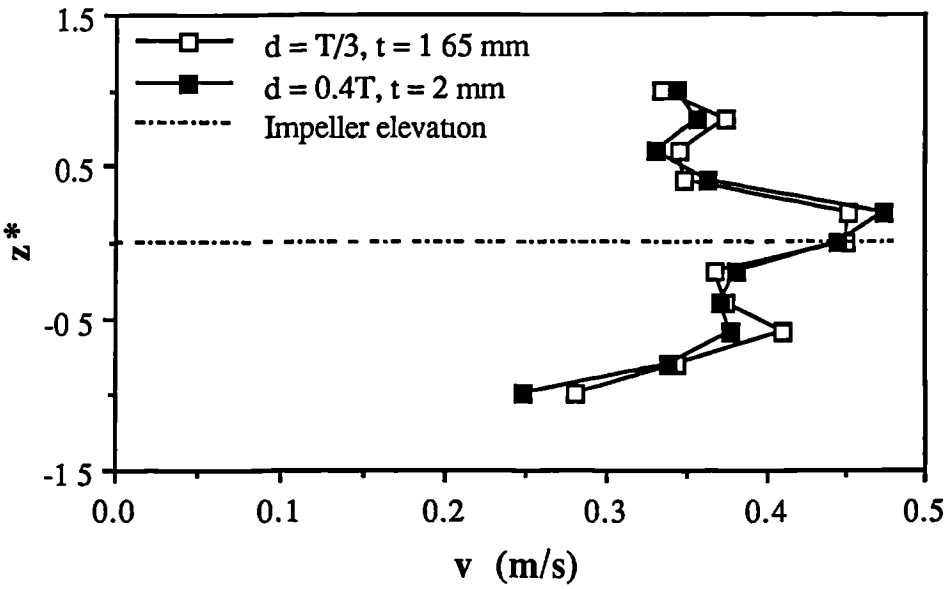

Figure 4.21. Effect of impeller size on the radial rms velocities at constant Reynolds number; C = T/3, t/d = constant, r* = 1.04, theta = 0°.

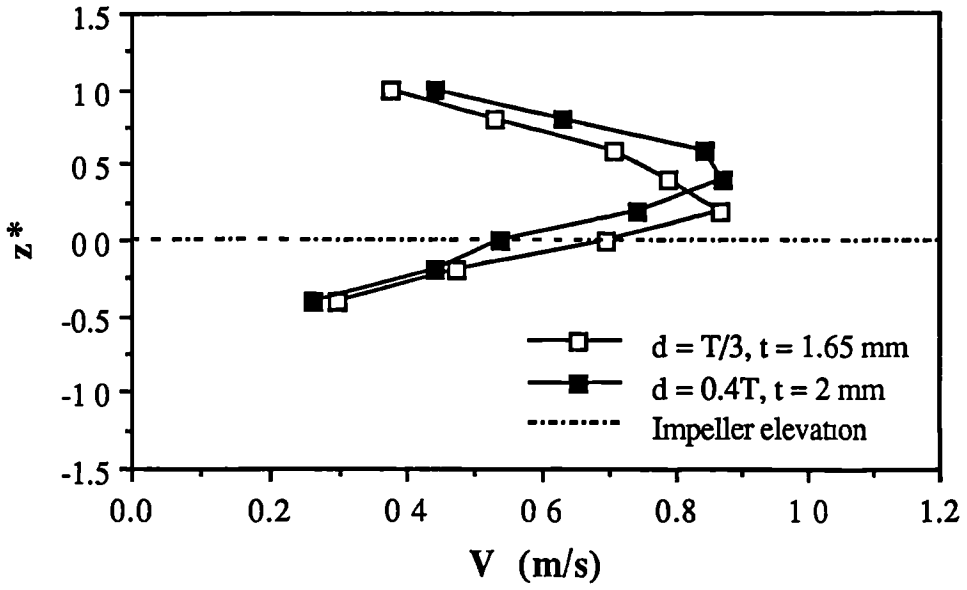

Figure 4.22. Effect of impeller size on the radial mean velocities at constant Reynolds number; C = T/3, t/d = constant, r* = 1.428, theta = 0°.

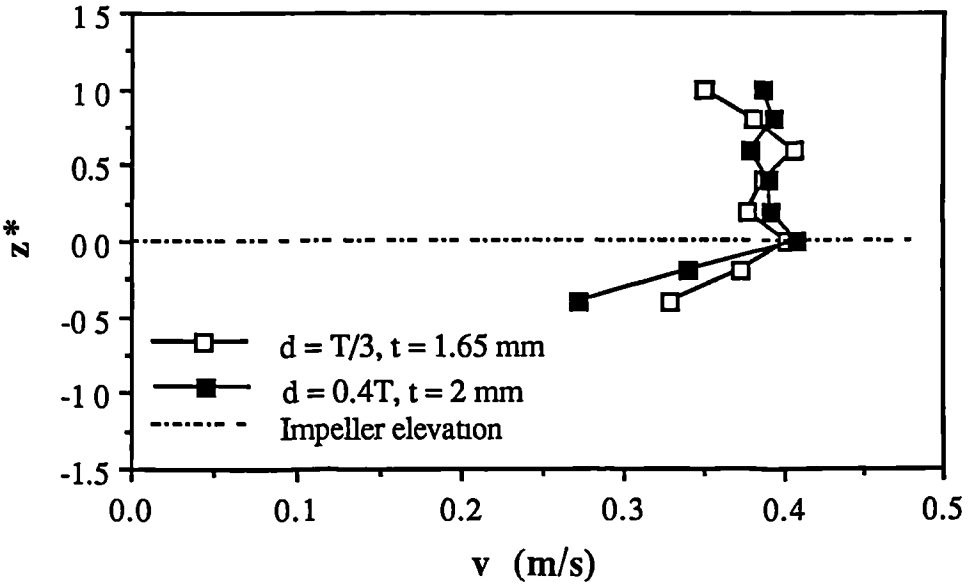

Figure 4.23. Effect of impeller size on the radial rms velocities at constant Reynolds number; C = T/3, t/d = constant, r* = 1.428, theta = 0°.

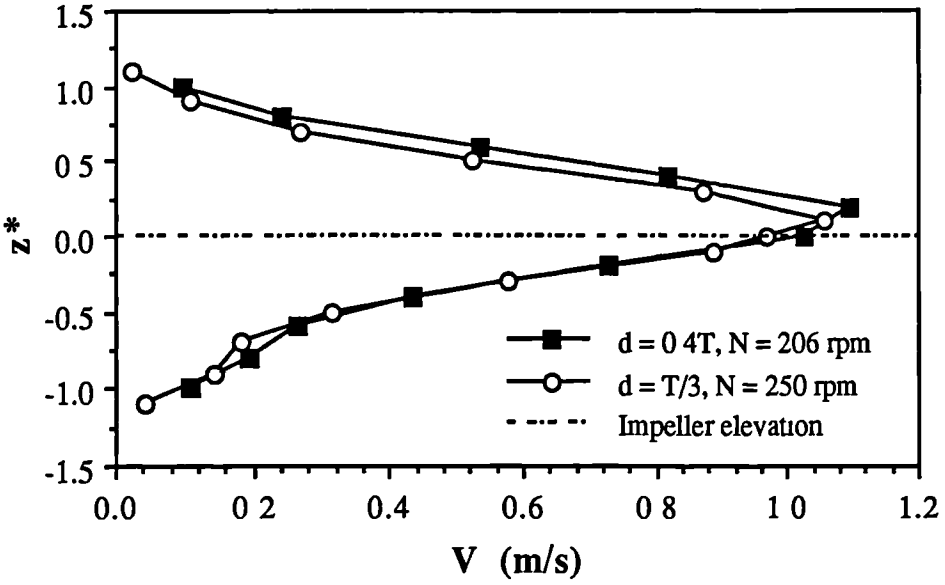

Figure 4.24. Effect of impeller diameter on the radial mean velocities at constant Reynolds number; C = T/3, t = 2 mm, r* = 1.04, theta = 0°.

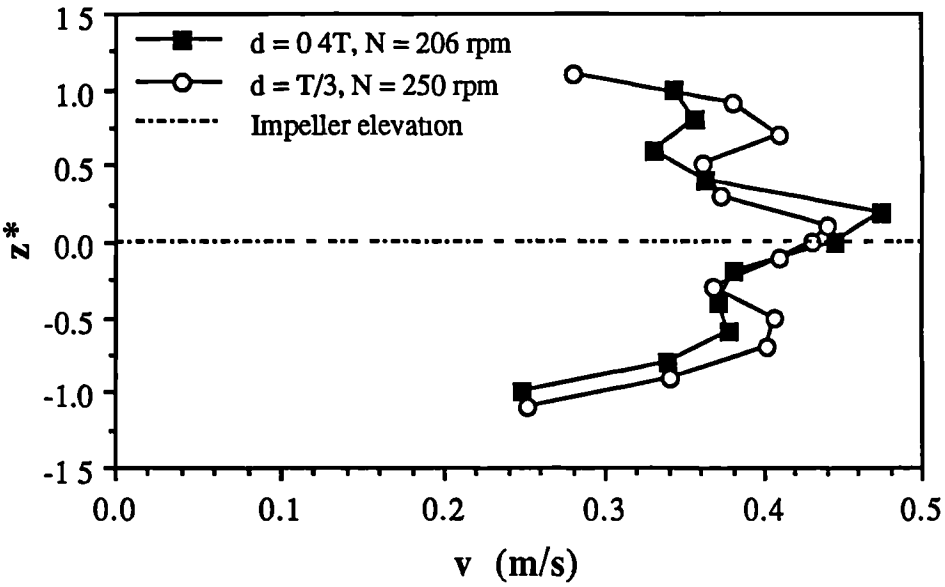

Figure 4.25. Effect of impeller diameter on the radial rms velocities at constant Reynolds number; C = T/3, t = 2 mm, r* = 1.04, theta = 0°.

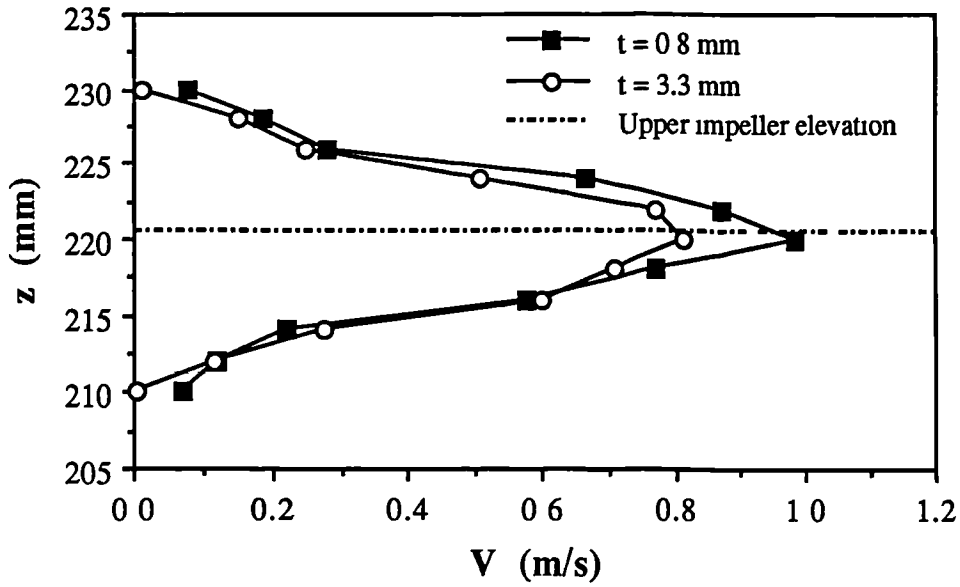

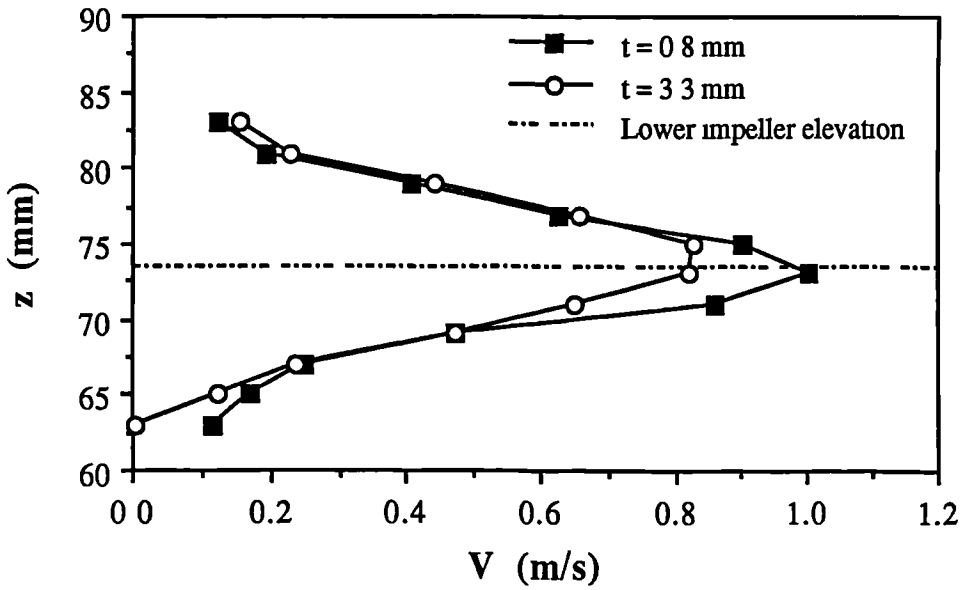

Figure 4.26. Effect of impeller thickness on the radial mean velocities in the impeller streams; C1 = T/4, C2 = T/2, N = 250 rpm, r = 51 mm, theta = 0°.

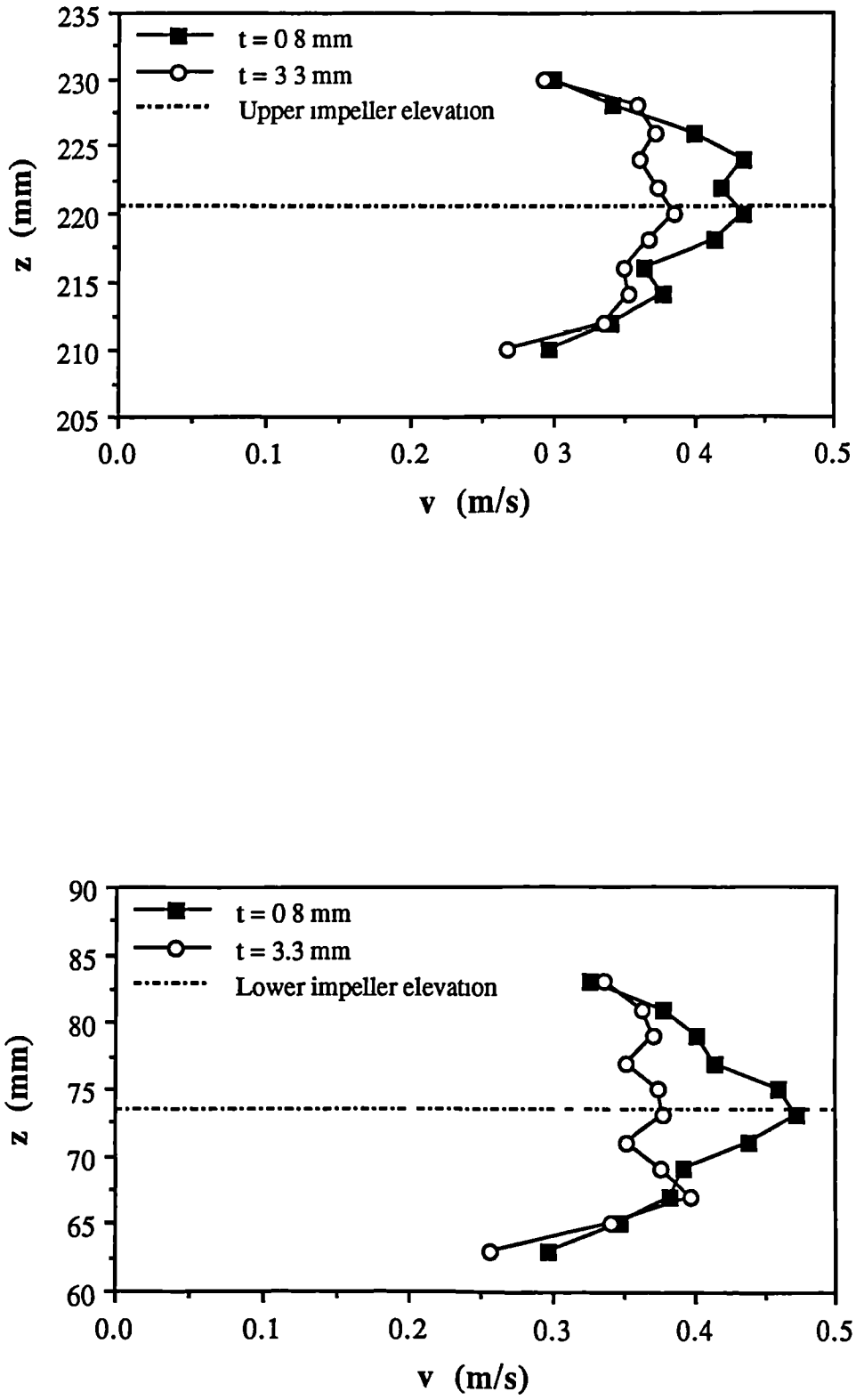

Figure 4.27. Effect of the impeller thickness on the radial rms velocities in the impeller streams; C1 = T/4, C2 = T/2, N = 250 rpm, r = 51 mm, theta = 0°.

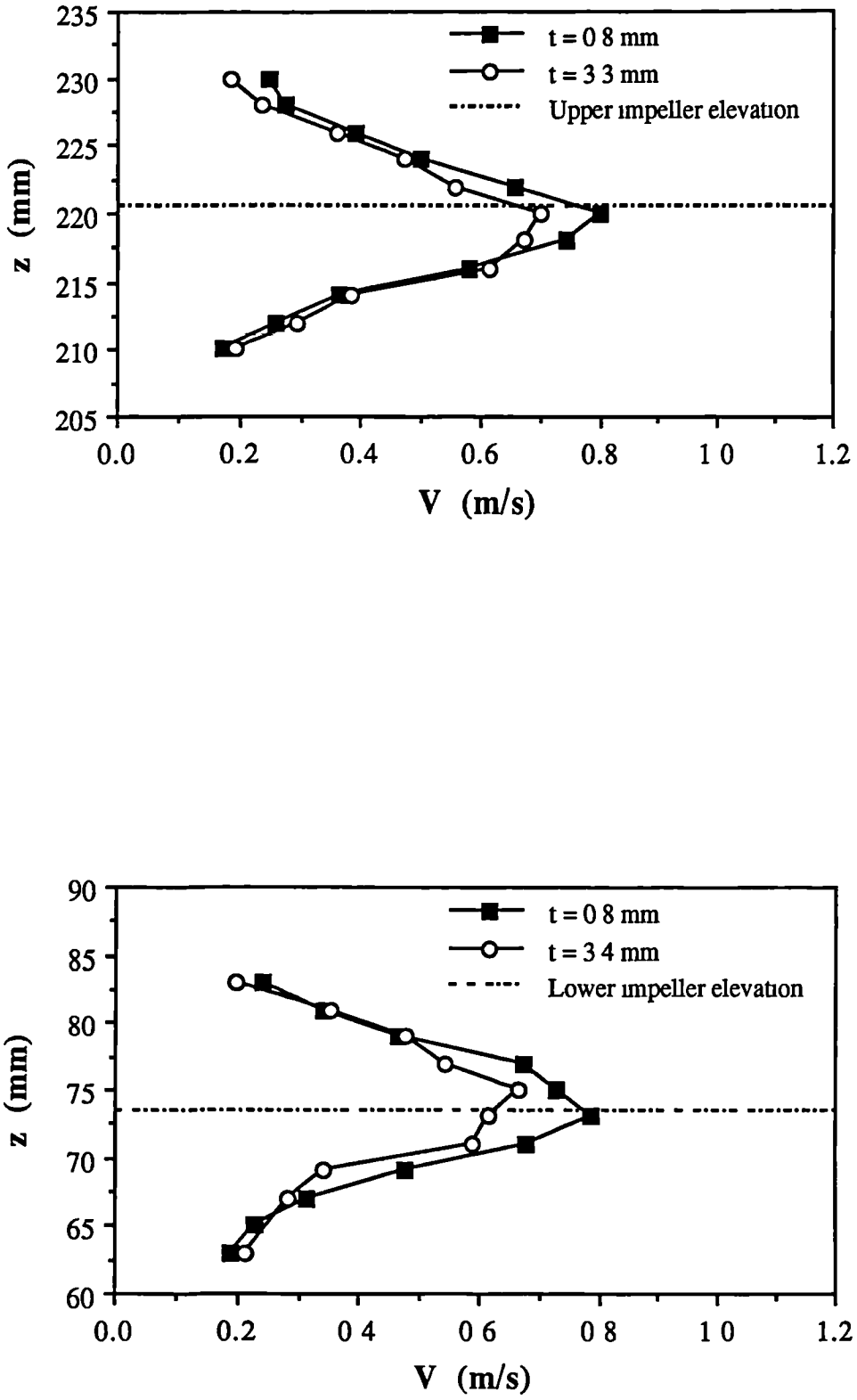

Figure 4.28. Effect of impeller thickness on the radial mean velocities in the impeller streams; C1 = T/4, C2 = T/2, N = 250 rpm, r = 70 mm, theta = 0°.

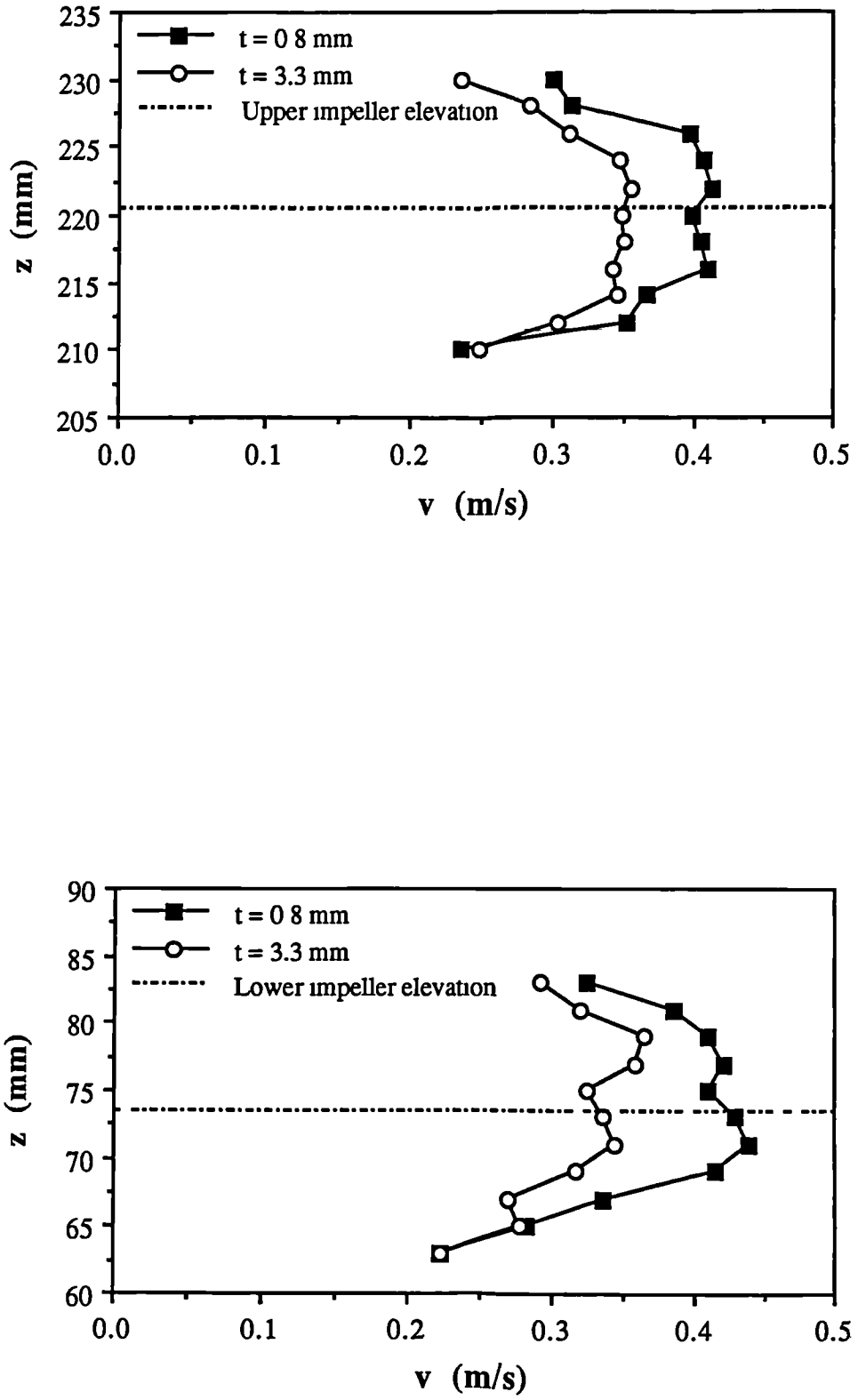

Figure 4.29. Effect of impeller thickness on the radial rms velocities in the impeller streams; C1 = T/4, C2 = T/2, N = 250 rpm, r = 70 mm, theta = 0°.

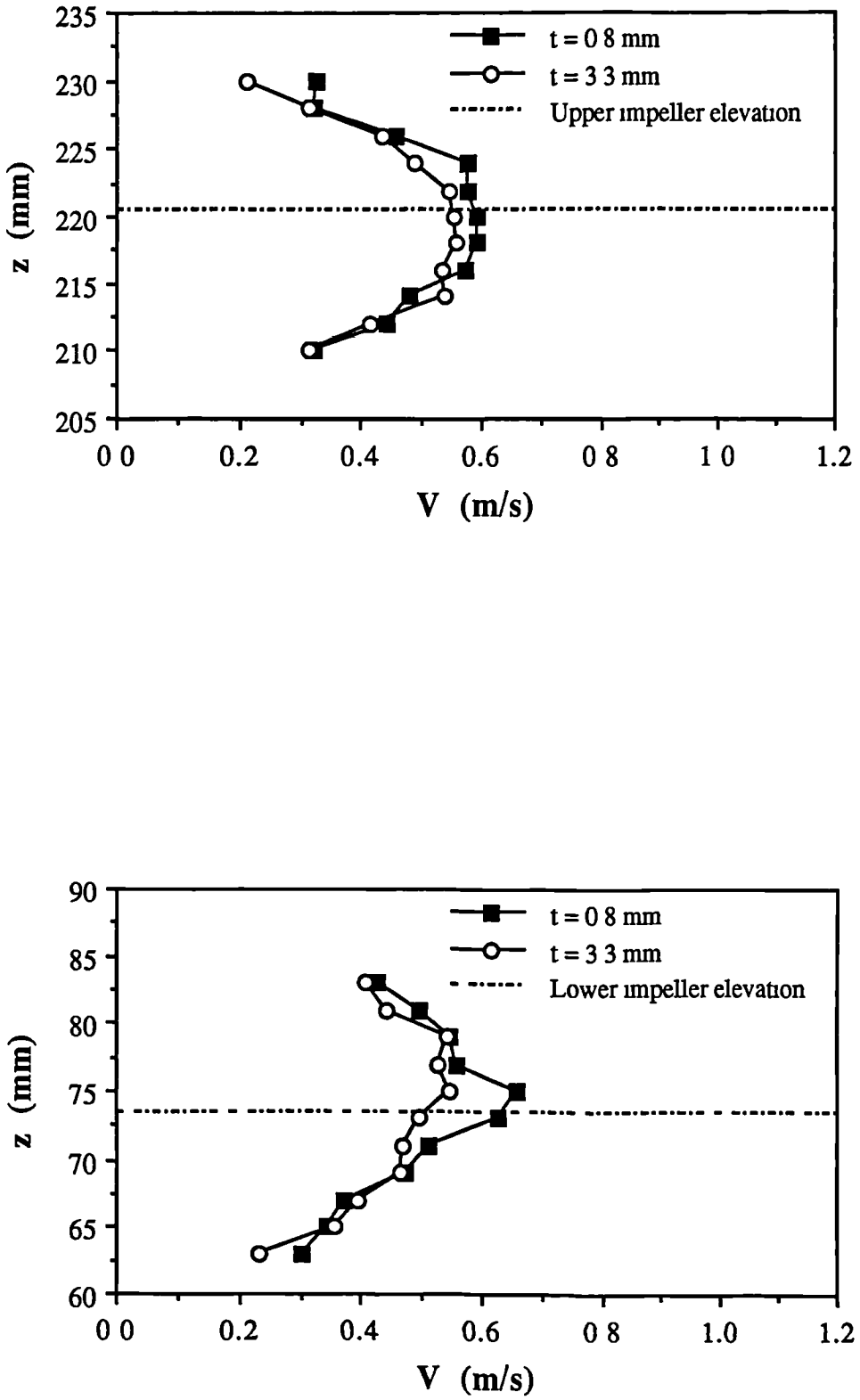

Figure 4.30. Effect of impeller thickness on the radial mean velocities in the impeller streams; C1 = T/4, C2 = T/2, N = 250 rpm, r = 85 mm, theta = 0 °.

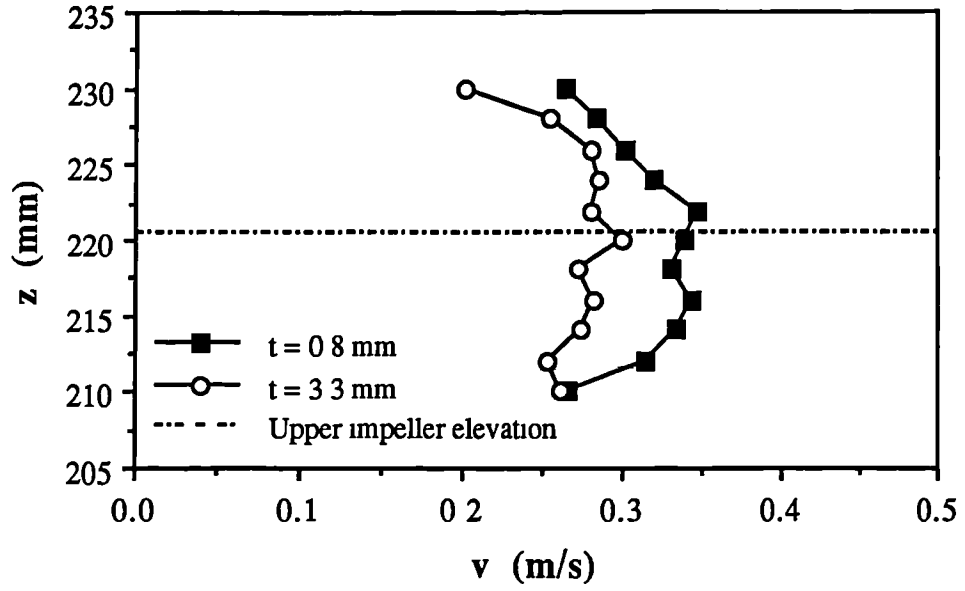

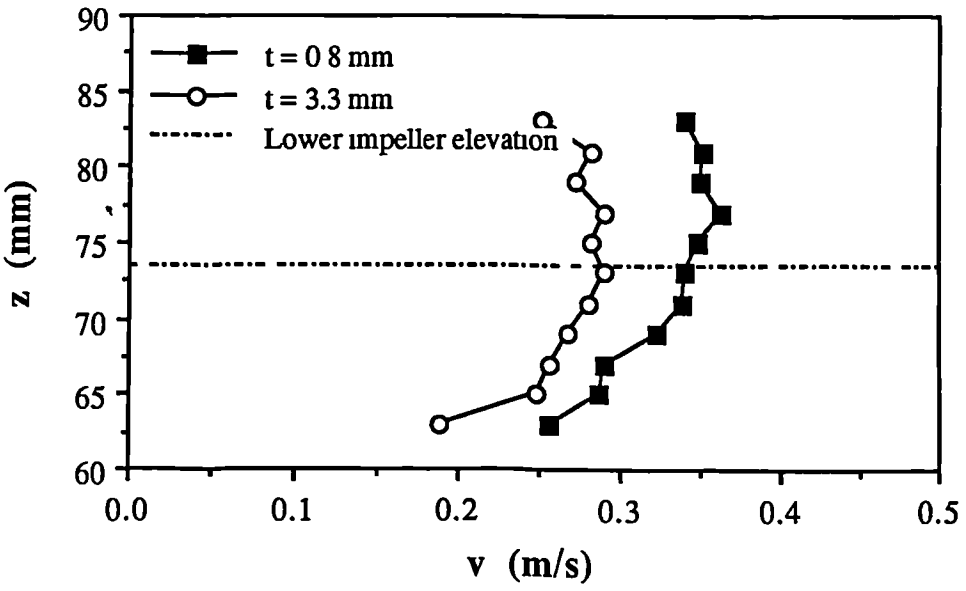

Figure 4.31. Effect of impeller thickness on the radial rms velocities in the impeller streams; C1 = T/4, C2 = T/2, N = 250 rpm, r = 85 mm, theta = 0°.

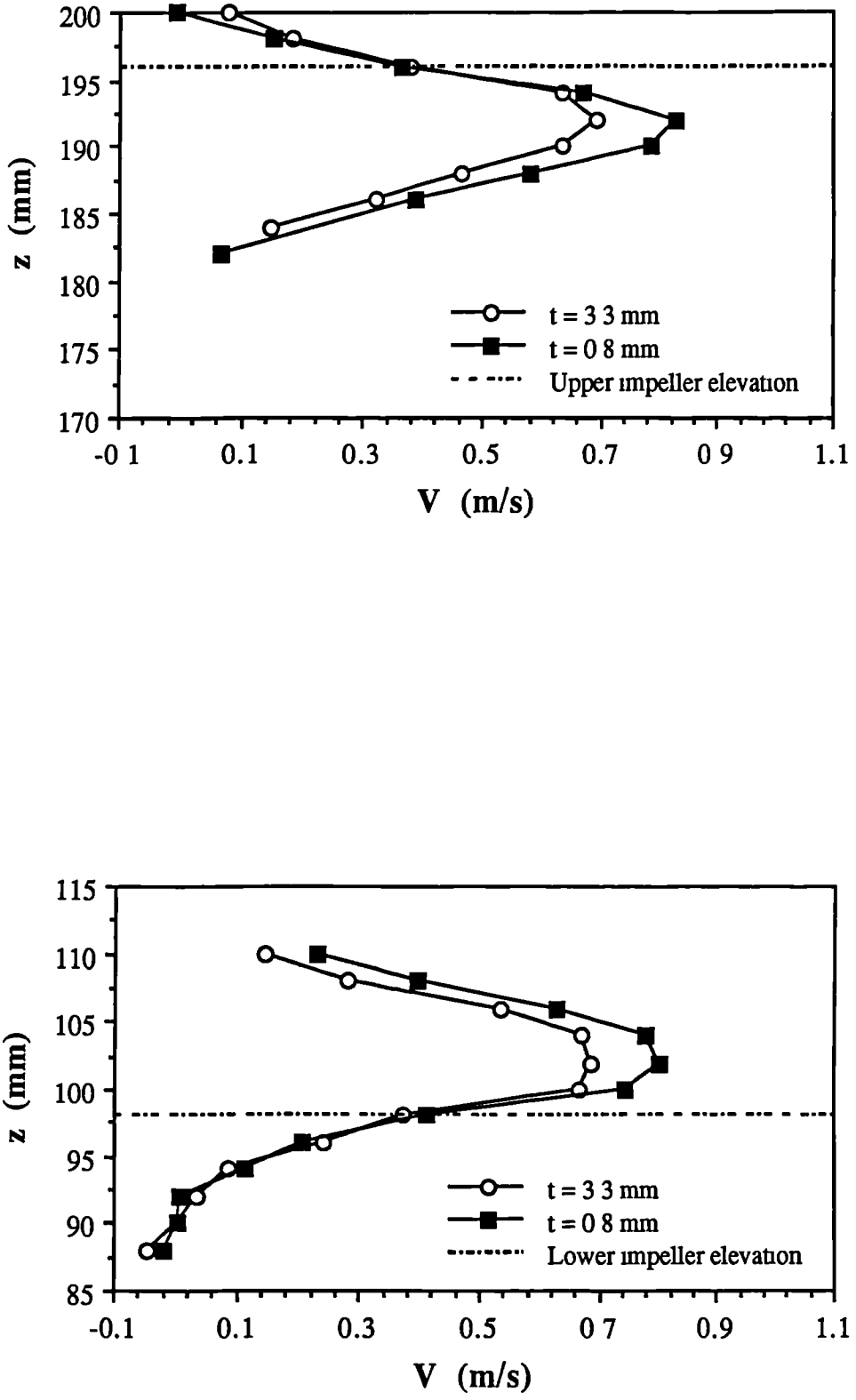

Figure 4.32. Effect of impeller thickness on the radial mean velocities in the impeller streams; C1 = C2 = T/3, N = 250 rpm, r = 51 mm, theta = 0°.

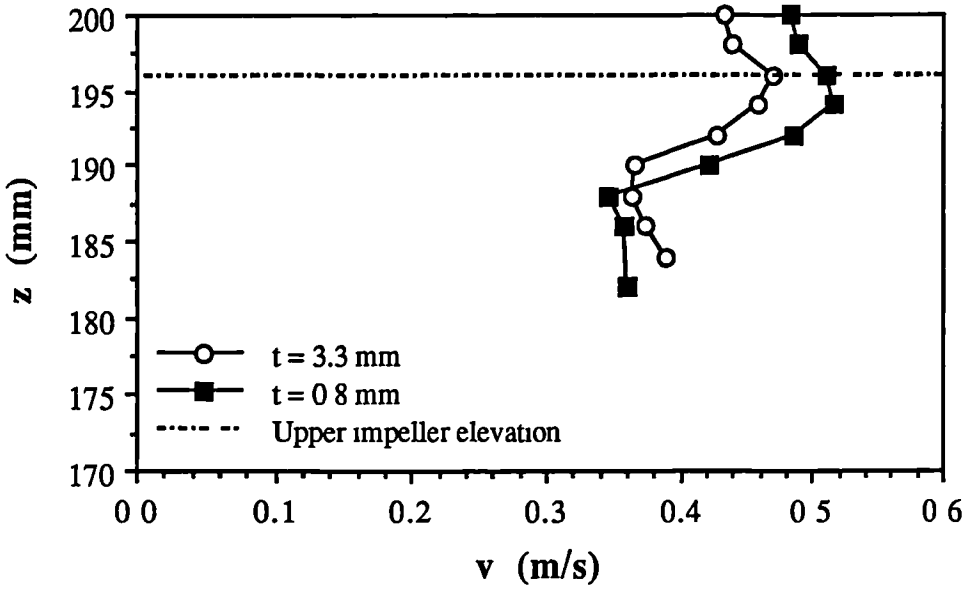

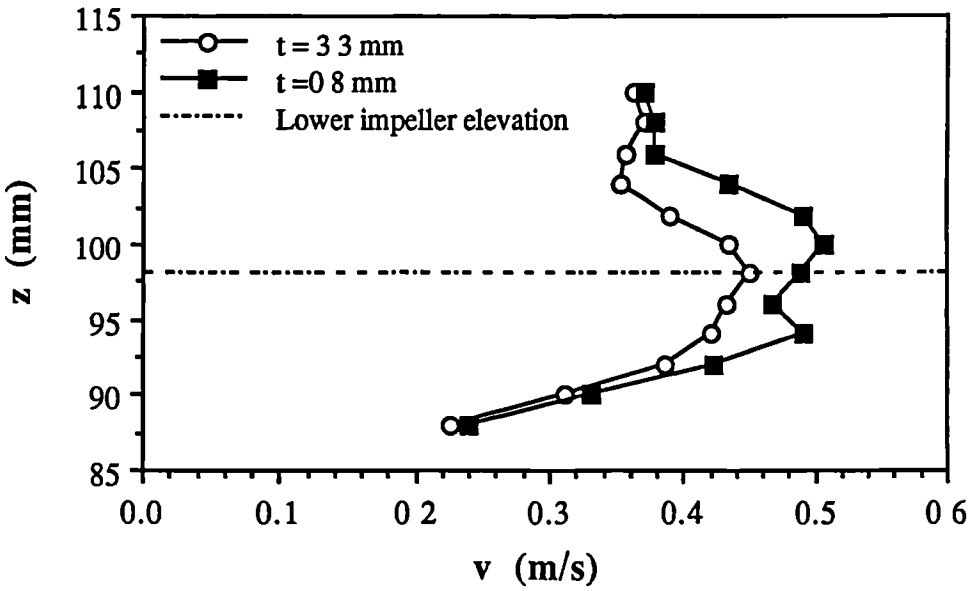

Figure 4.33. Effect of impeller thickness on the radial rms velocities in the impeller streams; C1 = C2 = T/3, N = 250 rpm, r = 51 mm, theta = 0°.

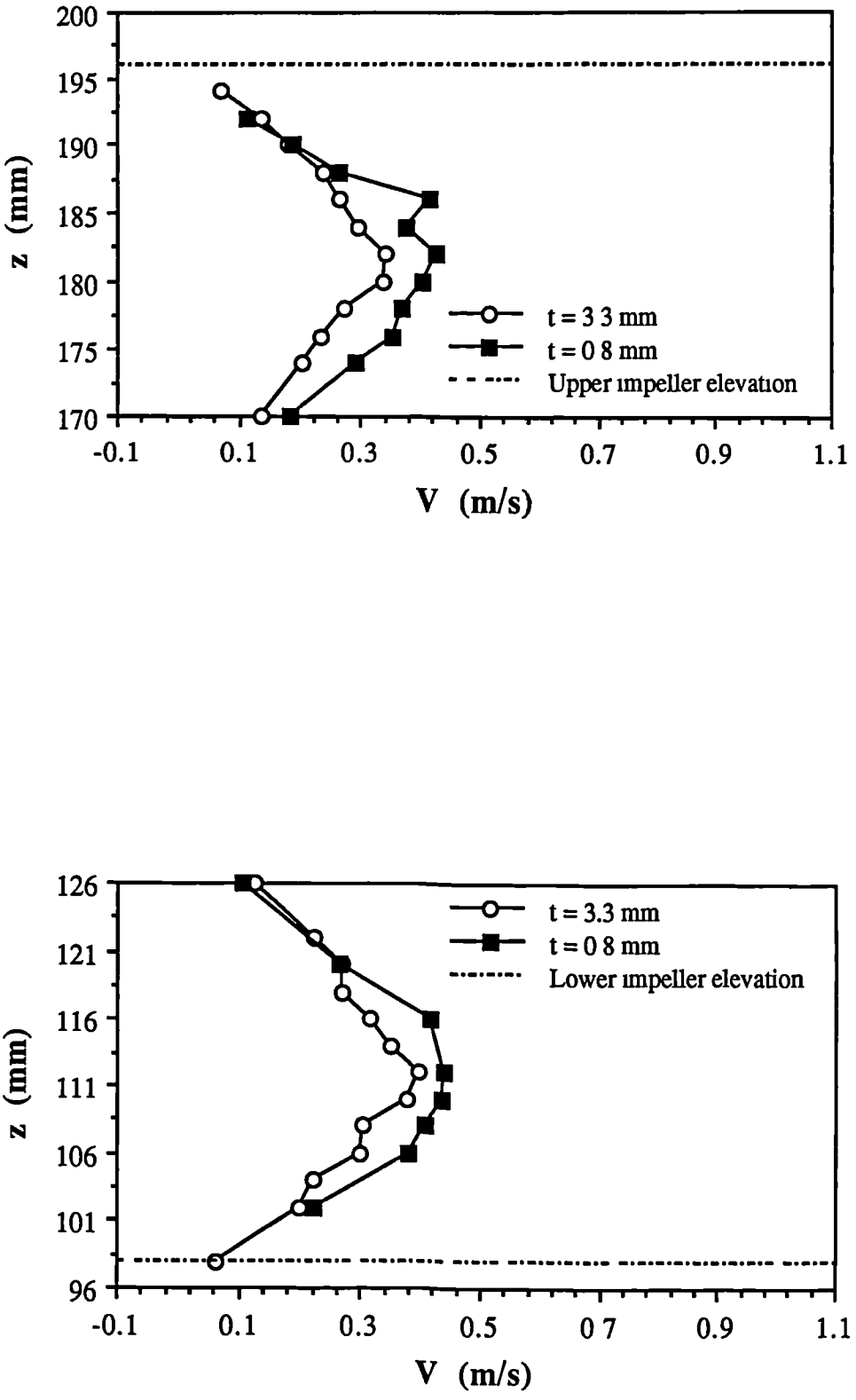

Figure 4.34. Effect of impeller thickness on the radial mean velocities in the impeller streams; C1 = C2 = T/3, N = 250 rpm, r = 70 mm, theta = 0°.

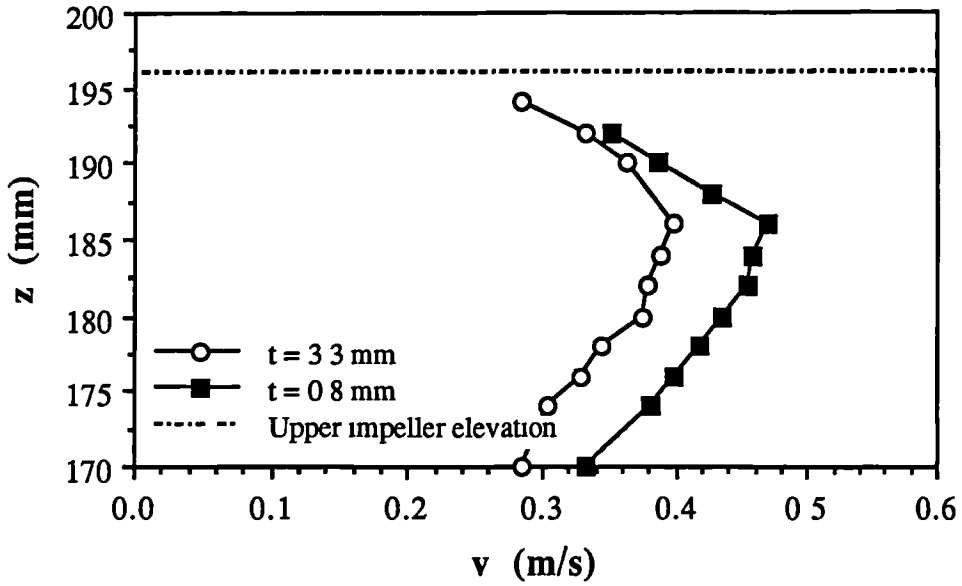

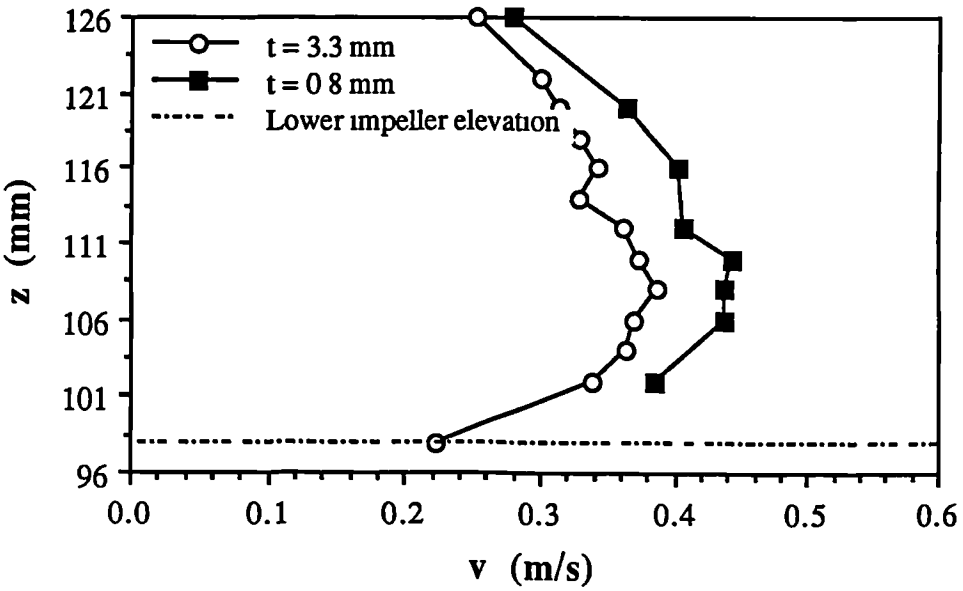

Figure 4.35. Effect of impeller thickness on the radial rms velocities in the impeller streams; C1 = C2 = T/3, N = 250 rpm, r = 70 mm, theta = 0°.

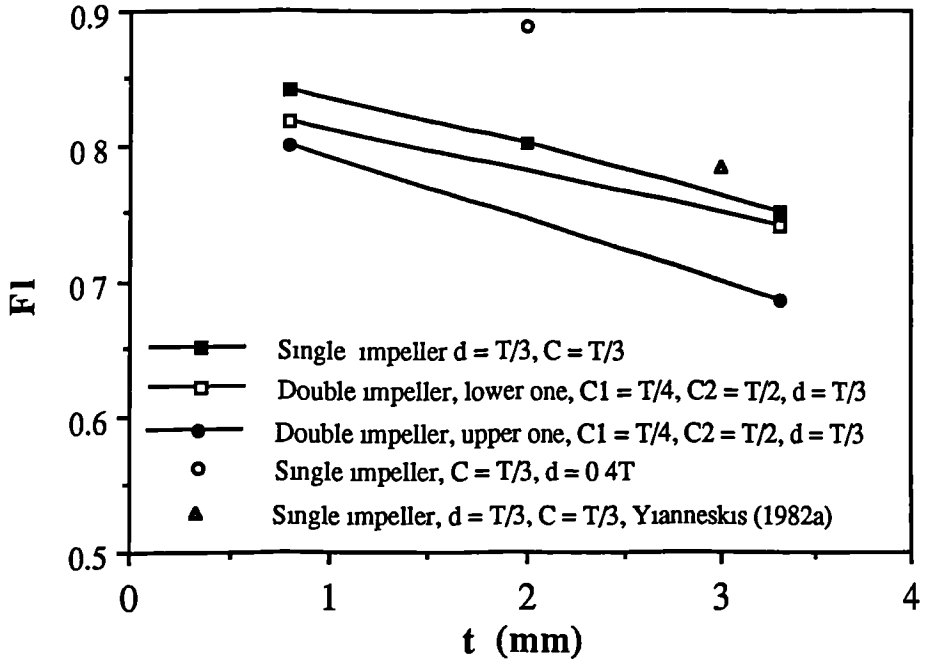

Figure 4.36. Variation of flow number with impeller thickness and impeller diameter, r* = 1.04, theta = 0°.

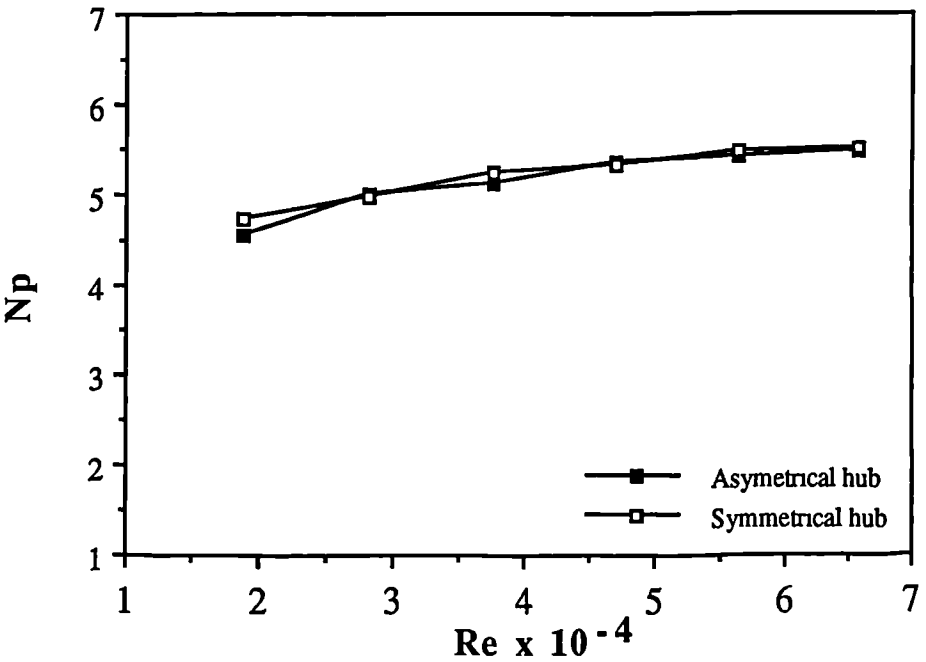

Figure 4.37. Effect of impeller hub on the power number of Rushton impeller, t = 1.65 mm.

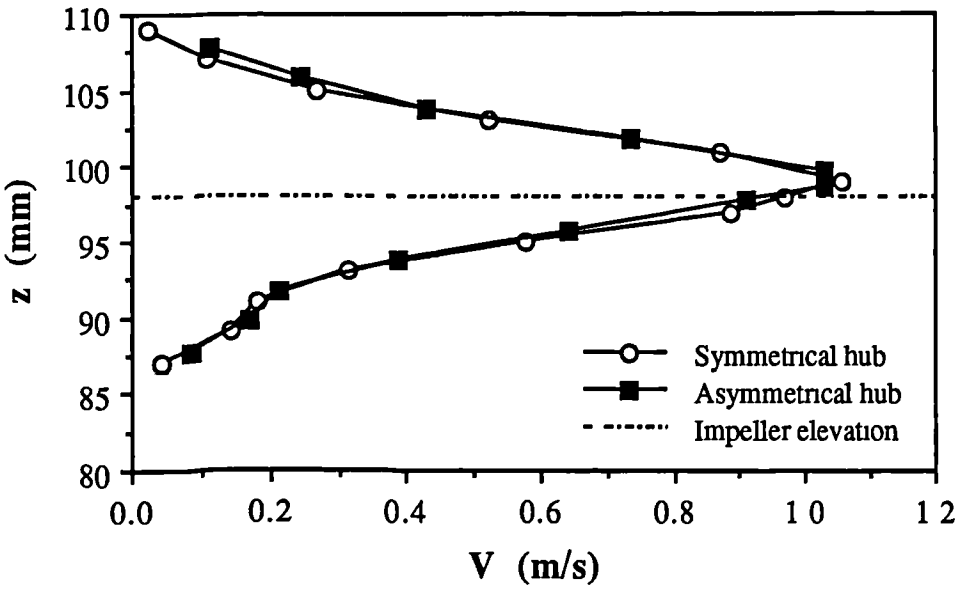

Figure 4.38. Comparison of the radial mean velocity profiles generated by single Rushton impeller with symmetrical and asymmetrical hub; C = T/3, r = 51 mm, theta = 0°.

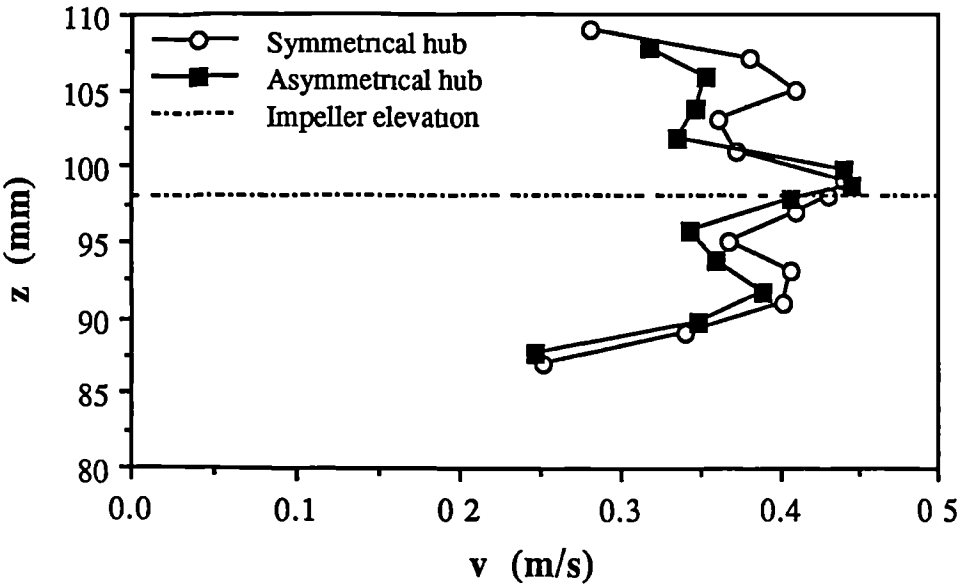

Figure 4.39. Comparison of the radial rms velocity profiles generated by single Rushton impeller with symmetrical and asymmetrical hub; C = T/3, r = 51 mm, theta = 0°.

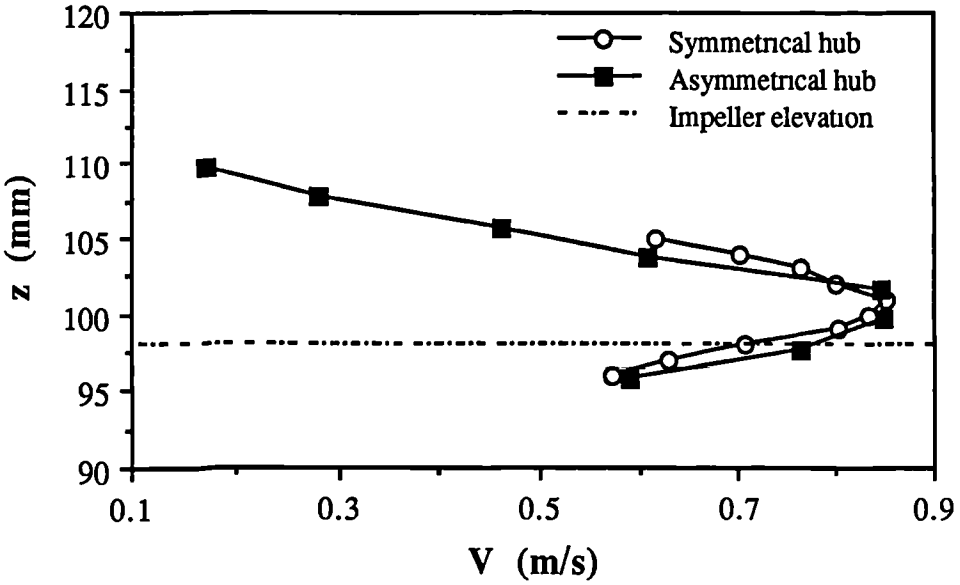

Figure 4.40. Comparison of the radial mean velocity profiles generated by single Rushton impeller with symmetrical and asymmetrical hub; C = T/3, r = 70 mm, theta = 0°.

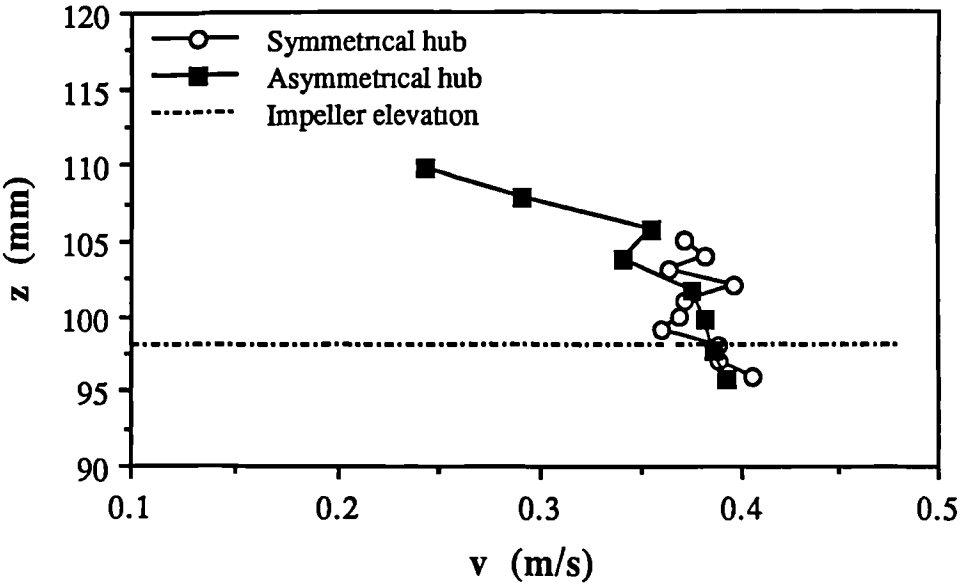

Figure 4.41. Comparison of the radial r.m.s. velocity profiles generated by single Rushton impeller with symmetrical and asymmetrical hub; C = T/3, r = 51 mm, theta = 0°.

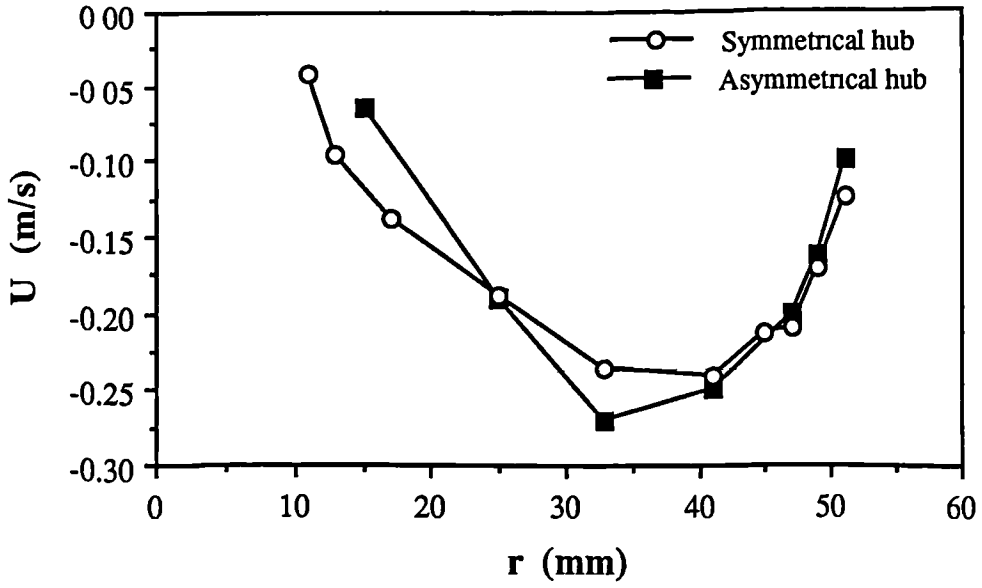

Figure 4.42. Comparison of the axial mean velocity profiles generated by single Rushton impeller with symmetrical and asymmetrical hub; C = T/3, z = 113 mm, theta = 0°.

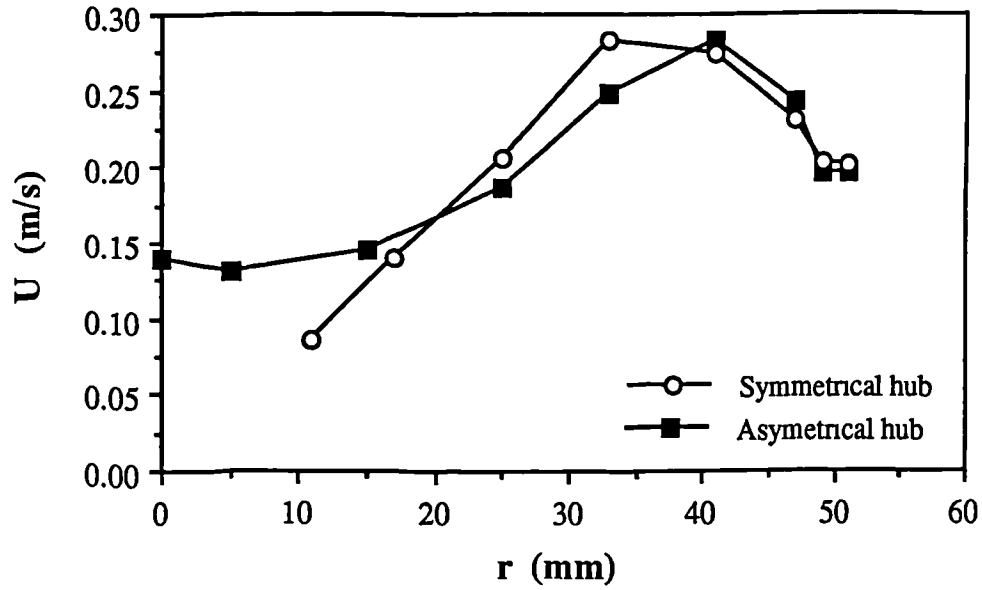

Figure 4.43. Comparison of the axial mean velocity profiles generated by single Rushton impeller with Symmetrical and asymmetrical hub; C = T/3, z = 83 mm, theta = 0°.

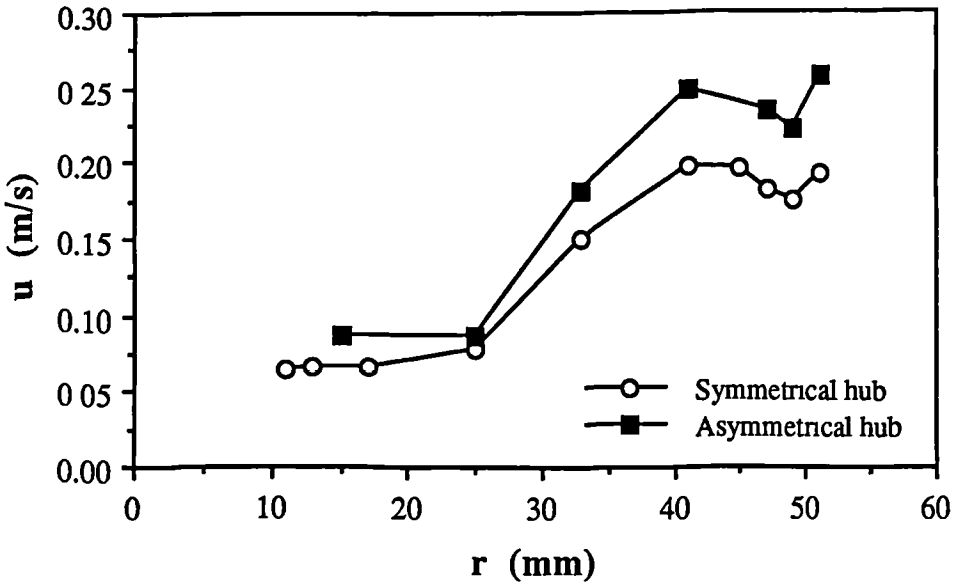

Figure 4.44. Comparison of the axial rms velocity profiles generated by single Rushton impeller with symmetrical and asymmetrical hub; C = T/3, z = 113 mm, theta = 0°.

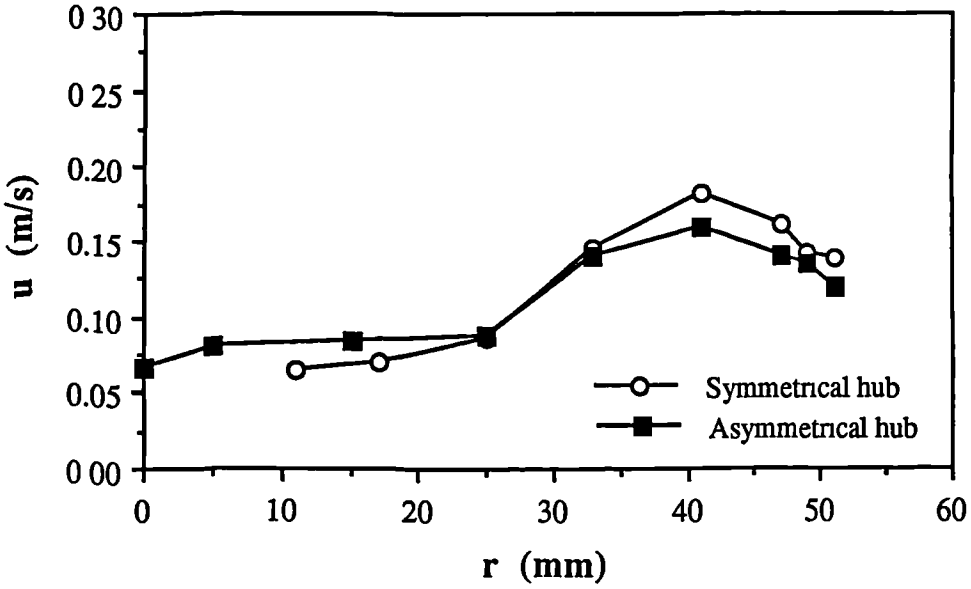

Figure 4.45. Comparison of the axial rms velocity profiles generated by single Rushton impeller with symmetrical and asymmetrical hub; C = T/3, z = 83 mm, theta = 0°.

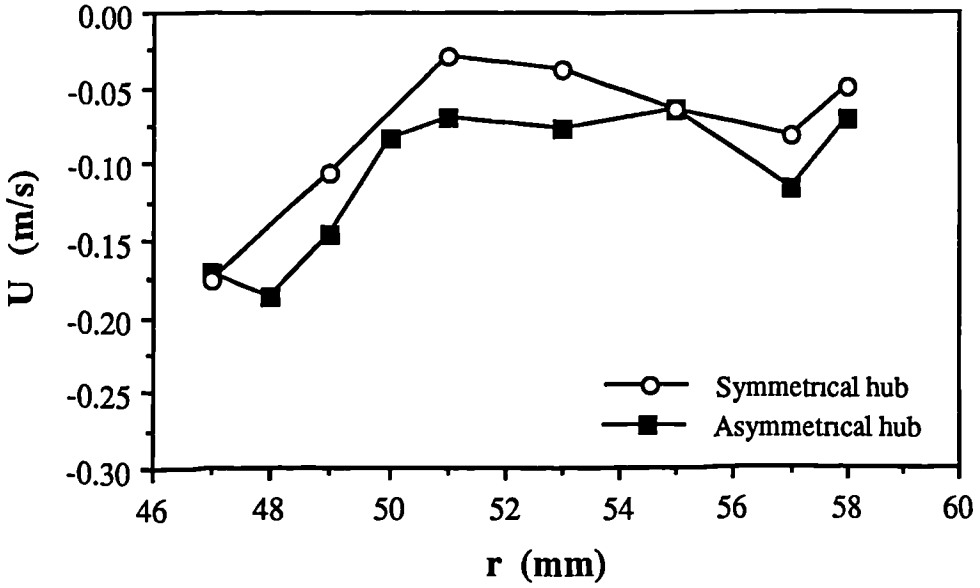

Figure 4.46. Comparison of the axial mean velocity profiles generated by single Rushton impeller with symmetrical and asymmetrical hub; C = T/3, z = 110 mm, theta = 0°.

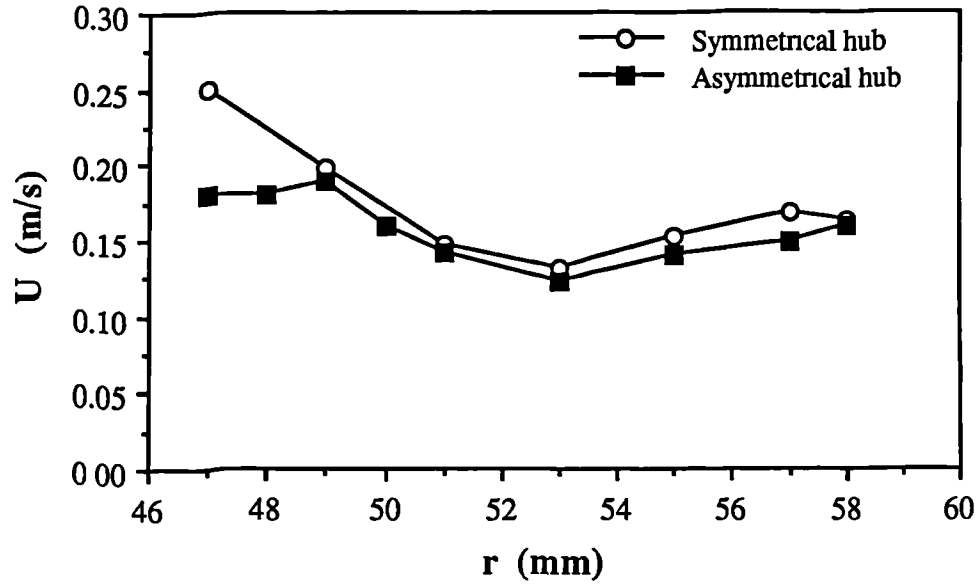

Figure 4.47. Comparison of the axial mean velocity profiles generated by single Rushton impeller with symmetrical and asymmetrical hub; C = T/3, z = 86 mm, theta = 0°.

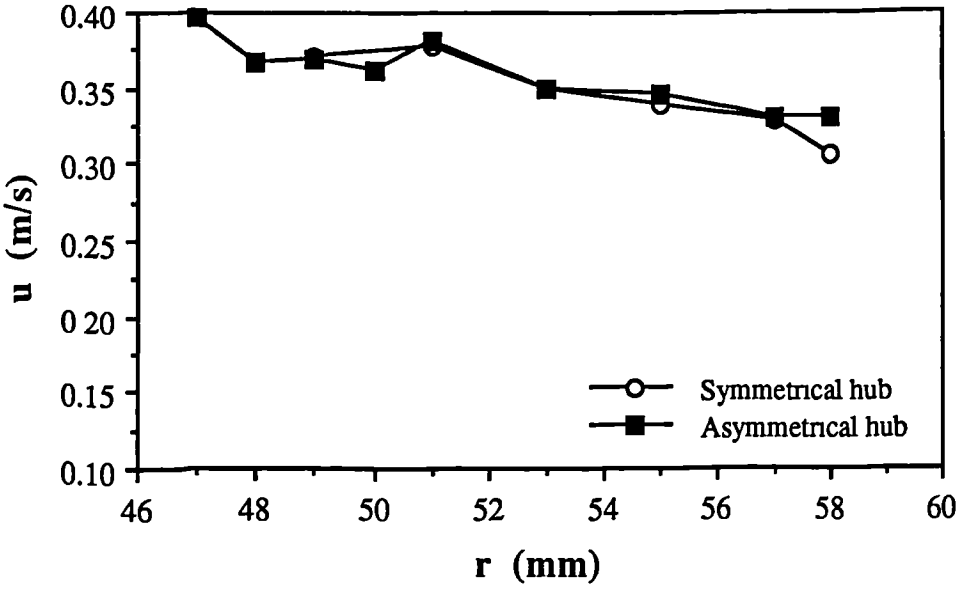

Figure 4.48. Comparison of the axial rms velocity profiles generated by single Rushton impeller with symmetrical and asymmetrical hub; C = T/3, z = 110 mm, theta = 0°.

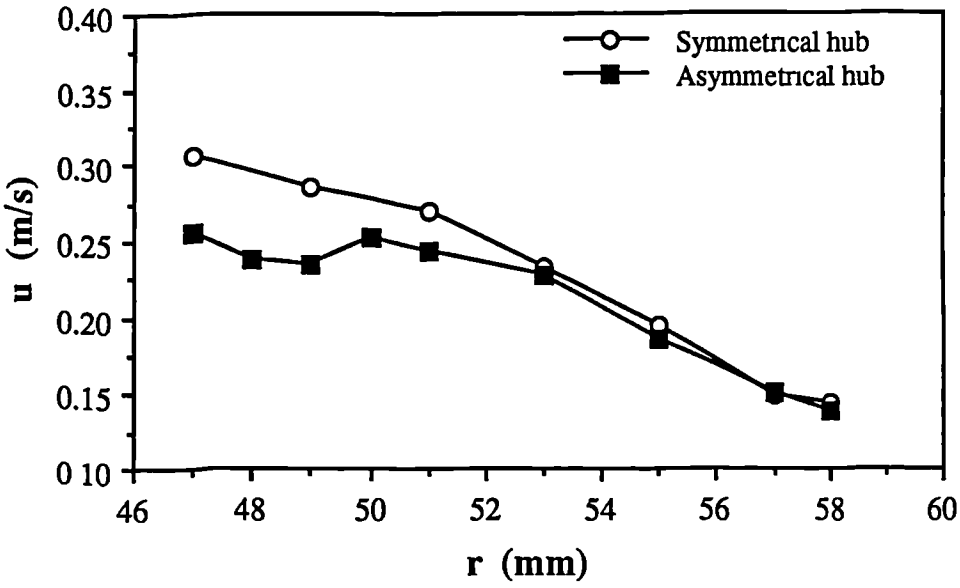

Figure 4.49. Comparison of the axial rms velocity profiles generated by single Rushton impeller with symmetrical and asymmetrical hub; C = T/3, z = 86 mm, theta = 0°.

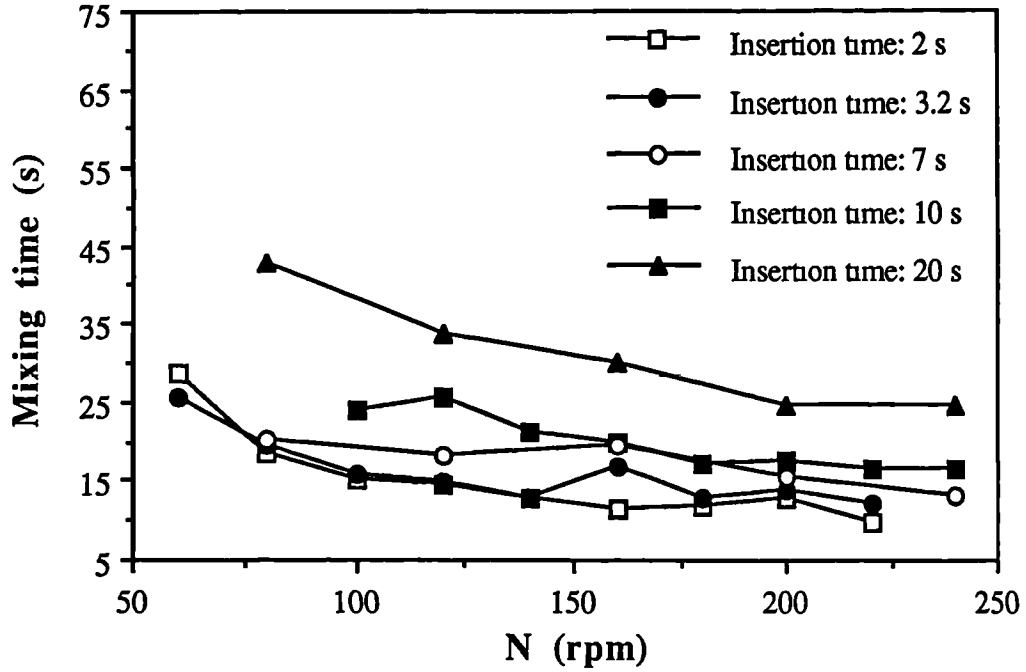

Figure 4.50. Effect of the impeller speed on local mixing time: C1 = 0.3 T, C2 = 0.4 T; probe located at r = 60 mm, z = 0.7 T; theta = 0 °.

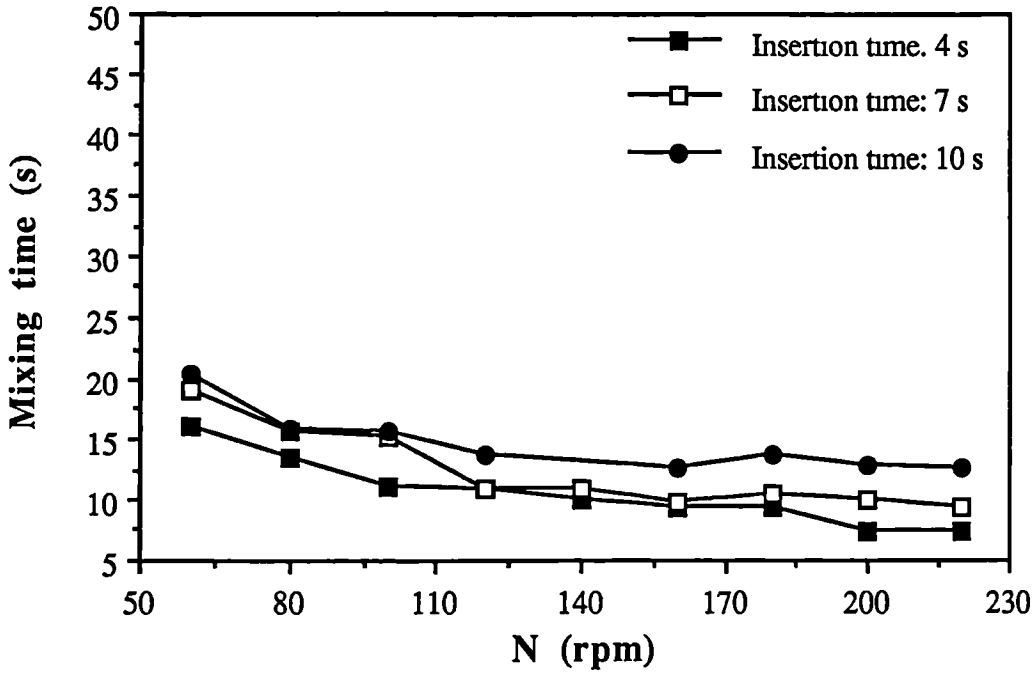

Figure 4.51. Effect of impeller speed on local mixing time: C1 = C2 = T/3, probe located at r = 30 mm, z = T/2, theta = 0°.

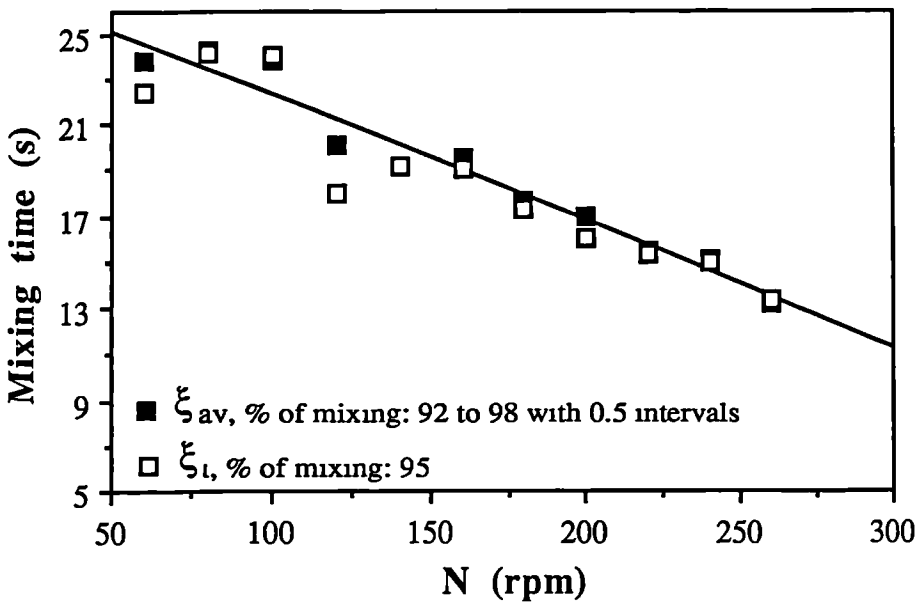

Figure 4.52. Effect of impeller speed on average mixing time; C1 = 0.3 T, C2 = 0.4 T, insertion time = 6.5 s, theta = 0° .

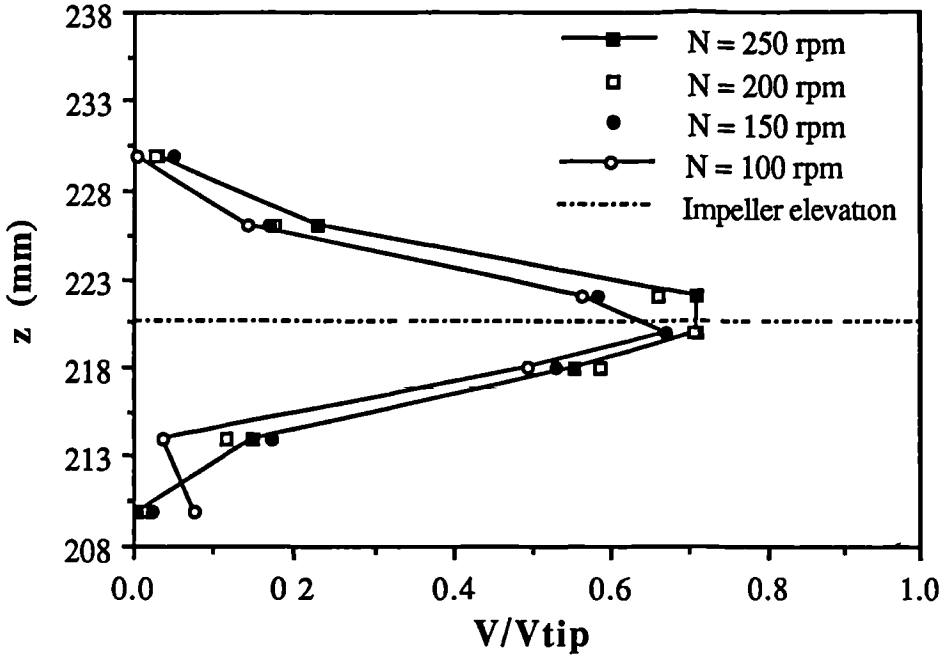

Figure 4.53. Effect of impeller speed on the normalized radial mean velocities in the upper impeller stream: C1 = T/4, C2 = T/2, r = 51 mm, theta = 0°.

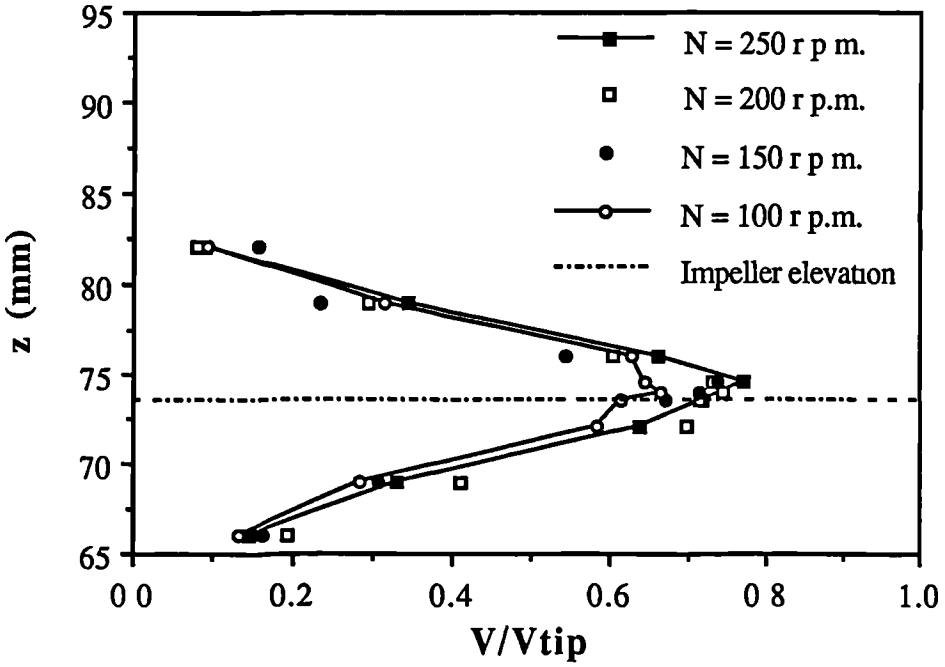

Figure 4.54. Effect of impeller speed on the normalized radial mean velocities in the lower impeller stream: C1 = T/4, C2 = T/2, r = 51 mm, theta = 0°.

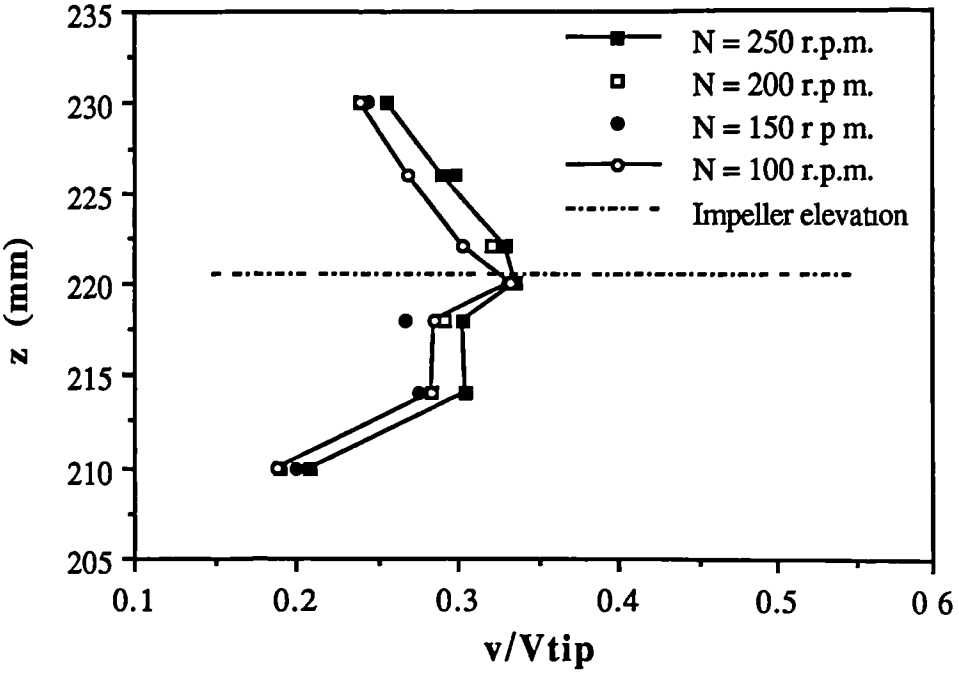

Figure 4.55. Effect of impeller speed on the normalized radial rms velocities in the impeller stream; C1 = T/4, C2 = T/2, upper impeller, r = 51 mm, theta = 0°.

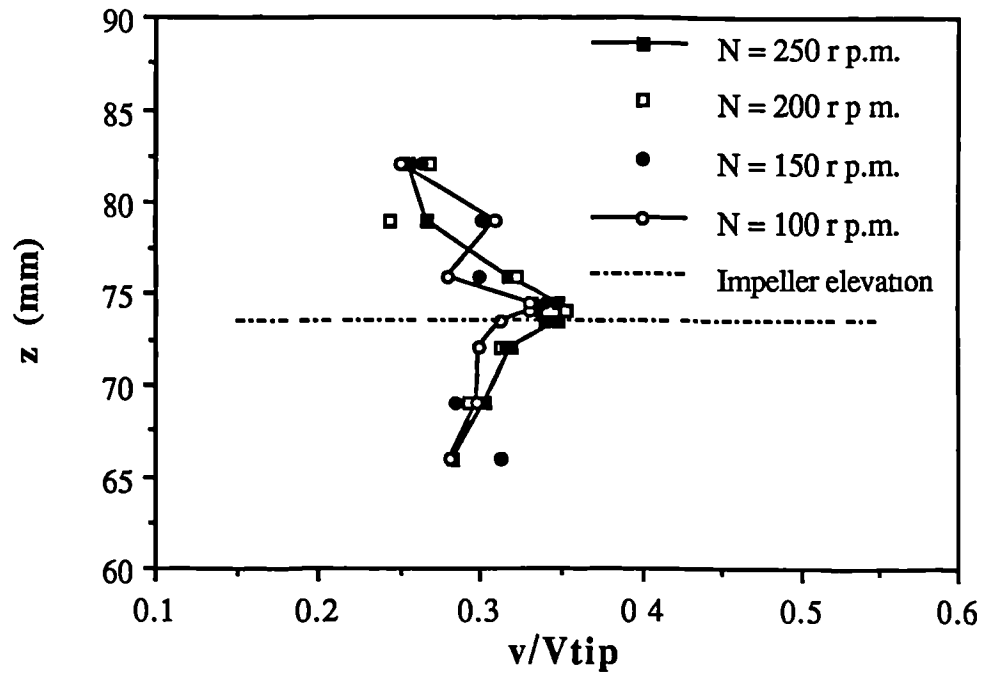

Figure 4.56. Effect of impeller speed on the normalized radial rms velocities in the impeller stream; C1 = T/4, C2 = T/2, lower impeller, r = 51 mm, theta = 0°.

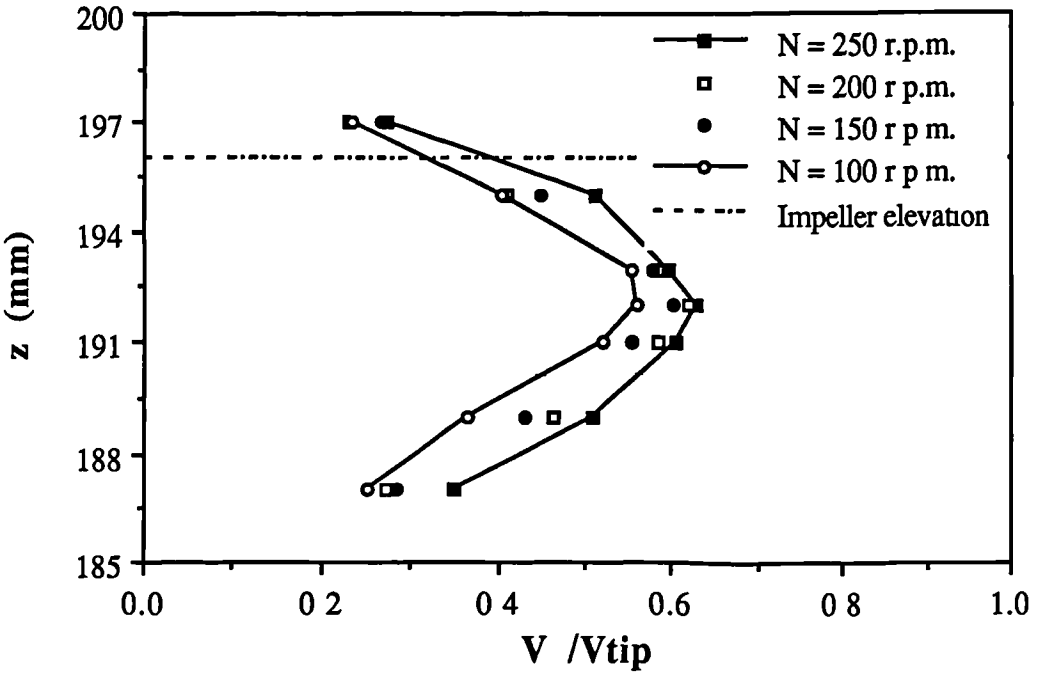

Figure 4.57. Effect of impeller speed on the normalized radial mean velocities in the impeller stream; C1 = C2 = T/3, upper impeller, r = 51 mm, theta = 0°.

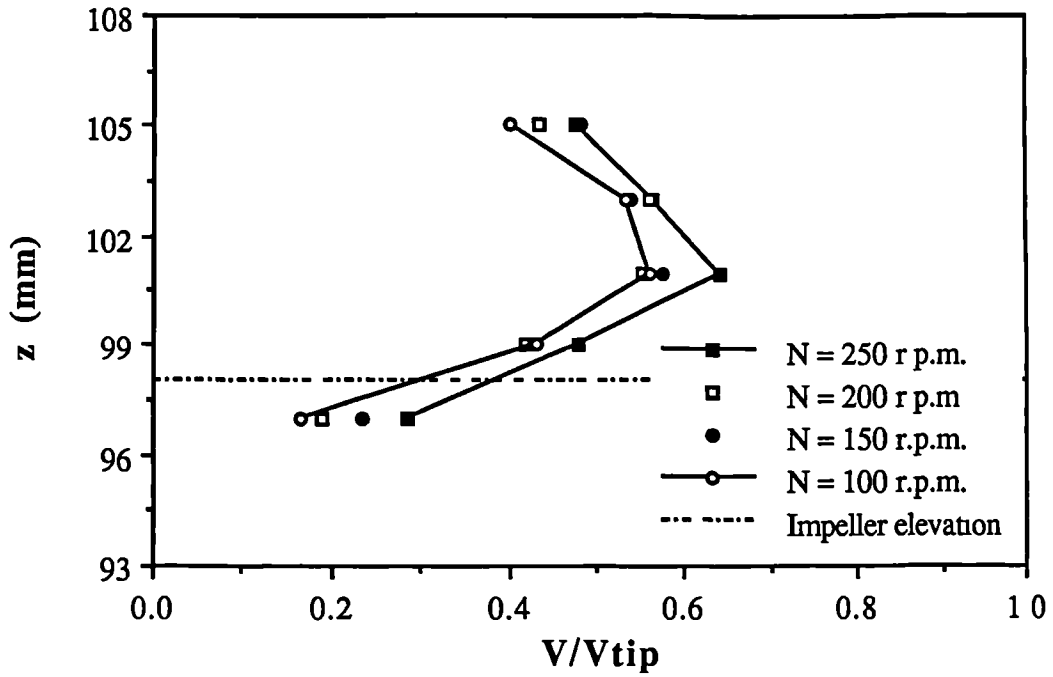

Figure 4.58. Effect of impeller speed on the normalized radial mean velocities in the impeller stream; C1 = C2 = T/3, lower impeller, r = 51 mm, theta = 0°.

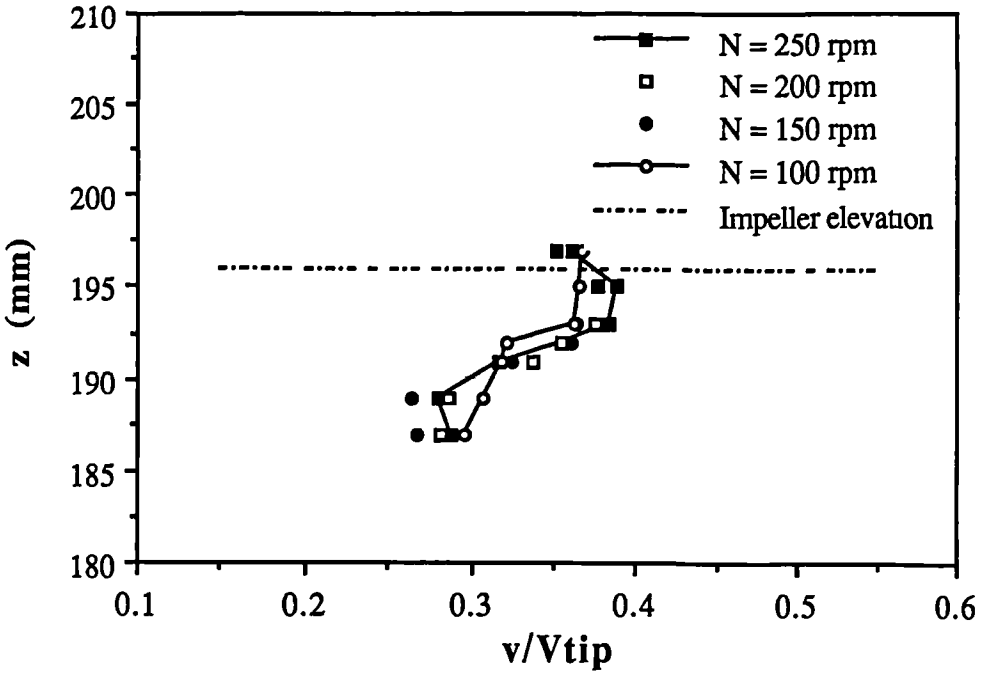

Figure 4.59. Effect of impeller speed on the normalized radial rms velocities in the impeller stream; C1 = C2 = T/3, upper impeller, r = 51 mm, theta = 0°.

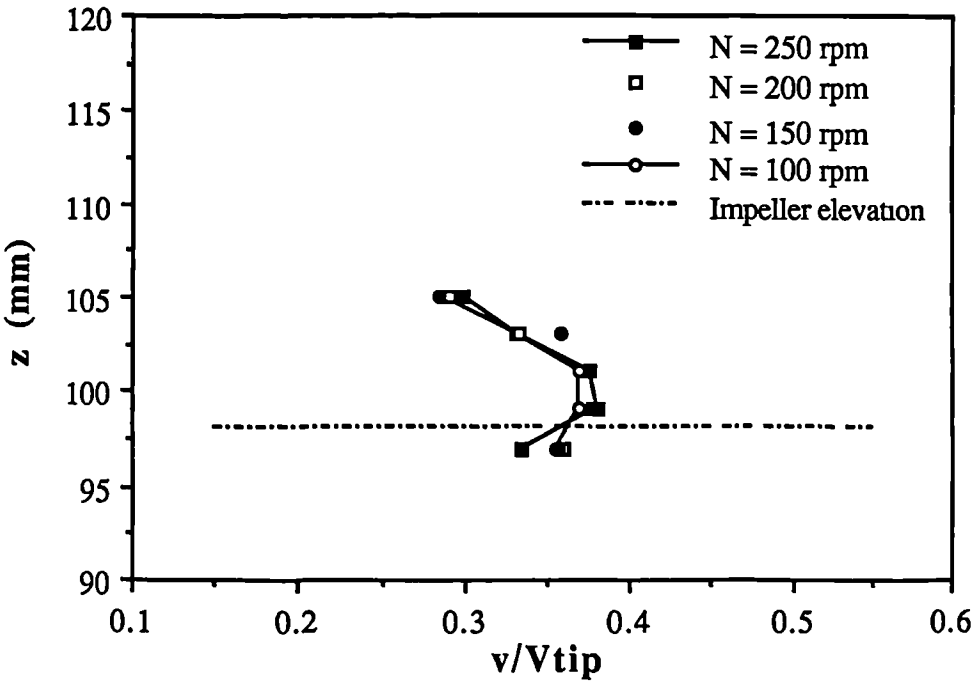

Figure 4.60. Effect of impeller speed on the normalized rms velocities in the impeller stream; C1 = C2 =T/3, lower impeller r = 51 mm, theta = 0°.

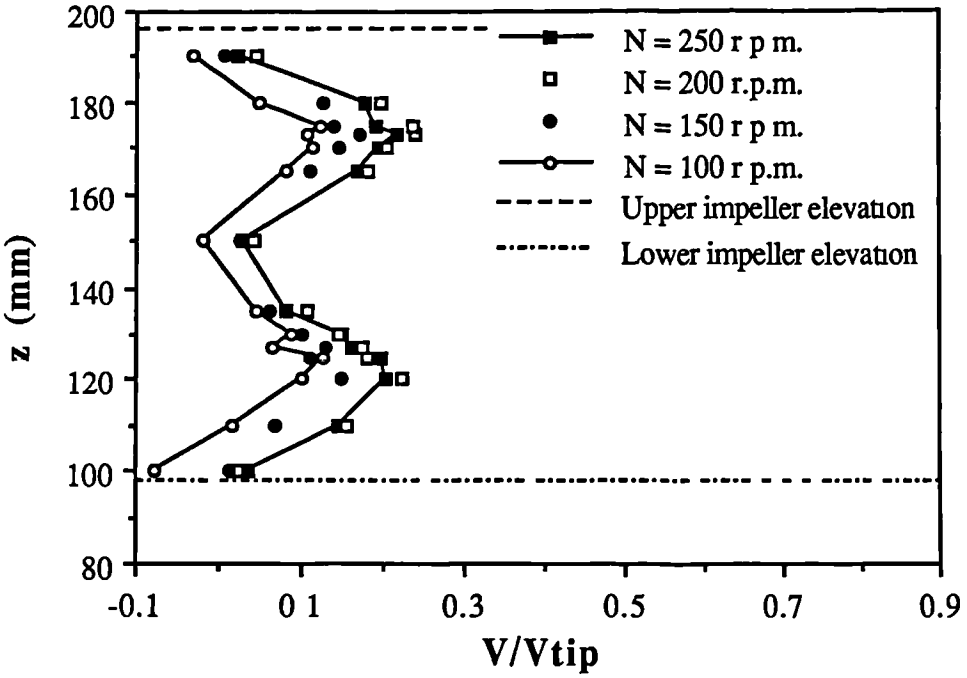

Figure 4.61. Effect of impeller speed on the normalized radial mean velocities in the impeller stream; C1 = C2 = T/3, r = 85 mm, theta = 0°.

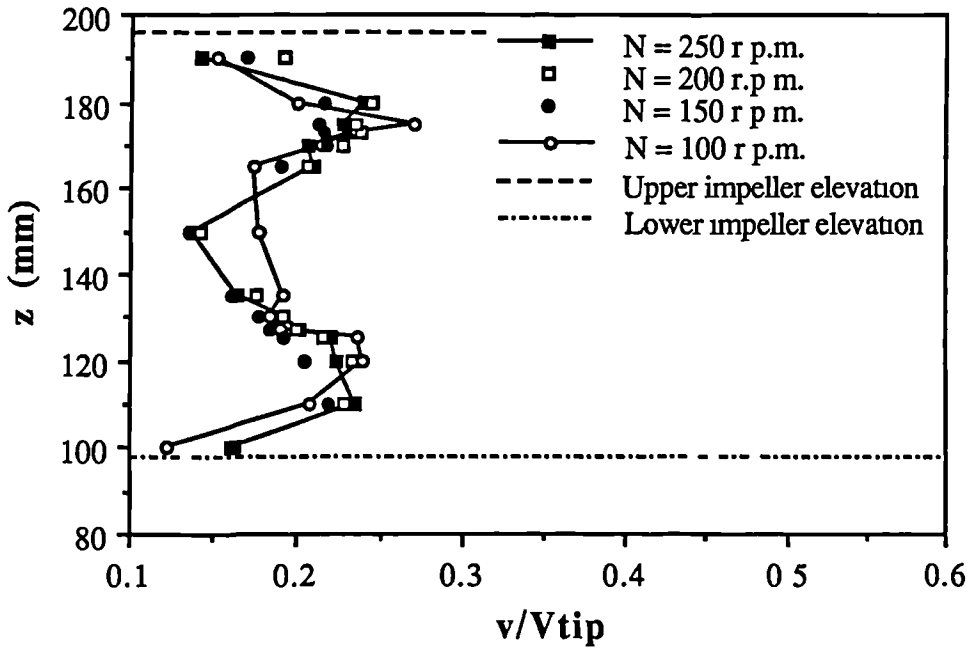

Figure 4.62. Effect of impeller speed on the normalized radial r.m.s. velocities in the impeller stream; C1 = C2 = T/3, r = 85 mm, theta = 0° .

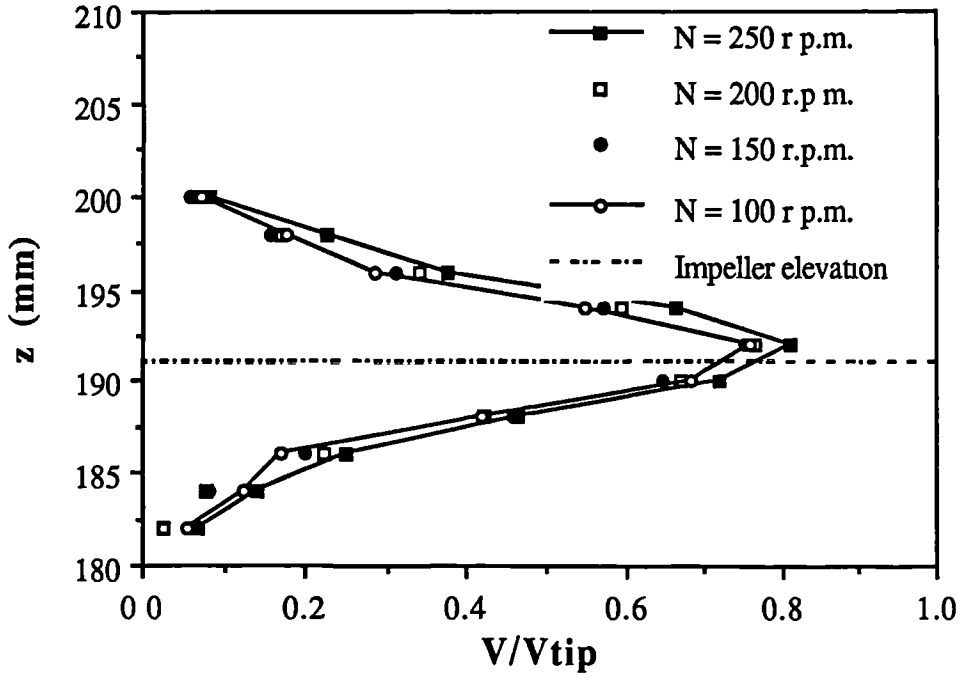

Figure 4.63. Effect of impeller speed on the normalized radial mean velocities in the impeller stream; C1 = 0.15T, C2 = 0.5T, upper impeller, r = 51 mm, theta = 0°.

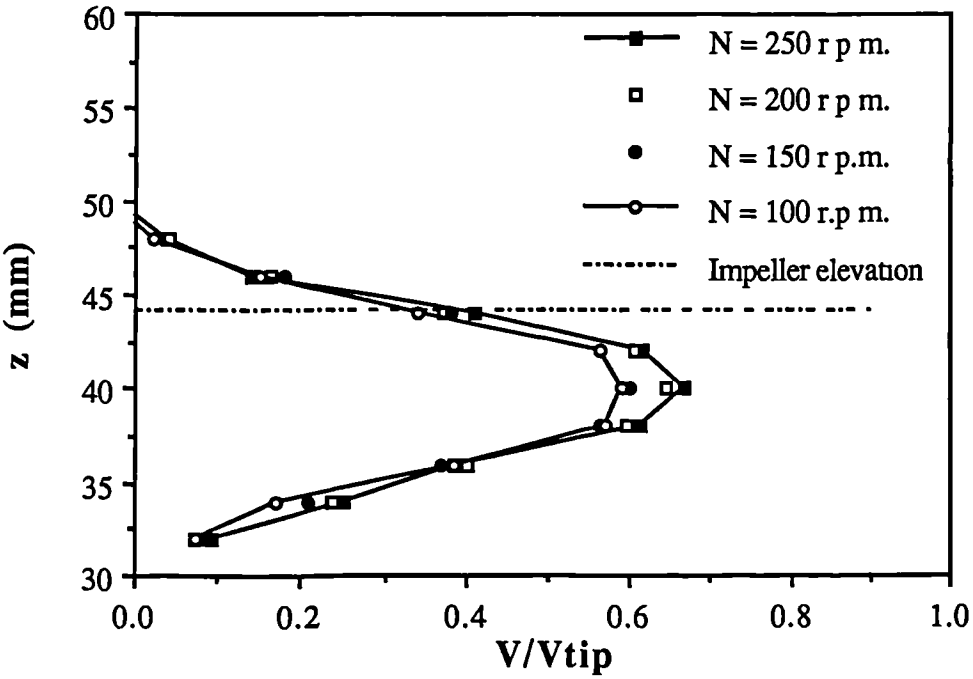

Figure 4.64. Effect of impeller speed on the normalized radial mean velocities in the impeller stream; C1 = 0.15T, C2 = 0.5T, lower impeller, r = 51 mm, theta = 0°.

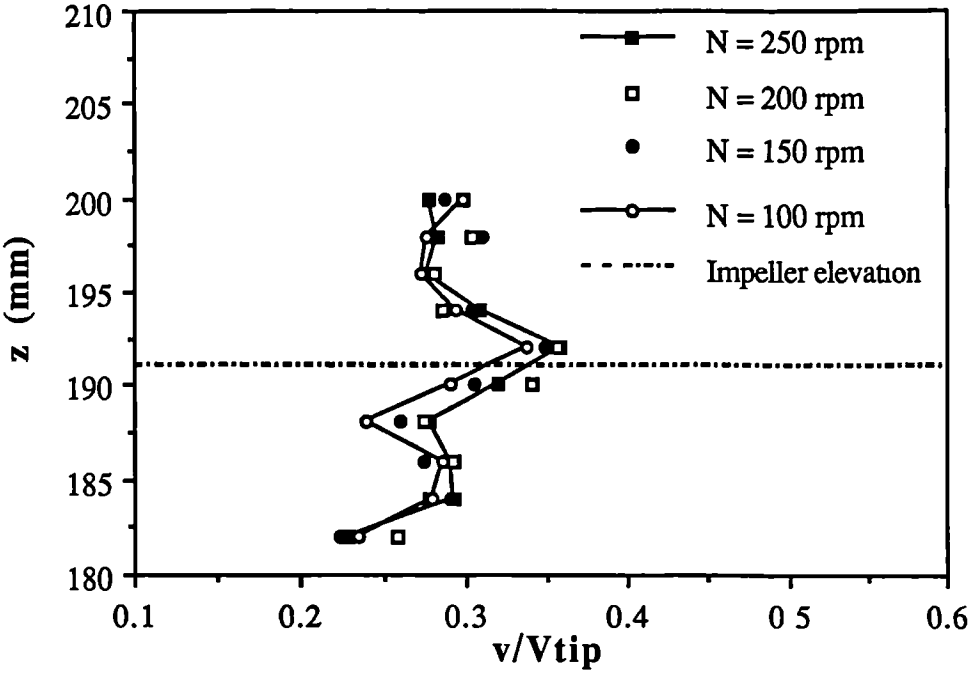

Figure 4.65. Effect of impeller speed on the normalized radial rms velocities in the impeller stream; C1 = 0.15T, C2 = 0.5T, upper impeller, r = 51 mm, theta = 0°.

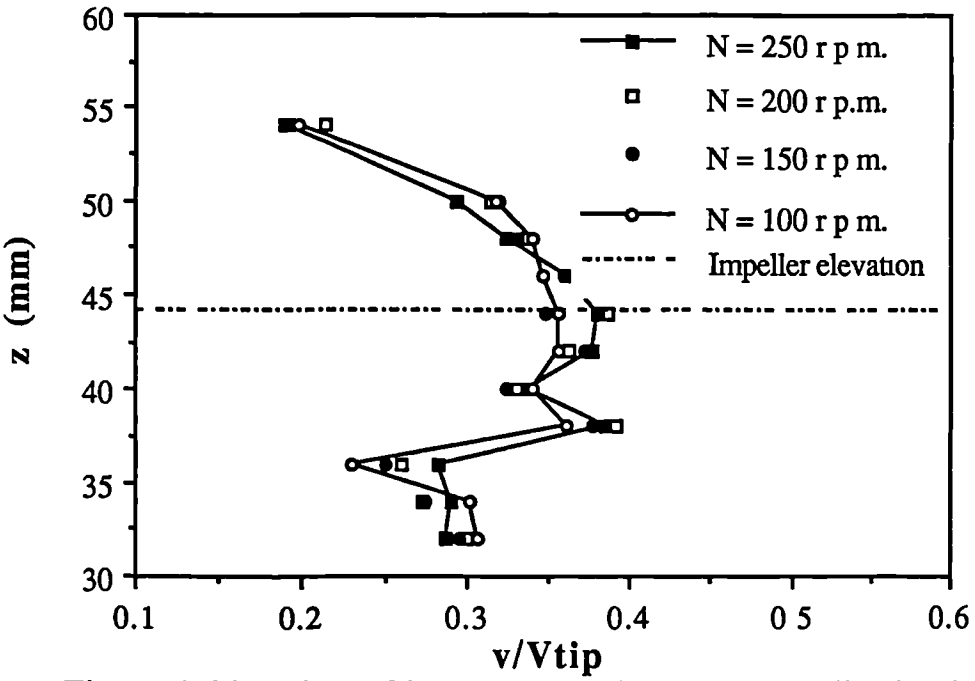

Figure 4.66. Effect of impeller speed on the normalized radial rms velocities in the impeller stream; C1 = 0.15T, C2 = 0.5T, lower impeller, r = 51 mm, theta = 0°.

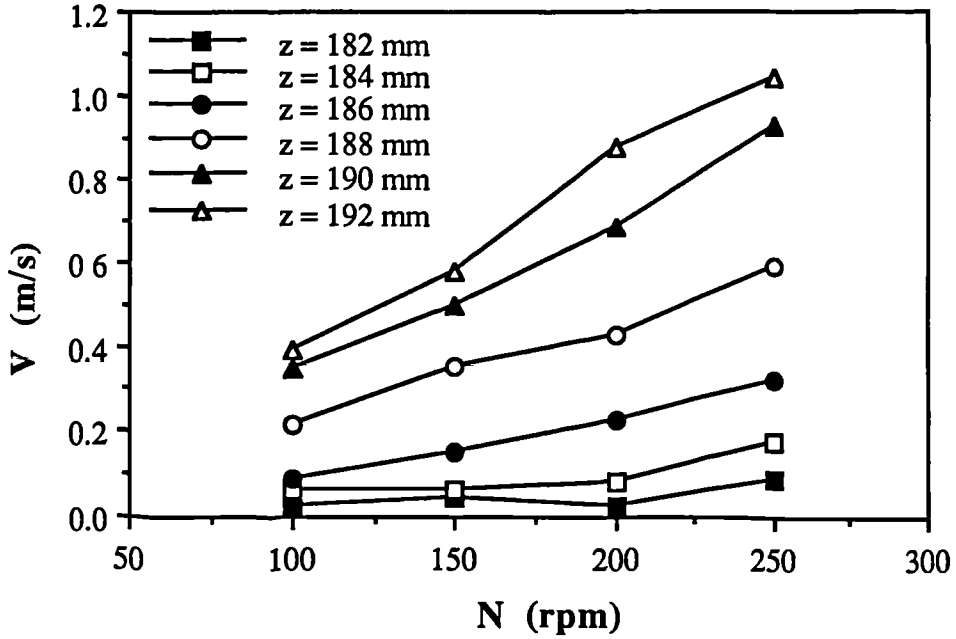

Figure 4.67. Effect of impeller speed on the radial mean velocity gradient in the impeller stream; C1 = 0.15T, C2 = 0.5T, r = 51 mm, upper impeller, theta = 0°.

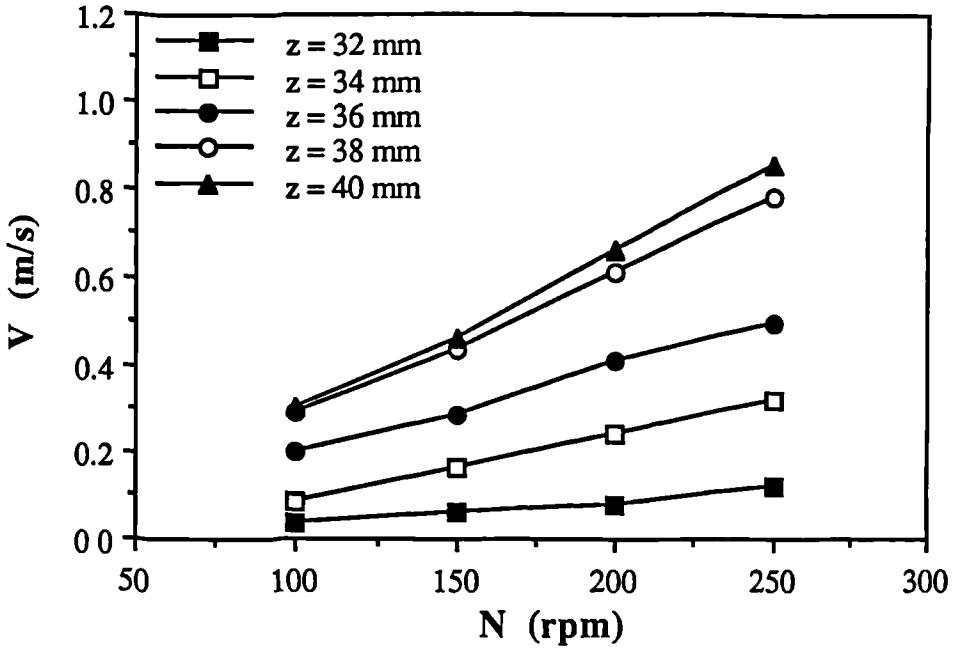

Figure 4.68. Effect of impeller speed on the radial mean velocity gradients in the impeller stream; C1 = 0.15T, C2 = 0.5T, r = 51 mm, lower impeller, theta = 0°.

CHAPTER 5

MIXING CHARACTERISTICS OF VESSELS STIRRED BY DIFFERENT COMBINATIONS OF PITCHED BLADE AND RUSHTON IMPELLERS

5.1 Introduction

The mixing characteristics of a vessel stirred by two Rushton impellers were described and discussed in Chapter 3. In that investigation the variation in the impeller spacings was found to be quite significant for the performance of the stirred tank. This Chapter is concerned with an investigation similar to that of Chapter 3, but employing combinations of either pitched blade and Rushton impellers or two pitched blade impellers.

All the impellers used in the experiments described below had a diameter d = T/3 and a blade/disk thickness t = 1.65 mm. Two types of pitched blade impellers were used with a blade inclination of either 60° or - 60° (see Figure 2.5). Flow visualisation was carried out with different combinations of impellers. For every combination the impeller spacings and the liquid height was varied. The results revealed that the flow patterns induced by all the combinations were unstable, the sole exemption being when two pitched blade impellers pumping towards each other were employed. The flow pattern in the latter case with a liquid height H = T and impeller spacings $C_1 = C_2 = T/3$ showed many similarities with the merging flow identified in Chapter 3. This stable flow pattern was quantified by detailed LDA measurements of all three velocity components and the distribution of turbulence kinetic energy was determined and compared with that obtained in the merging flow pattern generated by two Rushton impellers.

With a liquid height of H = T the effect of C_2 on the mixing time was investigated employing different combinations of Rushton and pitched blade impellers. Also the power numbers of all impeller combinations with impeller spacings $C_1 = C_2 = T/3$ were measured and compared with each other. All the power measurements were carried out with the flywheel attached to the shaft and only the mean values of power numbers are presented.

5.2 Flow visualisation

The flow patterns were observed at the $\theta = 0^\circ$ r-z plane for every combination of impellers for at least twenty minutes by the flow visualisation technique described in Chapter 2. The combinations of impellers with various impeller spacings and liquid heights examined in the vessel are shown in Table 5.1 in the following page. In this table different impellers have been named as explained in the caption. Hereafter in the text when referring to a combination of impellers the first acronym indicates the type of the lower impeller and the second acronym indicates the type of the upper impeller. The general features of the flow patterns observed are shown schematically in Figures 5.1 to 5.7.

5.2.1 Combination DT / PBD

Effect of impeller separation C_2 with H = 1.5 T

The effect of the spacing between the two impellers (C_2) was investigated with the lower impeller located at $C_1 = T/4$. The impeller generated flows did not interact significantly when the impellers were located at a distance

Case	Lower impeller	Upper impeller	H	C_1	C_2	N (rpm)
1	DT	PBD	1.5 T	0 25 T	T	100 to 300
2					0 80 T	250, 300
3					0 55 T	250
4			1.3 T		0 80 T	250
5			1.1 T		0 55 T	250
6			T		0 50 T	250
7				0 33 T	0 33 T	80 to 250
8	DT	PBU	T	0 25 T	0.50 T	250
9				0.33 T	0.33 T	250
10	PBD	PBD	1.5 T	0 25 T	T	250
11				0.33 T	0.84 T	250
12				0.40 T	0.70 T	250
13				0.40 T	0 50 T	250
14			T	0 25 T	0 50 T	250
15				0 25 T	0 33 T	250
16	PBU	PBU	1.5 T	0 25 T	T	250
17				0.33 T	0 84T	250
18	PBU	PBD	1 5 T	0.25 T	0.50T	200, 250
19			T		0.50 T	200, 250
20					0.33 T	200, 250
21				0.33 T	0.33 T	200, 250

Table 5.1. Combinations of impellers investigated

DT: disk turbine (Rushton impeller)

PBU: upward pumping pitched blade impeller

PBD: downward pumping pitched blade impeller

of C_2 = T. With this spacing the lower impeller formed two ring vortices as a result of the radial impeller stream, which was inclined slightly upwards (Figure 5.1(a)). The upper ring vortex of the Rushton impeller extended up to a height of around H = 0.6T. The upper impeller formed only one ring vortex as it was pumping downwards. The flow in the region between the upper vortex of the lower impeller and the vortex generated by the upper impeller was unstable, with a ring vortex formed occasionally with the same rotational direction as that of the ring vortex produced by the pitched blade impeller.

More interaction of the impeller streams was observed as C_2 was decreased to 0.8T (Figure 5.1(b)). The upper impeller stream was unstable flapping from the dominant direction (at around 45° to the vessel axis) to the axial direction. This axial flow was entrained by the lower impeller. A region of strong shear was formed by two counter flowing streams near the middle of the vessel when the upper impeller stream was inclined to the horizontal.

As the impeller spacing between two impellers was decreased further to C_2 = 0.55T, Figure 5.1(c), the flow was unstable everywhere in the vessel except below the lower impeller where a stable ring vortex could be observed. The upper ring vortex of the lower impeller was being formed continually and destroyed by the flapping upper impeller stream. The dominant direction of the upper impeller stream was axial. Occasionally the lower impeller stream was redirected upward, reaching above the upper (PBD) impeller and being entrained into the flow of that impeller.

Effect of liquid height

With C_2 = 0.8T, the flow pattern shown in Figure 5.1 (b) did not vary significantly when the liquid level was reduced from H = 1.5T to H = 1.3T. However, the dominant direction of the upper impeller stream changed to axial as the liquid level decreased. A similar change was also noticed in the flow pattern shown in Figure 5.1(c) (C_2 = 0.55T) as the liquid height was reduced from 1.5T to 1.1T.

With H = 2T the observations were almost the same as that with H = 1.5T. Recent time-resolved LDA measurements have shown that with H = 2T the mean velocity in a location between the two impellers changed significantly with time (Rutherford et al, 1994).

Effect of C_2 with H = T

The influence of C_2 on the flow pattern was investigated with the impellers located symmetrically in the vessel (C_1 = C_3). The flow visualisation observations for two cases C_2 = T/2 and C_2 = T/3 are shown schematically in Figures 5.2 (a) and 5.2 (b) respectively. In both cases the flow below the Rushton impeller was stable, forming a ring vortex as usual.

With C_2 = T/2 (Figure 5.2(a)) the upper impeller stream was unstable flapping from a vertical direction to an inclined one. When the stream was inclined it was mixed with the lower impeller stream before reaching the vessel wall at a height slightly above the elevation of the lower impeller. When the upper impeller stream was vertical, it was being entrained by the flow of the lower impeller. At times, the flow between the two impellers formed a ring vortex as a result of the interaction of the redirected lower

impeller stream and the upper impeller stream. This ring vortex was not stable. Occasionally the re-directed lower impeller stream was being entrained into the flow of the upper impeller in the same way as in the flow pattern shown in Figure 5.1(c).

With C_2 = T/3 (Figure 5.2(b)) the entrainment of the flow from one impeller stream into the flow of the other impeller was more evident in comparison with the C_2 = T/2 case. The ring vortex above the lower impeller was not well defined and the centre of this unstable vortex was moving around in the region above and below the upper impeller elevation and close to the vessel wall.

The effect of speed was also studied for this flow pattern. At the lower impeller speeds (around N = 80 rpm) the upper impeller stream could be distinguished in the region above the lower impeller. At impeller speeds higher than 150 rpm the upper impeller stream merged with Rushton impeller stream.

It is interesting to note that with this combination but using a 45° PBD instead of 60° PBD impeller, Nienow and Kuboi (1984) reported that the induced flow pattern was almost stable. However, in that investigation the high viscosity fluids and larger impellers (d = T/2) were employed. In view of the report by Nienow and Kuboi and the observations made in this work further investigations are clearly required in order to establish the variation of the flow pattern as the viscosity of the working fluid and/or impeller geometry changes.

It has been previously found that in general DT / PBD impeller combinations provide poor gas dispersion, as reported by Kuboi and

Nienow (1982), and also show some instabilities at impeller speeds which are just sufficient to overcome the upward movement of the gas (Chapman, 1981). Taken together with the present findings, these previous observations indicate that flow instabilities may have predominantly undesirable effects on fluid mixing and gas dispersion. Similar detailed investigations are therefore required in gassed vessels in order to provide more appropriate guidelines for aerated mixing processes.

5.2.2 Combination PBD / PBD

Effect of impeller separation C_2 with H = 1.5 T

The impellers were located symmetrically in the vessel ($C_1 = C_3$), and the influence of C_2 on the flow pattern induced by the above combination of impellers was investigated. The observations are shown schematically in Figures 5.3(a) and (b). With $C_2 = T$ or $C_2 = 0.83T$ (Figure 5.3(a)) the flow between the two impellers was unstable, constantly forming a ring vortex. This vortex was being deformed by either the re-directed lower impeller stream or the upper impeller stream. The top vortex was stable and its centre was roughly at r = 100 mm and just below the upper impeller.

A more pronounced instability of the flow between the two impellers was observed when C_2 was reduced to 0.7T. With this spacing a pronounced flow stream from the upper impeller to the lower one could be observed occasionally as shown in Figure 5.3(b).

Effect of C_2 with H = T

The lower impeller was located at a spacing C_1 = T/4 and the spacing between the impellers was varied from T/2 to T/3. Figure 5.4 shows the

flow pattern with a spacing of T/2 between the two impellers. The flow was completely unstable. The lower impeller stream was re-directed either toward the top of the lower impeller (forming a large ring vortex) or to the top of the upper impeller. The upper impeller stream was sometimes vertical and sometimes inclined, while at other times it was split into two, one stream directed in each of the two directions. In the inclined case the upper stream was mixed with the re-directed lower impeller stream and subsequently flowed towards the top of the lower impeller. However, in all cases some part of the upper impeller stream was directed towards the top of the lower impeller and entrained into the flow of that impeller. This flow entrainment was occasionally being interrupted by the re-directed lower impeller stream. Frequently the upper impeller stream and the redirected lower impeller stream were moving towards each other and formed an unstable ring vortex which rotated in the same direction as either the upper or the lower unstable ring vortex.

The instability of the flow pattern became more intensive as the spacing between the two impellers was reduced, as might be expected.

5.2.3 Combination PBU / PBD

In this combination with a liquid height H = T and spacings $C_1 = C_2 = T/3$ the impellers were pumping towards each other and formed two stable ring vortices, as shown in Figure 5.5. The centres of the lower and the upper ring vortices were roughly at a radius r = 100 mm and around the lower and upper impeller elevations respectively. The meeting point of the two impeller streams was located half way between the two impellers. This point was moved slightly upwards when the lower impeller elevation was

reduced to C_1 = T/4 and the separation between the two impellers was kept the same (C_2 = T/3).

With this combination of impellers and $C_1 = C_2$ = T/3, the flow pattern was very similar to the merging flow pattern produced by two Rushton impellers. However, the flow in the region confined by the impellers was not as rotational as observed with the merging flow pattern (see Figure 3.53). It has been reported that the combination 45° PBU / 45° PBD disperses gas in a power and speed considerably lower than that required with DT / DT and/or DT / PBU impeller combinations (Kuboi and Nienow, 1982). As the DT / PBD and DT /DT combinations produce unstable flows for all or many impeller spacings respectively, the PBU / PBD combination appears to offer an attractive alternative for the generation of stable and predictable flow patterns. Hereafter in the text the merging flow pattern induced by this combination of impellers will be referred to as 'PBTs merging flow pattern'.

5.2.4 Combination PBU / PBU, H = 1.5T, $C_1 = C_3$

With this combination and C_2 = 0.83T three ring vortices were observed in the vessel as shown schematically in Figure 5.6. The upper ring vortex was stable and its centre was roughly at r = 100 mm and just above the upper impeller. The lowest ring vortex was also stable and its centre was roughly at r = 100 mm just above the lower impeller. The flow in between the two impellers formed a ring vortex but not as strong as the other two vortices. The discharge flow from the lower impeller was partly returned back to the suction region of the impeller (by the lower ring vortex) and partly formed the weak middle ring vortex. Occasionally the lower impeller stream was entrained into the flow of the upper impeller via the middle vortex. The

induced flow pattern did not change significantly when the separation between the impellers was increased to $C_2 = T$.

The PBU / PBU combination as well as the DT / PBU combination described in section 5.2.5 below, are rarely used in practice. They were studied however for two reasons. First for completeness in order to determine whether any interesting and/or useful flow patterns were produced by such combinations. It has been reported that in gassed systems upward pumping impellers do not show instabilities (Chapman, 1981) but their ability to disperse gas is poor at lower impeller speeds (Kuboi and Nienow, 1982). The combination DT / 45° PBU was reported to be an effective configuration for mixing of aerated high viscosity fluids (Solomon et al 1981) and to show a complex variation of the flow pattern and of individual impeller power consumption in gassed units (Kuboi and Nienow, 1982).

Second, it has been found in gassed systems that dual impeller combinations with an upward-pumping impeller above may be beneficial. The power versus gas flow rate curves in systems with a downward-pumping impeller above show a step-like variation, with the power dropping considerably at the higher gas rates, probably due to the flow instabilities. In contrast, the corresponding curves in dual impeller systems with an upward-pumping impeller above are almost flat (Middleton, 1993). Although gas bubbles may be expected to escape to the free surface more easily with an upward-pumping impeller above, the power-gas flow rate curve may be preferable for both new reactor design as well as for retrofitting existing vessels.

5.2.5 Combination DT / PBU, H = T, $C_1 = C_3$

The flow pattern generated by this combination and C_2 = T/2 is shown schematically in Figure 5.7 (a). The lower impeller stream was flapping at an angle of up to ± 10° to the horizontal and formed two ring vortices, one above and one below the impeller. The upper impeller stream was also flapping at an angle of 0 - 30° to the horizontal and formed one large ring vortex. The boundary between the upper and the middle ring vortices was not stationary. Occasionally the flow from the re-directed upper impeller stream was dispersing the middle vortex and was entrained into the flow of the Rushton impeller as shown by the thinner line in Figure 5.7(a).

The flow pattern was also observed with C_2 = T/3. With this spacing flow entrainment occurred from the stream of one impeller into the flow of the other impeller most of the time as shown in Figure 5.7(b). A small part of the upper impeller stream generated a small and less defined ring vortex above the upper impeller.

The observations with $C_1 = C_2$ = T/3 were similar to those reported by Nienow and Kuboi (1984) although they used larger impellers (d = T/2), a 45° PBU and high viscosity fluids.

5.3 Mixing time measurements

With a liquid height of H = T in the vessel, the effect of impeller spacing C_2 on the average mixing time (obtained from measurements at eight locations, see Figure 3.26 (b)) was investigated for three combinations of Rushton and pitched blade impellers and the results are shown in Figure

5.8. For the purpose of comparison the mixing time results obtained by two Rushton impellers (presented in Chapter 3) are also shown in this Figure.

The variation of mixing time with C_2 in the combinations PBU / PBD, DT / PBD and PBD / PBD is insignificant in contrast to that obtained with the two Rushton impellers. The lowest mixing time was obtained by the combinations of (PBD / PBD) and/or (DT / PBD). The combination forming the PBTs merging flow pattern resulted in an average mixing time slightly shorter than that obtained with the merging flow pattern generated by two Rushton impellers and varied only slightly with C_2.

The results of Figure 5.8 are very informative for design purposes: They indicate that some unstable flows can result in lower mixing times. The mixing times with PBD / PBD and DT / PBD are around 20% lower than with the stable PBU / PBD and around 25 - 50% lower than with the DT / DT combinations.

In the DT / DT investigations presented in Chapter 3 (Figures 3.31 - 3.34) unstable flows (for C_2 around 0.385T) resulted in higher mixing times. This can be clearly seen from the results for DT / DT reproduced in Figure 5.8, and may appear to contradict the above findings for the other impeller combinations where, in general, unstable flow patterns resulted in smaller mixing times. The DT / DT mixing results show as well that the stable merging flow pattern yields considerably lower mixing times than the stable parallel flow pattern.

From the above, it may be concluded that in dual impeller combinations:

1. Flow patterns induced by mixed, i.e. inclined to both the axial and radial direction, impeller streams result in lower mixing times than radial direction flows.
2. Unstable mixed flow patterns result in considerably lower mixing times than both stable mixed flow and stable radial flow patterns.

Therefore, from mixing time criteria alone, unstable mixed flow patterns are preferable for mixing process operations where minimisation of the blending time is a process requirement.

5.4 Power measurements

With the PBU / PBD and DT / PBD combinations and a liquid height H = T the power numbers of the impellers, spaced at $C_1 = C_2 = T/3$, were measured at different impeller speeds using the technique outlined in Chapter 2. These measurements are presented in Figures 5.9(a) and 5.9(b) for both impellers and for the lower impeller respectively. In addition the measurements of the impeller power numbers with the Rushton merging flow in the vessel (presented in Chapter 3) are shown in these Figures for the purpose of comparison.

At impeller speeds of 200 - 250 rpm the power numbers are almost the same. The lowest total power number was measured with the impeller combination PBU / PBD and valued at Np = 6.4. In this combination the power numbers of the upper and lower impeller were almost identical, whereas with the DT / PBD combination the upper (PBD) impeller power number was about 50% that of the lower (DT) impeller, as might be expected.

The highest total power number Np = 8.4 was obtained with the two Rushton impellers. The highest and the lowest individual impeller power numbers were obtained in the combination DT / PBD and valued at Np = 5.3 and Np = 2.7 for the Rushton and pitched blade impellers respectively.

The above results reveal a number of interesting variations:

1. The total power number is clearly affected by the power number of each impeller in the combination: it is the highest for two DTs followed by that for one DT and one PBT and that for two PBTs. The higher total power number measured with the DT / DT combination is expected, as a DT has a higher power number than a PBT. With the DT / DT combination the total power number is smaller than the sum of the two single-impeller power number. With the DT / PBD combination the total Np is nearly equal to the sum of the single impeller N_ps and with the PBU / PBD combination the total Np is higher (by around 20%) than the sum of the single impeller N_ps.

2. The power number of a DT when in the lower position may vary by as much as 20%, being around 5.3 for the DT / PBD and around 4.2 for the DT / DT combination (Figure 5.9 (b)). This may be related to more efficient pumping of the lower DT in the DT / PBD case, where the PBD stream is fed directly in to that of the DT (Figure 5.2(b)).

3. The power number of the PBD impeller in the PBU / PBD combination was higher by around 20%, than the power number of the same impeller in the DT / PBD combination. This power number in the latter combination was almost identical to a single PBD impeller, in agreement with the findings of Machon et al (1985) for H = 2T and C_2 = T system.

The above provide useful guidelines for process design. The power numbers of the various impeller combinations can be predicted, as a first approximation, from those of the individual impellers, but an 'efficiency' factor must be applied to predict the total and individual impeller power numbers. This factor will depend on the impeller combination and impeller spacing and therefore the flow stability and flow pattern in the vessel. However, due to the complexity of the flow processes, extremely extensive power measurements are necessary with various C_1, C_2, H and N for all impeller combinations in order to determine a practical correlation for power number prediction.

5.5 Mean and rms velocity with the PBTs merging flow pattern

The PBTs merging flow pattern was quantified by LDA measurements at an impeller rotational speed of 230 rpm. Measurements at higher impeller speeds were not possible due to the air entrainment into the liquid in the vessel which took place at speeds above 230 rpm. The three components of the mean and rms velocities were measured at radii of r = 0.0, 10, 20, 40, 51, 60, 75, 90, 115, 130 and 140 mm in the impeller and bulk flow region at the $\theta = 0^{\circ}$ r-z plane. More attention was paid to the region confined between the impellers, i.e. to the discharge side of the impellers.

5.5.1 Axial velocity profiles

Axial mean velocity profiles of the flow with this pattern are presented in Figure 5.10. The measured velocities at a height of 147 mm are almost zero. This confirms the division of the flow in the vessel into the two ring vortices observed in flow visualisation experiments. The highest mean velocity was measured at the discharge of the upper impeller and valued at

$V = 0.6\ V_{tip}$. The velocities in the bulk flow change direction at a radius of around 115 mm in the upper-half of the vessel and at a radius of around 105 mm in the lower-half of the vessel.

Figure 5.11 shows the rms velocity profiles corresponding to the mean values presented in Figure 5.10. In general, the rms velocities measured in the region above the lower impeller and below the upper impeller are higher than those measured in the rest of the tank. These higher rms velocities are more pronounced at radii between 30 and 115 mm being maximum ($u = 0.32\ V_{tip}$) at r = 51 mm and z = 147 mm where the cores of the two impeller streams join. The high rms velocities in the region with radii between 85 and 130 mm and at mid-way between two impellers (where the mean velocities are near zero (Figure 5.10)) may indicate that a flow interchange takes place from one ring vortex into another. Generally in the region above the upper impeller and in the region below the lower impeller the rms velocities measured in the vicinity of the vessel wall are slightly higher than those measured at the same height close to the shaft.

Comparison between Figures 5.11 and 3.50 (showing the axial rms profiles of the Rushton merging flow pattern) shows that the axial rms velocities at z = 147 mm are relatively higher with the PBTs merging flow pattern in the vessel albeit they were measured with a lower impeller rotational speed. These higher rms velocities may indicate relatively better mixing between the upper and lower ring vortices with the PBTs merging flow pattern in the vessel.

5.5.2 Radial velocity profiles

Figure 5.12 shows the distribution of the radial mean velocities in the vessel with the PBTs merging flow pattern. The unification of the impeller

streams can easily be seen from the velocity profiles obtained at the mid-section of the vessel. The highest radial mean velocities (around 0.42 V_{tip}) were measured at the locations z = 147 mm, r = 75 and 90 mm where the impeller streams are joined. In general, the radial velocities below the lower impeller are comparatively higher than those measured above the upper impeller at the same radius. However, a similar comparison for the mean axial velocities (Figure 5.10) shows lower values below the lower impeller. Therefore, the flow above the upper impeller is more axial and that below the lower impeller is more radial. The radial mean velocities measured at radii of r = 20 mm or less were almost zero.

Figure 5.13 shows the radial rms-velocities corresponding to the mean values presented in Figure 5.12. Little variation of the rms velocities with elevation can be seen at radii smaller than 20 mm. This is also the case in the region below the lower impeller for all the measurement locations in every radius. In the vicinity of each impeller (in the upper and lower impeller streams) the maximum rms velocities were measured around 0.42 V_{tip} at r = 51 mm. The locations of these two rms velocity maxima moved towards each other as the radius of the measurement locations increased. At a radius of r = 75 mm the two peaks have almost vanished and the profile of the rms velocities in the merged impeller streams is practically flat. The rms velocities in these locations were typically 0.22 V_{tip}.

5.5.3 Tangential velocity profiles

Figure 5.14 shows the profiles of the tangential mean velocities corresponding to the other two components presented in Figures 5.10 and 5.12. Near zero mean velocities were measured at the locations below the lower impeller and above the upper impeller at radii smaller than 60 mm.

The mean velocities are also nearly zero in the region between the impellers and at radii r = 10 and 20 mm. This is one of the major differences between the PBTs merging flow pattern and the merging flow pattern produced by two Rushton impellers: the flow with the latter combination was highly rotational in the region between the impellers.

As shown in Figure 5.14, the highest mean velocities (W = 0.48 V_{tip}) were measured in the vicinity of each impeller at r = 45 mm (in the impeller stream). At this radius the mean velocities at the locations between the impellers changed significantly along the axial direction, and a minimum value W = 0.13 V_{tip} was measured at a height z = 147 mm. At a radius of 60 mm and in the region between the two impellers, the mean velocities did not vary significantly with the height of measurement locations. These velocities were valued typically at W = 0.25 V_{tip}. In addition the mean velocities measured at radii greater than 115 mm did not change significantly with elevation except those obtained at a height z = 11 mm, which were nearly zero.

Comparison of the mean tangential velocity profiles shown in Figure 5.14 with those obtained with Rushton merging flow pattern (Chapter 3, Figure 3.53) indicates that, in addition to the major difference mentioned above, the tangential mean velocities in the impeller streams are generally higher with the Rushton merging flow pattern while in general in the bulk flow the velocities are higher with the PBTs merging flow pattern at radii larger than 75 mm.

Figure 5.15 shows the profiles of rms velocities corresponding to the mean velocities presented in Figure 5.14. At each radius, the rms velocities did not vary much along the axial direction, except for the impeller stream

regions. Even in the impeller stream regions the rms velocities do not show as significant variation as with the radial components.

5.5.4 Velocity vectors in r-z plane

The velocity vectors ($\vec{U} + \vec{V}$) with this flow pattern in the $\theta = 0^{\circ}$ r-z plane are presented in Figure 5.16. The two ring vortices formed, the direction of discharge flow from the impellers and also the merging of the impeller streams can clearly be seen from this Figure. The centre of the lower and upper vortices are roughly at the points r = z = 105 mm and r = 115 mm, z = 200 mm respectively. Comparing this Figure with that obtained with the merging flow pattern generated by two Rushton impellers (Figure 3.62, Chapter 3) the following differences can be deduced:

a) The impeller streams with the Rushton merging flow pattern are directed towards each other in almost straight-line paths and the radius of the meeting point is around r = 100 mm. With the PBTs merging flow pattern the streams follow curved paths and merge in a region comparatively closer to the shaft as it is clearly shown in Figure 5.16.

b) In general mean velocities in the bulk flow of the vessel (in each location) are relatively higher with the PBTs merging flow pattern in spite of being measured with a smaller impeller speed.

c) In terms of the axial and radial flow, better circulation is obtained with PBTs merging flow pattern, which is desirable for better mixing. This is in agreement with the lower mixing times recorded with the PBTs, as discussed earlier.

5.5 5 Rms velocity contours

For clarity of presentation the rms velocities presented in Figures 5.11, 5.13 and 5.15 are shown in the form of contour plots in Figures 5.17 (a), (b) and (c) respectively. In general the patterns are symmetrical with respect to the mid-height of the vessel. In the region where the impeller streams are interacting the axial rms velocities are significantly higher than those measured in the rest of the tank (Figure 5.17(a)). Comparison of Figures 5.17(a), (b) and (c) show that in the impeller streams the axial rms velocities are higher than the radial ones and radial rms velocities are higher than the tangential ones. Therefore, the turbulence in the impeller streams is not isotropic. These comparisons also indicate that in the region above the upper impeller and below the lower impeller and at radii smaller than 70 mm, the axial rms velocities are smaller than the other two components. In the vicinity of the impellers the highest rms velocities (in all the three directions) were measured at the lower tip of the upper impeller and at the upper tip of the lower impeller.

For ease of comparison between the distribution of rms velocities with the PBTs and the Rushton merging flow patterns, in the legend of the former pattern the value denoted for each colour is smaller than that denoted for the same colour in the legend of the Rushton merging flow pattern. These reductions were made in proportion to the reduction in the impeller tip (or rotational) speed, i.e. the values in the legend of the Rushton merging flow pattern (Figure 3.67) were multiplied by the ratio of the impeller speeds (230 / 250) and the new values were denoted for the legend of the PBTs merging flow pattern (Figure 5.17). In this way a colour-based comparison is the same as if the rms velocities normalised by V_{tip} were compared.

Comparisons of the rms velocities measured with the two merging flow patterns (Figure 3.67 and 5.17) show that, in general, in the impeller streams and away from the impellers the axial and radial rms velocities are relatively higher with the PBTs merging flow pattern. This is not the case for the tangential components particularly in the locations close to the impellers and at a radius of around r = 51 mm. These comparisons also indicate that in the bulk flow, there is little variation in the axial rms velocities from one pattern to another and at radii roughly greater than 70 mm the radial and tangential rms velocities are relatively higher with the PBTs merging flow pattern.

An interesting feature is the high w region near the shaft and the free surface obtained with the DTs which is not found in the w distribution with the PBTs. This may be related to the free surface vortex (Yianneskis et al, 1987) which is not as prominent with the PBTs.

5.5.6 Turbulence kinetic energy contours

The distribution of the turbulence kinetic energy (Eq. 3.3) in the vessel with the PBTs merging flow pattern is shown in Figure 5.18. As expected from the rms velocity contours presented in Figure 5.17 the turbulence kinetic energy is maximum in the impeller streams. The lowest turbulence kinetic energy levels are around 0.017 $(m/s)^2$ and are found in the region near to the free surface and near the bottom corner of the vessel. The k values in the legend of this Figure are different to those of Figure 3.70 which shows the distribution of the k values in Rushton merging flow pattern. Similarly to the rms contour values, the various contour bands for the k values were arranged by changing the band range by the ratio (230 /

$250)^2$ to enable direct comparison of the colour bands as if the k values were normalised by V_{tip}^2.

Comparison of the distribution of k in the vessel with the two merging flow patterns, (Figures 3.70 and 5.18), shows that:

1. On average the turbulence kinetic energies above the upper impeller are higher with the Rushton merging flow pattern in the bulk flow region.
2. In the region between the two impellers higher values were obtained with the PBTs merging flow pattern.
3. In the impeller streams away from the impellers, the k values are higher with the PBTs merging flow pattern, while close to the impellers the Rushton impellers produce higher levels of turbulence kinetic energies.
4. In the region below the lower impeller and at radii smaller than 60 mm the turbulence levels are relatively higher with Rushton impellers while at radii greater than 60 mm relatively higher k values can be found with the pitched blade impellers.

With the PBTs merging flow pattern the area-weighted average value of the kinetic energy, over the whole of the vessel, was determined and valued at $k_{avr} = 3.453 \times 10^{-2}$. This value was normalised with the V_{tip}^2 and compared with the normalised k_{avr} obtained for the Rushton merging flow pattern. The comparison indicates that around 4% higher k is obtained with the Rushton merging flow pattern.

The efficiencies of the mixing tank with the two merging flow patterns can be compared from the measurements of power consumption, mixing time and velocity characteristics presented in this Chapter and in Chapter 3. As the mixing time and the total power number are smaller (around 10% and

30% respectively) with the PBTs merging flow pattern, more efficient blending of liquids takes place with this flow pattern. However, it is interesting to note that the PBTs merging flow pattern may provide a higher macro-mixing rate as the mean velocities in the bulk of tank are comparatively higher with this flow pattern. Micro-mixing may be expected to take place with a slightly lower rate with the PBTs merging flow pattern since the trailing vortices behind the blades of pitched blade impellers are relatively weak (Tatterson et al, 1980 and Hockey, 1988b). This suggestion is supported by the lower average value of k obtained with the PBU / PBD combination.

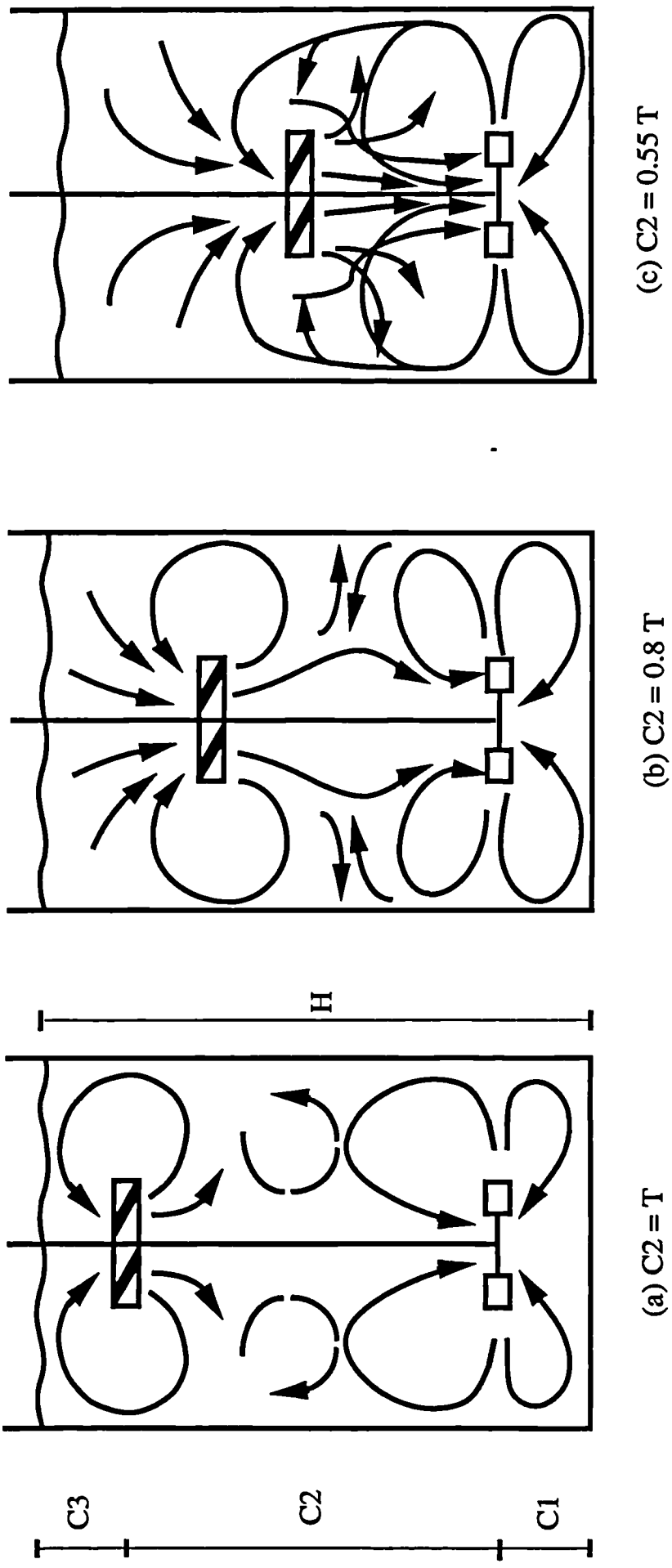

Figure 5.1. Variation of flow pattern in the stirred tank agitated by two impellers (DT / PBD), H = 1.5 T, C1 = T/4.

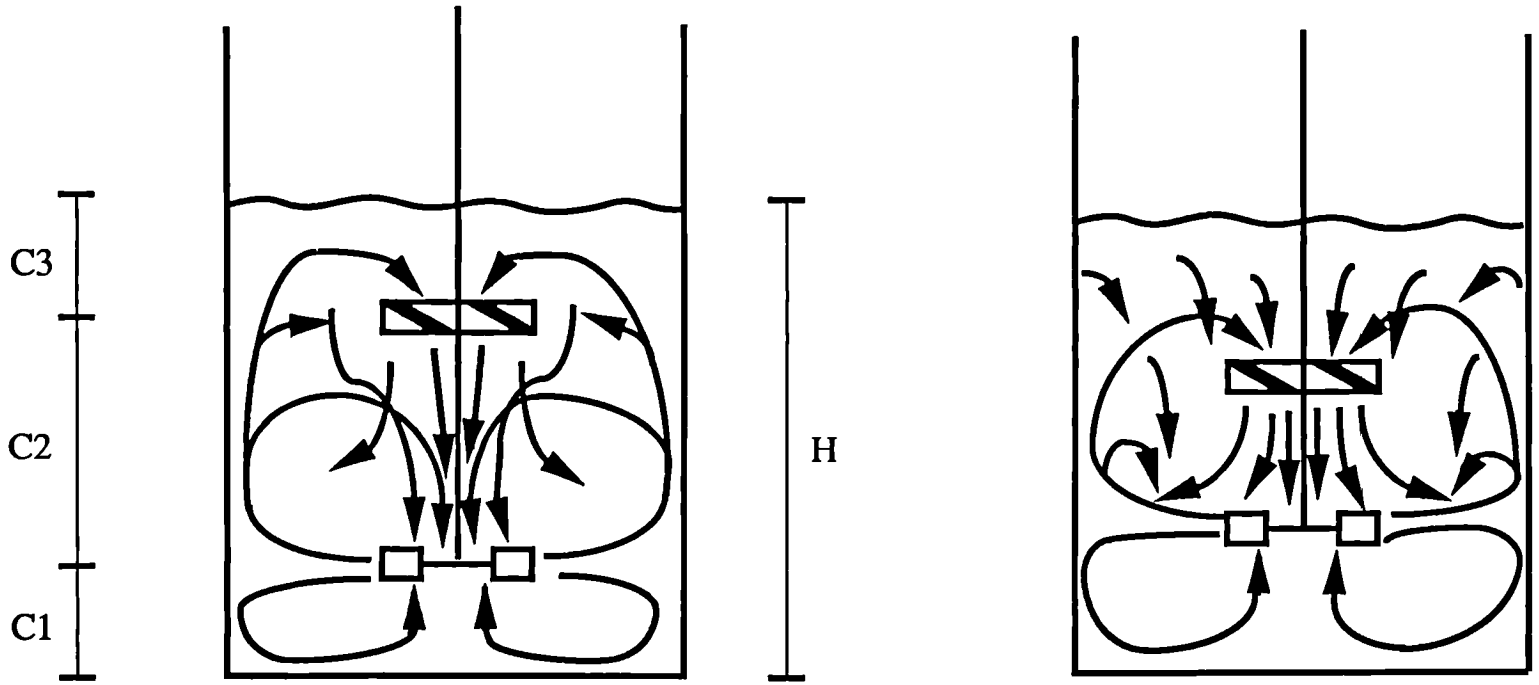

(a) H = T, C1 = T/4, C2 = T/2

(b) H = T, C1 = T/3, C2 = T/3

Figure 5.2. Variation of flow patterns in the stirred tank agitated by two impellers (DT / PBD), H = T, C1 = C3.

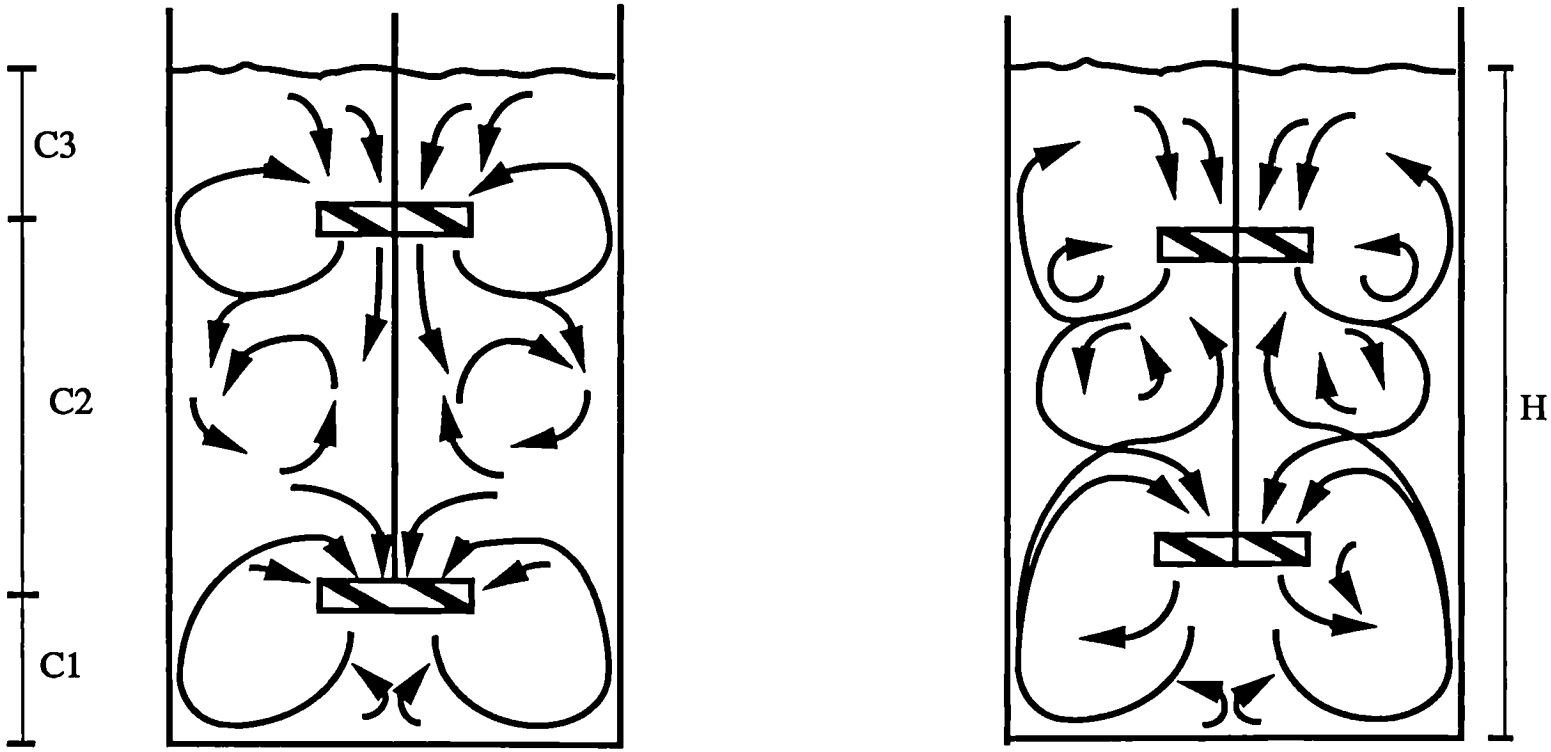

(a) C2 = T or 0.83T

(b) C2 = 0.7T

Figure 5.3. Variation of flow pattern in the stirred tank agitated by two impellers (PBD / PBD), H = 1.5T, C1 = C3.

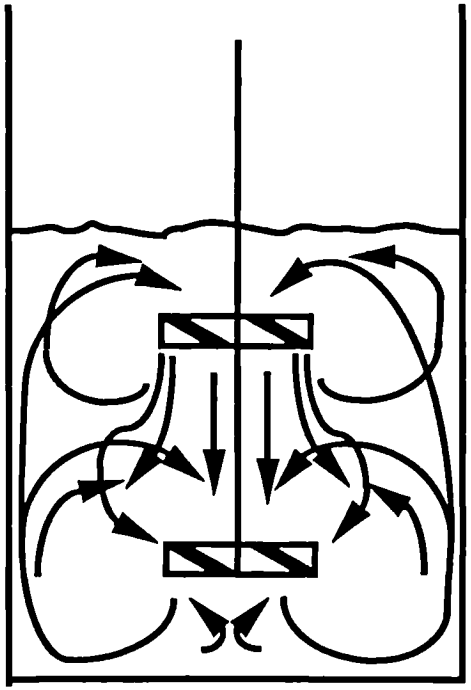

Figure 5.4. Flow pattern in the stirred tank agitated by two impellers (PBD / PBD), H = T, C1 = T/4, C2 = T/2 or 2T/5 or T/3.

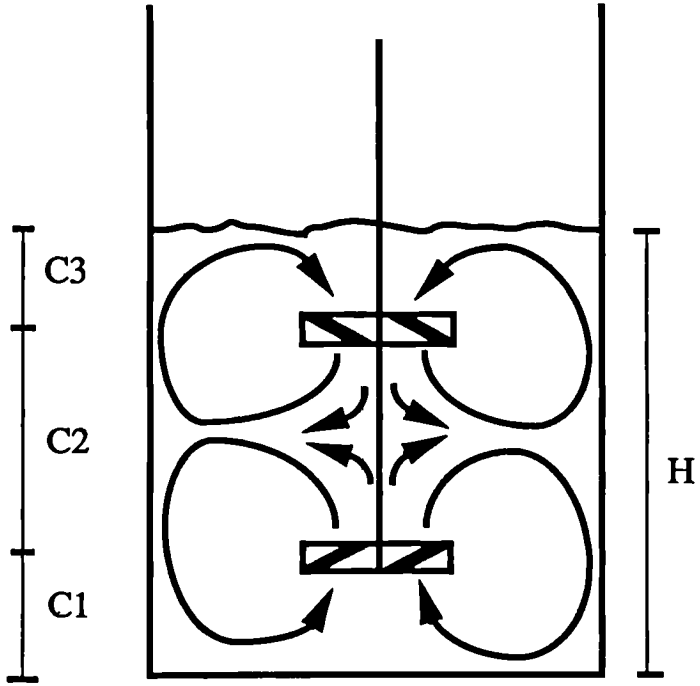

Figure 5.5. Flow pattern in the stirred tank agitated by two impellers (PBU / PBD), H = T, C1 = C2 = T/3.

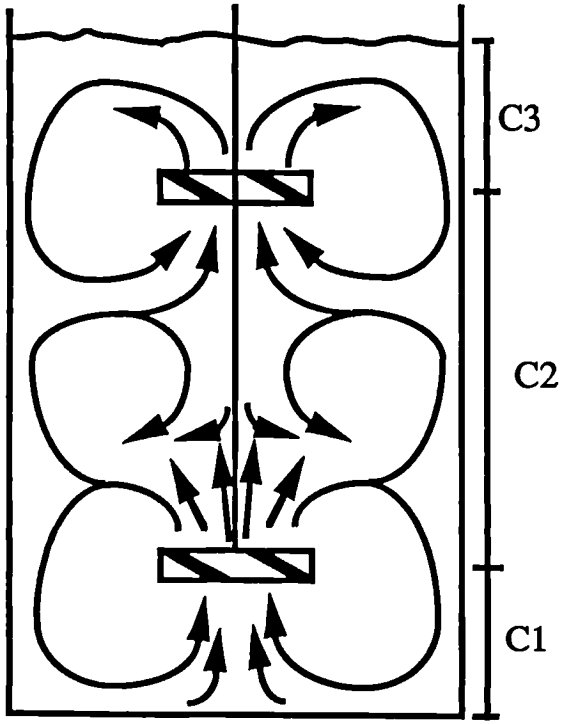

Figure 5.6 Flow pattern in the stirred tank agitated by two impellers (PBU / PBU), H =1.5 T, C1 = C3 = T/3 or T/4.

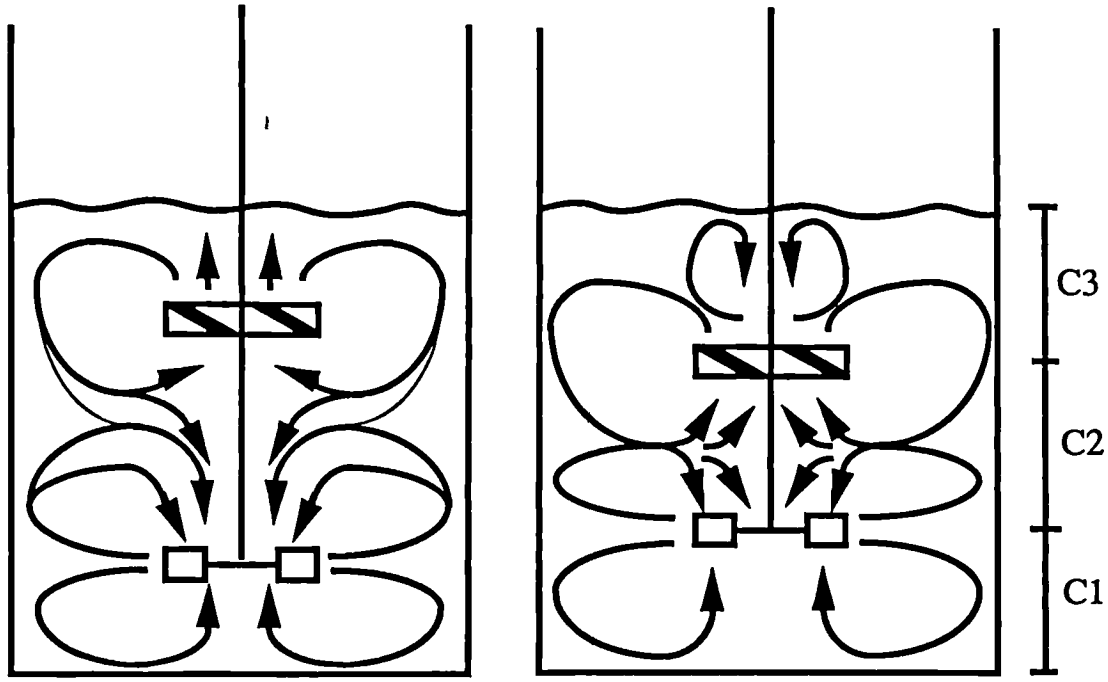

(a) C1 = T/4, C2 = T/2

(b) C1 = C2 = T/3

Figure 5.7. Flow patterns in the stirred tank agitated by two impellers (DT / PBU), H = T.

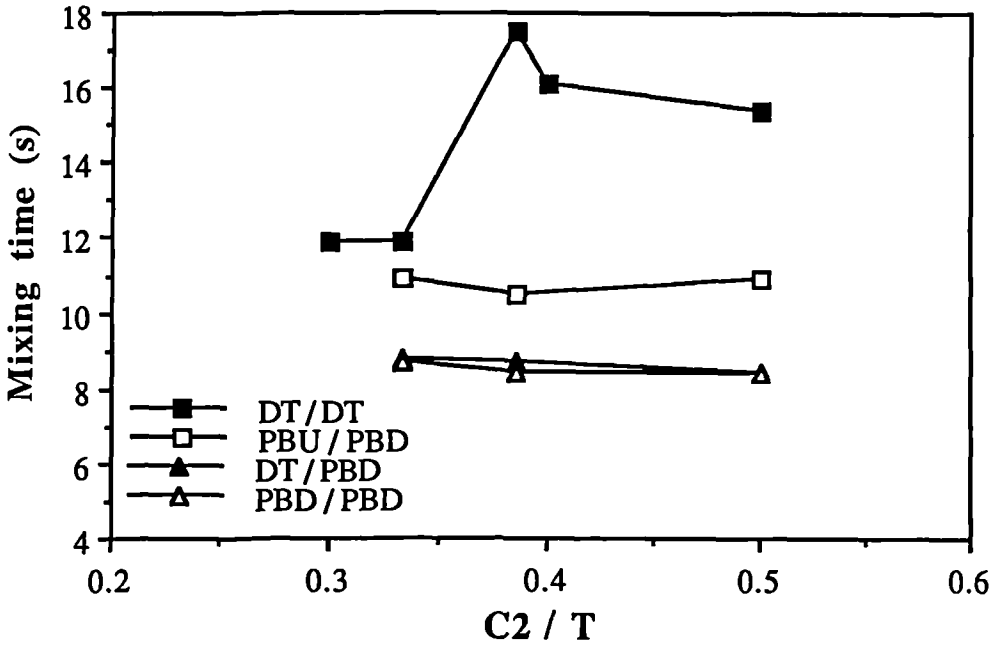

Figure 5.8. Effect of impeller spacing on mixing time averaged at 8 points; different two-impeller combinations, N = 200 rpm, insertion time 6.5 s.

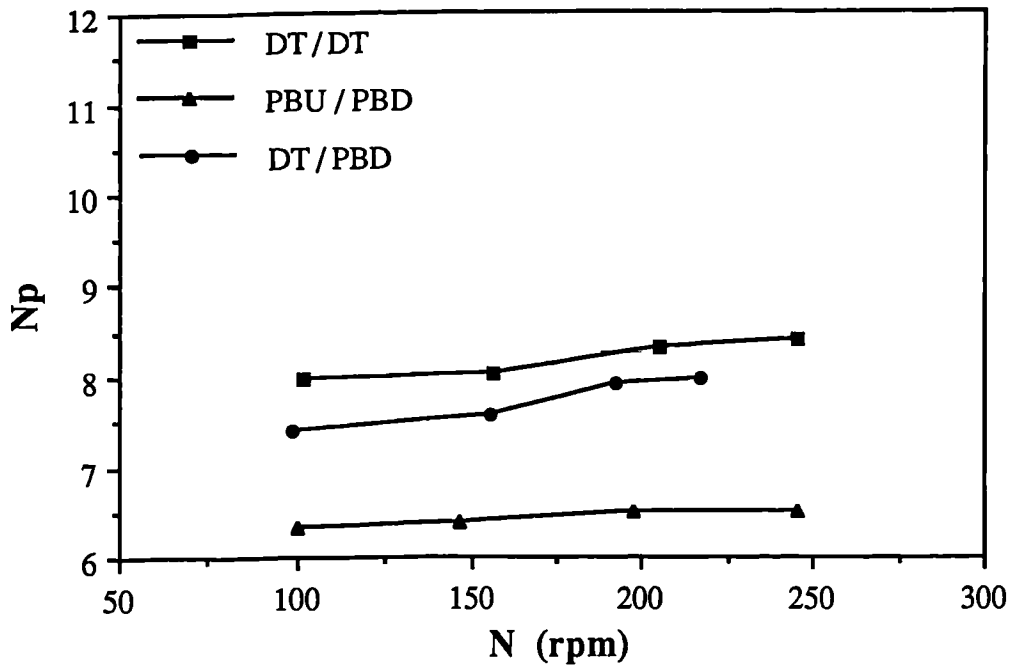

Figure 5.9 (a). Comparison of the power number for both impellers for different impeller combinations, C1 = C2 = T/3, t = 1.65 mm.

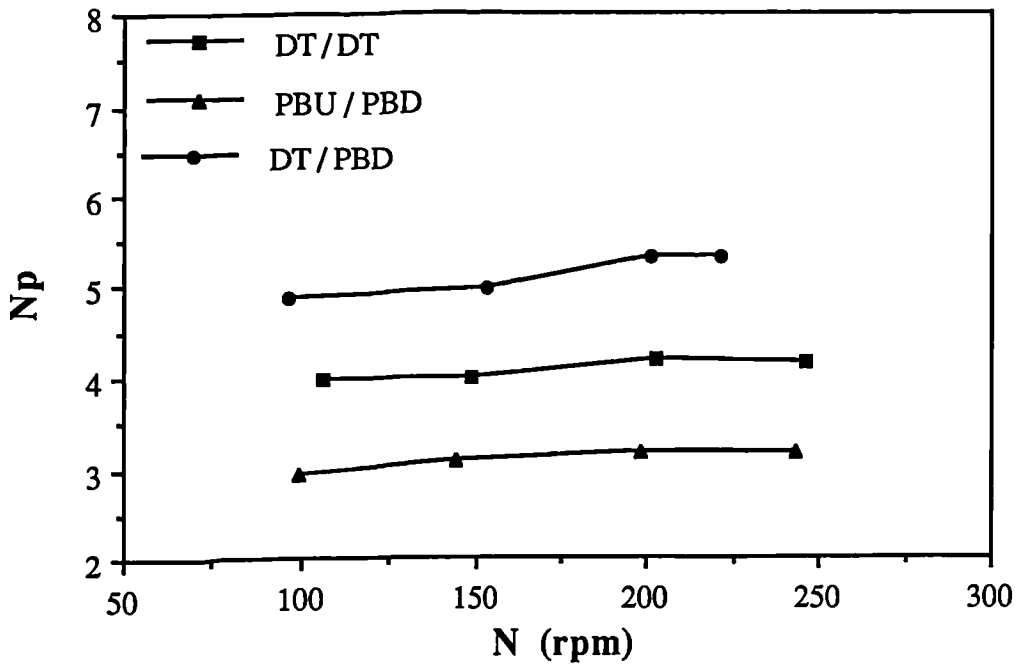

Figure 5.9 (b). Comparison of the power number for the lower impeller with different impeller combinations, C1 = C2 = T/3, t = 1.65 mm.

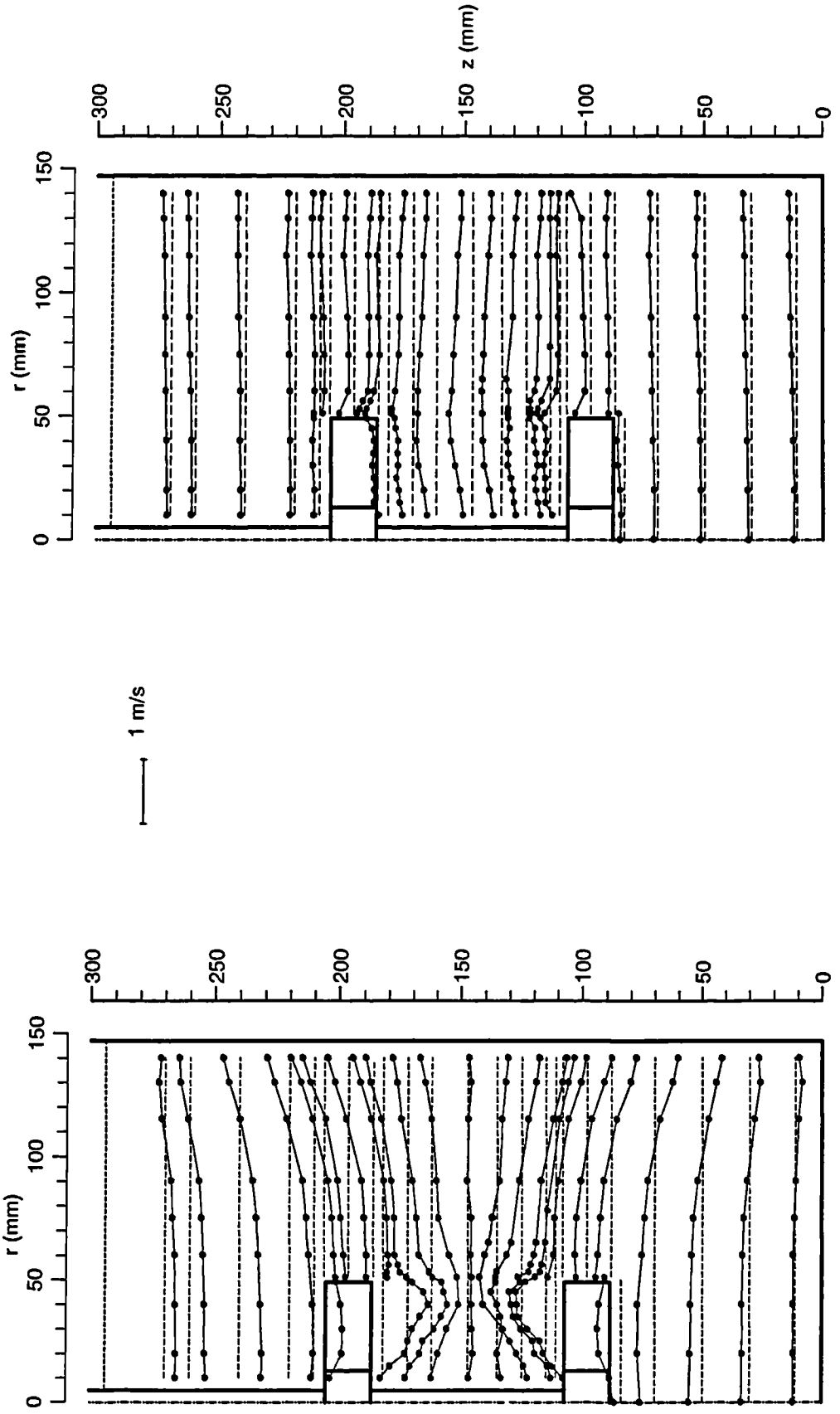

Figure 5.10. Axial mean velocity profiles; C1 = C2 = T/3.

Figure 5.11. Axial rms velocity profiles, C1 = C2 = T/3.

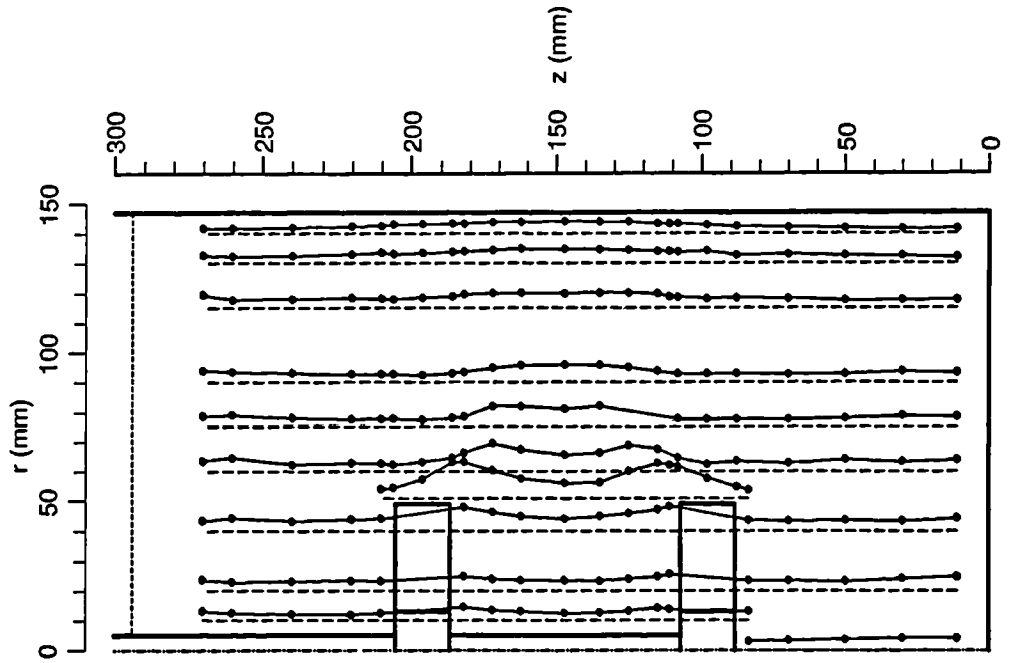

Figure 5.13. Radial rms velocity profiles; C1 = C2 = T/3.

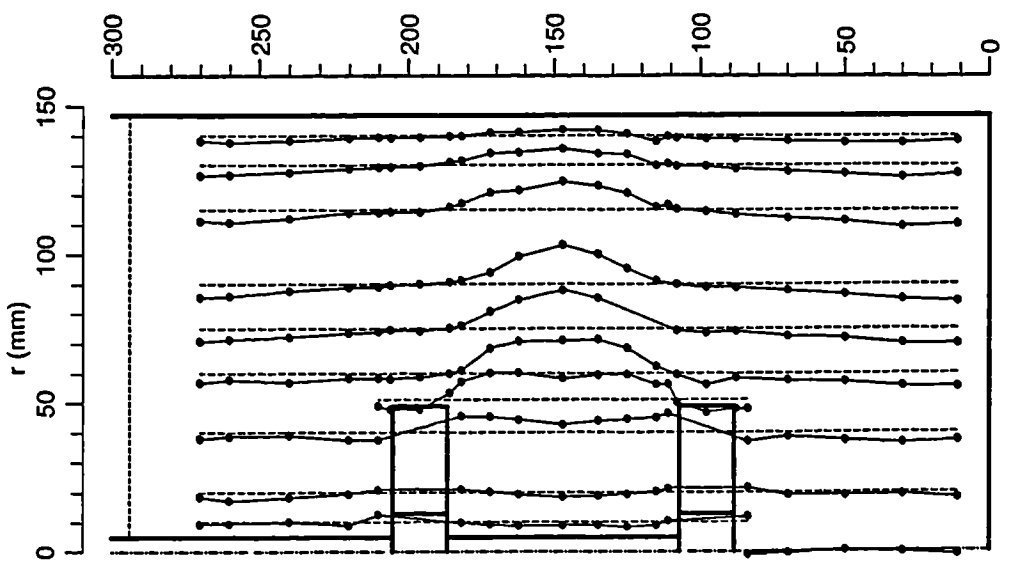

1 m/s

Figure 5.12. Radial mean velocity profiles; C1 = C2 = T/3.

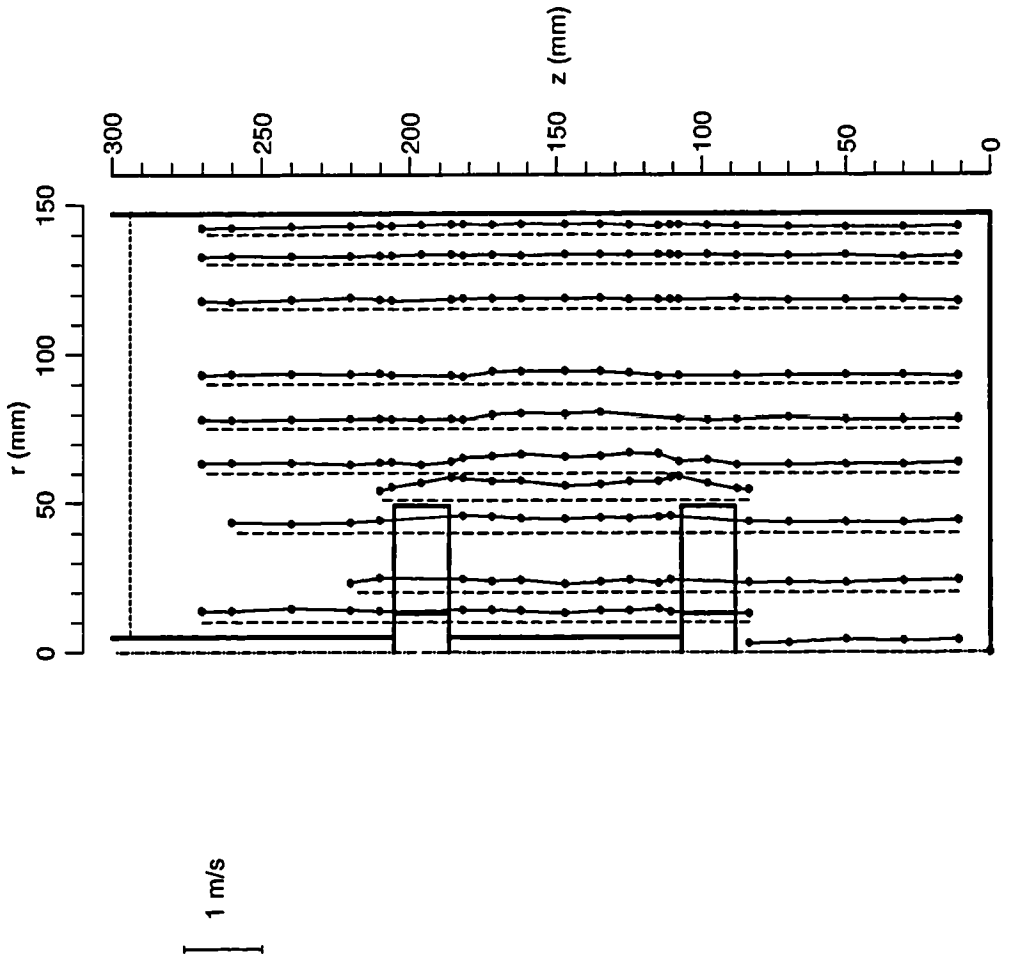

Figure 5 15. Tangential rms velocity profiles; C1 = C2 = T/3.

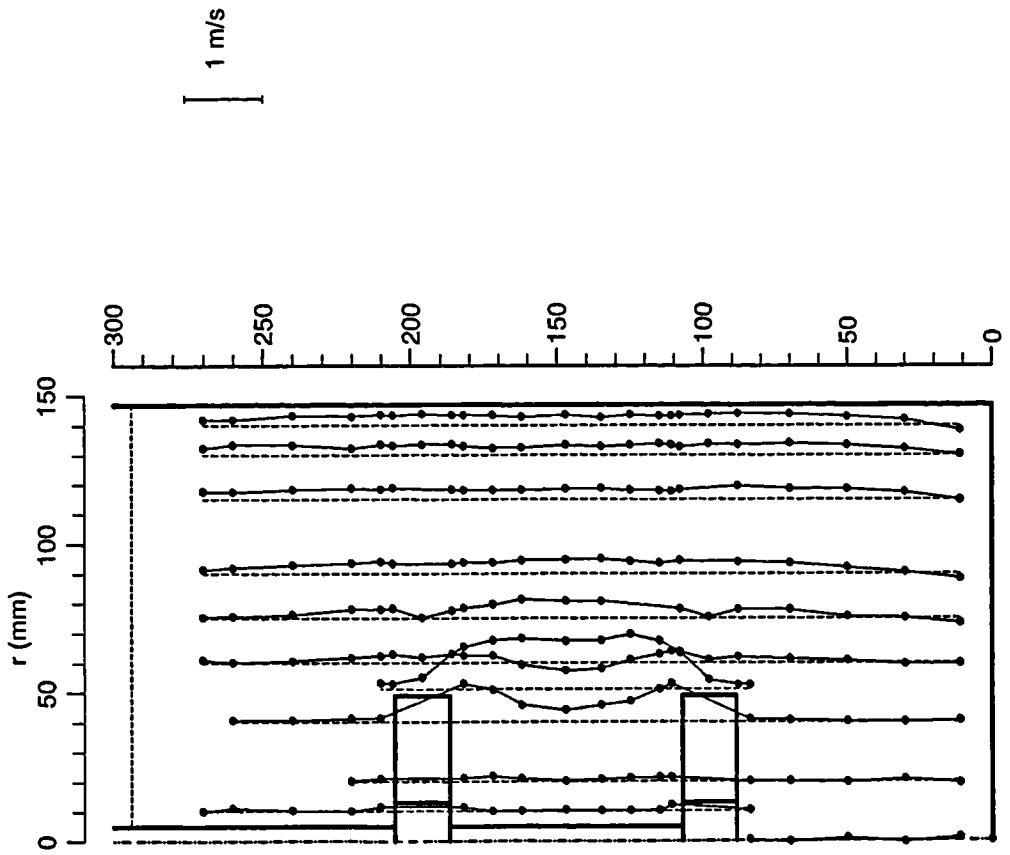

Figure 5.14. Tangential mean velocity profiles; C1 = C2 = T/3.

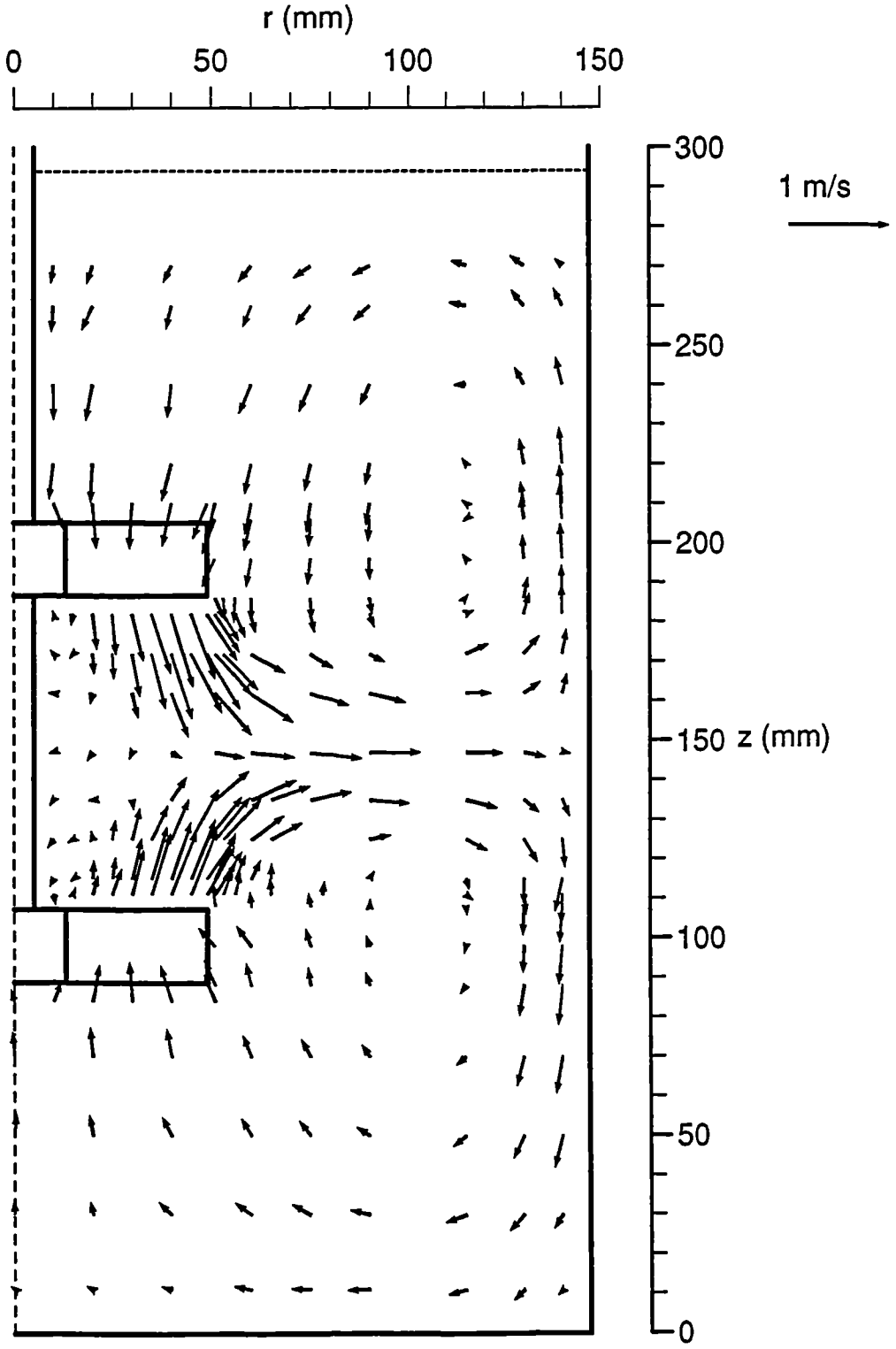

Figure 5.16. Velocity vectors in $\theta = 0^{\circ}$ r-z plane; C1 = C2 = T/3.

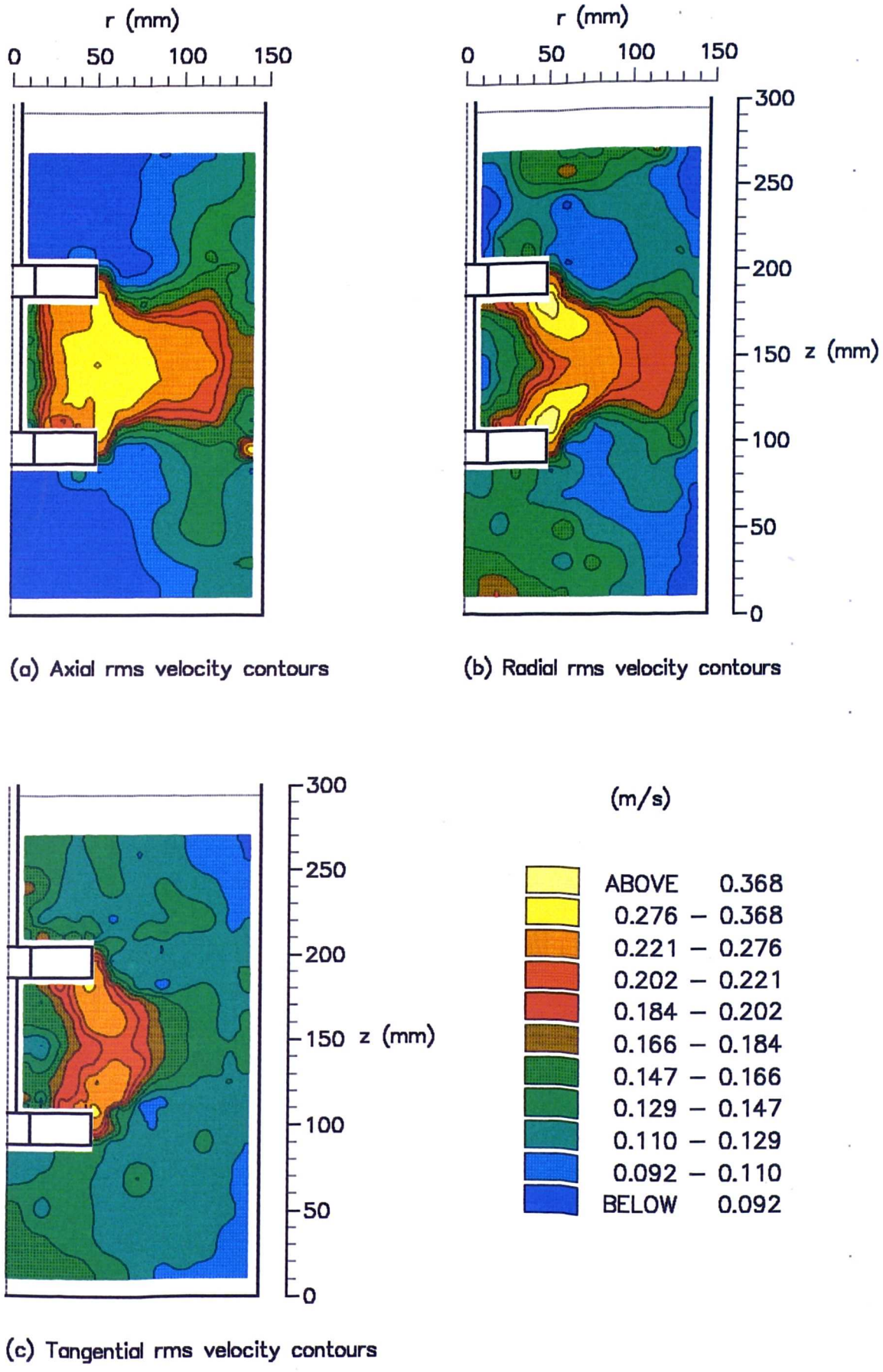

(a) Axial rms velocity contours

(b) Radial rms velocity contours

(c) Tangential rms velocity contours

Figure 5.17. Rms velocity contours in $\theta = 0^{\circ}$ r-z plane; C1 = C2 = T/3.

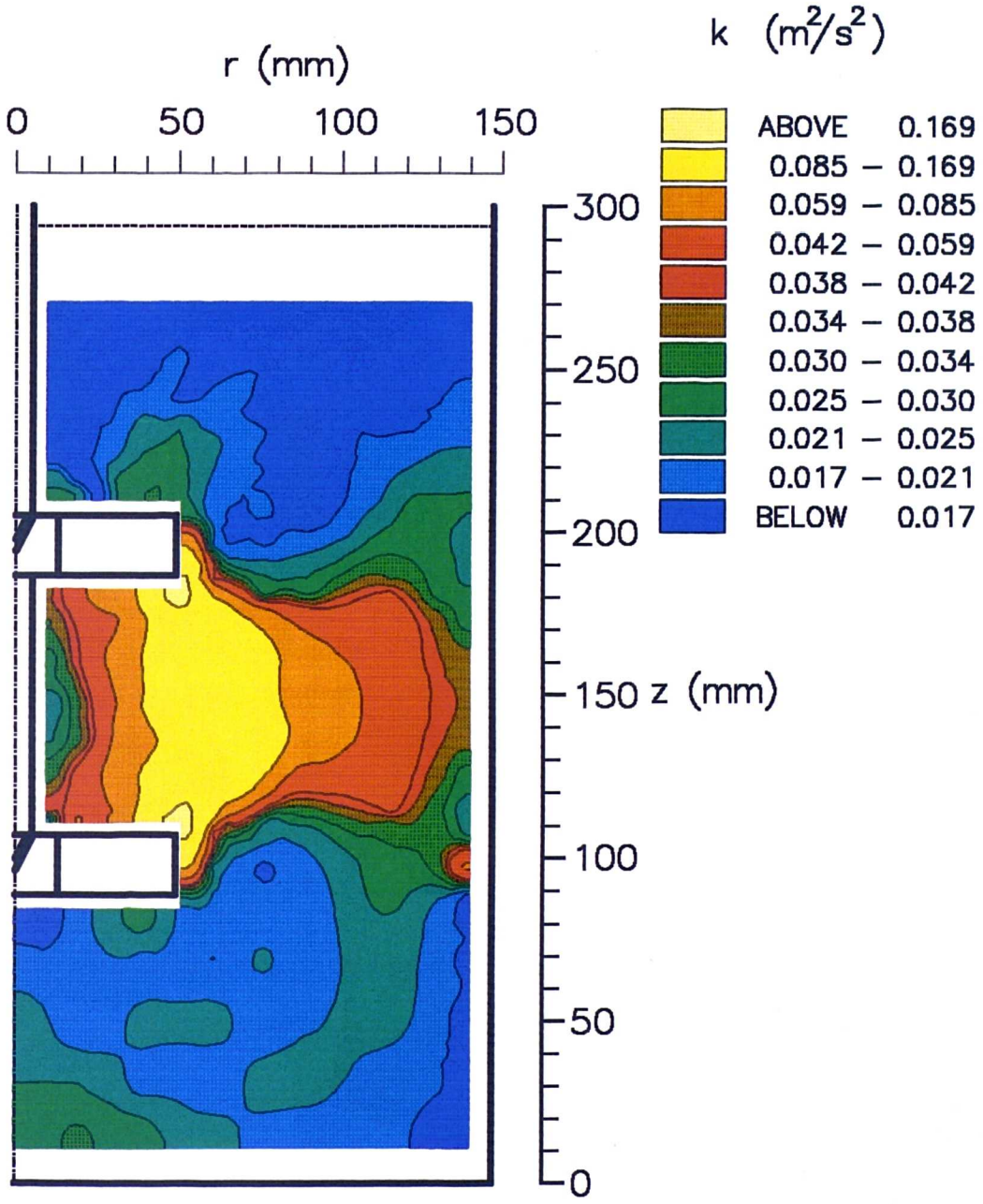

Turbulence kinetic energy contours, C1 = C2 = T/3.

Figure 5.18

CHAPTER 6

CLOSURE

This chapter is divided into three sections. In the first a very brief account of the research carried out is given. In the second the main findings and achievements of the thesis are outlined and in the third areas in which further investigation is needed are identified.

6.1 The present contribution

The object of the research in this thesis was to investigate the mixing characteristics of a stirred tank agitated by two impellers. A considerable amount of time was devoted to the design and construction of the mixing tank and of the Rushton and pitched blade impellers of different shapes. For different impeller configurations, flow visualisation was carried out prior to quantitative study of the flow for which a LDA system was developed and used as a measuring tool.

Flow visualisation was performed in order to obtain qualitative information about the structure of the flow and also to identify the regions where quantitative studies were mostly needed. In all the quantitative studies the liquid height was equal to the tank diameter. The overall mixing performance of single- and/or two-impeller systems was determined by performing power and mixing time measurements. For the former measurements a telemetric strain gauge torque measuring system was developed and used. This system was suitable for dual-impeller mixing systems as the power drawn by each impeller could be determined. A conductivity method was employed for mixing time measurements. With

each impeller configuration the overall mixing time was obtained by repeating the measurements in different parts of the vessel in order to overcome the shortcomings of this technique.

A parametric study was also carried out for both single- and two-Rushton impeller systems and the effects of impeller geometry and speed on the mixing characteristics of the stirred tank were investigated.

6.2 Achievements and conclusions

Flow visualisation with three impeller combinations were performed, these were: two Rushton, two pitched blade, and Rushton and pitched blade impellers. The observations clearly demonstrated a complex variation of flow pattern as the impeller combination, impeller spacings, liquid height and impeller speed were varied.

More attention was paid to the two Rushton impeller combination with which a small change in the impeller spacings resulted in a significant variation in the direction of the impeller streams and consequently in the generated flow pattern. With this combination three stable and four unstable flow patterns were identified. With the stable flow patterns either both the impellers were pumping in a horizontal direction and generating four main ring vortices (parallel flow pattern) or the two impeller streams were merging and forming two main ring vortices (merging flow pattern) or the upper impeller was pumping horizontally and generating two main ring vortices while the lower impeller was pumping towards the vessel bottom and generating one main ring vortex (diverging flow pattern).

Although the variations in the liquid height and in the impeller speed affected the kind of flow pattern in the vessel to some extent, the presence of the two former stable flow patterns was strongly dependent on the spacing between the two impellers while the presence of the third stable flow pattern was strongly dependent on the clearance of the lower impeller from the bottom of the vessel. Each of the unstable flow patterns observed with the two Rushton impellers was a combination of either two or three of the above mentioned stable flow patterns depending on the impeller spacings, liquid height and impeller speed.

Extensive power measurements revealed a fluctuating torque exerted on the shaft by the impellers in two-impeller systems. These fluctuations intensified as the impeller speed was made more stable by mounting a flywheel on the shaft. The maximum fluctuation of the power number was typically 25% of the mean values when the flow pattern was stable. With an unstable flow pattern the fluctuation was even higher. Comparatively the maximum fluctuation of the power number measured for a single Rushton impeller was very small (around 3.7%).

Among the different combinations of Rushton and/or pitched blade impellers studied, the highest combined power number for two impellers (Np = 10) was obtained for two Rushton impellers generating the parallel flow pattern (C_1 = T/4, C_2 = T/2), and the lowest (Np = 6.5) was obtained with the two pitched blade impellers (C_1 = C_2 = T/3) pumping towards each other. With the combination DT / DT the total Np was always less than the sum of the single impeller power numbers while with the PBU / PBD combination the total Np was greater (by around 20%) than the sum of the single impeller power numbers.

Mixing time measurements revealed useful information for mixing process design and the results showed that the mixing time could be increased by up to 100% by using different combinations of impellers. With the two Rushton impellers there were significant variations of mixing time with the spacing between the two impellers. With these two impellers, the shortest mixing time was obtained with the merging flow pattern ($C_1 = C_2 = T/3$) and the longest was obtained when the flow was unstable, changing between the parallel and merging flow patterns.

With every impeller combination studied other than the two Rushton impellers the mixing time was almost independent of the clearance between two impellers as a variation in this spacing did not cause a significant change in the induced flow pattern. Among all the impeller combinations examined, the shortest mixing time was obtained with the combinations DT / PBD and/or PBD / PBD and the longest mixing time was obtained with two Rushton impellers producing an unstable parallel / merging flow pattern.

The flow pattern induced by two pitched blade impellers pumping towards each other, was found to be stable and showed a lot of similarities with the merging flow pattern generated by two Rushton impellers. Measurements were made of the three mean and rms velocity components with every stable flow pattern in the vessel. The measurements with the flow patterns induced by two Rushton and two pitched blade impellers were presented and discussed in Chapters 3 and 5 respectively. These LDA results confirmed the flow visualisation observations and provided distribution of the flow characteristics in the vessel with every stable flow pattern. The flow with all the four flow patterns was highly vortical and three

dimensional and the most important features of these flows were as follows.

With every pattern the flow around the axis and along the wall of the vessel was predominantly in the axial direction. With the parallel flow pattern, each (horizontal) impeller stream generated two ring vortices, one on each side of the stream. With this pattern flow entrainment to each of the impeller streams occurred from both sides of the stream. The flow number of the lower impeller was slightly higher than that of the upper impeller and both these flow numbers were smaller than that of an identical single impeller.

With the Rushton merging flow pattern the impeller streams merged in almost straight line paths and the flow was predominantly tangential in most of the regions in the middle of the vessel and particularly in the region confined between the two impellers where the flow exhibited a solid body rotation around the shaft. In terms of radial velocity magnitudes in the bulk flow this flow pattern was the poorest among all the others. Most of the flow entrainment from the bulk flow to the impeller streams occurred from the upper side of the upper impeller stream and from the lower side of the lower impeller stream.

With the diverging flow pattern the radial discharge flow rate from the upper impeller was slightly higher than those obtained for the impellers generating the parallel flow pattern. The lower impeller stream was directed towards the vessel base at an average angle of 30° to the horizontal in the impeller vicinity and 60° to the horizontal close to the vessel bottom. The flow beneath the lower impeller formed a weak ring vortex. In the vicinity of the lower impeller and along the upper half of the impeller blade

the mean radial velocities were small and directed towards the impeller axis. However, the inclination of the lower impeller stream is convenient for particle suspension in the stirred tanks due to the sweeping action of the lower impeller stream. A detailed account of the effect of impeller spacing on the flow patterns, mixing time and velocity profiles in double Rushton impeller systems has been given by Mahmoudi and Yianneskis (1991, 1992) and Lee, Mahmoudi and Yianneskis (1993).

The similarities and differences between the Rushton and PBTs merging flow patterns were discussed in detail in Chapter 5. Although the average level of k in the vessel is slightly higher with the Rushton merging flow pattern, the values of k in the region between the two impellers and in most regions near the walls are higher with the PBTs. Consequently better local and probably overall mixing could be achieved with the PBTs if feed pipes in stirred reactors are positioned in regions of high k.

The turbulence quantities measured over 360° of impeller rotation decayed with distance from the impellers with all the flow patterns. With the three stable flow patterns generated by two Rushton impellers the turbulence can be considered only approximately as being isotropic in some locations in the impeller stream and anisotropic in the bulk flow. With the PBTs merging flow pattern the turbulence was anisotropic everywhere in the vessel. The area-weighted average turbulence kinetic energy was found to be the highest with the parallel flow pattern and the lowest with the diverging flow pattern.

The effects of Rushton impeller rotational speed and geometry on the flow in the impeller region were presented and discussed in Chapter 4. It was shown that the radial mean and rms velocities (normalised by the impeller

tip speed) do not vary significantly with impeller speed. However, in general, with lower impeller speeds the normalised mean velocities were slightly smaller. A higher flow number and power number was obtained with a thinner impeller. An increase in the size and thickness of a Rushton impeller resulted in a slightly higher discharge efficiency (F_l/Np) of the impeller.

6.3 Recommendations for future work

In this work a change in the separation between two Rushton impellers was found to have a significant effect on the induced flow pattern and it would be interesting and useful to extend the research by variation in the sizes of the impellers and the mixing tank in order to predict the variations in the flow pattern as the impeller spacings, liquid height and impeller speed change.

The working fluid used in the experiments described in this thesis was water. However, it would be useful to carry out similar investigations with fluids of different viscosities in order to establish stability criteria with different spacings and impeller combinations. This is particularly important in view of the related findings of other researchers who studied different fluids, as mentioned in section 5.2.1.

Similar investigations in gassed flows are also required, especially in view of the frequent use of double impeller (DT / PBD) combinations for gas dispersion. Finally, combinations of axial (hydrofoil) and hollow-blade impellers with Rushton and pitched blade turbines are also used for a large number of mixing processes and they should be investigated in similar detail to the ones studied here to establish accurate mixing criteria.

The flow with Rushton merging flow pattern was highly rotational in the middle part of the vessel and an increase of the number or width of the baffles might be useful to improve the vertical circulation of the flow in the tank as the baffles influence the mean flow in the tank extensively (Bissel et al, 1947 and Reed et al, 1977).

Time-resolved measurements and angle-resolved measurements over 1° interval of impeller rotation in the impeller region would be useful to quantify the changes in the trailing vortices as a result of a variation in the impeller spacing (or correspondingly in the flow pattern) or variation in the impeller geometry. It is known that the rms velocities measured over 360° of impeller rotation (which include "pseudo-turbulence" - van't Riet et al, 1976) can be overestimated by 400% in comparison to angle-resolved measurements (Yianneskis et al, 1987). Comparisons of angle-resolved measurements with the results obtained in this work could help establish the effects of flow periodicity on the measured velocities in the impeller region. The ensemble-averaged measurements are however very useful for computational predictions of the flows as these results can be used as boundary conditions.

The Rushton and PBTs merging flow patterns showed a lot of similarities and differences. In particular with the former flow pattern the total Np was significantly lower than the sum of the power numbers of the single impellers while in the latter flow pattern this variation was reversed. With both flow patterns the power numbers varied with time, resulting in an almost identical fluctuation intensity of the total power number, $[rms]_{Np}/Np$, (Mahmoudi et al, 1994). Further investigation is clearly needed particularly with different impeller spacings for the PBU / PBD

combination. In addition time- and/or angle-resolved measurements are needed in the impeller region of both combinations and especially with the DT / DT combination in order to identify any possible changes in the structure and extent of the trailing vortex region behind the blades. This is important as these vortices may affect the torque exerted by the impellers (Nienow and Wisdom, 1974). Such work is in progress at King's College London and will be reported shortly.

In this work the impeller blade and disk were of the same thickness. Further work is needed to investigate whether the effects of these two thicknesses on the power and velocity characteristics can be separated.

The conductivity technique used in the present work, although accurate, suffers from the disadvantage that it only provides a measurement at a single point and is not representative of the conditions in the vessel as a whole. A novel technique is urgently required to allow the accurate determination of mixing time across the whole vessel. It would be interesting and useful to perform mixing time measurements using a liquid crystal tracer as a passive scalar and image processing techniques to determine the overall mixing time. This will also be beneficial for the accurate determination of stagnant regions in the vessel with different flow patterns. Preliminary investigations prompted by the above recommendations have shown very promising results for determination of the mixing time throughout the vessel (Lee and Yianneskis, 1994)

REFERENCES

S G. **Armstrong** and S **Ruszkowski (1986)**
"Measurement and comparison of flows generated by different types of impeller in a stirred tank". In: Colloque Agitation Mecanique, Toulouse, pp. 1 9 - 1.16.

S G. **Armstrong and S. Ruszkowski (1988)**
"The flow field in the discharge stream of disk turbines", 6th European Conference on Mixing, Pavia, Italy, pp. 1 - 6.

F.G. **Bader (1986)**
"Mass transfer in a multiturbine fermentor. I Gassed and ungassed power inputs", International Conference on Bioreactor Fluid Dynamics, Cambridge, paper 20, pp. 269 - 277.

K. M **Baker,** Astech Electronics Ltd **(1974)**
"Balancing techniques for strain gauge bridges", 'Strain', pp 73 - 82.

K. M. **Baker,** Astech Electronics Ltd **(1992)**
"Personal communication "

H **Benkreira (1990)**
"Fluid Mixing 4", Institution of Chemical Engineers, Rugby, U.K.

E. S. **Bissel,** H. C. **Hesse,** H. J. **Everett** and J. H. **Rushton (1947)**
"Design and utilization of internal fittings for mixing vessels", Chem Eng Prog , Vol 43, pp. 649 - 658.

W. **Bruijn,** K. **van't Riet** and J. M. **Smith (1974)**
"Power consumption with aerated Rushton turbines", Trans. Instn Chem. Engrs, Vol. 52, pp 88 - 104.

W. **Bujalski,** A. W. **Nienow,** S. **Chatwin** and M **Cooke (1986)**
"The dependency on scale and material thickness of power numbers of different impeller types", Proc. Int. Conf. on Mechanical Agitation, Toulouse, E. N. S Ass of Chem. Eup., pp. 1 37 - 1.46.

R V. **Calabrese** and C. M. **Stoots (1989)**
"Flow in the impeller region of a stirred tank", Chemical Engineering Progress, pp 43 - 50

C. M. **Chapman (1981)**
"Studies of gas-liquid-particle mixing in stirred vessels", Ph D. Thesis, University of London, cited by Kuboi and Nienow (1982)

R. G **Cooper** and D **Wolf (1968)**
"Velocity profiles and pumping capacities for turbine type impellers", The Canadian Journal of Chemical Engineering, Vol. 46, pp 94 - 100.

D. G **Cronin (1988)**
"The design of a pilot-scale protofermenter and its application to mixing, power consumption, heat-transfer and mass-transfer studies", Ph D Thesis, University of Birmingham.

D. B A. **Crozier (1989)**
"A detailed study of the flow characteristics in a tall stirred tank", Third International Conference on Laser Anemometry-Advances and Applications, Wales, pp 16 1 - 16 10.

L. A. **Cutter (1966)**
"Flow and turbulence in a stirred tank", A I Ch E. Journal, Vol 12, No 1, pp 35 - 45.

L. E. **Drain (1980)**
"The Laser Doppler Technique", John Wiley and Sons, Chichester.

D. F G **Durao and** J H **Whitelaw (1975)**
"The influence of sampling procedures on the velocity bias in turbulent flows", Proc. of the LDA Symp on The Accuracy of Flow Measurements by Laser Doppler Methods, Copenhagen, cited by K. O. Suen (1992).

F. **Durst**, A. **Melling** and J H **Whitelaw (1981)**
"Principles and practice of laser Doppler anemometry", 2nd edition, Academic Press, London.

K. N. **Dyster**, E. **Koutsakos**, Z. **Jaworski** and A W. **Nienow (1993)**
"An LDA study of the radial discharge velocities generated by a Rushton turbine: Newtonian fluids, Re $\geq$ 5", Trans IChemE, Vol. 71, Part A, pp. 11 - 23.

M **Greaves** and K A H. **Kobbacy (1981)**
"Surface aeration in agitated vessels", IChemE Symposium Series No 64, pp. H1 - H22.

A A. **Gunkel** and M E. **Weber (1975)**
"Flow phenomena in stirred tanks, part I. The impeller stream, AIChE Journal Vol. 21, No 5, pp 931 - 948

N. **Harnby**, M F. **Edwards**, A. W **Nienow (1985)**
"Mixing in the process industries", Butterworths, London.

R. R **Hemrajani (1985)**
"Mixer configuration, design guidline and scale-up criteria for effective mixing of immiscible liquids", Proc. 5th European Conference on Mixing, pp. 63 - 79.

S **Hiroka** and R. **Ito (1975)**
"On the relation between power input and impeller jet flow rate", J. Chem Eng. Japan, 8, No. 4, pp. 323 - 326.

R. M **Hockey (1988a)**
"Stirred reactor flow patterns with a pitched blade impeller", Mechanical Engineering Department, Imperial College of Science and Technology, Report No FS/88/07

R. M **Hockey (1988b)**
"Flow around a 60^{o} pitched blade impeller", Mechanical Engineering Department, Imperial College of Science and Technology, Report No FS/88/32

W. **Hoesel and** W. **Rodi (1977)**
"New biasing elimination method for laser-Doppler velocimeter counter processing", Rev. Sci. Instrum , Vol 48, No. 7, cited by Suen (1992).

D. B **Holmes**, R M.**Voncken** and J. A. **Dekker (1964)**
"Fluid flow in turbine stirred, baffled tank-I: Circulation time", Chemical Engineering Science, Vol. 19, pp 201 - 208

V. **Hudcova**, V. **Machon** and A W. **Nienow (1989)**
"Gas-liquid dispersion with dual Rushton turbine impellers", Biotechnology and Bioengineering, Vol. 34, pp 617 - 628

S. **Ito**, K. **Ogawa**, N. **Yoshida (1975)**
"Turbulence in impeller stream in a stirred vessel", Journal of Chemical Engineering of Japan, Vol. 8, No. 3, pp 206 - 209

Z. **Jaworski**, A. W **Nienow**, E. **Koutsakos**, K. **Dyster** and W. **Buljalski (1991)**
"An LDA study of turbulent flow in a baffled vessel agitated by a pitched blade turbine", Tras IChemE, Vol 69, Part A, pp. 313 - 320

H. **Kramers** G. M **Baars** and W. H **Knoll (1953)**
"A comparative study on the rate of mixing in stirred tanks", Chemical Engineering Science, Vol. 2, pp 35 - 42.

S J. **Khang** and T. J. **Fitzgerald (1975)**
"A new probe and circuit for measuring electrolyte conductivity", Ind Eng. Chem , Fundam., Vol. 14, No. 3, pp. 208 - 213.

S. J. **Khang** and O. **Levenspiel (1976)**
"New scale-up and design method for stirrer agitated batch mixing vessels", Chemical Engineering Science, Vol. 31, pp 569 - 577.

R **Kuboi**, A. W. **Nienow (1982)**
"The power drawn by dual impeller systems under gassed and ungassed condition", Forth European Conference on Mixing, Noordwijkerhout, Netherlands, pp. 247 - 261.

R **Kuboi** , A W. **Nienow** and K. **Allsford (1983)**
"A multipurpose stirred tank facility for flow visualization and dual impeller power measurment", Chem Eng. Commun., Vol 22, pp 29 - 39.

K C. **Lee** and M. **Yianneskis (1994)**
"Transient temprature measurements in a stirred vessel with liquid crystal tracers", Submitted to the ASME 2nd Biennial European Joint Conference on Engineering Systems Design and Analysis, London, 4 - 7 July.

K. C. **Lee**, S. M. S **Mahmoudi** and M **Yianneskis (1993)**
"Mean flow and turbulence energy distribution in vessels stirred by two Rushton impellers using ensemble-averaged and time-resolved LDA", Proc. AIChE, Annual meeting, St Louis, Missouri, 7 - 12 November.

V. **Machon**, J. **Vlcek**, J. **Skrivanek (1985)**
"Dual impeller systems for aeration of liquids· An experimental study", 5th European Conference on Mixing, pp. 155 - 169

S. M S. **Mahmoudi** and M **Yianneskis (1991)**
"The variation of flow pattern and mixing time with impeller spacing in stirred vessels with two Rushton impellers", 7th European Conference on Mixing, pp. 17 - 24.

S. M. S. **Mahmoudi** and M. **Yianneskis (1992)**
"The effect of impeller spacing on the mean flow and turbulence in stirred vessels with two Rushton impellers", Proc IChemE Reasearch event, Manchester, pp. 380 - 382

S. M. S. **Mahmoudi** and M **Yianneskis (1993)**
"The influence of Rushton impeller blade and disk thickness on the mixing characteristics of stirred vessels", Submitted for publication to Journal of Process Mechanical Engineering.

S. M. S. **Mahmoudi, K Rutherford,** K C. **Lee** and M. **Yianneskis (1994)**
"A study of the turbulence characteristics of dual-impeller mixing systems using LDA", Submitted to 8th European Conference on Mixing, Cambridge, 21 - 23 September.

D. K. **McLaughlin** and W. G. **Tiederman (1973)**
"Biasing Correction for individual Realisation of Laser Anemometry Measurements in Turbulent Flows", Physics of Fluids, Vol. 16, p. 2082, cited by Suen (1992).

J. **Middleton (1993)**
"Imperial Chemical Industries", personal comunication.

A. S **Mujumdar,** B **Huang,** D. **Wolf,** M. E **Weber** and W. J. M. **Douglas (1970)**
"Turbulence parameters in a stirred tank", The Canadian Journal of Chemical Engineering, Vol. 48, pp 475 - 483.

S **Nadaradjah (1992)**
"An experimental investigation of flows through inlet ports and valves" PhD Thesis, King's College, University of London.

S. **Nagata (1975)**
"Mixing, Principles and application", Kodansha, Tokyo, Japan

A. W. **Nienow** and R **Kuboi (1984)**
"A technique for studying intervortex mixing rates in a dual impeller agitated vessel in high viscosity fluids", Fluid mixing II, Chem E. Symp Series No. 89, pp. 97 - 106.

A. W. **Nienow** and M D.**Lilly (1979)**
"The power drawn by multiple impellers in sparged agitated vessels, Biotechnology and Bioengineering, Vol XXI, pp. 2341 - 2345

A W. **Nienow** and D. **Miles (1971)**
"Impeller power numbers in closed vessels", Ind Eng Chem. Process Des. Develop., Vol. 10, No 1, pp 41 - 43.

A. W. **Nienow** and D. J. **Wisdom (1974)**
"Flow over disc turbine blades", Chemical Engineering Science, Vol. 29, pp. 1994 - 1997.

J M. **Nouri (1988)**
"Single and two phase flows in ducts and stirred reactors", PhD thesis, Imperial College of Science and Technology, University of London.

J M. **Nouri** and J. H. **Whitelaw (1990)**
"Effect of size and confinement on the flow characteristics in stirred reactors", Proc of 5th International Symposium on Application of Laser Techniques to Fluid Mechanics, Lisbon, Portugal, paper 23 2.

J. M. **Nouri**, J H. **Whitelaw** and M **Yianneskis (1987)**
" The scaling of the flow field with impeller size and rotational speed in a stirred reactor", Proc. of 2nd Int Conf. on Laser Anemometry - Advances and Applications, Strathclyde, Scotland, September 1987, pp 489-500.

P. **Ramage (1992)**
"Techni Measure Ltd", private comunication

N. B **Reed**, M **Princz** and S. **Hartland (1977)**
"Laser Doppler measurements of turbulence in a standard stirred tank", Proc. 2nd. Eur. Conf. on Mixing, paper B1, pp B1 1 - B1.26

J. **Rennie** and F. H. H **Valentine (1968)**
"Gas dispersion in agitated tanks", Chemical Engineering Science, Vol. 23, pp 663 - 664.

B. K **Revill (1982)**
"Pumping capacity of disc turbine agitators - A literature review", Forth European Conference on Mixing, paper B1, pp. 11 - 24.

J. W. **Richards (1963)**
"Power input to fermenters and similar vessels", British Chemical Engineering, Vol. 8, No. 3, pp. 158 - 163

M. **Roustan (1985)**
"Power consumed by Rushton turbines in nonstandard vessels under gassed conditions", 5th European conference on Mixing, pp 127 - 141.

J. H. **Rushton**, E. W. **Costich** and H J **Everett (1950)**
"Power characteristics of mixing impeller, Part I", Chemical Engineering Progress, Vol 46, No 8, pp 395 - 404

K. **Rutherford**, S. M S. **Mahmoudi**, K. C. **Lee** and M. **Yianneskis (1994)**
"A study of the flows induced by a pitched blade / Rushton dual impeller system with LDA and flow visualization", IChemE Research Event, January, 4 - 6.

J. P. **Sachs** and J H **Rushton (1954)**
"Discharge flow from turbine-type mixing impellers", Chemical Engineering Progress, Vol. 50, No. 12, pp. 597 - 603

Y. **Sano** and H **Usui (1985)**
Interrelation among mixing time, Power number and discharge flow rate number in baffled mixing vessels", Journal of Chemical Engineering of Japan, Vol 18, No 1, pp. 47 - 52

C. **Schofield (1974)**
"The definition and assessment of mixture quality in liquids and pastes", First European Conference on Mixing and Centrifugal Separation, pp C1-1 - C1-13.

J. M. **Smith**, M M C. G. **Warmoeskerken** and E. **Zeef (1986)**
"Gas liquid dispersion with multiple impellers", AIChE annual meeting, Paper 117.

J **Solomon**, A. W **Nienow** and G. W **Pace (1981)**
"Flow patterns in agitated plastic and pseudoplastic viscoelastic fluids", IChemE Symposium Series No 64. pp. A1-A13

K O. **Suen (1992)**
"Investigation of gas flow in a motored high speed diesel engine by laser-Doppler anemometry", PhD thesis, King's College, University of London

H **Taguchi** and T. **Kimura (1970)**
"Studies on geometric parameters in fermentor design, (I) Effects of impeller spacing on power consumption and volumetric oxigen transfer coefficient", J Ferment. Techno., Vol. 48, No. 3, pp. 117 - 124.

G. B **Tatterson**, H -H S. **Yuan** and R. S. **Brodkey (1980)**
"Stereoscopic visualization of the flows for pitched blade turbines", Chemical Engineering Science, Vol. 35, pp 1369 - 1375

J **Thyn**, V. **Novak and** P. **Pock (1976)**
"Effect of measured volume size on the homogenization time", The Chemical Engineering Journal, Vol. 12, pp 211 - 217.

V. W. **Uhl** and J. B **Gray (1966)**
"Mixing, Theory and Practice", Academic Press", London

K. **van der Molen** and H. R E. **van Maanen (1978)**
"Laser-Doppler measurements of the turbulent flow in stirred vessels to stablish scaling rules", Chem. Eng Sci., Vol. 33, pp 1161 - 1168.

K. **van't Riet** and J M. **Smith (1973)**
"The behaviour of gas-liquid mixtures near Rushton turbine blades", Chemical Engineering Science Vol. 28, pp 1031 - 1037.

K. **van't Riet** and J. M **Smith (1975)**
"The trailing vortex system produced by Rushton turbine agitators", Chemical Engineering Science, Vol 30, pp 1093 - 1105.

K. **van't Riet**, W. **Bruijn** and J. M. **Smith (1976)**
"Real and pseudo-turbulence in the discharge stream from a Rushton turbine", Chemical Engineering Science, Vol. 31, pp. 407 - 412.

R M. **Voncken**, D. B. **Holmes**, H. V **Den Hartog (1964)**
"Fluid flow in turbine-stirred, baffled tanks-II: Dispertion during circulation", Chemical Engineering Scince, Vol. 19, pp. 209 - 213.

R J. **Weetman** and J. Y. **Oldshue (1988)**
"Power, flow and shear characteristics of mixing impellers", 6th European Conference on Mixing, Pavia, Italy, pp. 43 - 50.

H. **Wu** and G. K. **Patterson (1989)**
"Laser-Doppler measurements of turbulent-flow parameters in a stirred mixer", Chemical Engineering Science, Vol 44, No. 10, pp. 2207 - 2221

W. J. **Yanta (1973)**
"Turbulence measurements with a laser-Doppler velocimeter", Naval Ordnance Labs, White Oak, Silver spring, Report NOLTR 73-94.

M **Yianneskis (1982a)**
"Flow characteristics in a standard configuration stirred reactor", Imperial College, Mechanical Engineering Department, Report No. FS/82/23

M. **Yianneskis (1982b)**
"Flow in reciprocating engin cylinders and curved ducts", PhD Thesis, Imperial College, University of London.

M **Yianneskis, Z. Popiolek** and J H **Whitelaw (1987)**
"An experimental study of the steady and unsteady flow characteristics of stirred reactors", J. Fluid Mech., Vol 175, pp. 537 - 555.

M **Yianneskis** and J. H. **Whitelaw (1993)**
"On the structure of the trailing votices around Rushton turbine blades", Trans IChemE, Vol. 71, Part A, pp. 543 - 550.